Filter Bank based MultiCarrier (FBMC) for Cognitive Radio Systems

Haijian Zhang

Modulations multiporteuses à base de bancs de filtres pour la radio cognitive

présentée par

Haijian ZHANG

pour obtenir le grade de

Docteur du Conservatoire National des Arts et Métiers et Wuhan Université

Spécialité: Lasers, Métrologie et Communications

Soutenue le 15 novembre 2010 devant le jury composé de

Rapporteurs:	Aawatif HAYAR
	Jacque PALICOT
Examinateurs:	Pierre SIOHAN
	Jean-François HELARD
	Maurice BELLANGER
Directeurs:	Didier LE RUYET
	Daniel ROVIRAS
	Hong SUN

Acknowledgements

<div align="right">

Haijian ZHANG

Paris, September 2010

</div>

Abstract

Cognitive Radio (CR) is a fully reconfigurable radio that can intelligently change its communication variables in response to network and user demands. The ultimate goal of CR is to allow the Secondary User (SU) to utilize the available spectrum resource on a non-interfering basis to the Primary User (PU) by sensing the existence of spectrum holes. Therefore, the detection of PU is one of the main challenges in the development of the CR technology. Moreover, compared to conventional wireless communication systems, CR system poses new challenges to Resource Allocation (RA) problems because of the Cross-Channel Interference (CCI) from the adjacent channels used by SU to PU. In the CR context, most past efforts have been spent on Orthogonal Frequency Division Multiplexing (OFDM) based CR systems. However, OFDM technique exhibits some shortcomings in application due to its significant spectrum leakage. Filter Bank based Multi-Carrier (FBMC), as another promising Multi-Carrier Modulation (MCM) candidate, has been recently proposed for CR applications. In this dissertation, three important issues in developing a FBMC based CR system are discussed.

The three prime issues can be summarized: we firstly survey the spectrum sensing problems of OFDM and FBMC signals by using Cyclostationary Signature (CS) detector. Furthermore, we propose a Polyphase Filter Bank (PFB) based multi-band sensing architecture, and argue for its advantage; secondly, the comparison of OFDM and FBMC from the spectral efficiency point of view is discussed; and lastly, our emphasis is placed on the strategic resource allocation algorithms for non-cooperative multi-cell CR systems.

The overall proposed algorithms have been verified by simulation. Numerical results show that FBMC, as opposed to OFDM, could achieve higher spectrum efficiency and attractive benefit in spectrum sensing. The contributions of this dissertation have heighten the interest in applying FBMC in the future CR systems.

Keywords: Cognitive Radio; FBMC; OFDM; Spectrum Sensing; Spectral Efficiency Comparison; Resource Allocation;

Résumé

La radio cognitive (CR) est une radio entièrement reconfigurable qui permet de changer intelligemment ses paramètres de communication en réponse à l'activité des autres réseaux radios et demandes d'utilisateur. L'objectif ultime de la CR est de permettre à l'utilisateur secondaire (SU) d'utiliser la ressource de spectre disponible sans interférer sur l'utilisateur primaire (PU) en utilisant des trous de spectre. Par conséquent, la détection du PU est l'un des défis principaux dans le développement de la CR. Par rapport aux systèmes conventionnels de communication sans fil, le système CR introduit de nouveaux problèmes d'allocation de ressource (RA) en raison de l'interférence des canaux adjacents utilisés par le SU et le PU. Dans le contexte de la CR, la plupart des efforts ont été menés sur les systèmes de CR basés sur le multiplexage par division de fréquences orthogonales (OFDM). Toutefois, la technique de l'OFDM montre quelques points faibles dans l'application à cause des remontées significatives du spectre. Les modulations multiporteuses à base de bancs de filtre (FBMC) ont été récemment proposées pour des applications de CR. Dans cette thèse, trois points importants pour le développement d'un système de CR basé sur le FBMC sont discutés.

Les trois points principaux peuvent être résumés ainsi: nous examinons premièrement les problèmes de détection de spectre des signaux OFDM et FBMC en employant le détecteur de signature de cyclostationnarité (CS). En outre, nous proposons une architecture de détection multi-bande basée sur le banc de filtre polyphasé (PFB), et montrons son avantage; deuxièmement, la comparaison entre l'OFDM et le FBMC du point de vue de l'efficacité spectrale est discutée; et enfin, nous proposons un algorithme stratégique d'allocation de ressource pour les systèmes cognitifs multi-cellulaires et multi-utilisateurs.

Les algorithmes proposés dans cette thèse ont été testés par simulation. Les résultats numériques prouvent que le FBMC, par opposition à l'OFDM, pourrait réaliser une efficacité spectrale plus élevée et offre un avantage attrayant dans la détection de spectre. Les contributions de cette thèse ont accru l'intérêt d'appliquer FBMC dans les systèmes de CR à l'avenir.

Mots-clés: radio cognitive; FBMC; OFDM; détection de spectre; comparaison de l'efficacité spectrale; allocation de ressource;

Résumé des travaux de thèse

Motivation

La demande pour des nouveaux services et applications sans fil, ainsi que le nombre d'utilisateurs, sont en constante augmentation. Cependant, cette croissance est finalement limité par la quantité et la largeur des bandes de fréuences disponibles dans le spectre radiofréuence. Des mesures récentes effectués par plusieurs agences indiquent que les ressources du spectre sous licence ne sont pas pleinement exploités en fonction de l'heure et de l'emplacement gégraphique. Ces observations suggèrent que l'attribution fixe du spectre donne lieu à la pénurie spectrale, ce qui motive l'introduction des techniques d'accès dynamique au spectre (DSA). La radio cognitive (CR), inventé par Mitola, a été récemment proposé comme une solution prometteuse pour améliorer l'utilisation du spectre par DSA. L'objectif de la CR est d'améliorer l'efficacité spectrale par la superposition d'un système de radio mobile secondaire sur un système primaire sans nécessiter aucune modification du système sous licence. Au moment d'écrire cette thèse, il n'y a toujours pas d'approches communes sur la façon de définir et de mettre en œuvre les systèmes utilisant la CR. Bien que beaucoup d'efforts soient consacrè à l'étude de faisabilité de la CR, des méthodes plus efficaces et fiables doivent être développés en raison des ressources limités du spectre.

Ainsi les systèmes de la future CR devraient fournir une capacité plus élevé que les systèmes sous licence par une utilisation efficace des ressources disponibles. les modulations multi-porteuses (MCM) ont attirés beaucoup d'attention dans la communauté des communication, par opposition à la modulation simple porteuse en raison de la capacité à faire face efficacement aux canaux à évanouissements sélectifs en fréuence et de la flexibilité pour allouer les ressources de chaque sous-canal sur un base individuelle. Le multiplexage par division de fréuences orthogonales (OFDM) a été étudié de manière intensive ces dernières annés. Une grande partie de l'attention dans la littéature actuelle met l'accent sur l'utilisation de l'OFDM, qui est en mesure d'éviter les interféences inter-symbole (ISI) et interféences inter-canaux (ICI) en utilisant un préfixe cyclique prolongé (CP). l'OFDM a été proposé comme candidat pour les systèmes de la CR mais en dépit de ces avantages, l'OFDM est très sensible à l'offset de fréuence rèiduel (CFO) et au décalage temporel due à une
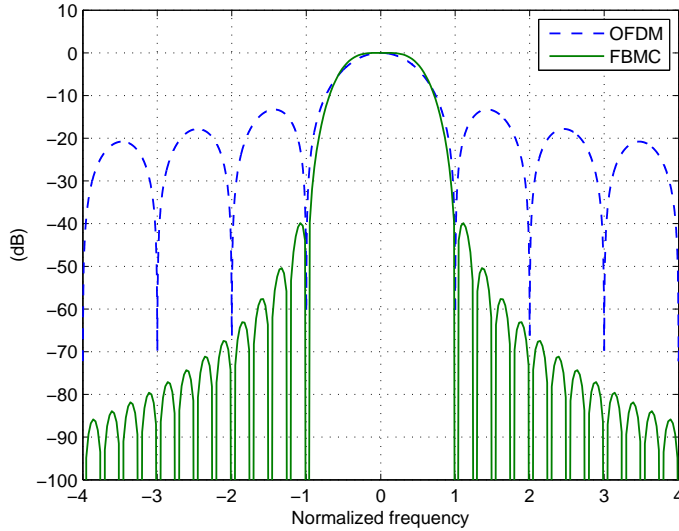
Comparaison des réponses en fréuence de l'OFDM et FBMC

synchronisation imparfaite. En outre, les systèmes utilisant l'OFDM sacrifient une partie du débit de transmission en raison de l'insertion du CP.

Dans cette thèse, nous proposons une autre classe de MCM: les modulations multiporteuses à base de bancs de filtre (FBMC), qui ne nécessitent pas de CP et montrent une meilleure robustesse au décalage de fréuence rèiduelle en tirant parti de la basse fuite spectrale de son filtre de prototype. Les modulations FBMC sont également un candidat pour la couche physique de la radio cognitive. En outre, les bancs de filtres au niveau du récepteur peuvent être utilisè comme un outil d'analyse de CR pour la détection du spectre. L'application des bancs de filtres pour la détection de spectre se révèle être plus approprié que la transformé de Fourier rapide (FFT) et la méthode Multi-Taper (MT) en raison de ses hautes performances et de son faible coût. Par conséuent les FBMC sont un candidat potentiel pour les systèmes de la CR en raison de leurs capacitè à offrir une capacité élevé et leurs bonnes cohabitations avec les systèmes de communication actuels.

La difféence essentielle entre les modulations OFDM et FBMC rèide dans la propriété de la fuite spectrale, comme indiqué dans la figure ci-dessus [1], dans laquelle leurs réponses en fréuence sont prèentés. Il peut être observé que la modulation OFDM possède des lobes latéaux importants, qui impose des contraintes d'orthogonalité stricte pour toutes les sous-porteuses. Au contraire, la modulation FBMC a des lobes latéaux négligeables dans le domaine fréuentiel. Avec une fuite spectrale très limité, une analyse spectrale de haute rèolution et de faibles interféences sur les bandes de fréuences adjacentes peuvent être atteintes. Récemment, il y a eu une prise de conscience croissante

---

[1]Le prototype de filtre utilisé pour la comparaison est la celui conçu dans le projet PHYDYAS.

du potentiel de l'utilisation de FBMC dans le domaine de radio communications, en particulier avec l'utilisation du filtre prototype Isotropic Orthogonal Transform Algorithm (IOTA). La pleine exploitation des modulations FBMC ainsi que leurs combinaisons avec les systèmes multi-antenne (MIMO) dans le cadre de la CR, a été étudié dans le projet europén PHYDYAS.

L'objectif de cette thèse est de proposer et développer des systèmes de CR utilisant les modulations FBMC. Bien que certains progrès ait été accompli dans ce domaine, beaucoup d'obstacles doivent être surmontè avant qu'un système de radio cognitive entièrement automatisé puisse être réalisé. Les modulations FBMC n'ont jusqu'à prèent reçu qu'une attention limité et n'ont pas été largement étudiés comme l'OFDM. Par conséuent, un autre objectif de cette thèse est de diffuser les connaissances de base de FBMC et de renforcer ainsi la littéature des bancs de filtres.

Porté de la recherche

La proposition d'utiliser les modulations FBMC dans le domaine de la CR est relativement récente et beaucoup d'efforts devraient être consacrè à sa mise en œuvre et de nombreuses questions en suspens restent à rèoudre. Dans cette thèse, l'accent est mis sur plusieurs axes de recherche des systèmes de CR basè sur les modulations FBMC. Plus précisément, le champ d'application de cette thèse comporte trois tâches principales:

Détection du spectre

Tout d'abord, nous soulignerons l'importance fondamentale de la détection du spectre. Dans le contexte de la CR, la détection du spectre est une fonctionnalité essentielle pour détecter les bandes inoccupés dans le spectre et avec un niveau relativement faible de SNR, puis ajuster dynamiquement les paramètres de fonctionnement de la CR. Ainsi, la détection des utilisateurs principaux est l'un des défis dans le développement de la technologie de la CR, avec pour objectif d'obtenir des méthodes de détection fiable et efficace. Ici la détection du signal FBMC basé sur la signature cyclostationnaire (CS) est proposé et étudié. Ensuite, la détection multi-bandes exploitant le rèeau de filtres polyphasè (PFB) est analysé et comparé par rapport à la détection basé sur une structure FFT.

Comparaison de l'efficacité spectral

Pour évaluer les modulations multiporteuses appliqués aux systèmes CR réls, nous devons faire attention au problème de son efficacité spectrale. Les capacitè du système secondaire des systèmes à base de FBMC et OFDM sont examinè et comparè sur la base d'un scénario de liaison montante dans le contexte de la CR.

Allocation des ressources

Un autre axe de recherche abordé est l'allocation des ressources (RA). Les défis de la RA dans un contexte de CR sont difféents de ceux de la RA classique sur deux aspects: l'interféence de l'utilisateur secondaire (SU) sur l'utilisateur principal (PU) doit être considéé, d'autre part, les trous de fréuences disponibles sont variables dans le temps, alors que les algorithmes de RA conventionnels supposent que les ressources du spectre disponible sont fixes. Dans la dernière partie de cette thèse, nous mettrons l'accent sur les algorithmes de RA pour les systèmes de CR non-coopéatif et multi-cellulaire.

Cette thèse tente de développer un système de radio cognitive basé sur les modulations FBMC par opposition à l'OFDM en couvrant plusieurs sujets de recherche importants. Nous donnons un aperçu de la radio cognitive et FBMC dans le premier chapitre. Trois questions de recherche: la détection du spectre, la comparaison de l'efficacité spectrale, l'allocation des ressources, dans les systèmes de CR basè sur les modulations FBMC sont étudiés par rapport aux systèmes de CR basè sur l'OFDM.

Chapitre 2 - Introduction sur la radio cognitive et les modulations FBMC

Radio cognitive

L'approche de radio cognitive proposé par Mitola est la plus originale mais ses fonctionnalitè sont encore trè en avance sur les technologies actuelles. En conséuence, la plupart des travaux de recherche se concentre actuellement sur la radio cognitive à base de détection du spectre (SSCR) avec moins de fonctionnalitè. Il convient de souligner que la CR mentionné dans cette thèse se réfère à la SSCR.

Une illustration du système SSCR est reprèenté sur la figure ci-dessous, où deux systèmes primaires opèrent respectivement dans deux bandes de fréuences difféentes f1 et f2, attribués sous licence à ces deux systèmes primaires. Plus précisément, un système de CR pourrait établir des liens de communication dans la limite de porté de chaque système principal. Un SU mesure tout d'abord l'environnement du spectre afin de déterminer les bandes de fréuences inoccupés. Une fois qu'un trou spectral est détecté, le SU adapte sa puissance d'émission, sa bande de fréuence, et sélectionne sa modulation, etc, de sorte qu'il minimise les interféences vis à vis du PU. L'utilisation du spectre est difféente dans les difféents domaines, donc les emplacements des trous spectraux et leurs durés varient. L'utilisation du plan temps-fréuence-espace est prèenté dans la figure suivante. Il est à noter que les SUs dans le domaine de fréuence f1 peuvent utiliser la fréuence f2 tout le temps parce qu'ils sont hors de porté de communication du système primaire dans la zone de fréuence f2, et *vice versa* pour d'autres systèmes de CR dans le domaine de fréuence f2. Ainsi, un système idéal de SSCR permet à ses utilisateurs d'accéder à une bande de fréuence de façon opportuniste dans le temps et l'espace, ce qui conduit à une augmentation significative de l'efficacité du spectre total. Dès que le
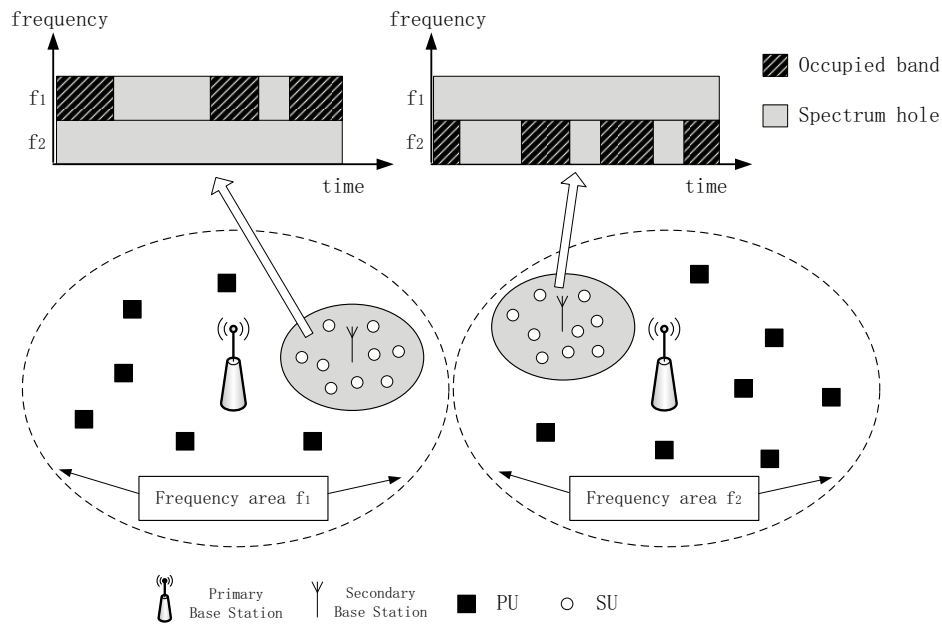
Un scénario Espace-Temps-Fréuence du système SSCR

SU commence la transmission, il devrait être en mesure de détecter ou prévoir l'apparition d'un PU afin qu'il quitte la bande de ce PU. Fondamentalement, la détection et l'adaptation des SUs doit être faite indépendamment des PUs afin de permettre au système primaire de maintenir son infrastructure de communication existante. Ainsi, afin de réaliser le concept de SSCR, l'analyse spectrale à haute rèolution, mise en forme du spectre agile, et la prédiction du spectre fiable sont nécessaire.

FBMC

La discussion dans cette thèse se consacre principalement à l'utilisation des modulations FBMC-OQAM basés sur la thérie du banc de filtres. Le principe de FBMC-OQAM consiste à diviser le débit de transmission en M flux indépendants en utilisant M sous-porteuses. Une condition d'orthogonalité est introduite entre les sous-porteuses pour garantir que les symboles transmis arrivent au récepteur sans ISI et ICI. Ceci est réalisé par une transmission des composantes en phase et en quadrature des symboles avec un décalage d'une demi-péiode de symbole. Le système FBMC-OQAM se compose d'un banc de filtres de synthèse (SFB) à l'émetteur et d'un banc de filtres d'analyse (AFB) au niveau du récepteur.

La technique FBMC-OQAM a une complexité de mise en œuvre un peu plus élevé que l'OFDM. Toutefois, dans le projet PHYDYAS il a été montré que la complexité de mise en œuvre de FBMC-OQAM est encore acceptable. la technique FBMC-OQAM a les caractéistiques principales suivantes:

1. Aucun préfixe cyclique n'est nécessaire et de petites bandes de garde sont suffisantes pour supprimer les interféences entre canaux;

2. En raison de ses lobes latéaux faibles, la technique FBMC-OQAM est beaucoup moins sensible aux décalages temporels que l'OFDM. En outre, FBMC-OQAM est moins sensible au décalage de fréence rèiduelle et est plus robuste à l'effet Doppler;

3. Le même dispositif peut être utilisé simultanément pour la détection des fréuences et la réception. La capacité du spectre d'analyse des bancs de filtres à haute rèolution peut être exploité pour les systèmes de CR. Les bancs de filtre permettent d'augmenter une plus grande dynamique spectrale que la FFT classique. Ainsi, la probabilité de collisions indèirables entre les SUs et PUs est considéablement réduite;

4. FBMC-OQAM divise le canal de transmission du système en un ensemble de sous-canaux et chaque sous-canal chevauche seulement avec ses voisins les plus proches. Les sous-canaux peuvent être regroupè en blocs indépendants, ce qui est crucial pour la compatibilité et les techniques d'accès dynamique;

Le blocs de filtrage polyphasé remplace les blocs pour l'insertion / suppression préfixe utilisés dans les terminaux de OFDM. On voit que la FFT est commune aux modulations OFDM et FBMC-OQAM, ce qui est un aspect important pour les problèmes de compatibilité. Par souci de simplicité, le terme FBMC sera utilisé au lieu de FBMC-OQAM dans le reste de cette thèse.

Chapitre 3 - Détection du spectre

Détecteur de signature cyclostationnaire

Dans le contexte de la CR, la détection du spectre se compose de la détection d'occupation et l'identification. La détection d'occupation consiste à détecter l'occupation du spectre dans une région et d'identifier les bandes libres et les bandes occupés. Le détecteur d'énergie peut être appliqué à cet effet. L'identification permet de de faire la distinction entre l'utilisation sous licence par les utilisateurs principaux, l'utilisation opportuniste par les utilisateurs de CR, et le bruit. Cette distinction est cruciale dans un scénario CR avec une forte densité d'utilisateurs. Un détecteur cyclostationnaire peut aussi être appliqué pour traiter le bruit, les interféences, et d'autres utilisateurs secondaires différemment. Dans la suite, le détecteur cyclostationnaire basé sur la signature cyclostationnaire pour les signaux FBMC est étudié.

La théorie de la corrélation spectrale des signaux cyclostationnaires a été étudié pendant des décennies. Les formules explicites de la fonction de corrélation spectrale (SCF) pour différents types

de signaux de modulations analogiques et numéiques ont déjà été déivè. Dans cette section, nous étudions et exploitons les caractéistiques cyclostationnaires pour le signal FBMC. La caractéisation de la corrélation spectrale du signal FBMC peut être décrite par un système péiodique linéaire variant dans le temps (LPTV). Grâce à cette écriture, nous avons obtenu des formules explicites thériques de la SCF pour le signal FBMC. Après une analyse thérique, des signatures cyclostationnaires (CSs) ont été artificiellement incorporés au signal FBMC et un détecteur de signature de faible complexité est prèenté pour la détection du signal FBMC. Les rèultats de l'analyse thérique et les simulations démontrent l'efficacité et la robustesse de ce détecteur de CS par rapport au détecteur d'énergie traditionnel.

Nous avons malheureusement constaté que le signal FBMC a une très faible propriété inhéente cyclostationnaire en raison des faibles lobes latéaux de la fonction prototype. La pauvre cyclostationnarité limite l'application pratique dans le contexte de la CR. Même pour les signaux OFDM qui contiennent des caractéistiques cyclostationnaires en raison de l'insertion de CP, la puissance est faible par rapport à la puissance du signal et une détection fiable de ces cyclostationnaritè requiert une architecture complexe et une longue observation.

Dans cette partie nous étudions le problème de la détection du signal FBMC en prèence d'un canal additif à bruit blanc gaussien (AWGN) en utilisant les CSs. Les CSs sont effectivement appliqués pour surmonter les limitations associés à l'absence des caractéistiques cyclostationnaires pour la détection du signal. La détection et l'analyse des CS peuvent aussi être obtenues en utilisant des architectures de récepteur à faible complexité et de courte duré d'observation.

Comme illustré dans la figure ci-dessous, les CSs sont facilement créè par mapper un ensemble des sous-porteuses sur une deuxième séie comme suit

$$\gamma_{n,l} = \gamma_{n+p,l} \qquad n \in N$$

oú $\gamma_{n,l}$ est le l^{ieme} message distribué indépendant et identiquement sur la n^{ieme} sous-porteuse, N est l'ensemble des sous-porteuses à mapper et p est le nombre de sous-porteuses entre sous-porteuses mappés. Ainsi, un motif de corrélation est créé et une CS est incorporé dans le signal par la transmission redondante des symboles.

D'après la thérie des LPTV, nous pouvons calculer la formule du SCF du signal FBMC avec les
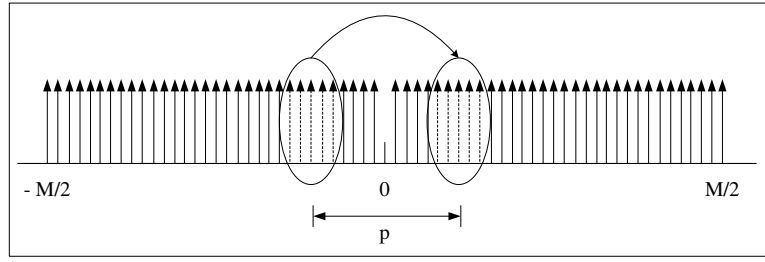
Généation de CSs par répétition des symboles

CSs

$$S^{\alpha}_{fbmc \cdot cs}(f) =$$

$$
\begin{cases}
\frac{2\sigma^2}{T_0} \sum_{n=-M/2}^{M/2-1} P(f + \frac{\alpha}{2} - \frac{n}{T_0})P^*(f - \frac{\alpha}{2} - \frac{n}{T_0}), & \alpha = \frac{2 \cdot integer}{T_0}, 2 \cdot integer \neq -p; \\
\\
\frac{2\sigma^2}{T_0} \sum_{n \in N} P(f + \frac{\alpha}{2} - \frac{n}{T_0})P^*(f - \frac{\alpha}{2} - \frac{n+p}{T_0}), & \alpha = -\frac{p}{T_0}; \\
\\
0, & \alpha \neq \frac{2 \cdot integer}{T_0}, \alpha \neq -\frac{p}{T_0};
\end{cases}
$$

où $P(f)$ est la transformé de Fourier du filtre prototype, N est l'ensemble des sous-porteuses à associer et $p \in \mathcal{P}(\mathcal{P} = \pm 2i, i = 1, 2, 3, 4, \cdots)$.

L'amplitude du SCF du signal FBMC avec les CSs est prèenté dans la figure ci-dessous, où deux CSs sont incorporés correspondant à deux valeurs difféentes de p (en choisissant $p = 2$ et $p = 4$). Nous pouvons voir que pour le signal FBMC les caractéistiques cyclostationnaires fortes (CSs) apparaissent à la fréence cyclique $\alpha = -2/T_0$ et $\alpha = -4/T_0$ (T_0 est un symbole de FBMC).

Comme le bruit ne prènte pas de cyclostationnarité, la détection de la prènce du signal FBMC est éuivalente à la détection de la prènce de cyclostationnarité dans le signal composite reçu $x(t) = s(t) + n(t)$ sur la fréence prédéterminé cyclique, où $n(t)$ est la contribution du bruit.

Un détecteur de CS peut être utilisé pour la détection du signal FBMC. Les caractéistiques cyclostationnaires généés par l'association des sous-porteuses peuvent être détectés avec succès en utilisant une rèolution spectrale Δf (espacement sous-porteuse). Ainsi, le détecteur de CS de faible complexité peut être conçu en glissant une fenêtre W avec la largeur $N_s \cdot \Delta f$ (N_s est le nombre de sous-porteuses dans l'ensemble mappé) sur le SCF estimé à la fréence cyclique α_0

$$T_{x^{(*)}} = \max_m \sum_n \widehat{S}^{\alpha_0}_{x^{(*)}}(n)W(m-n)$$

où $\widehat{S}^{\alpha_0}_{x^{(*)}}$ est estimé en utilisant un cross-péiodogramme cyclique avec filtrage temporel.

Les courbes ROC sont donnés dans les deux figures ci-dessous pour une moyenne de 500 simulations de Monte Carlo et un canal AWGN. La première figure donne les rèultats expéimentaux à
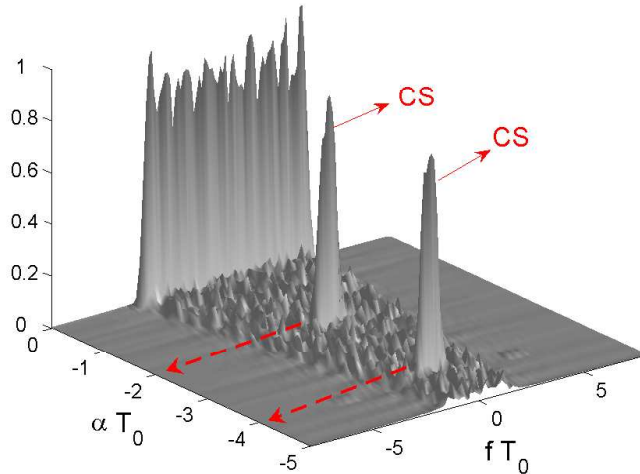
SCF pour signal FBMC avec deux CSs aux fréuences cycliques $\alpha = -2/T_0$ **et** $\alpha = -4/T_0$

des SNR difféents ($0dB$, $-3dB$, $-6dB$, $-9dB$ and $-12dB$) avec 6 sous-porteuses mappés et un temps d'observation $T = 1ms$ (10 symboles FBMC). A titre de comparaison, le détecteur d'énergie avec une incertitude de bruit $U = 0.12dB$ est utilisé. On peut voir que les performances de détection souhaités peuvent être atteintes pour le détecteur de CS avec un niveau de SNR faible, et un taux de détection de 100% peut être atteint lorsque le niveau de SNR est supéieur à $0dB$. Nous pouvons également observer que le détecteur d'énergie surpasse de manière significative le détecteur de CS lorsque la puissance du bruit est bien estimé.

Les effets du temps d'observation et de l'ensemble mappé sont prèentè dans la deuxième figure pour $SNR = -12dB$, où les courbes ROC montrent que la performance du détecteur de CS s'améliore lorsque le temps d'observation et le nombre de sous-porteuses mappés augmentent. En outre, les performances du détecteur d'énergie pour difféentes valeurs d'incertitude de bruit sont prèentés et on véifie que le détecteur d'énergie est très sensible à l'incertitude de bruit lorque le SNR est faible. En raison de l'incertitude de bruit, les performances du détecteur d'énergie ne s'améliore pas, même si nous augmentons le temps d'observation. Ce comportement est prédit par la limite que l'on appelle le mur SNR. A savoir, le détecteur d'énergie ne peuvent pas distinguer le faible signal reçu du bruit lorsque le SNR est supéieur à un certain niveau.

Détection multi-bande à base de banc de filtre polyphasé

La détection du spectre est une fonctionnalité essentielle pour les systèmes de CR afin de garantir que les utilisateurs puissent partager les ressources du spectre avec les utilisateurs autorisè. Récemment,
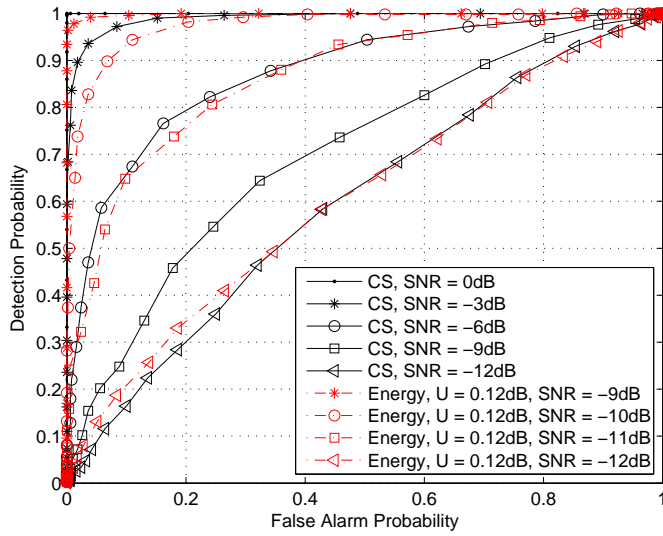
Courbes de ROC pour canal AWGN avec $N = 6$ sous-porteuses mappés et un temps d'observation $T = 1ms$
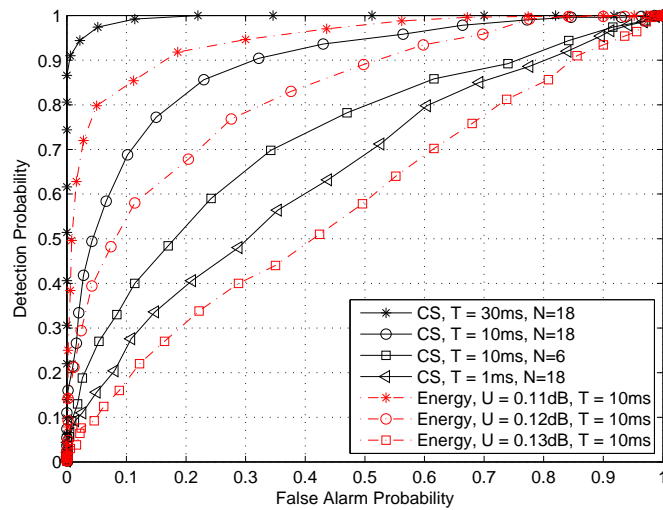
Courbes de ROC pour canal AWGN avec $SNR = -12dB$

la détection multi-bande de l'activité des utilisateurs sous licence a fait l'objet de plusieurs travaux de recherches.

Dans cette thèse, nous étudions une architecture de détection multi-bandes basé sur les bancs de filtres polyphasè (PFB). Nous avons obtenus thériquement les expressions de la probabilité de détection et de fausse alarme des détecteurs basè sur la FFT et le PFB, en déterminant au préalable un seuil de détection thérique. Les rèultats expéimentaux sont prèentè pour véifier notre analyse thérique et démontrer que la détection basé sur le PFB a une meilleure performance que la détection basé sur la FFT.

Le concept de base de la détection multi-bande est d'estimer la densité spectrale de puissance (PSD) puis d'appliquer la détection de puissance dans le domaine des fréuences à partir des PSD estimés. Le PFB est proposé comme un outil efficace pour l'analyse spectrale, sans coût supplémentaire, puisque chaque utilisateur secondaire pourrait être éuipé de PFB. Cela signifie que la structure PFB utilisé pour les communications offrira une nouvelle opportunité pour la détection, sans coûts supplémentaires. Dans la littéature, les performances de la détection multi-bande sont en généal comparés avec un estimateur basé sur le péiodogramme (PSE), et les rèultats de la simulation montrent un avantage significatif du PFB par rapport aux PSE. Néanmoins, la plupart de ces travaux utilise le Prolate Sequence Window (PSW) comme filtre prototype du PFB. Cependant, ce filtre ne peut pas être réutilisé pour la communication.

Dans cette section, nous avons considéé pour la détection multi-bandes un PFB basé sur un filtre prototype qui peut être utilisé pour la transmission Les expressions thériques des probabilitè de détection et de fausse alarme des détecteurs à base de PFB et PSE sont obtenues, respectivement. Ainsi, les niveaux de seuil appropriè pour les difféents détecteurs peuvent être choisis pour assurer une comparaison éuitable. Plus précisément, le PFB utilisant le filtre du projet PHYDYAS et le filtre PAW sont étudiè et comparè avec le PSE, et les rèultats expéimentaux véifient l'analyse thérique et révèlent que le PFB est un meilleur analyseur de spectre que le PSE.

Occupation du canal primaire
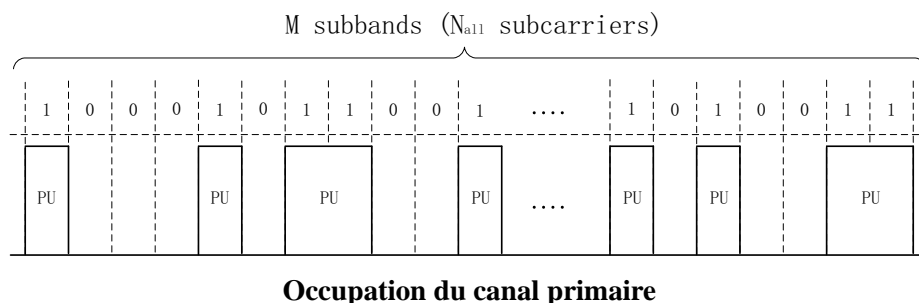
Dans le cadre de la CR, nous considéons un système primaire à base de FBMC sur une large bande avec N_{all} sous-porteuses. Comme indiqué sur la figure ci-dessus, la bande de fréuences utilisé

par les PUs est divisé en M sous-bandes avec N_s sous-porteuses par sous-bande. Dans un intervalle ou dans une région géographique, certaines des M sous-bandes peuvent ne pas être occupés par les PUs et sont donc disponibles pour les SUs. La figure prènte le canal de distribution primaire dans un intervalle de temps pour lequel les sous-bandes occupés par les PUs sont dèignés par des "1", alors que les sous-bandes disponibles pour SUs sont dèignés par des "0".

Dans la suite, nous évaluons numéiquement la détection multi-bande d'un point de vue pratique. En supposant un système sous license avec une bande passante $B = 30MHz$ contenant $N_{all} = 8192$ sous-porteuses où la bande entière est également séparé en $M = 128$ sous-bandes avec $N_s = 64$ sous-porteuses par sous-bande. Il est également supposé que le canal est additif à bruit blanc gaussien de moyenne nulle et la densité de bruit de puissance $-174dBm/Hz$. Le taux de charge du système principal est de 50%. La longueur des filtres prototypes PFB est égale à $\beta = 4M = 512$. La fréuence centrale est $f_c = 3.6GHz$. Le signal est supposé reçu après démodulation sans décalage de fréuence. $K = 250$ groupes de signaux échantillonnè avec 128 échantillons par groupe sont utilisè pour simuler la détection multi-bandes.

Compte tenu d'une probabilité fixe de fausse alarme $P_f = 5\%$, un seuil thérique peut être calculé, puis ce seuil est utilisé pour calculer la probabilité de détection. De même, la probabilité de fausse alarme peut être calculé pour une probabilité de détection donné $P_d = 95\%$. Les courbes de performance de la probabilité de détection et de la probabilité de fausse alarme en fonction du niveau SNR sont tracés dans les figures ci-dessous, respectivement. Nous pouvons observer que la performance du PFB (PHYDYAS et PSW) prènte une amélioration significative (gain de performance maximale de 25%) par rapport au PSE en raison de la faible fuite spectrale de PFB. Il est intéessant de constater que les performances du filtre PHYDYAS sont légèrement meilleures que celles du PSW ce qui peut s'expliquer par le fait que la variance de fréuence variable de PSW est le double de celle de PHYDYAS.

Chapitre 4 - Comparaison de la capacité de l'OFDM / FBMC pour les systèmes de la CR

Les communications multiporteuses ont été proposés comme candidat pour la radio cognitive en raison de leurs souplesses pour exploiter les bandes spectrales inutilisés. Dans ce chapitre, nous comparons l'efficacité spectrale d'un rèeau de CR en utilisant deux types de communications multi-porteuses: l' OFDM avec un préfixe cyclique et le FBMC. En supposant que la détection du spectre est parfaitement mis en œuvre, l'efficacité spectrale sur les bandes libres détectés dépend de la modulation multiporteuse utilisé et de la stratégie d'allocation de ressources que le système secondaire adopte. Afin de réduire la complexité, nous proposons un algorithme d'allocation des ressources
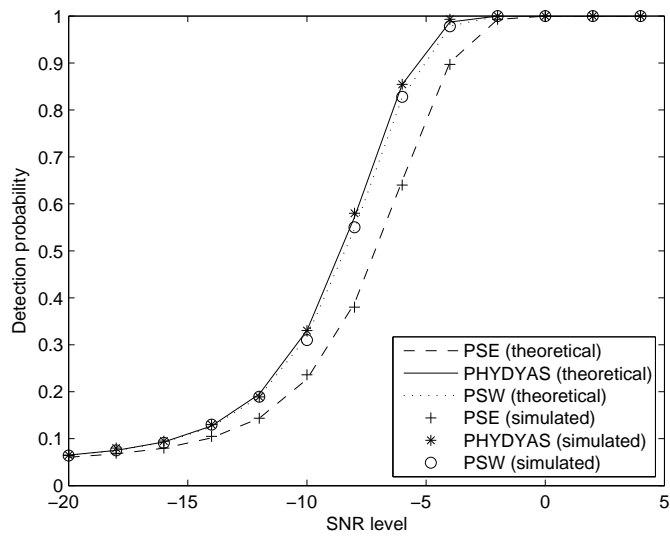
Probabilité de détection par rapport au niveau SNR ($P_f = 5\%$)
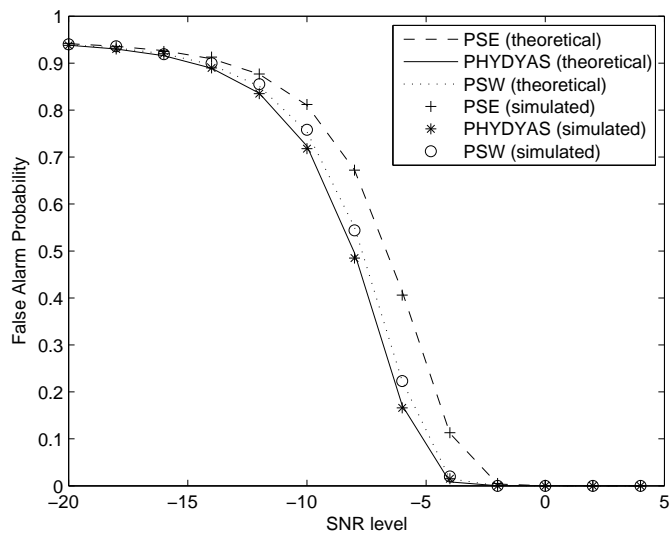
Probabilité de fausse alarme par rapport au niveau SNR ($P_d = 95\%$)

dans lesquel la répartition des sous-porteuses et l'allocation de puissance sont réalisés de manière séuentielle.

En pratique, les problèmes d'interféence entre les PUs et les SUs dans un rèeau CR rélle ne dépend pas des lobes secondaires de la PSD mais de la synchronisation imparfaite. Dans cette thèse, nous étudions et comparons tout d'abord les interféences inter-cellulaire causés par les décalages temporels pour les systèmes basè sur l'OFDM et le FBMC. Les tables d'interféences moyennes des modulations OFDM et FBMC sont donnés. Ces tables offrent un modèle pratique de l'interféence inter-cellulaire, et seront utilisés pour analyser les performance des algorithmes d'allocation des ressources dans ce chapitre au lieu de la densité spectrale de puissance. Dans ce travail, nous nous concentrons sur la comparaison de l'OFDM et FBMC en termes d'efficacité spectrale du système secondaire, qui dépend de sa stratégie d'allocation des ressources adopté par le système secondaire. Nous proposons un schéma d'allocation de ressources dans un scénario de liaison montante et en prenant en compte l'atténuation et en considéant des canaux de Rayleigh. L'objectif de maximiser la somme des taux est formulé avec une contrainte de puissance et une contrainte sur l'interféence inter-cellulaire basé sur les tables des interféences.

Sans pertes de généalité, notre procédure d'allocation des ressources est divisé en deux étapes. Tout d'abord, les SUs sont affectè aux trous du spectre détectè en utilisant une métrique de capacité moyenne (AC-métrique) et l'algorithme hongrois (HA). Nous montrons que l'algorithme AC-métrique permet d'atteindre de meilleures performances que l'algorithme basé sur des SNR-métriques. Lorsque les SUs sont affectè à des trous du spectre, la deuxième partie de la procédure (allocation de puissance) est rèolue par la méthode de projection du gradient (GPM) au lieu d'utiliser des lagrangiens. Le GPM est un outil mathématique efficace pour les problèmes d'optimisations convexes ayant des contraintes linéaires et une allocation de puissance optimale peut être obtenue avec une complexité de calcul limité. Les rèultats numéiques montrent que l'efficacité spectrale des systèmes CR basè sur la FBMC est proche de celle d'un système parfaitement synchronisè et bien supéieure à efficacité spectrale des systèmes CR basè sur l'OFDM.

Comme montré dans la figure ci-dessous, un scénario de liaison montante des rèeaux de CR composé d'un système primaire avec un PU et un système secondaire avec un SU est reprèenté graphiquement, où D est la distance entre la station de base primaire (PBS) et la station de base secondaire (SBS), et R_p et R_S sont les rayons de système primaire et secondaire, respectivement. Une bande de fréuence composé de $N_c = 48$ clusters et $L = 18$ sous-porteuses dans chaque cluster est autorisé par le système primaire.

Lorsque nous transmettons une rafale de symboles complexes indépendants, l'interféence relative à une sous-porteuse est égale à la somme des interféences pour toutes les intervalles de temps. Les interféences inter-cellulaires supéieures à "10^{-3}" pour OFDM et FBMC sont donnés dans la figure
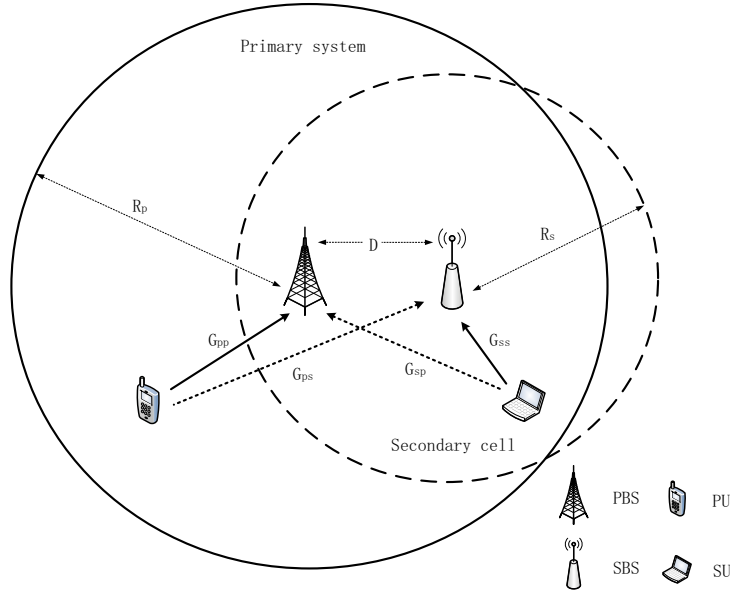
Radio cognitive avec un système primaire et une cellule secondaire

ci-dessous. On peut observer que le nombre de sous-porteuses qui induisent des interféences nuisibles à l'utilisateur principal de l'OFDM et FBMC est égal à "8" et "1", respectivement.

La cellule secondaire souhaite maximiser son débit total en allouant de la puissance dans les trous du spectre pour ses propres utilisateurs, ce problème peut être formulé comme suit :

$$\max_{\mathbf{p}} : C(\mathbf{p}) = \sum_{m=1}^{M} \sum_{k=1}^{K} \sum_{f=1}^{F_k} \theta_m^{kf} log_2 \left[1 + \frac{p_m^{kf} G_{ss}^{mkf}}{\sigma_n^2 + I_f^k} \right]$$

$$s.t.$$

$$\begin{cases} \sum_{k=1}^{K} \sum_{f=1}^{F_k} \theta_m^{kf} p_m^{kf} \leq P_{th}, \quad \forall m \\ 0 \leq p_m^{kf} \leq P_{sub} \\ \sum_{m=1}^{M} \sum_{n=1}^{N} \theta_m^{k_{l(r)}n} p_m^{k_{l(r)}n} G_{sp}^{mk_{l(r)}} V_n \leq I_{th}, \quad \forall k \end{cases}$$

où M est le nombre d'utilisateurs secondaires, K est le nombre de trous du spectre, et F_k est le nombre de sous-porteuses dans le k^{ieme} trou du spectre. $\theta_m^{kf} \in \{0, 1\}$ est la sous-porteuse indicatrice d'affectation, soit $\theta_m^{kf} = 1$ si la f^{ieme} sous-porteuse dans le k^{ieme} trou spectre est alloué à SU m, p_m^{kf} est la puissance de SU m sur la f^{th} sous-porteuse dans le k^{ieme} trou du spectre, G_{ss}^{mkf} est le gain du canal de propagation du SU m vers le PU sur la f^{th} sous-porteuse dans le k^{ieme} trou du spectre, σ_n^2 est la puissance de bruit, et I_f^k est l'interféence cellulaire du PU vers le SU sur la f^{ieme} sous-porteuse dans le k^{ieme} trou du spectre. P_{th} et P_{sub} sont respectivement la puissance limite par utilisateur et la puissance limite par sous-porteuse. N est la longueur du vecteur d'interféences V (ses valeurs sont donnè dans la figure d'interféence), $p_m^{k_{l(r)}n}$ est la puissance du SU m sur la gauche (la droite) de la
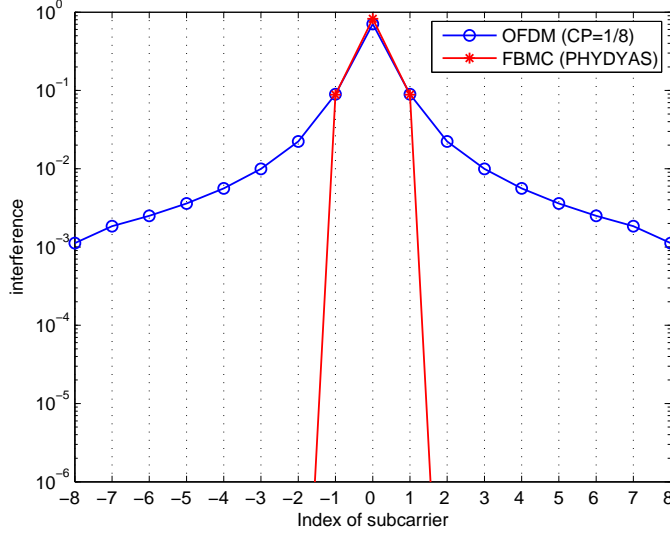
Les puissances d'interféences moyennes de l'OFDM et FBMC

n^{ieme} sous-porteuse dans le k^{ieme} trou du spectre, $G_{sp}^{mk_{l(r)}}$ est le gain du canal de propagation de SU m à PBS sur la gauche (la droite) de la première sous-porteuse primaire à côté du k^{ieme} trou du spectre, et I_{th} dèigne le seuil d'interféence fixé par le PU sur la première sous-porteuse primaire à côté du SU.

En pratique, le gain du canal entre les SU et PU G_{sp} ne peut pas être estimé de façon précise et la quantité d'interféence apporté du SU au PU est calculé sur la base de la connaissance du canal estimé. Nous supposons qu'une estimation approximative du gain du canal de SU vers PU peut être obtenue par le SU pendant la phase de détection. L'erreur d'estimation est déterminé par la probabilité de coupure prescrit des systèmes primaires. Basé sur un gain de canal estimé, les rèultats de simulation obtenus montrent que le gain de performance augmente entre les systèmes FBMC et OFDM par rapport au cas de connaissance parfaite des gains de canaux.

Les rèultats expéimentaux du cas parfaitement synchronisé (PS) sont donnè à titre de comparaison. En outre, la performance du cas avec parfaite connaissance des gains de canal est également étudié. Les capacitè moyennes pour des interféences différentes (coefficient de perte de capacité $\lambda = 0.02 \sim 0.2$) avec une probabilité de coupure $P_{out} = 0.06$, une puissance maximale d'utilisateur $P_{th} = 36mWatt$, et une distance $D = 0.2km$ sont donnés dans la première figure ci-dessous. Comme prévu, la performance du FBMC surpasse toujours celle de l'OFDM, qui montre une diminution rapide de la capacité lorsque une moindre perte de capacité est requise par le PU, alors FBMC est légèrement affecté par les différents niveaux d'interféence. Dans le même temps, nous pouvons voir un grand écart de capacité entre le cas avec le canal de gain idéal et le cas avec un gain de canal estimé

36 PUs, 6 SUs, 12 free clusters, P_{th}= 36 mWatt, D= 0.2 km, P_{out}=0.06
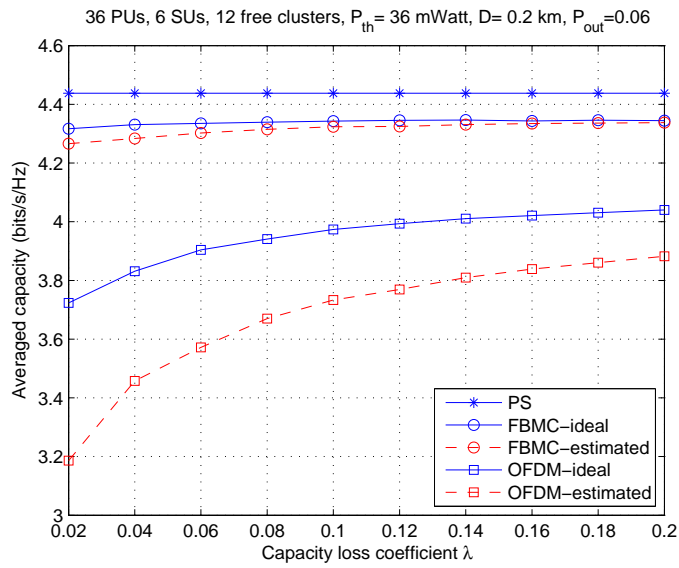
Les capacitè moyennes par rapport au niveau d'interféence

36 PUs, 6 SUs, 12 free clusters, λ= 0.04, P_{th}= 36 mWatt, D= 0.2 km
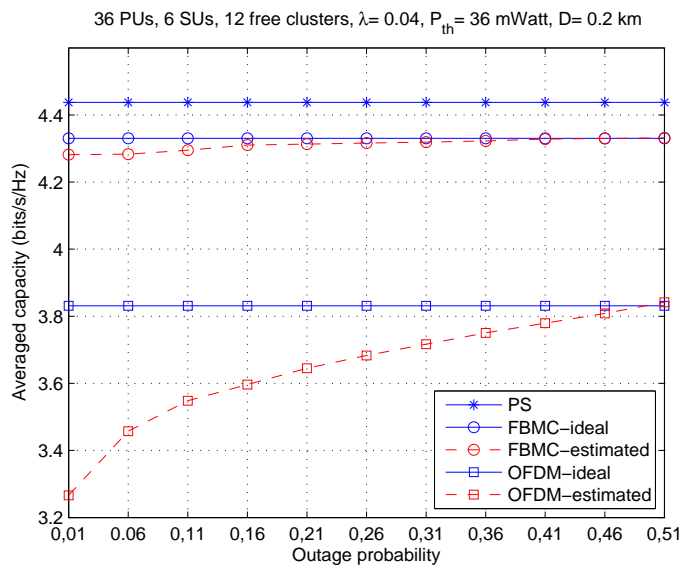
Les capacitè moyennes par rapport à la probabilité de coupure

pour le système CR basé sur l'OFDM, alors qu'il existe une difféence de capacité légère en appliquant le système CR basé sur FBMC. Cela s'explique par le fait que le nombre de sous-porteuses de OFDM et FBMC qui induisent des interféences nuisibles aux PU est de "8" et "1", respectivement. Quand une faible probabilité de coupure est nécessaire, plusieurs sous-porteuses adjacentes à PU doivent être dèactivés ou sous-utilisés pour l'OFDM ce qui dégrade en conséuence la capacité. Finalement, on peut noter que la performance du FBMC est proche de celle du cas PS. La deuxième figure montre la moyenne des capacitè par rapport aux difféents probabilitè de coupure. La capacité moyenne (avec un gain de canal estimé) à base de OFDM s'effondre quand une faible probabilité de coupure est dèiré alors que le système CR basé sur le FBMC est beaucoup moins vulnéable aux probabilitè de coupure.

Chapitre 5 - Allocation des ressources non-coopéatifs des Systèmes de CR basé sur FBMC

Dans le chapitre précédent, la question de l'allocation des ressources dans le contexte d'une seule cellule de CR a été étudié. Afin d'étudier plus avant cette question, ce chapitre traite de problème d'allocation des ressources en prèsence de multiples cellules de CR à base de FBMC avec plusieurs SUs par cellule et où les utilisateurs de CR dans des cellules difféentes partagent les mêmes ressources du spectre afin d'accroître l'efficacité spectrale. Par conséquent, les utilisateurs utilisant la même bande de fréuences vont s'interféer entre eux c'est à dire que l'interféence inter-cellule existera entre les cellules difféentes. Dans ce travail nous proposons un algorithme d'allocation de ressource non-coopéatif qui cherche à maximiser la somme des débits d'information de chaque cellule avec une contrainte sur la puissance de chaque utilisateur de manière distribué. La thérie des jeux (GT) est un outil mathématique utile pour analyser les processus de décision interactive et peut être utilisé pour étudier les problèmes d'allocation de ressources distribués. Puisque la formulation de la maximisation des débits des utilisateurs multiples dans chaque cellule est un problème d'optimisation non-concave, la technique d'accè multiple(MAC) est proposé. Avec le MAC, le problème devient un problème d'optimisation concave. Lorsqu'il n'y a qu'un utilisateur dans chaque cellule de CR, l'algorithme de remplissage itéatif (IWFA) peut être une bonne solution pour le jeu multi-cellule distribué. Toutefois, l'algorithme IWFA n'est plus adapté lorsqu'il y a plusieurs utilisateurs dans une cellule, car la question de l'affectation des sous-porteuses pour multi-utilisateurs de chaque cellule doit être aussi traité. Par conséuent, l'algorithme proposé dans chapitre est une généalisation de l'algorithme IWFA pour l'allocation des ressources distribués dans plusieurs cellules avec de multiples utilisateurs dans chaque cellule.

Ce chapitre se concentre sur l'algorithme d'allocation des ressources non-coopéatif entre multiples cellules secondaires indépendantes. Dans ce travail, nous étudions cette question en utilisant

les outils de la thérie des jeux. Plus précisément, nous proposons un algorithme d'allocation de ressources non-coopéatif pour les liaisons en voie montante en utilisant la thérie des jeux et la technique MAC entre plusieurs cellules à base de FBMC avec multiples utilisateurs par cellule. La station de base secondaire dans chaque cellule CR, en essayant d'optimiser le débit de ses propres utilisateurs, est un joueur. La maximisation du débit total d'information dans une cellule est considée, sous des contraintes de puissance de chaque utilisateur CR. Grâce à la propriété de la technique MAC, le problème de maximisation de débit peut être formulé comme un problème d'optimisation concave. Comme il est compliqué d'obtenir une solution analytique pour la répartition de puissance de multi-utilisateurs, l'algorithme de Lagrange (LA) et la méthode de projection du gradient (GPM) sont utilisè pour rèoudre ce problème d'optimisation concave. L'algorithme proposé basé sur la GT et la technique MAC permet d'effectuer itéativement l'affectation des sous-canal et allocation de puissance pour les multi-utilisateur. Il peut être considée comme une extension de l'algorithme IWFA qui est classiquement appliqué pour l'allocation de puissance itéative dans le cas mono-utilisateur.

Les rèultats de simulations montrent que l'algorithme proposé basé sur la thérie des jeux permet de partager un ou plusieurs sous-canaux entre de multiples utilisateurs permet d'obtenir un débit d'information plus élevé et une meilleure convergence des rèultats (convergence vers l'éuilibre de Nash (NE) avec un petit nombre d'itéations) que l'accè classique par multiplexage fréuentiel (FDMA). Comme la mise en œuvre de l'accè MAC nécessite une complexité matéielle supplémentaire, nous avons proposé un algorithme MAC-FDMA où nous transformons le rèultat de l'allocation des ressources obtenu en MAC en une solution FDMA. Par rapport à la solution traditionnelle FDMA, cette transformation MAC en FDMA permet d'obtenir de meilleures performances en particulier lorsque la dimension du système est élevé.
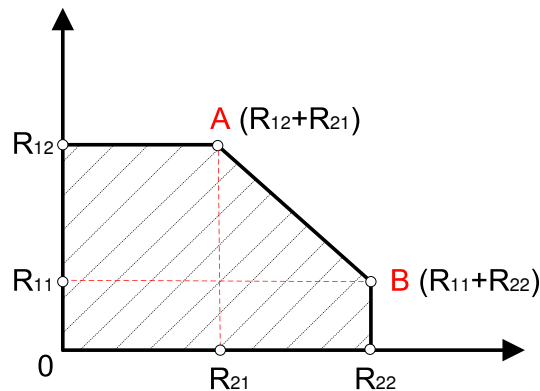
La région de capacité de MAC pour deux utilisateurs

Afin de transformer le problème d'optimisation traditionnel en un problème d'optimisation concave, nous utilisons l'accè MAC, ce qui signifie que de multiples utilisateurs de CR dans la même

cellule peuvent occuper une ou plusieurs bandes de fréuences. Lorsqu'il est possible d'utiliser la technique MAC pour la transmission des donnés dans un système, la région de capacité est supéieure à celle obtenue par les accès TDMA ou FDMA. La limite de région de capacité de l'accè MAC pour $M = 2$ utilisateurs avec des puissances (p_1, p_2) est donné par

$$R_1 + R_2 \leq log_2[1 + \frac{p_1 G_1 + p_2 G_2}{N_0}]$$

où G est le gain de canal, et N_0 est la puissance du bruit ambiant.

Dans le contexte de la thérie des jeux, les stations de base secondaires sont les joueurs, qui réagissent et luttent entre-elles pour les ressources communes.

En rèumé, soit $\mathcal{G} = \{\mathcal{N}, \{\mathbf{p}_n\}_{n \in \mathcal{N}}, \{u_n\}_{n \in \mathcal{N}}\}$ la structure des jeux non-coopéatifs, où $\mathcal{N} = \{1, 2, \cdots, N\}$ est l'ensemble des indices des joueurs (SBS), $\mathbf{p}_n = [p_1^{n1}, p_1^{n2}, \ldots, p_1^{nM}, p_2^{n1}, p_2^{n2}, \ldots, p_F^{nM}] \in \mathbb{R}^{MF}$ est l'espace de stratégie de puissance du n^{ieme} joueur (M est le nombre d'utilisateur dans une cellule et F est le nombre de bande libre), et u_n est la fonction d'utilité du n^{ieme} joueur.
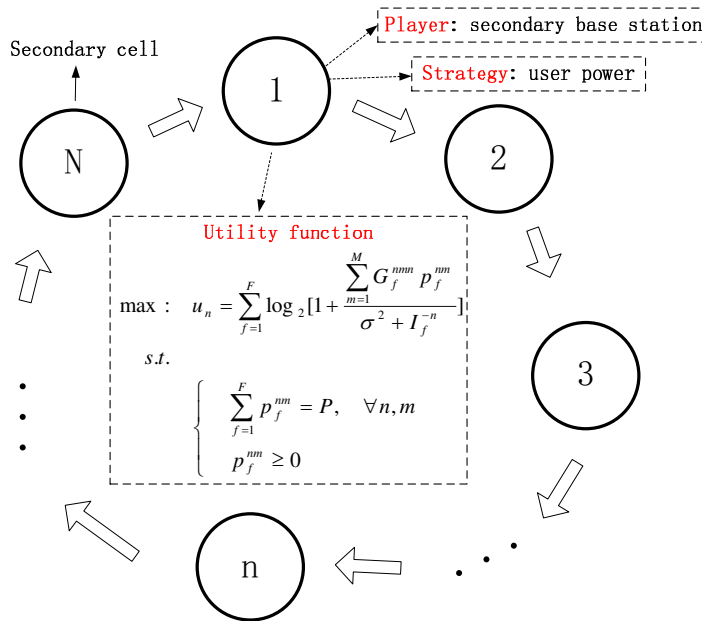
Approche de la thérie des jeux: joueur, stratégie et fonction d'utilité

Le jeu non-coopéatif est mis en œuvre de manière séuentielle. Cet algorithme séuentiel est illustré dans la figure ci-dessous. Le rèultat du jeu proposé impliquant N joueurs devrait permettre d'atteindre un éuilibre de Nash (NE).

Afin d'évaluer la thérie des jeux proposé basé sur l'accè MAC (MAC-GT), un jeu basé sur l'accè FDMA (FDMA-GT) est également mis en œuvre afin que chaque station de base secondaire exhaustive recherche la stratégie optimale qui maximise le débit d'information dans un ordre séuentiel. Pour un grand nombre d'utilisateurs par cellule CR, un problème de calcul apparaît pour l'algorithme

FDMA-GT, car au cours de chaque processus d'itéation, nous devons essayer tous les candidats possibles afin d'obtenir la solution FDMA optimale. Cette recherche exhaustive rend l'algorithme FDMA-GT impossible à implémenter et d'autres heuristiques doivent être recherchés pour rèoudre ce problème en particulier pour les grandes dimensions. Dans ce chapitre, grâce à l'algorithme de MAC-GT, nous proposons un algorithme de transformation MAC-FDMA. Cet algorithme est décrit dans la table ci-dessous.

Étant donné une cellule avec M utilisateurs et F bandes libres ($F = M$),
nous transformons la matrice $M \times F$ de MAC **P** en une matrice FDMA **P'**
selon les étapes suivantes:
étape 1: Initialisation: **P'**= **zeros** (M, F), et de définir deux ensembles
$$\mathscr{M} = \{1, 2, \ldots, M\}, \mathscr{F} = \{1, 2, \ldots, F\};$$
étape 2:   **for**   i = 1:M
      Calculer
$$[m', f'] = arg\,max_{m \in \mathscr{M}, f \in \mathscr{F}}\,\mathbf{P}(m, f)$$
      répartir ensuite la sous-porteuse f' à l'utilisateur m', et éliminer
      l'utilisateur m' et la sous-porteuse f' des ensembles $\mathscr{M}$ and $\mathscr{F}$, à savoir
      P'(m', f')= P;
      $\mathscr{M} = \mathscr{M} \setminus \{m'\}, \mathscr{F} = \mathscr{F} \setminus \{f'\};$
   end

Dans la première étude, nous considéons que le nombre de bandes est toujours égal au nombre d'utilisateurs par cellule ($M = F$). Nous effectuons plusieurs simulations afin de corroborer les rèultats thériques. Tout d'abord, les rèultats de simulation avec 5 utilisateurs par cellule de CR sont prèentè. La somme des débits du système en fonction de la distance D entre les stations de base est comparé pour les algorithmes FDMA-GT et MAC-GT. 500 topologies indépendantes et réalisations de canaux sont simulés. Nous pouvons voir que l'algorithme MAC-GT a toujours de meilleures performances que l' algorithme FDMA-GT. En outre, il est intéessant de constater que l'algorithme MAC-FDMA surpasse la recherche exhaustive FDMA-GT.

Les taux de convergence associè pour le FDMA-GT et le MAC-GT sont également prèentè dans les figures ci-dessous. Nous observons que plusieurs itéations sont nécessaires lorsque la distance D devient faible. l'algorithme FDMA-GT converge un peu plus vite que le MAC-GT, mais il existe certains cas de non convergence), dont le taux augmente avec le nombre d'utilisateurs. Inversement, l'algorithme MAC-GT permet de garantir que le jeu non-coopéatif converge vers un éuilibre de Nash ((NE Nash equilibrium) avec peu d'itéations.
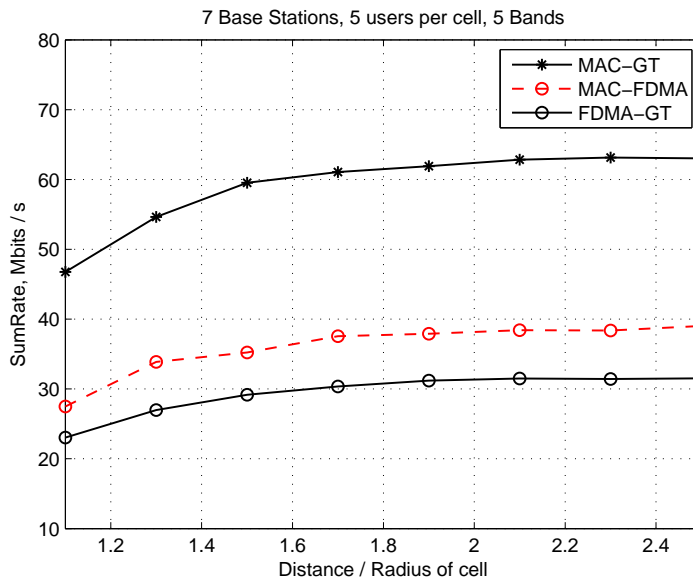
La somme des débits du système en moyenne par rapport à la distance entre SBS
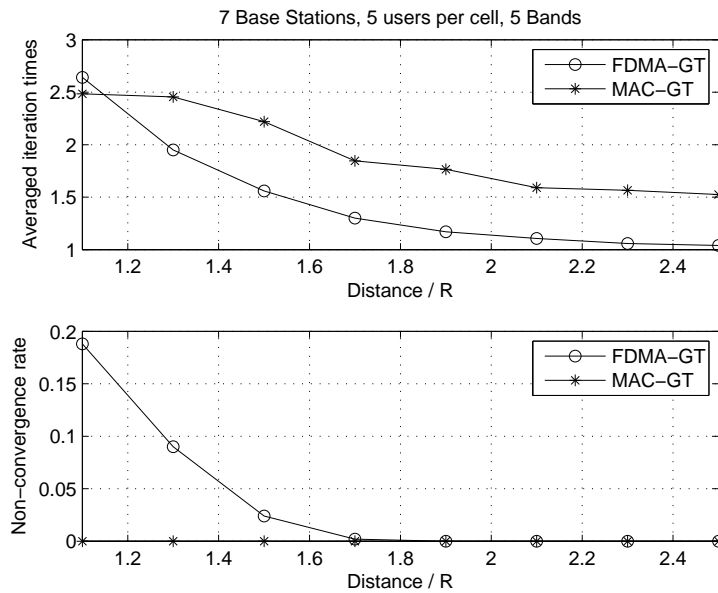
Le nombre d'itéation et les taux de non-convergence en moyenne

Chapitre 6 - Conclusion

La radio cognitive jouera un rôle clé dans le domaine des communications sans-fil en raison de l'augmentation des besoins en service et par conséquent, une couche physique bien adaptée à la CR est nécessaire. L'objectif de cette thèse est de démontrer l'apport des modulations multiporteuses à base de bancs de filtres FBMC pour les futurs systèmes de CR , qui sont plus efficaces et flexibles que les systèmes de CR basés sur les modulations multiporteuses classiques OFDM. Récemment, un grand nombre de recherches a concentré son attention sur l' OFDM pour les systèmes de CR, mais peu d'études dans la littérature ont considéré les FBMC, en particulier associées à la modulation OQAM. Ainsi, un autre objectif de cette thèse est de diffuser les connaissances de base des FBMC et de motiver les chercheurs afin de renforcer la recherche sur les FBMC.

En tant que candidat potentiel pour les systèmes de communication de prochaine génération, le FBMC conserve non seulement les caractéristiques de l'OFDM comme par exemple un débit élevé, une robustesse aux évanouissements par trajets multiples, une mise en forme spectrale flexible, etc, mais améliore aussi les points faibles de l'OFDM grâce à ses capacités intrinsèques. Tout d'abord, le FBMC permet de maximiser l'efficacité spectrale d'un système de CR en éliminant le CP. Deuxièmement, le FBMC exploite les faibles lobes secondaires de son filtre prototype ce qui conduit à une plus grande robustesse au décalage résiduelle de fréquence et une meilleure suppression de l'ISI et de l'ICI par rapport à l'OFDM. Pour le FBMC, aucune bande de garde supplémentaire n'est nécessaire pour garantir la qualité des services de système sous licence. Enfin, il a été montré que les bancs de filtre peuvent être utilisés comme un analyseur de spectre précis sans ajout de complexité. Dans cette thèse, nous avons montré que les bancs de filtre d'analyse au niveau du récepteur peuvent atteindre une meilleure résolution spectrale que les solutions basées sur la transformée de Fourier classique. En outre, par rapport à l'OFDM, les modulations FBMC peuvent permettre une gestion de fréquence très souple grâce à une granularité d'une sous-porteuse et peuvent garantir une mise en forme du signal émis pour occuper les trous du spectre sans interférer les utilisateurs autorisés.

En résumé, les modulations FBMC offrent une résolution spectrale plus élevée ainsi qu'une meilleure efficacité et exigent seulement une petite augmentation de la complexité de calcul par rapport à l 'OFDM. Toutes ces propriétés importantes des modulations FBMC en font un candidat prometteur pour la couche physique de CR pour l'accès dynamique au spectre.

Contents

CONTENTS

List of Figures

LIST OF FIGURES

List of Tables

LIST OF TABLES

List of Symbols

$*$	the conjugate operator
$\otimes$	the convolution operator
$\triangleq$	defined as
$\cap$	the intersection operator
$\cup$	the union operator
$|x|$	the absolute value of the scalar x
$||\mathbf{x}||$	certain norm of the vector $\mathbf{x}$
$\mathbf{I}$	the identity matrix
$\mathbf{X}^{-1}$	the inverse of the matrix $\mathbf{X}$
$(\cdot)^T$	the transpose of $(\cdot)$
$e^{(\cdot)}$	the exponential function
$log(\cdot)$	the natural logarithm
$log_b(\cdot)$	the logarithm in base b
$Tr(\cdot)$	the trace operator
$Rank(\cdot)$	the rank operator
$\mathbb{R}^n$	the the set of n-dimensional real vectors
$\mathbb{E}(\cdot)$	the statistical expectation
$Var(\cdot)$	the statistical variance
$Re(\mathbf{x})$	the real part of $\mathbf{x}$
$Im(\mathbf{x})$	the imaginary part of $\mathbf{x}$
$\nabla_x f(x)$	the gradient of function f with respect to x
$\mathcal{F}(f)$	the Fourier transform of function f
$\mathcal{F}^{-1}(f)$	the inverse Fourier transform of function f
$\mathcal{N}(\mu, \sigma^2)$	the Gaussian distribution with mean μ and variance σ^2
$min\{x, y\}$	equal x when $x < y$
$max\{x, y\}$	equal x when $x > y$
$argmin$	the argument of the minimum
$argmax$	the argument of the maximum
$cf.$	the abbreviation of *confer*
$Q.E.D.$	the abbreviation of *completion of the proof*

LIST OF SYMBOLS

List of Abbreviations

3GPP	**3**rd **G**eneration **P**artnership **P**roject
AC	**A**veraged **C**apacity
AFB	**A**nalysis **F**ilter **B**ank
AWGN	**A**dditive **W**hite **G**aussian **N**oise
BPSK	**B**inary **P**hase **S**hift **K**eying
CAF	**C**yclic **A**utocorrelation **F**unction
CCI	**C**ross-**C**hannel **I**nterference
CDF	**C**umulative **D**istribution **F**unction
CDMA	**C**ode **D**ivision **M**ultiple **A**ccess
CFO	**C**arrier **F**requency **O**ffset
CMT	**C**osine **M**odulated Multi-**T**one
CP	**C**yclic **P**refix
CR	**C**ognitive **R**adio
CS	**C**yclostationary **S**ignature
CSI	**C**hannel **S**tate **I**nformation
DARPA	**D**efense **A**dvanced **R**esearch **P**rojects **A**gency
DFT	**D**iscrete **F**ourier **T**ransform
DSA	**D**ynamic **S**pectrum **A**ccess
DSL	**D**igital **S**ubscriber **L**ine
FBMC	**F**ilter **B**ank based **M**ulti-**C**arrier
FCC	**F**ederal **C**ommunications **C**ommission
FCR	**F**ull **C**ognitive **R**adio
FDD	**F**requency **D**ivision **D**uplex
FDMA	**F**requency **D**ivision **M**ultiplexing **A**ccess
FFT	**F**ast **F**ourier **T**ransform
FMT	**F**iltered **M**ulti**T**one
FT	**F**ourier **T**ransform
GPM	**G**radient **P**rojection **M**ethod
GT	**G**ame **T**heory
HA	**H**ungarian **A**lgorithm
HMM	**H**idden **M**arkov **M**odel
HOS	**H**igher **O**rder **S**tatistic
ICI	**I**nter-**C**arrier **I**nterference
IEEE	**I**nstitute of **E**lectrical and **E**lectronics **E**ngineers
IFFT	**I**nverse **F**ast **F**ourier **T**ransform

IOTA	**I**sotropic **O**rthogonal **T**ransform **A**lgorithm
ISI	**I**nter-**S**ymbol **I**nterference
ISM	**I**ndustrial **S**cientific and **M**edical
IWFA	**I**terative **W**ater-**F**illing **A**lgorithm
KKT	**K**arush-**K**uhn-**T**ucker
LA	**L**agrangian **A**lgorithm
LAPTV	**L**inear **A**lmost **P**eriodic **T**ime-**V**ariant
LBCR	**L**icensed **B**and **C**ognitive **R**adio
LICQ	**L**inear **I**ndependence **C**onstraint **Q**ualification
LPTV	**L**inear **P**eriodic **T**ime-**V**ariant
LTE	**L**ong **T**erm **E**volution
MAC	**M**ultiple **A**ccess **C**hannel
MCM	**M**ulti-**C**arrier **M**odulation
MC-MU	**M**ulti-**C**ell with **M**ulti-**U**ser per cell
MIMO	**M**ultiple-**I**nput **M**ultiple-**O**utput
MT	**M**ulti-**T**aper
NE	**N**ash **E**quilibrium
NP	**N**onconvergent **P**oint
NRA	**N**on-cooperative **R**esource **A**llocation
OCR	**O**verlay **C**ognitive **R**adio
OFDM	**O**rthogonal **F**requency **D**ivision **M**ultiplexing
OQAM	**O**ffset **Q**uadrature **A**mplitude **M**odulation
PAPR	**P**eak-to-**A**verage **P**ower **R**atio
PBS	**P**rimary **B**ase **S**tation
PFB	**P**olyphase **F**ilter **B**ank
PHYDYAS	**PHY**sical layer for **DY**namic spectrum **A**cces**S** and cognitive radio
PSD	**P**ower **S**pectral **D**ensity
PSE	**P**eriodogram **S**pectrum **E**stimator
PSW	**P**rolate **S**equence **W**indow
PU	**P**rimary **U**ser
QAM	**Q**uadrature **A**mplitude **M**odulation
QoS	**Q**uality **o**f **S**ervice
RA	**R**esource **A**llocation
ROC	**R**eceiver **O**perating **C**haracteristic
SBS	**S**econdary **B**ase **S**tation
SCF	**S**pectral **C**orrelation **F**unction
SDR	**S**oftware-**D**efined **R**adio
SFB	**S**ynthesis **F**ilter **B**ank
SINR	**S**ignal to **I**nterference-plus-**N**oise **R**atio
SNR	**S**ignal to **N**oise **R**atio
SS	**S**econdary **S**ystem
SSCR	**S**pectrum **S**ensing based **C**ognitive **R**adio
SU	**S**econdary **U**ser
TDMA	**T**ime **D**ivision **M**ultiplexing **A**ccess
UBCR	**U**nlicensed **B**and **C**ognitive **R**adio
UCR	**U**nderlay **C**ognitive **R**adio

USB	**U**niversal **S**erial **B**us
UWB	**U**ltra **W**ide**B**and
WiMAX	**W**orldwide **I**nteroperability for **M**icrowave **A**ccess
WLAN	**W**ireless **L**ocal **A**rea **N**etwork
WMAN	**W**ireless **M**etropolitan **A**rea **N**etwork
WPAN	**W**ireless **P**ersonal **A**rea **N**etwork
WRAN	**W**ireless **R**egional **A**rea **N**etwork

LIST OF ABBREVIATIONS

Introduction

1.1 Motivation

The demand for new wireless services and applications, as well as the number of wireless users, are progressively increasing. However, this growth is ultimately restricted by the amount of available radio frequency spectrum. Recent measurements by several agencies [1]∼[4] indicate that the licensed spectrum resources have not been fully exploited depending on the time and the geographic location. These observations suggest that the fixed spectrum allocation approach has given rise to spectral scarcity, which motivates the introduction of some Dynamic Spectrum Access (DSA) techniques. Cognitive Radio (CR), which is coined by Mitola [5], has recently been proposed as a promising solution to improve spectrum utilization via DSA. The goal of the CR is to enhance spectral efficiency by overlaying a secondary mobile radio system on an existing primary one without requiring any change to the actual licensed system. At the time of this writing, there is still no common way on how to define and implement CR systems. Although a lot of effort is being spent on investigating the feasibility and effectivity of CR, more efficient and reliable methods should be developed due to the limited and costly spectrum resources.

Hence, for the sake of commercial and technological improvement, future CR systems should provide higher capacity and meanwhile lower impairment to licensed system by means of an efficient utilization of the available resources. Multi-Carrier Modulations (MCMs) have attracted a lot of attention ranging from wireline to wireless communications as opposed to single-carrier modulation because of the capability to efficiently cope with frequency selective fading channels and the flexibility to allocate the resources of each subchannel on an individual basis. Conventional Orthogonal Frequency Division Multiplexing (OFDM), as a physical MCM scheme, has been investigated quite intensively in recent years. Much of attention in the present literature emphasizes on the use of OFDM, which is able to avoid both Inter-Symbol Interference (ISI) and Inter-Channel Interference (ICI) making use of an extended Cyclic Prefix (CP). In [6], OFDM has been suggested as a candidate for CR systems. Nevertheless, in spite of these advantages, OFDM is very sensitive to residual Carrier Frequency Offset (CFO) and to timing offset due to imperfect synchronization. In addition, OFDM systems sacrifice data transmission rate because of the insertion of CP.
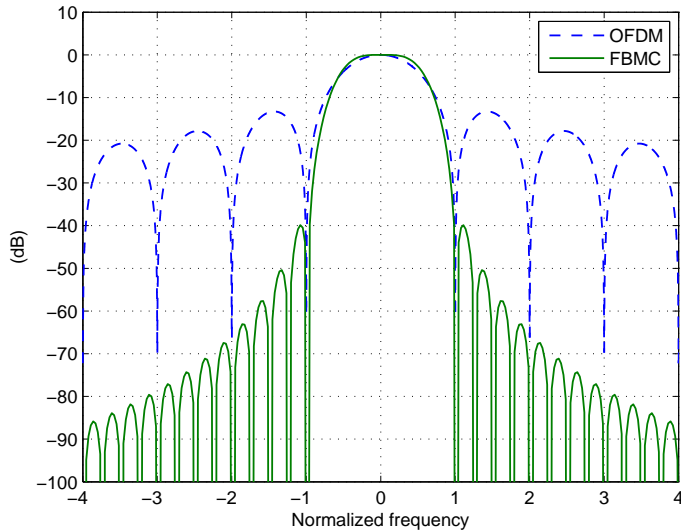
Figure 1.1: Comparison of frequency responses of OFDM and FBMC

In this dissertation, we propose another MCM scheme: Filter Bank based Multi-Carrier (FBMC) [7]~[13], which does not require CP extension and shows higher robustness to residual frequency offset than CP-OFDM by taking advantage of the low spectral leakage of its modulation prototype filter. FBMC has been already considered as a physical layer candidate for CR systems [14]. Moreover, filter banks at the receiver can be used as an analytical tool in CR for spectrum sensing. In [15][16], application of filter banks to spectrum sensing is proved to be more suitable than Fast Fourier Transform (FFT) and Thomson's Multi-Taper (MT) method because of its high performance and low cost. Consequently, FBMC is envisaged to be a potential candidate for future CR systems because of its capability to provide high capacity and low impairment to legacy system.

The essential difference between OFDM and FBMC lies in the spectral leakage property, as shown in Fig. 1.1, in which [1] their frequency responses are drawn in a comparable way. It can be observed that OFDM exhibits significant frequency side-lobe, which imposes strict orthogonality constraint for all the sub-carriers. On the contrary, FBMC has a negligible side-lobe in the frequency domain. With insignificant spectral leakage, high resolution spectrum analysis and low interference to adjacent frequency bands can be achieved. Recently, there has been an increasing awareness of the potential of using FBMC in the radio communications area, in particular the Isotropic Orthogonal Transform Algorithm (IOTA) technique [17][18]. The full exploitation of FBMC techniques as well as their combination with Multiple-Input Multiple-Output (MIMO) in the context of CR, has been considered and developed in the European project PHYDYAS [19].

---

[1]The prototype filter used for comparison is the one designed by Bellanger in [9].

The objective of this dissertation is to propose and develop FBMC based CR systems. Although some progress has been made in this area, a lot of obstacles must be overcome before a fully automated CR system can be realized. As mentioned in [15], FBMC has so far received limited attention and not been extensively studied like OFDM. Therefore, another goal of this dissertation is to disseminate the basic knowledge of FBMC and thereby to reinforce the filter bank literature.

1.2 Research Scope

Since FBMC is a somewhat new concept in CR domain, a great deal of effort should be devoted to implement it and many open issues remain to be resolved. In this dissertation, emphasis is placed on several research issues of FBMC based CR systems. Specifically, the scope of this dissertation involves three main tasks:

- *Spectrum Sensing*: first of all, we shall stress the fundamental importance of spectrum sensing. In CR context, spectrum sensing is an essential enabling functionality to detect unoccupied spectrum holes as reliably and efficiently as possible in relatively low SNR level, and then dynamically adjust the radio operating parameters accordingly. Thus, the detection of primary users is one of the main challenges in the development of the CR technology, and more and more attention has been paid to obtain various reliable and efficient spectrum sensing methods. Herein the detection of FBMC signal based upon Cyclostationary Signature (CS) is proposed and investigated. Additionally, multi-band sensing built on Polyphase Filter Bank (PFB) is analyzed and compared to FFT based sensing structure.

- *Spectral Efficiency Comparison*: it has been believed that in order to evaluate a type of MCM scheme applied to real CR systems, we have to pay attention to the problem of its spectral efficiency. The secondary system capacities of FBMC and OFDM based CR systems are examined and compared based on an uplink CR scenario.

- *Resource Allocation*: an additional research issue to be tackled is the Resource Allocation (RA). The challenges of RA in CR context differing from conventional RA algorithms lie in two aspects: the Cross-Channel Interference (CCI) from Secondary User (SU) to Primary User (PU) should be considered; secondly, the available spectrum holes have the property of time-varying, whereas conventional RA algorithms assume that the available spectrum resource is fixed. In the last part of this dissertation, we emphasize on the RA algorithms for non-cooperative multi-cell CR systems.

1.3 Literature Review

Little research has been conducted in applying FBMC to CR applications. In the sequel, the existing literature corresponding to spectrum sensing, spectral efficiency comparison, and resource allocation is presented, respectively.

Spectrum Sensing

A cyclostationary process is an appropriate probabilistic model for the signal that undergoes periodic transformation, such as sampling, modulating, multiplexing, and coding operations, provided that the signal is appropriately modeled as a stationary process before undergoing the periodic transformation [20]. Increasing demands on communication system performance indicate the importance of recognizing the cyclostationary character of communicated signals. The growing role of the cyclostationarity is illustrated by abundant works in the detection area and other signal processing areas. Spectral correlation is an important characteristic property of wide sense cyclostationarity, and a Spectral Correlation Function (SCF) is a generalization of the Power Spectral Density (PSD) function. Recently, the SCF has been largely exploited for signal detection, estimation, extraction and classification mainly because different types of modulated signals have highly distinct SCFs and the fact stationary noise and interference exhibit no spectral correlation property. Furthermore, the SCF contains phase and frequency information related to timing parameters in modulated signals.

In [20][21], explicit formulas of the Cyclic Autocorrelation Function (CAF) and SCF for various types of single carrier modulated signals are derived. The cyclostationary properties of OFDM have been analyzed in [22][23], and the formulas of CAF and SCF of OFDM signal are derived by a mathematic deduce process in [22], whereas the authors in [23] provide a straightforward derivation of CAF and SCF for OFDM signal by a matrix-based stochastic method without involving complicated theory. As for FBMC signals, the second-order cyclostationary properties of FBMC signal are exploited in [24][25] for blind joint CFO and symbol timing estimation.

Spectrum sensing on a single frequency band has a relatively rich literature. However, the literature of multi-band sensing which monitors multiple frequency bands simultaneously is very limited. The basic concept of multi-band sensing is to firstly estimate the PSD and then power detection (which is simple and can locate spectrum occupancy information quickly) is applied in the frequency domain based on the observed power spectrum. In [26], a wideband dual-stage sensing technique: a coarse and a fine spectrum sensing architecture is proposed. These two sensing stages collaborate with each other to enhance the accuracy of spectrum sensing performance. In [27], three widely used spectrum estimation methods: weighted overlapped segment averaging approach, multi-taper spectrum estimator and multiple signal classification algorithm are introduced and compared for wideband detection.

The authors in [28] consider making joint decisions over multiple frequency bands. The spectrum sensing problem is formulated as a class of optimization problems in interference limited cognitive radio networks. In [29], a novel approach called segmented periodogram for wideband spectrum segmentation is proposed. The proposed scheme is based on the posterior expectation of the piece-wise flat realizations of the underlying signal spectrum, which is obtained using the reversible jump Markov chain Monte Carlo technique. According to the estimated segmented periodogram, the wideband detection performance can be improved compared to conventional periodogram.

However, few of the aforementioned studies consider the PSD estimation applying polyphase filter bank. PFB is proposed as an efficient tool for spectral analysis [16] without additional cost since each secondary user can be equipped with PFB as the receiver front end. This means that the PFB structure for communication will offer a new opportunity for sensing at no extra cost. Furthermore, the complexity issues associated with PFB for spectrum sensing are investigated in [30], and a new low complexity PFB architecture for multi-standard cognitive radios is presented. The previous works using PFB and energy detector for multi-band sensing can be found in [31][32]. In these papers, the performance of the PFB based multi-band sensing is evaluated in comparison with conventional Periodogram Spectrum Estimator (PSE), and the final simulation results demonstrate the significant advantage of the PFB multi-band sensing compared to conventional PSE. Nevertheless, both of these papers employ an optimal Prolate Sequence Window (PSW) as the prototype filter of PFB. This PSW prototype filter as a spectral analysis can not be reused for communication.

Spectral Efficiency Comparison

In a real OFDM based CR system problems arise from the IFFT / FFT operations, which result in additional interference from the CR system to the primary system and *vice versa* [6][33]. Using the IFFT transmitter implementation, the temporal pulse shape of one symbol is rectangular, resulting in a sinc-shaped frequency response on each subcarrier, thus OFDM systems suffer from high side-lobe radiation.

In the literature, some system performance comparisons between OFDM and FBMC can be found in [34]~[41]. However, optimal resource allocation problem in multicarrier CR context with both power and mutual interference constraints is still an open topic. In [42]~[46], downlink power allocation problems in multicarrier based CR systems are investigated. In [43], maximization of the capacity with per subchannel power constraints is considered, but the influence of side-lobes of neighboring subcarriers is omitted. Conversely, the authors in [44] propose an optimal scheme with the interference induced to primary user, but the total power constraint is not considered. In [45],

a power loading scheme to maximize the downlink capacity of the CR system under the interference and power constraints is proposed, and then according to this proposed scheme, the CR systems based on OFDM and FBMC are evaluated and compared in terms of power allocation and the system throughput in [46], in which an iterative Power Interference constraint algorithm (PI-algorithm) to iteratively allocate the subcarrier power is proposed. However, the interference induced from PU to SU is assumed to be negligible and channel pathloss is not considered.

Resource Allocation

In [47], the original distributed power control for frequency selective multi-user interference channel is modeled as a non-cooperative game and implemented by means of Iterative Water-Filling Algorithm (IWFA) in the context of Digital Subscriber Line (DSL) systems, where each user water-fills its power to different subchannels regarding the power of other users as interference. A distributed non-cooperative game to perform subchannel assignment, adaptive modulation, and power control for multi-cell OFDM networks with one user per cell is proposed in [48]. In order to achieve Pareto improvement compared to the solution in [48], a pricing policy to the users' transmit power by adding a penalty price is proposed in [49]. However, the authors in [48][49] have not provided provable uniqueness of NE and the global convergence to a Nash Equilibrium (NE). In [50], the optimization problem maximizing the information rate of each link for Rayleigh frequency selective interference channel is formulated as a static non-cooperative game, and an asynchronous IWFA is proposed to reach the NE of the game. In this asynchronous algorithm, each user updates its PSD in a completely distributed and asynchronous way. Moreover, the authors provide the conditions which ensure the global convergence of the asynchronous IWFA to the unique NE point. In [51], a distributed power allocation algorithm based on a new class of games, called *potential game* is proposed. Convergence rule and steady state characterization are analyzed using potential game theory. The proposed potential game algorithm is shown to achieve higher energy efficiency in comparison with pure IWFA. In [52], a full distributed resource allocation in multi-cell with multiple users per cell is firstly presented by adopting a game theoretic approach. The unique NE point is proved to exist in some constrained environment. However, at each iteration, subchannel assignment and power control are separately implemented by the player (base station), which requires iterative calculations of the subchannel assignment matrix and the power vector. Except the distributed algorithms based on game theory, a heuristic resource allocation approach is presented in [53], in which a *selfish* and a *good neighbor* decentralized dynamic spectrum access strategies are proposed. However, dynamic resource allocation for non-cooperative multi-cell with multiple users per cell in the context of CR is still an open topic.

1.4   Thesis Outline

This dissertation attempts to develop a FBMC based CR system as opposed to OFDM by covering several important research issues. We give a basic overview of CR and MCM techniques in the first chapter, which is a necessary part for the understanding of subsequent chapters. After the statement of CR and MCM, three research issues: spectrum sensing, spectral efficiency comparison, resource allocation, in FBMC based CR systems are investigated compared with OFDM based CR systems. The structure of this dissertation is as follows:

Chapter 2 - Overview of CR and MCM Techniques

The literature overview of CR and MCM is provided in this chapter, where we present the history, development, application, key research issues of CR and MCM schemes.

Chapter 3 - Spectrum Sensing

We start by introducing a brief summary of spectrum sensing methods existing in current literature, and then this chapter proceeds by proposing two sorts of spectrum sensing strategies: cyclostationary signature based single-band sensing and polyphase filter bank based multi-band sensing.

Concerning the single-band sensing, we investigate and exploit the cyclostationarity characteristics of OFDM and FBMC signals. The spectral correlation characterization of MCM signal can be modeled by a special Linear Periodic Time-Variant (LPTV) system. Using this LPTV model, we have derived the explicit theoretical formulas of nonconjugate and conjugate cyclic autocorrelation function and spectral correlation function of OFDM and FBMC signals. According to foregoing theoretical spectral analysis, cyclostationary signatures are artificially embedded into MCM signal and a low-complexity CS detector is therefore presented for detecting MCM signals.

Finally, we investigate a multi-band detection architecture based on polyphase filter bank, which aims to reliably sense multiple active bands by exploiting the low leakage property of PFB. We have theoretically obtained the expressions of detection probability and false alarm probability for PFB and FFT based detectors, respectively, and thereby a theoretical detection threshold can be defined.

Chapter 4 - Capacity Comparison of OFDM / FBMC for Uplink CR Systems

In this chapter, we emphasize the channel capacity comparison of a CR network using two types of multicarrier communications: CP-OFDM and FBMC modulation schemes. We use a resource allocation algorithm in which subcarrier assignment and power allocation are carried out sequentially. By taking the impact of inter-cell interference resulting from timing offset into account, the maximization

of total information rates is formulated under an uplink scenario with pathloss and Rayleigh fading, subject to maximum power constraint as well as mutual interference constraint between primary user and secondary user.

Chapter 5 - Non-Cooperative Resource Allocation of FBMC-based CR Systems

We propose a game theoretic algorithm to perform uplink frequency allocation and power control between non-cooperative multi-cell with multi-user per cell in FBMC based CR systems. The maximization of total information rates of multiple users in one cell is considered for Rayleigh channel with pathloss, subject to power constraint on each user. By using Multiple Access Channel (MAC) technique, the original integer optimization problem is transformed into a concave optimization problem and we establish a distributed game model, in which each base station, trying to maximize the sum-rate of its own users, is a player. The proposed game theoretic algorithm for distributed multi-user power allocation is viewed as an extension of iterative water-filling algorithm applied to distributed single-user power allocation.

Chapter 6 - Conclusions and Perspectives

This chapter summarizes the main contributions of the dissertation and some possible steps for future research are provided.

1.5   Publications

Some of the researches presented in this dissertation have been published, submitted, or under preparation at the time of submission of this dissertation:

Journal Papers

1. **H.Zhang**, D. Le Ruyet, and M. Terré, "Spectral Efficiency Comparison between OFDM / OQAM and OFDM based CR Networks," *Wireless Communications and Mobile Computing, Wiley*, vol. 9, pp. 1487-1501, Nov. 2008.

2. **H.Zhang**, D. Le Ruyet, and M. Terré, "Spectral Correlation of Multicarrier Modulated Signals and Its Application for Signal Detection," *EURASIP Journal on Advances in Signal Processing*, vol. 2010, Article ID 794246, 14 pages, 2010. doi:10.1155/2010/794246.

3. **H.Zhang**, D. Le Ruyet, D. Roviras, Y. Medjahdi, and H. Sun, "Spectral Efficiency Comparison of OFDM / FBMC for Uplink Cognitive Radio Networks," *EURASIP Journal on Advances in Signal Processing*, vol. 2010, Article ID 621808, 14 pages, 2010. doi:10.1155/2010/621808.

4. **H**.**Zhang**, D. Le Ruyet, D. Roviras, and H. Sun, "Filter Bank based Multi-Band Spectrum Sensing for Cognitive Radio Networks," *in preparation*.

5. **H**.**Zhang**, D. Le Ruyet, D. Roviras, and H. Sun, "A Resource Allocation Strategy of Noncooperative Multi-cell for FBMC based Cognitive Radio Networks," *in preparation*.

Conference Papers

1. **H**.**Zhang**, D. Le Ruyet, and M. Terré, "Signal Detection for OFDM/OQAM System Using Cyclostationary Signatures," *in Proc. of IEEE International Symposium on Personal Indoor and Mobile Radio Communications (PIMRC)*, Sep. 2008, pp. 1-5.

2. **H**.**Zhang**, D. Le Ruyet, and M. Terré, "On Spectral Efficiency Analysis between OFDM/OQAM and OFDM based CR Networks," *in Proc. of IEEE Vehicular Technology Conference VTC'09*, Apr. 2009, pp. 1-5.

3. **H**.**Zhang**, D. Le Ruyet, D. Roviras, and H. Sun, "Resource Allocation of Noncooperative Multi-cell for Cognitive Radio Networks," *in Proc. of ISWCS'09*, Sep. 2009, pp. 101-105.

4. **H**.**Zhang**, D. Le Ruyet, D. Roviras, and H. Sun, "Uplink Capacity Comparison of OFDM / FBMC based Cognitive Radio Networks," *in Proc. of ICC'10*, Cape Town, South Africa, May. 2010.

5. **H**.**Zhang**, D. Le Ruyet, D. Roviras, and H. Sun, "Capacity Analysis of OFDM / FBMC based Cognitive Radio Networks with Estimated CSI," *in Proc. of CrownCom'10*, Cannes, France, Jun. 2010.

Other Publications not Presented in This Dissertation

1. **H**.**Zhang**, W. Yang, J. Chen, and H. Sun, "Improved Classification of Polarimetric SAR Data Based on Four-component Scattering Model," *in Proc. of 2006 CIE International Conference on Radar*, Oct. 2006, pp. 555-558.

2. W. Yang, H. Wang, Y. Cao, and **H**.**Zhang**, "Classification of Polarimetric SAR Data Based on Multidimensional Watershed Clustering," *in Proc. of Lecture Notes in Artificial Intelligence, ADMA'06*, 2006, pp. 157-164.

3. W. Yang, **H**.**Zhang**, J. Chen, and H. Sun, "Automatic Detection of Power Transmission Network in Full Polarimetric SAR Imagery," *in Proc. of IEEE Radar Conference'07, Boston, USA*, Apr. 2007, pp. 789-793.

4. **H**.**Zhang**, W. Yang, T. Zou, and H. Sun, "Automatic Extraction of Power Transmission Tower Series from PolSAR Imagery Based on MRF Model," *in Proc. of 2007 Asian and Pacific Conference on Synthetic Aperture Radar*, Nov. 2007, pp. 788-792.

5. W. Yang, H. Sun, **H**.**Zhang**, X. Xu, "Study on Extracting Information from Spaceborne Polarimetric Synthetic Aperture Radar Data," *SPACE ELECTRONIC TECHNOLOGY*, vol. 4, no. 2, pp. 1-6, 2007. (in Chinese)

6. **H**.**Zhang**, W. Yang, T. Zou, and H. Sun, "Classification of Polarimetric SAR Image Based on Four-component Scattering Model," *Geomatics and Information Science of Wuhan University*, vol. 34, no. 1, pp. 122-125, 2009. (in Chinese)

Overview of CR and MCM Techniques

Wireless technologies and devices have proliferated over the past decades, which considerably increases the demand for electromagnetic spectrum. This ever-increasing demand gives us an impression that we would encounter the problem of spectrum scarcity in the future. However, the truth is that the available spectrum is abundant but inadequately utilized owing to the conventional spectrum allocation policy. The advent of Cognitive Radio (CR) has a significant impact on the efficient use of limited radio spectrum. A wealth of information of CR can be found in [54][55]. Due to the huge body of research literature and the interdisciplinary nature of CR, it is not possible to provide an exhaustive overview of current CR knowledge. Instead, this chapter presents a concise overview of the emerging CR solution for spectrum scarcity. The purpose here is to provide a preliminary summary before offering a more detailed exposition of CR techniques in the following chapters. The realization of CR requires a highly adaptive and flexible physical layer so that the sensing and adaptation can be implemented efficiently. In the second part of this chapter, Multi-Carrier Modulation (MCM), as the candidate transmission technology for CR physical layer, is discussed.

We begin this chapter by stating the background of CR in *Section 2.1.1*, where the CR evolution, CR definitions, and CR classifications are presented. In *Section 2.1.2*, we survey the current CR developments and future applications in different wireless systems, and then this chapter lists the key research issues posed by the characteristic of CR systems in *Section 2.1.3*. Next, *Section 2.2*, two MCM techniques: Orthogonal Frequency Division Multiplexing (OFDM) and Filter Bank based Multi-Carrier (FBMC), are compared, and FBMC, proposed in this dissertation, is elaborated in theory. In *Section 2.3*, the European project PHYDYAS [1] supporting FBMC technique is briefly introduced. Finally, conclusion is made in *Section 2.4*.

2.1 Cognitive Radio

2.1.1 Background

It is well recognized that wireless access has become an integral and vital component of our daily life (e.g. entertainment, education, healthcare, public safety, military, and many other aspects). For

---

[1]Some work of this dissertation is done in the context of this project.

instance, more and more people have the habit of carrying their laptops into public places in order to surf on the Internet. Imagining what will happen when more future devices evolve into wireless: not only laptops, but also mobile phones, sensors, monitors, home appliances, radio wireless tags, and etc. This development tendency signifies that, in the long term, a great variety of new wireless services will spring up quickly, which requires a revolutionary change in how the future radio spectrum is regulated.

However, government regulatory agencies have adopted until now a fixed spectrum assignment policy to the licensing of finite amounts of spectrum to various wireless services, in a way that is referred to as legacy *command and control*. Open spectrum access to most of the radio spectrum is only allowed for radio systems with limited transmission powers like the underlay Ultra WideBand (UWB) approach. The overlay sharing approach is generally not permitted. Most of the key radio bands less than 3 GHz are already exclusively assigned, and the deployment of new wireless services is confined to either some unlicensed bands, such as the Industrial, Scientific, and Medical (ISM) bands, or bands above 3 GHz. Nevertheless, the existing unlicensed bands are far from sufficient to satisfy the need of future wireless services. This implies that the fixed radio regulation is too inflexible to handle the emerging wireless applications and might hamper the progress of wireless access.

Careful studies of the current usage of the radio spectrum by several agencies [1]∼[4] have revealed that a large portion (up to 85%) of the licensed spectrum below 3 GHz, while even noticeably higher at the frequencies above 3 GHz, is not occupied most of the time and space. The spectrum scarcity and the inefficiency of the spectrum usage necessitate an open access paradigm to adequately exploit the existing wireless spectrum. Moreover, the highly commercial success of wireless applications on an unlicensed basis with relaxed regulations (e.g. Wireless Local Area Network (WLAN) and Wireless Personal Area Network (WPAN)) indicates that it is profitable to change the legacy radio regulatory policy towards an open spectrum access. In order to support this open spectrum access, new wireless systems are required to be able to autonomously organize their spectrum usage without regulating the incumbent system. Thus, the essential problem is not the shortage of radio spectrum but the way that spectrum is used and how a self-organizing system is built. Naturally, the foregoing realistic facts motivate the development of Dynamic Spectrum Access (DSA) technique to share the existing wireless spectrum.

The term *dynamic spectrum access* has a broad connotation which is categorized into three models in [56]: dynamic exclusive use model, open sharing model, and hierarchical access model. The dynamic exclusive use model keeps the basic structure of the legacy spectrum regulation policy, i.e. spectrum bands are licensed to wireless services for exclusive use. The licensee has the right to lease or share the spectrum for business profit, but such sharing is not mandated by the regulation policy. Open sharing model is also referred to as *spectrum commons*, this model means an open

sharing among peer users like the sharing in ISM radio bands. The last hierarchical access model involving Primary Users (PUs) and Secondary Users (SUs) is subdivided into: underlay and overlay approaches. The basic idea of this model is to open licensed spectrum to SUs while limiting the interference perceived by PUs. Specifically, the overlay approach (also referred to as *opportunistic spectrum access*) aims at opportunistically utilizing spatial and temporal spectrum white space by allowing SUs to identify and exploit local spectrum availability in a non-interfering manner. In contrast, the underlay approach operating over UWB is a simple approach to occupy a wide licensed spectrum without interfering with PUs based on strict restrictions on transmitted power level. The important thing to note is that this approach does not rely on detection of white space. Compared to the former two models, hierarchical access model is regarded as the most compatible model with the current spectrum assignment policy and legacy wireless systems. Although the underlay approach is the first step approved by Federal Communications Commission (FCC) forward to improve spectrum utilization through open sharing, this approach do not exploit the existence of idle spectrum, and just appropriate for short-range communications due to the low transmission power. Moreover, sophisticated spread spectrum techniques are required for this approach. While for overlay approach the transmission power of SUs can be comparable to the power of PUs, therefore long-range communications will be feasible. After realizing these limitations of UWB, FCC has issued a proposed rule making opportunistic overlay approach as a candidate to implement efficient spectrum utilization.

In this dissertation, we focus on the opportunistic spectrum access under the hierarchical access model. Over the recent decades, the concepts of Software-Defined Radio (SDR) and Cognitive Radio (CR) are introduced to realize the idea of opportunistic spectrum access. The pioneer work can be traced to the introduction of SDR, which was firstly proposed by Mitola in [57][58] in 1991. SDR system is a radio communication system in which some or all of the communication functions are realized as programs running on standard computers or embedded devices. The architecture and computational aspects of the ideal SDR have been defined formally in [59]. Software radios recently have significant applications for the military services and commercial standards. In the long term, SDR is expected by its advocators to produce a radical change in radio design. However, there is no reliable technology to guarantee spectrum use of PUs, which enables the emergence of the cognitive radio (CR) [60].

The concept of CR was first presented officially in [5] by Mitola in 1999. CR is thought of as a logical evolution of SDR. Based on the SDR technologies, CR could additionally incorporate flexible and sophisticated algorithms to control the interference to PUs. Employing adaptive software, intelligent CR devices could be designed to reconfigure their communications functions to meet the requirements of the wireless system and SUs. Based on the idea that SUs access the spectrum dynamically for available bands without causing harmful interference to PUs, as a result, spectrum usage

increases, the CR is therefore the key enabling technology of next generation wireless systems and opportunistic spectrum access systems.

In recent years, a number of technical terms related to CR are coined: opportunistic spectrum access, adaptive radio, agile radio, spectrum pooling, spectrum overlay, etc. In order to avoid definition confusion, the term *cognitive radio* will be adopted throughout this dissertation.

CR Definitions

Ever since the notion of CR was firstly introduced in 1999, different interpretations of what an ideal CR may look like have been much discussed in the literature [61][62]. However, there is no consensus on the formal definition of CR until now, the concept has evolved over the past few years to include various meanings in different scenarios. The exact definition of CR is still under debate. An unified definition of CR is difficult to make mainly because different researchers and organizations have different expectations about levels of situation awareness and cognitive functionality. Various definitions are summarized in [63]. The standard definition of CR is expected to come out over time stemming from either an international consensus or from the future CR system which firstly dominates the market. The author in [63] reveals some commonalities among different CR definitions, and finally give their originally definition of CR by synthesizing their common features:

"A cognitive radio is a radio whose control processes permit the radio to leverage situational knowledge and intelligent processing to autonomously adapt towards some goal."

The SDR Forum [64], which has several initiatives under way to support the development of cognitive radio, is under way to draft a definition that explains CR as shown below:

"A cognitive radio is an adaptive, multi-dimensionally aware, autonomous radio system that learns from its experiences to reason, plan, and decide future actions to meet user needs."

To some extent, we can simply understand that a cognitive radio is a radio that can alter its operating parameters (e.g. transmit power, carrier frequency, modulation scheme, etc) intelligently and dynamically based on the surrounding environment or user demands.

CR Classifications

It is generally thought that dynamic spectrum access is merely one of the important applications of CR, and CR system can stand for any wireless paradigm that operates with cognition. In a broad sense, the existing CR in the literature can be mainly categorized into three classifications by different

ways according to *system functionality*, *available spectrum property*, and *spectrum access technique*, respectively.

The first classification depends on the differences of the functionality that a CR can exhibit. More specifically, there are two types of CR with different system functionalities: Full Cognitive Radio (FCR) and Spectrum Sensing based Cognitive Radio (SSCR).

- **FCR** (also referred to as *Mitola radio* [5][65]): in which every possible operating parameter observable by a wireless device or network should be taken into account. This kind of CR system incorporates full cognitive radio functionality, e.g. the cognitive radio described in [65] incorporates nine levels of CR functionality, however, some of which cannot be supported by the current techniques.

- **SSCR**: in which only the radio frequency spectrum is considered. Specifically, SSCR is a secondary system which is able to sense its radio environment and then adjust its operating parameters to reuse idle spectrum bands and meanwhile to meet Quality of Service (QoS) of primary system.

The second classification is based on the available spectrum property, by which CR is separated into: Licensed Band Cognitive Radio (LBCR) and Unlicensed Band Cognitive Radio (UBCR).

- **LBCR**: in which the radio frequency is licensed to so-called primary users, and the CR users are referred to as secondary users. SUs are capable of sharing the spectrum bands assigned to PUs. The interference avoidance with PUs is the most significant issue in this architecture. More specifically, SUs aim at sensing the availability of licensed spectrum bands, or controlling the transmission power in order not to interfere with PUs. One of such systems is described in the IEEE 802.22 work group, which is developing a standard for Wireless Regional Area Network (WRAN) operated in licensed TV bands [66].

- **UBCR** (also referred to as *open sharing model*): in which one CR user can only utilize the unlicensed radio frequency spectrum and compete with other peer CR users. More specifically, there is no license holder, all system entities have the same right and priority to access the common unlicensed band. Unlike LBCR, CR users in UBCR focus on detecting the activities of other CR users rather than PUs. One known unlicensed band is the ISM band, which is originally reserved for the use of industrial, scientific and medical purposes. One of such systems is described in the IEEE 802.15.2 task group, which has been formed specifically to focus on the coexistence between Bluetooth and IEEE 802.11 devices.

2. OVERVIEW OF CR AND MCM TECHNIQUES

The last classification is characterized based on spectrum access technique: Overlay Cognitive Radio (OCR) and Underlay Cognitive Radio (UCR).

- **OCR**: in which CR nodes access the network by using a portion of frequency bands that is not used by other system nodes. Each CR node detects temporary unused frequency and then communicates on these bands. Similar to LBCR, the interference with other nodes should be canceled or limited.

- **UCR**: in which CR nodes spread their transmitted power over a large bandwidth to minimize the interference. The idea of UCR lies in the facts that most wireless systems can tolerate interference to some degree and that reliable transmission can occur even at a low power level if the bandwidth is large. The typical example is the UWB transmission, where the extremely low power spectral density minimizes coexistent interference to incumbent narrow band communication. However, the low transmitted power constrains UCR suitable only for short-range applications (e.g. WPAN or wireless Universal Serial Bus (USB)).

Although Mitola radio is more representative of original CR research direction, this CR with full functionality is more or less too far ahead of current technologies. Moreover, most of the research work is currently focusing on SSCR with less levels of functionality. It should be pointed out that the CR mentioned in this dissertation refers to as SSCR, and the CR techniques investigated herein are mainly in the context of LBCR and OCR.

An illustration of SSCR system is shown in Fig. 2.1, where two primary systems respectively operate in the frequency area f_1 and f_2, which are different licensed frequency bands assigned to these two primary systems. Specifically, a CR system could build communication links within the communication range of each primary system. A SU first senses the spectrum environment in order to learn the frequency bands unoccupied by PUs. Once such a spectrum hole [1] is found, the SU adapts its transmission power, frequency band, modulation selection, etc., so that it minimizes the interference to the PUs. In different areas the usage of the spectrum differs, so spectrum hole locations and their durations vary. The time-frequency utilization of PUs in the two frequency areas can be seen in Fig. 2.1. It is noted that the SUs in the frequency area f_1 can utilize the frequency f_2 all the time because they are out of communication range of primary system in the frequency area f_2, and *vice verse* for the other CR system in the frequency area f_2. Thus, an ideal SSCR system allows its users to access a frequency band opportunistically in time and space, thereby leading to a significant increase of the total spectrum efficiency. As soon as the SUs start the transmission, they should be able to detect or

---

[1]Spectrum hole represents a frequency band assigned to a primary users exclusively, but is not utilized by that user at a particular time and specific geographic location. Spectrum holes can be considered as multidimensional regions within frequency, time, and space.
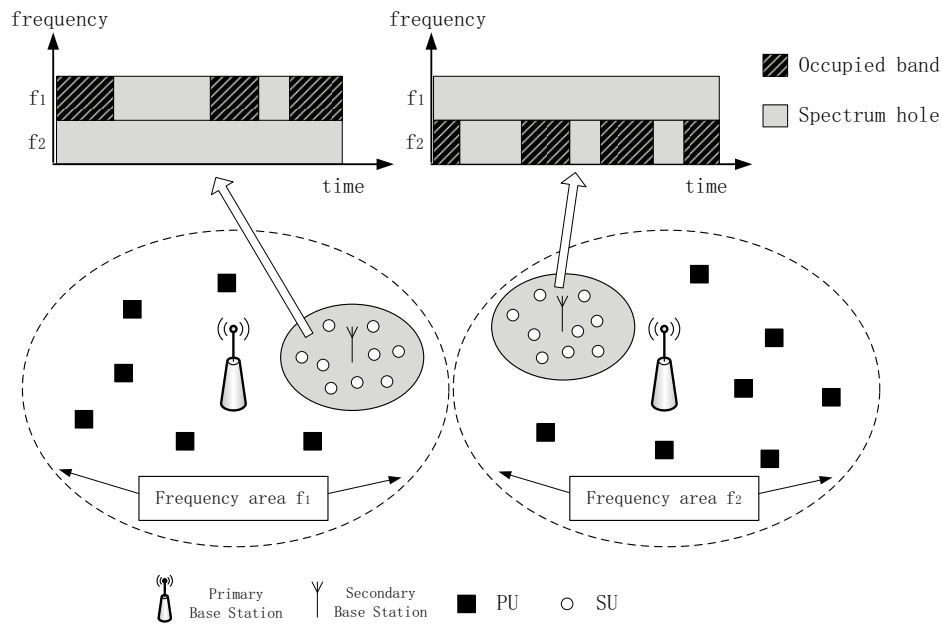
Figure 2.1: A Space-Time-Frequency scenario of SSCR system

predict the appearance of a PU so that it vacates the spectrum for that PU. Basically, the sensing and adaptation of the SUs must be done independently of the PUs to make the primary system maintain its legacy communication infrastructure. Thus, in order to realize the concept of SSCR, high resolution spectral analysis, flexible spectrum shaping, and reliable idle spectrum prediction are required.

2.1.2 Developments and Applications

Cognitive radio can be considered as a logical extension of SDR, therefore CR concepts and features can be implemented based on SDR technology and architecture, which are well studied by the SDR Forum. Moreover, the SDR forum has now several CR initiatives under way. Despite these initiatives by SDR Forum, most of the researches about CR are still at a conceptual level, and there are few cognitive radio networks in practical deployment. More advanced technologies and flexible spectrum management policies for realizing CR network are being invented and developed. This section describes some of the recent advances in CR communications, where the current CR developments and future possible CR applications are presented.

Developments

It has been gaining a growing interest among academic, industry, and regulatory communities in searching for all-profitable CR techniques. In academic, many researchers are currently engaged

in developing the sound communication technologies and protocols required for CR networks, and tremendous amount of academic papers and books related to CR have been published in literature [54][55]. The ever-increasing research efforts have made a significant progress on CR both in theory and in practical implementation.

In addition to academic area, commercial, civil and military areas all exhibit much interests in this type of highly intelligent radio. Initial work on CR is developed at the Defense Advanced Research Projects Agency (DARPA) in the United States for the military use. DARPA is responsible for funding the development of new technologies in order to enhance the national security, which not only has strengthened the defense capability but also has had a significant effect on the CR technique improvement. It is widely known that the realization of CR idea in industry largely depends on the development of regulatory communities. Nowadays, European and American regulatory communities are putting emphasis on CR for the commercial use, because new wireless services can be provided to meet future user demands. Many large-scale projects addressing CR topics for commercial purpose are recently approved and are under way, and some new companies are emerging to apply CR sensing techniques to efficiently exploit the radio spectrum resources. Moreover, FCC has built several CR test trials to investigate the impact of CR in white space, and then a white space coalition comprising of eight companies is set up aiming at efficient use of the future available analog television frequency bands. In a word, there is a tendency that more industrial activities will spring up to realize the CR technique.

The regulatory reform is regarded as the key factor for future CR network development. Most of the current spectrum assignment policies around the world pose a challenge to the dynamic spectrum access due to the inflexible allocation approaches. Efforts are being made by regulatory communities to promote the possibility of allowing dynamic spectrum access. Pre-regulatory activity has already started in all the international telecommunication union regions. For instance, FCC as one of the proactive regulatory bodies supports CR via recent spectrum policy task force and CR notice of proposed rules. The revised rules permit the 3650-3700 MHz band for terrestrial wireless broadband operations incorporating a contention-based protocol, which can be interpreted as benefiting from CR technologies.

The core regulation that can accelerate CR development and deployment lies in the standardization. Many standardization efforts already include some degree of CR technology today. In [67], the on-going standards activities of interest for CR within IEEE have been reviewed, and the prospects and issues for future standardization have been also provided. The existing standards mainly supporting dynamic spectrum access are IEEE 802.22 and IEEE P1900:

- *IEEE 802.22* (WRAN in unused TV bands): this is the first international wireless standard [66] adopting intelligent CR with tangible frequency bands for its operation, and will be also the first step to convince the regulators to open other licensed spectrum for spectrum sharing by successful co-existing network architecture. More specifically, this standard is defined for WRANs to provide broadband Internet connectivity, and will operate in the licensed bands from 54 to 862 MHz allocated for TV services since most of TV channels in these frequency spectra are largely unused especially in rural regions.

- *IEEE P1900*: the IEEE P1900 standards committee was established in 2005 jointly by the IEEE communications society and the IEEE electromagnetic compatibility society to develop supporting standards dealing with new techniques being developed for next generation radio and advanced spectrum management.

Other standards having CR features can be found in IEEE 802.11 and IEEE 802.16. In IEEE 802.11h, dynamic frequency selection and transmit power control are implemented for WLAN sharing. Another technology that is receiving interest lately in both academic and industry is Worldwide Interoperability for Microwave Access (WiMAX), e.g. the natural band from 3 to 10 GHz for CR operation is utilized by the UWB radios, where the primary users of this spectrum are WiMAX systems. The strategy to avoid interference between UWB and WiMAX systems is called *detect and avoid*, which involves some basic cognitive functions like sensing and power adaptation. In the future, more efficient spectrum management and planning are required for heterogeneous CR networks, such as IEEE 802.11-based WLANs and IEEE 802.16-based Wireless Metropolitan Area Networks (WMANs) may operate in the same unlicensed frequency band.

Future Applications

CR is already being considered as one of the key candidate technologies for the fourth generation wireless systems. There is no doubt that the CR technologies will have a great impact on wireless communication commercial area, where CR techniques will bring profit to each network entity: device manufacturer, license holder and secondary user. More specifically, equipment manufactures can benefit from the increased demand for wireless devices. The same trend as the introduction of *unlicensed bands* which has caused a substantial increase of short-range devices such as WLAN and Bluetooth, the implementation of CR techniques will induce similar changes by efficiently using the existing radio frequency resources. Likewise, license holders can increase additional revenues by renting their spectrum bands to new wireless services, which reduces the large burden for keeping expensive licensed spectrum. Thanks to the above benefits brought to manufactures and license holders, secondary users can obtain cheap services with higher quality.

In addition to the potential application in commercial area, the CR paradigm is expected to enable a variety of new applications in demanding environments [62], e.g. cognitive mesh network, civil emergency network, military network, and roaming network:

- *Cognitive mesh network*: mesh network is a mesh connectivity technology that can significantly enhance network performance. Recently, wireless mesh network is undergoing rapid progress and inspiring substantial deployments. With the growing commercial deployments of mesh networks and other WLAN networks, the ISM band is getting saturated. In order to relieve this congestion, CR techniques can be used for mesh networks to obtain higher throughput since they can opportunistically access to finite amount of spectrum. Thus, dynamic spectrum usage of the scarce spectrum resource will be the next stage of evolution in mesh network research, which is referred to as cognitive mesh network.

- *Civil emergency network*: which includes various emergency networks. CR has the potential to mitigate the consequences of natural diasters by temporarily building coordination without any infrastructure. CR will be also useful for emergency healthcare services. For example, transmission of video or images from an accident site to the hospital can help the medical staffs to prepare emergency medicines and equipments for the victims ahead of time.

- *Military network*: which has a strong need for rapid set-up time and security of the communication in hostile environment. CR could improve the reliability of communication, especially in the battlefield with high interference and vulnerability due to jamming. Moreover, CR could allow soldiers to perform spectrum handoff to find secure spectrum band for themselves or their allies.

- *Roaming network*: CR technologies offer the international roaming capability to CR terminals by autonomously exploit locally unused spectrum to provide new paths to spectrum access, and self-adjusting their transmission in compliance with local regulations.

2.1.3   Key Research Issues

Opportunistic use of spectrum in SSCR system poses critical challenges to the researchers. There are a lot of tasks that need to be accomplished before a fully functional SSCR network can be implemented. This section addresses the frequent research issues of cognitive radio, some of which will be dealt with in the subsequent chapters.

A time-frequency illustration of basic research tasks in SSCR system is given in Fig. 2.2. It is well known that the objective of SSCR is to enhance spectral efficiency by overlaying a secondary radio system on an existing primary one without requiring any change to this primary system. In order to
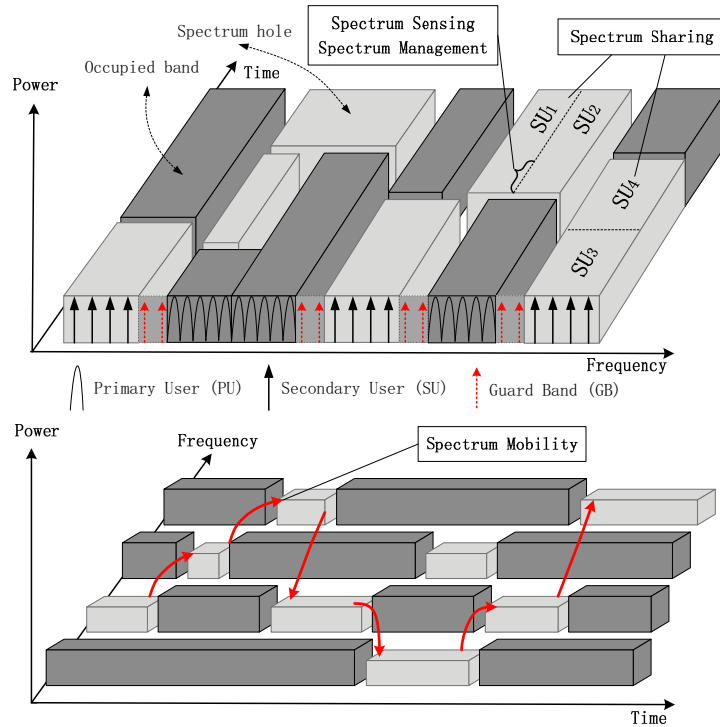
Figure 2.2: A Time-Frequency illustration of basic research tasks in cognitive radio system

achieve this goal, the future CR technology should enable the CR users firstly to accurately identify and intelligently track idle spectrum holes that are dynamic in time, frequency and location, and secondly to select the best available spectrum bands according to user or system requirements. Next, CR users are coordinated to access on the selected spectrum bands with fair spectrum scheduling approaches. Besides, CR techniques should guarantee that a CR user will vacate the channel currently occupied by this CR user when a primary user is detected on this channel, and meanwhile maintain seamless connection by changing over to another spectrum hole. The basic research issues can be summarized below:

Spectrum Sensing

Spectrum sensing is the key element of CR awareness, and plays a critical role on CR communication links since it provides reliable spectrum opportunities for them. The task of spectrum sensing is to determine which part of the licensed spectrum is idle and monitor the reappearance of licensed users. Spectrum sensing should be implemented such that it will result in high reliability in spectrum occupancy decision to guarantee the service quality of licensed system. On the other hand, it is essential for secondary users to establish the state of the spectrum and the nature of the interference

to evacuate immediately if there is a PU active in a band. However, noise and propagation conditions make spectrum sensing a very difficult task. It has been shown that a simple energy detector cannot guarantee the accurate detection of signal presence, therefore more sophisticated spectrum sensing techniques are required.

Spectrum Management

The task of spectrum management is to select the most suitable spectrum to meet user communication requirements over all available spectrum bands. The available spectrum bands detected through spectrum sensing show different characteristics according to not only the time-varying radio environment but also the spectrum band information, e.g. the operating frequency and the bandwidth. In order to capture the best spectrum, the quality of each spectrum hole should be characterized considering such as interference level, link layer delay, channel capacity, holding time interval, etc. The recent work only focuses on spectrum capacity estimation. In order to decide on the appropriate spectrum for different types of applications, it is desirable and still an open research issue to identify the spectrum bands combining all characterization parameters described above.

Spectrum Sharing

Another task in CR networks is spectrum sharing, which is in charge of coordinating access to the selected channels among coexisting secondary users. In spectrum sharing, fair resource allocation methods including interference avoidance need to be developed. However, substantially different challenges exist for spectrum sharing in CR network because of the coexistence with licensed users.

Spectrum Mobility

Spectrum mobility is needed when the following cases arise: CR users pass through the border from one region to the other one, current channel conditions become worse, or a primary user appears. The task of spectrum mobility is to dynamically change the operation frequency of CR users, and thus to maintain seamless communication during the transition to different frequency spectrum. Spectrum mobility gives rise to a new type of handoff in CR networks that we refer to as *spectrum handoff*. In other words, the purpose of spectrum mobility is to make sure that the spectrum handoff is implemented so efficient that a CR user can acquire minimum performance degradation under a non-interfering manner.

Apart from the above research tasks of CR networks, additional research in upper layer and cross-layer is also crucial for the realization of CR networks, more details can refer to [62]. Feasible CR implementation requires significant attention not only to the maturity of theoretical research, but also

to other aspects [68], such as standardization, commercial activities, hardware technique challenges (e.g. agile RF front-end, wideband adaptive filtering and amplification).

After providing a summary description and overview for CR, our focus, in the next section, is on the multi-carrier modulation schemes which are well suited for SSCR system.

2.2   Physical Layer MCM Schemes

The principle of MCM is to transmit data by splitting it into several components, and then send each of these components over separate carrier signals. MCM techniques occupy the overwhelming advantages than the single carrier modulation because of their high data rate, robustness to multipath fading, and enhanced resistance to Inter-Symbol Interference (ISI). Furthermore, MCM can provide a flexible spectrum shaping of the transmitted signal that fills the detected spectrum holes without causing interference to PUs. Another merit of MCM is that its processing structure employed for signal transmission and reception can be reused for spectral analysis. Consequently, spectrum sensing can be performed without any additional cost.

Recent works in CR have proposed the use of OFDM and FBMC, as natural candidates for the physical layer of CR systems [6][14][69]. In [70], Multi-Carrier Code Division Multiple Access (MC-CDMA) is suggested for CR systems when spectrum sensing is not available. Since the CR techniques in this dissertation are discussed in the context of SSCR, only OFDM and FBMC are investigated in the following part, where their pros and cons are listed and compared. Besides, the basic principle of FBMC is elaborated to provide an explicit understanding of this promising MCM technique.

2.2.1   OFDM

OFDM is one of the most widely used MCM technologies in current wireless communication systems and has been intensively studied in the literature. OFDM has also been preferred by many practical applications, e.g. in WLANs with IEEE 802.11n standard, in WMANs with IEEE 802.16e standard, in cellular networks with the 3GPP-LTE (3rd Generation Partnership Project-Long Term Evolution), etc, due to its simple concept, low complexity and minimum latency. Nowadays, OFDM has been proposed as a candidate for the CR systems in [6] because of its high-speed rate and inherent capability to combat multipath fading. These properties are obtained, firstly, by the decomposition of the transmitted signal into several narrow frequency bands, which makes it less sensitive to frequency selectivity, and, secondly, by the extension of the OFDM symbol duration using a Cyclic Prefix (CP) of sufficient length to avoid ISI. Additionally, the Fast Fourier Transform (FFT) as part of the OFDM demodulator can be used for spectral analysis.

However, despite these advantages, a number of shortcomings of OFDM in the application of CR have been presented in [33][71] and solutions to them have been proposed. These shortcomings of OFDM mainly originate from the significant side-lobe of the frequency response of the rectangular pulse shape and the extended CP which reduces spectral efficiency. Orthogonality cannot be guaranteed if adjacent subcarriers are used by non-synchronous users belonging to different OFDM systems, which results in severe interference between PUs and SUs or among SUs. To ease this dilemma, suggestions such as the extension of CP, the application of windowing techniques to suppress the side-lobe, and the usage of guard bands are proposed. Nevertheless, these solutions come at significant overhead and sacrifice an additional portion of time or bandwidth, otherwise these excessive time and frequency allocated to CP and guard bands could be used for data transmission. Other techniques proposed in the literature to reduce the spectrum leakage of OFDM can be found in [72][73]. These techniques achieve significant reduction of adjacent subcarriers interference, but increase the overall system complexity due to additional calculations. Analog or digital filters can suppress the undesirable spectrum portions of the OFDM signals before transmission, but this spectrum mask operation in CR context must be adaptive, which makes the use of filters difficult. In addition, the authors in [15] point out that in the CR setting, OFDM/FFT can lead to significant sensing errors, which is as well due to the large side-lobe of OFDM.

The drawbacks of OFDM in the CR context are listed as follows:

1. A CP is added at the end of each OFDM symbol to handle the channel impulse response, which causes a loss of symbol rate. Furthermore, there is extra overhead due to the guard-bands between the PU and SU transmission channels;

2. OFDM signal is very susceptible to residual frequency offset and timing offset, which results in high sensitivity to Doppler Effect, strict timing and frequency synchronization is required;

3. To implement spectrum sensing without additional cost, FFT as spectral analyzer cannot provide a high spectral dynamic spectrum range [1], thus OFDM cannot fulfill the prescribed out-of-band rejection specification of FCC [1]. Moreover, the significant spectral leakage among frequency subbands leads to serious influence on the performance of the spectrum sensing;

4. It requires block processing to maintain orthogonality among all the subcarriers, which is a major limitation to scalability;

5. Another drawback of OFDM is the increase of the Peak-to-Average Power Ratio (PAPR) that causes nonlinearities and clipping distortion;

---

[1]Here dynamic spectrum range refers to the difference between the weakest and the strongest signal which can be detected simultaneously by the estimator.

2.2.2 FBMC

It is worth noting that the influence of large side-lobe of OFDM is not important for the CR system in which its standard does not support Frequency Division Multiple Access (FDMA) operation (i.e. different clusters of subcarriers are allocated to different users), or in which the standard regulates sufficient guard bands to protect primary users, e.g. the FCC requires IEEE 802.22 to maintain large guard bands to adjacent TV channels. However, once the FDMA operation is adopted in a CR system with strict guard-band limitation, the aforementioned shortcomings of OFDM are likely to turn out to be significant. FBMC, to a large extent, inherits the benefits of OFDM, while exhibiting the potential to significantly enhance the spectral efficiency of the radio interface. Consequently, the attempts to overcome the limitations of OFDM in CR systems have promoted the development of FBMC.

There are mainly three FBMC techniques that have been studied in the literature: Offset Quadrature Amplitude Modulation (OQAM), Cosine Modulated multiTone (CMT), and Filtered MultiTone (FMT). Initial FBMC technique is referred to as OQAM, which is originally investigated in [74][75]. As opposed to OFDM, which transmits complex-valued symbols at a given symbol rate, OQAM transmits real-valued symbols by introducing a half symbol space delay between the in-phase and quadrature components of QAM symbols, it is possible to achieve a baud-rate spacing between adjacent subcarrier channels and recover the information symbol, free of ISI and Inter-Carrier Interference (ICI). Further progress is made by Hirosaki [76], who shows that the transmitter and receiver part of this modulation method can be implemented efficiently in a polyphase Discrete Fourier Transform (DFT) structure. More developments about OQAM can be found in [8]~[13].

Other FBMC techniques are motivated by the advanced Digital Subscriber Line (DSL) technology to better suit DSL channels. CMT using cosine-modulated filter banks is an early FBMC technique developed in DSL area [77][78], and has recently been applied to wireless applications. CMT owns high bandwidth efficiency and the capability for blind detection [78] owing to special structure of the underlying signals. When multiple adjacent bands are used for transmission, overlapped adjacent bands can be separated perfectly thanks to the reconstruction property of CMT. As well, FMT is an another FBMC technique originally developed for DSL applications [79]. Compared to CMT, which allows for overlapping of adjacent bands, the subcarrier bands in FMT are non-overlapping. Thus, the main difference between CMT and FMT lies in the way the spectral band is used. In FMT, different subcarrier signals can be separated by conventional filtering. In CMT, however, the overlapping subcarrier bands should be separated through sophisticated design of filtering, i.e. FMT allowing for easy and flexible handling of signals at the receiver may be attractive from an implementation point of view. As for CMT, in contrast, can offer higher bandwidth efficiency and blind detection capability.

2. OVERVIEW OF CR AND MCM TECHNIQUES

To conclude, the above three FBMC techniques could all theoretically offer a significant bandwidth efficiency advantage over OFDM due to their special filter bank based structure and the elimination of CP. In practice, the modulated signals need to be amplified by a non-linear power amplifier before to be transmitted, the authors in [80] propose a comparison between OFDM and FBMC using different types of memoryless power amplifiers. The numerical results show that FBMC can always obtain a better containment of the out-of-band energy than OFDM even if this advantage is partially reduced in the presence of a non-linearity. On the other hand, among different FBMC techniques, OQAM is preferred to be a suitable choice for CR applications in [81], where the performance of FMT, CMT and OQAM for CR networks are compared, and the conclusion is drawn that OQAM presents highest stopband attenuation among the three FBMCs for a fixed filter length and number of subcarriers. Moreover, FMT and CMT are originally introduced for DSL applications, and will be impractical and hard to meet the CR system requirements.

The discussion in this dissertation, therefore, mainly devotes to the use of OQAM based on filter bank theory for CR applications. The OQAM based transmission structure is introduced in the following.

The principle of OQAM is to divide the transmission flow into M independent transmission using M subcarriers. An introduced orthogonality condition between subcarriers guarantees that the transmitted symbols arrive at the receiver free of ISI and ICI, which are achieved through time staggering the in-phase and quadrature components of the subcarrier symbols by half a symbol period. Fig. 2.3 shows the OQAM based transmission system, which contains a Synthesis Filter Bank (SFB) at the transmitter and an Analysis Filter Bank (AFB) at the receiver.

At the transmitter, the input symbols are assumed to be complex-valued

$$x_k^l = a_k^l + j b_k^l \tag{2.1}$$

where a_k^l and b_k^l are respectively the real and imaginary part of the lth symbol in the kth subcarrier. The input signals to the synthesis filter bank at the kth subcarrier and the l'^{th} symbol are generated according to the offset QAM modulation rule

$$In\_SFB_k(l') = \begin{cases} a_k^{\frac{l}{2}} & if \quad k = even, l = even \\ j b_k^{\frac{l-1}{2}} & if \quad k = even, l = odd \\ j b_k^{\frac{l}{2}} & if \quad k = odd, l = even \\ a_k^{\frac{l-1}{2}} & if \quad k = odd, l = odd \end{cases} \tag{2.2}$$

Instead of a rectangular shape filter, a longer prototype filter is adopted in OQAM systems. It is possible to perform a filtering using a filter bank composed of a FFT and a polyphase filtering according to polyphase decomposition theory. Assuming $H(Z)$ is the transfer function of the prototype
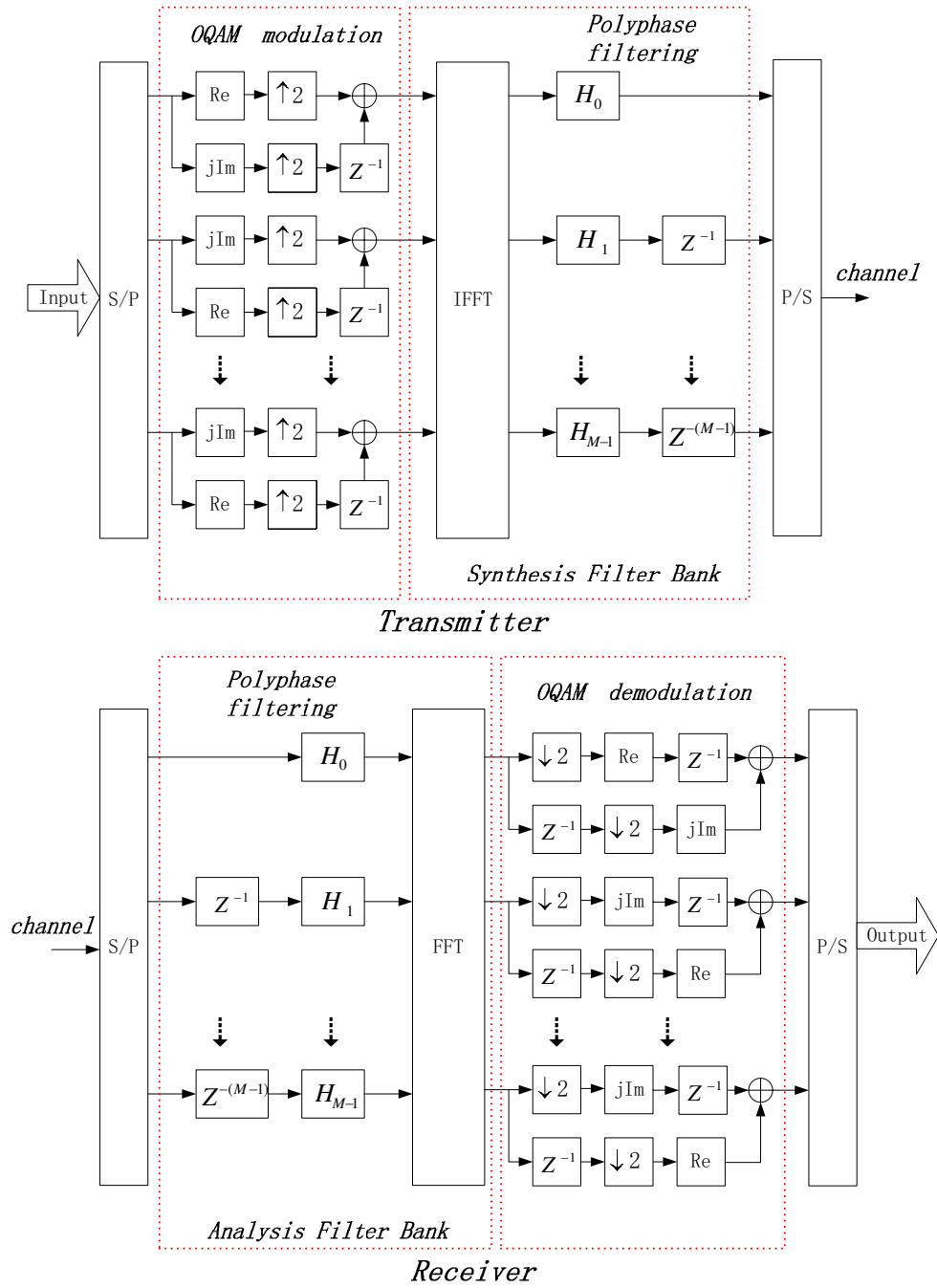
Figure 2.3: OQAM based transmission system

filter $h(n)$, using the polyphase decomposition, we have

$$H(Z) = \sum_{n=0}^{LM-1} h(n)Z^{-n} = \sum_{m=0}^{M-1} H_m(Z^M)Z^{-m} \tag{2.3}$$

where

$$H_m(Z^M) = \sum_{l=0}^{L-1} h_{lM+m}Z^{-lM} \tag{2.4}$$

where L denotes the overlapping factor of the prototype filter.

An uniform filter bank is obtained by shifting the response of a prototype on the frequency axis. At the transmitter side, we can write the transfer function of the mth filter as

$$B_m(Z) = H\left(Ze^{-j2\pi\frac{m}{M}}\right) = \sum_{m'=0}^{M-1} H_{m'}(Z^M)e^{j2\pi\frac{mm'}{M}}Z^{-m'} \tag{2.5}$$

Considering all the shifts by multiples of $1/M$ and the associated filters, a matrix equation for SFB is obtained as displayed in (2.6), where $W = e^{-j2\pi/M}$, and the square matrix is the inverse discrete Fourier transform matrix of order M. The structure of (2.6) is shown in Fig. 2.3, and it is referred to as synthesis filter bank.

$$\begin{bmatrix} B_0(z) \\ B_1(z) \\ \vdots \\ B_{M-1}(z) \end{bmatrix} = \begin{bmatrix} 1 & 1 & \dots & 1 \\ 1 & W^{-1} & \dots & W^{-(M-1)} \\ & \vdots & & \vdots \\ 1 & W^{-(M-1)} & \dots & W^{-(M-1)^2} \end{bmatrix} \begin{bmatrix} H_0(Z^M) \\ Z^{-1}H_1(Z^M) \\ \vdots \\ Z^{-(M-1)}H_{M-1}(Z^M) \end{bmatrix} \tag{2.6}$$

At the receiver side, we can write the transfer function of the mth filter as

$$B_m(Z) = H\left(Ze^{j2\pi\frac{m}{M}}\right) = \sum_{m'=0}^{M-1} H_{m'}(Z^M)e^{-j2\pi\frac{mm'}{M}}Z^{-m'} \tag{2.7}$$

Considering all the shifts by multiples of $1/M$ and the associated filters, in the same way the matrix equation for AFB is obtained as displayed in (2.8), where $W = e^{-j2\pi/M}$, and the square matrix is the discrete Fourier transform matrix of order M. The structure of (2.8) is shown in Fig. 2.3, which is referred to as analysis filter bank because it performs a frequency decomposition of the input signal.

$$\begin{bmatrix} B_0(z) \\ B_1(z) \\ \vdots \\ B_{M-1}(z) \end{bmatrix} = \begin{bmatrix} 1 & 1 & \dots & 1 \\ 1 & W & \dots & W^{M-1} \\ & \vdots & & \vdots \\ 1 & W^{(M-1)} & \dots & W^{(M-1)^2} \end{bmatrix} \begin{bmatrix} H_0(Z^M) \\ Z^{-1}H_1(Z^M) \\ \vdots \\ Z^{-(M-1)}H_{M-1}(Z^M) \end{bmatrix} \tag{2.8}$$

A simple postprocessing can be identified as an OQAM demodulation. The received symbols at the kth subcarrier and the lth symbol are generated from the output of the analysis filter bank according to the rule as displayed below

$$Out\_Sym_k(l) = \begin{cases} Re\Big[Out\_AFB_k(2l)\Big] + jIm\Big[Out\_AFB_k(2l+1)\Big] & if \quad k = even \\ jIm\Big[Out\_AFB_k(2l)\Big] + Re\Big[Out\_AFB_k(2l+1)\Big] & if \quad k = odd \end{cases} \tag{2.9}$$

where $Out\_AFB_k(l)$ denotes the output signal of the analysis filter bank at the kth subcarrier and the lth symbol.

In the literature, various prototype filters $h(n)$ are designed for their corresponding applications. In this dissertation, we use the prototype filter advocated in the European project PHYDYAS [9][19], which will be introduced in the following section.

The impulse response of PHYDYAS prototype filter with an overlapping factor $L = 4$ and $M = 512$ subcarriers is presented in Fig. 2.4. Assuming $N = LM$ is the number of prototype filter coefficients, and the prototype function $h(n)$ is symmetric around $Ł^{th}$ coefficient ($Ł = \frac{N}{2} + 1$), i.e. $h(n) = h(N + 2 - n), n = 2, 3, \cdots, N$ and $h(1) = 0$. The specific PHYDYAS filter coefficients in the time and frequency domains can be found in [9]. The frequency responses of OFDM and PHYDYAS prototype filter are compared in Fig. 2.5. We can see that OFDM subcarrier suffers from high side-lobe radiation as opposed to PHYDYAS filter bank.

In contrast to OFDM, OQAM technique has somewhat higher implementation complexity, together with the higher conceptual complexity and unfamiliarity to the engineering community. However, in the projet PHYDYAS [19], which will be presented in the next section, it has been demonstrated that the implementation complexity of FBMC is still acceptable. In addition to the implementation complexity, FBMC has the following salient features:

1. No cyclic prefix is needed and small guard-bands are sufficient to suppress cross-channel interference, therefore full capacity of the transmission bandwidth can be achieved using OQAM;

2. Due to its low side-lobe radiation, FBMC is much more insensitive to timing offset than classical OFDM. Furthermore, FBMC is less sensitive to residual frequency offset, which shows higher robustness to Doppler Effect;

3. The same device can be used for spectrum sensing and reception simultaneously, and the high resolution spectrum analysis capability of filter banks can be exploited for CR systems, which is proved in [15][16] that filter banks can obtain much larger dynamic spectrum range than the conventional FFT. Thus, the probability of undesirable collisions between secondary users and primary users is greatly reduced;
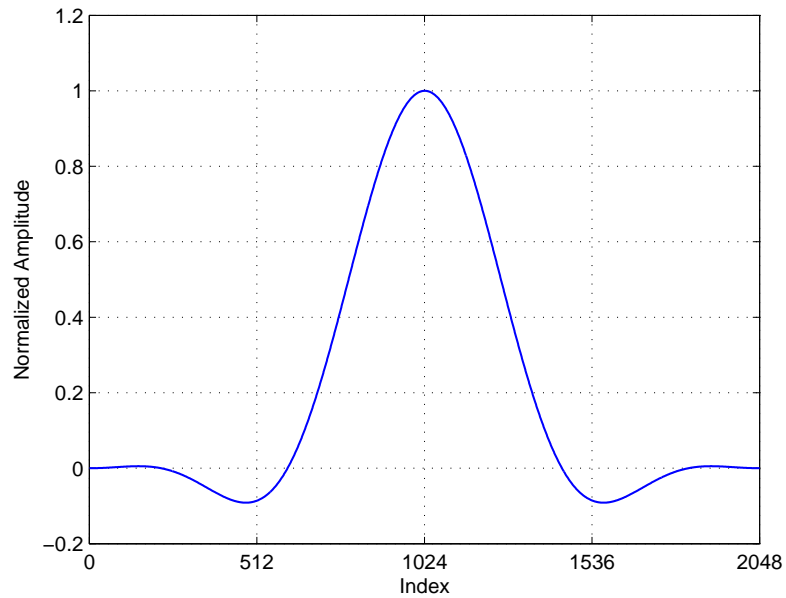
Figure 2.4: Impulse response of PHYDYAS prototype filter
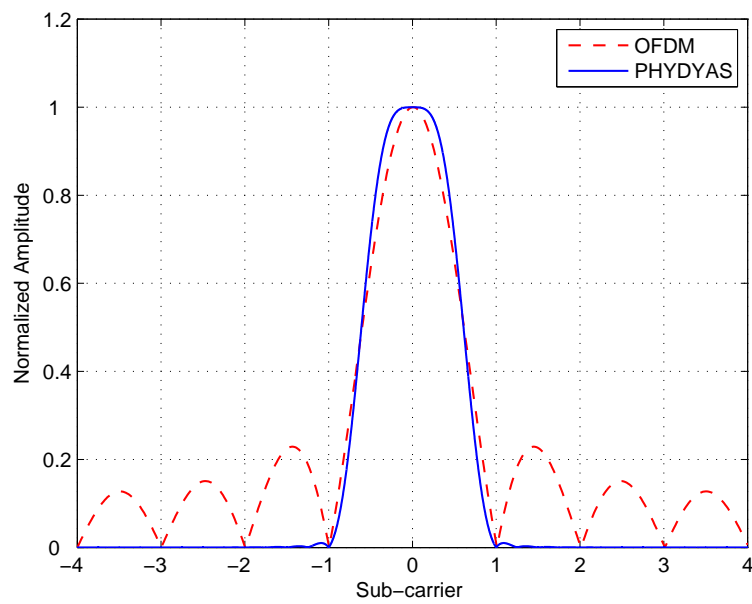
Figure 2.5: Frequency responses of OFDM and PHYDYAS prototype filter

4. OQAM divides the transmission channel of the system into a set of subchannels and each subchannel overlaps only with its neighbors. Subchannels can be grouped into independent blocks, which is crucial for scalability and dynamic access;

5. The PAPR characteristics of OFDM and FBMC are quite similar [82];

The polyphase filtering blocks replaces the blocks for prefix insertion / suppression used in OFDM terminals as shown in Fig. 2.3. It is seen that the FFT is common to both OFDM and OQAM, which is an important aspect for the compatibility issues. For simplicity, the term FBMC instead of OQAM will be used in the remainder of this dissertation.

2.3   PHYDYAS Project

PHYDYAS project [19] is an European project, which has a duration of 30 months [1] and has 13 consortium members consisting of academic teams, industrial partners and non-profit research organizations. The objective of PHYDYAS project is to propose FBMC as the CR physical layer candidate for future dynamic spectrum access and CR systems because traditional OFDM scheme is lack of flexibility and has poor spectral resolution. In contrast, FBMC can offer high spectrum resolution and provide independent sub-channels, while enhancing the high data rate capability. All of these advantages of FBMC technique fulfil the requirements of the new dynamic spectrum access and CR concepts.

Appropriate algorithms have been developed to cope with many situations, particularly fast initialization, equalization, single and multi-antenna processing. Other issues are the study of duplexing and multiple access techniques, interference management and cross-layer optimization in the FBMC context. The compatibility with OFDM is also an important work item in view of the smooth evolution of networks. Overall, three parts are distinguished: research in signal processing, research in communication and design and realization of the hardware/software demonstrator. These efforts have been carried out at the European level, in order to benefit from the vast amount of knowledge and experience available and make the time scale compatible with the on-going or planned standardization actions. The consortium has a strong academic participation, whose mission is to deliver the best methods and the most efficient algorithms. The industrial partners bring their experience in communication infrastructure design and deployment, in instrumentation and measurements and in circuit design. Non-profit research organizations facilitate the cooperation between academic and industry partners.

---

[1]The project started in 2008, January.

The most prominent impact of the project is to trigger the migration of radio systems from OFDM to a new FBMC based physical layer. Since several members of the consortium also are members of some standardization groups, this project has a direct impact on the future standard. Furthermore, the project has not only reinforced European industrial leadership in wired and wireless networks, but also stimulated and strengthened the European research in cognitive radio. In the perspective of the world, the success of the proposed physical layer has contributed to the dissemination and exploitation of the new radio concepts on a global scale.

2.4   Conclusion

Digital filter banks are occupying a progressively important role in both wireline and wireless communication systems. So far, some attempts have been made to introduce FBMC in the CR communications area, in particular, the Isotropic Orthogonal Transform Algorithm (IOTA) [17][18]. In [14], FBMC has been recommended as a physical layer candidate for CR systems, and has been investigated as a potential physical layer for future dynamic spectrum access and cognitive radio in the European project PHYDYAS [19].

As a physical layer candidate of CR networks, FBMC has the following advantages. Firstly, cyclic prefix is no longer required in the FBMC scheme in order to get high spectral efficiency, and FFT as in OFDM is completed by adding a polyphase filtering. The stop-band attenuation of each subcarrier can be controlled by designing the prototype filter with low side-lobe. In [15], the authors propose the use of FBMC to ease the leakage problem of OFDM due to its high robustness to residual frequency offsets by taking advantage of the low spectral leakage property of prototype filters. Because of its low spectrum leakage, FBMC has the advantage of feeding certain spectrum holes with certain transmission power resulting in no interference on the adjacent subcarriers that are occupied by PUs. Moreover, the additional polyphase filtering for communication can be reused for spectral analysis, and which can obtain larger dynamic spectrum range than OFDM/FFT.

The capabilities of FBMC for spectrum shaping and spectrum sensing well meet the essential requirements of SSCR, therefore, FBMC techniques are considered to be particularly suitable for CR physical layer transmission. The objective of this dissertation is to propose and investigate OQAM, one of promising FBMC techniques for the future CR systems. It is believed that FBMC will play an important role in realizing the concept of CR by providing an efficient, adaptive, and scalable technology because of its attractive features. Next chapter of this dissertation will deal with *spectrum sensing*, one of the key research issues of an SSCR system.

Spectrum Sensing

The objective of Cognitive Radio (CR) is to improve the efficient use of the spectrum by sensing the existence of spectrum holes. Therefore, spectrum sensing is the key technique to identify the unused frequency bands for access by the Secondary User (SUs), and to ensure that SUs would not interfere with Primary Users (PUs). In order to efficiently utilize the available spectrum opportunities, SUs are required to sense frequently the spectrum while minimizing the latency time spent in sensing.

In some cases, there exists the possibility of failing to detect primary activities due to channel fading and significant interference. To overcome this problem, IEEE 802.22 standardization is currently considering the network assisted detection by providing the continuously-updated spectrum usage tables or placing beacons in primary signals. However, in CR context, the PUs and SUs cannot necessarily exchange information. In this case, secondary nodes need to estimate the spectrum environment without assistance of primary system.

Reliable detection without assistance is mainly affected by two reasons: *silent receiver* and *hidden transmitter*. Specifically, the location of primary receivers are unknown due to the absence of signalling between primary receivers and the SUs, so it is very difficult for a CR terminal to have a direct measurement of a channel between a primary receiver and a secondary transmitter. Few research is focused on the detection of primary receivers [83], most of recent works focus on primary transmitter detection based on local observations of CR users. On the other hand, a CR terminal cannot detect a primary transmitter signal in the case of hidden transmitter (i.e. which is blocked by some obstacles), then the transmission of CR users will cause interference to the primary receiver. A robust approach so-called cooperative sensing is proposed for this hidden terminal problem by exchanging information among several CR terminals. The cooperative sensing decreases the probabilities of missing detection and false alarm considerably, and it can also decrease sensing time.

Primary receiver detection and cooperative detection are beyond the scope of this dissertation, where only primary transmitter detectors are investigated. In the following, a state of the art of transmitter detectors is summarized in *Section 3.1* together with their comparison. Next, two individual contributions are presented. Firstly, a Cyclostationary Signature (CS) based detector is proposed for Multi-Carrier Modulation (MCM) signal detection in *Section 3.2*, and we compare this CS detector

with traditional energy detector. Secondly, *Section 3.3* presents a multi-band detection architecture based on polyphase filter bank, which outperforms the FFT based multi-band detection.

3.1 State-of-The-Art of Transmitter Detectors

There are a number of spectrum sensing techniques proposed and theoretically analyzed for primary transmitter detection in the literature. The general approach of spectrum sensing is very difficult to draw up, and specific methods must be found according to the practical applications. To the best of our knowledge, there are four main signal detection techniques: matched filter, energy filter, higher order statistic, and cyclostationary feature detector [84][85][86].

The goal of our study in various sensing methods is to find a suitable detection method for CR application, where the following criteria require to be considered:

- *Criterion 1*: Minimum detectable signal levels and required sensing time to achieve the desired probabilities of detection and false alarm;

- *Criterion 2*: Robustness to noise uncertainty and background interference;

- *Criterion 3*: Implementation complexity and feasibility;

We motivate the strong need for sophisticated sensing techniques to satisfy the above three conditions. In the rest of this section, we introduce the aforementioned four detection methods by specifying their advantages and drawbacks, and characterize these detection methods by means of the above three criteria.

3.1.1 Matched Filter

Matched filter based spectrum sensing maximizes the received Signal to Noise Ratio (SNR) and performs optimal detection [87]. The main advantage of matched filter is that it can achieve high processing gain with the sensing time scale $\mathcal{O}(1/SNR)$ to meet a given probability of detection constraint [88]. If the number of samples used in sensing is not limited, this coherent detector can meet any desired probabilities of detection and false alarm simultaneously. Thus, given enough samples, arbitrary weak signals can be detected. Another advantage of matched filter is its capability to distinguish the primary signal from the interference and noise. Besides, it has low complexity and high agility. Most practical wireless network systems have pilots, preambles, or synchronization words (e.g. narrowed pilot in TV signals, dedicated spreading codes in CDMA systems, preamble words in OFDM systems), which can be utilized for coherent detection. As a result, if CR users have the sufficient knowledge on the primary signal, then a matched filter will be the optimal choice.

However, the benefit of high processing gain comes at the cost of knowing *a priori* knowledge of transmitted primary signal for demodulation, such as modulation scheme and order, pulse shaping, packet format, center frequency, etc. Moreover, timing synchronization, carrier synchronization, even channel equalization are indispensable for coherent demodulation. In the presence of frequency offset, matched filter has limitation on sensing time and detectable signal levels. Additionally, a significant drawback of a matched filter is that each CR terminal needs a special receiver for each primary transmitter class.

According to the aforementioned advantages and drawbacks of matched filter method, we can summarize its characteristic corresponding to the three criteria:

- *Criterion 1*: If the number of samples used in sensing is not limited, this detector can meet any desired probabilities of detection and false alarm;

- *Criterion 2*: It is robust to noise uncertainty and background interference;

- *Criterion 3*: Since the received signal may be totally unknown to the CR terminal, moreover, perfect carrier and timing synchronization are necessary, it has complex implementation structure and unrealistic feasibility in the context of CR;

3.1.2 Energy Detector

In some cases, an optimal detector based on matched filter is not an option since it requires *a priori* knowledge and perfect synchronization for coherent demodulation. Instead, a suboptimal and non-coherent energy detector also known as the radiometer [89] is adopted. In other words, if the CR terminal has no sufficient information about the primary user signal (e.g. if the power of the Gaussian noise is the only information known to the CR terminal), the optimal option will be an energy detector. Energy detector simply measures the energy of the input signal over a specific time interval. By knowing the noise variance, the obtained detection performance are satisfactory. Due to the negligence of signal structure information, which is considered by matched filter detector, energy detector needs longer detection time with the sensing time scale $\mathcal{O}(1/SNR^2)$ to achieve a given detection requirement [88]. Another advantage of the energy detector is its simple implementation structure, which benefits from the fact that it requires no prior knowledge of the current operating systems.

Despite the implementation simplicity and the applicability for various signals make the energy detector a favorable candidate, there are several drawbacks that might constrain the use of this detector. Firstly, a threshold used for primary user detection is highly susceptible to unknown or changing noise levels, fading, and channel interference. In practice, the quality of energy detection is strongly degraded due to noise power uncertainty, thus the main difficulty is to obtain a good estimate of the

variance of the noise. However, noise is an aggregation of various sources including the local thermal noise and the environment noise. The local thermal noise can vary over time owing to temperature variation, ambient interference, filtering, etc. The environment noise, which is an aggregation of random signals from various sources in the environment, also varies over time. Furthermore, there is always an estimation error due to limited amount of time. Thus, it is practically impossible to estimate the exact noise power. Even if noise power level is exactly estimated, in frequency selective fading it is intractable to set the threshold with respect to channel notches, and the presence of any in-band interference would also confuse the decision of energy detection. Consequently, the energy detector is prone to false detections at low SNR levels triggered by noise and interference uncertainties. Secondly, energy detector cannot discriminate between modulated signals, noise and interference but can only determine the presence of the signal, which means it cannot distinguish between the spectrum usage of the primary users and that of the other secondary users. Lastly, an energy detector does not work well for direct sequence spread signals and wideband frequency hopping signals.

In any case, energy detector is a good option when the CR terminal knows nothing about the primary signal or when implementation complexity is the main concern. More sophisticated detectors could be invented if additional information on primary user signal can be exploited.

We conclude the characteristic for energy detection method:

- *Criterion 1*: Signals can be detected at a SNR level as low as desired, provided the detection interval is long enough and the noise power level is perfectly known. However, the disadvantage suffering from noise and interference uncertainties puts limits on minimum detectable signal levels, and an increased sensing time is needed in this case;

- *Criterion 2*: It is highly susceptible to noise uncertainty and background interference. In most of practical situations, noise power is difficult to be estimated by the CR terminal;

- *Criterion 3*: It is a versatile detector with simple processing requirement, i.e. it can be applied for any signal type detection and does not involve complicated signal processing. However, it cannot differentiate signals, noise and interference. Therefore, it has low implementation complexity and limited feasibility;

3.1.3 Higher Order Statistic

During the past few years, there has been an increasing interest in applying Higher Order Statistics (HOSs) in many fields including the telecommunication. These statistics, known as *cumulants* [1] [90], and their associated Fourier transforms, known as *polyspectra*, not only reveal the amplitude

---

[1] The kth order cumulants is defined in terms of its joint moments of orders up to k, and the explicit relationship between cumulants and moments can be referred in [90].

information about a process, but also its phase information. Thus, cumulant-based signal processing methods which preserve the phase information, can handle Gaussian measurement noise automatically. In other words, HOSs are applicable for distinguishing the Gaussian noise and non-Gaussian signals. Many practical applications are truly non-Gaussian, for instance, experimental studies have confirmed that certain signals such as seismic reflectivities, electromagnetic interference, are non-Gaussian. HOSs, therefore, can be used to detect these non-Gaussian signals corrupted by Gaussian noise.

Since most of the theoretical results of HOS are scattered in the literature, a gathering of new theoretical results which are associated with HOSs in signal processing is collected in [90], which also demonstrates the utility of HOSs to practical problems. Some efforts using HOSs for detection, classification, and pattern recognition can be found in [91][92]. The goal in [91] is to discriminate single-carrier modulations from multi-carrier modulation of OFDM type. Because the single-carrier modulations are generally non-Gaussian and multi-carrier modulations are asymptotically Gaussian, then the problem is equivalent to the discrimination between Gaussian OFDM and non-Gaussian modulation signals. A detector using the HOS test based on fourth-order cumulants is therefore proposed for this discrimination. Similarly, the authors in [92] deal with the modulation classification of 4-state phase shift keying and 16-state quadrature amplitude modulation using a pattern recognition approach. The discriminating feature is build as an optimized combination of fourth and second order moments in order to maximize the probability of correct classification.

Finally, we conclude the characteristic for HOSs:

- *Criterion 1*: The processing time is proportional to the number of sampled data. It can achieve a good detection performance at a low SNR;

- *Criterion 2*: It is robust to noise uncertainty and background interference;

- *Criterion 3*: Computational complexity depends on the number of data samples, and no prior knowledge about primary users is needed. However, the application of HOSs in CR context is limited to differentiate the additive measurement noise (Gaussian) and non-Gaussian signals, it is not feasible for detecting different Gaussian signals (e.g. MCM signals and Gaussian noise);

3.1.4 Cyclostationary Feature Detector

An alternative detection method is the cyclostationary feature detection [95]. A cyclostationary detector can improve the performance over an energy detector by exploiting the built-in periodicity in the modulated signals. Modulated signals are usually aligned with sine wave carriers, hopping sequences, pilots, preamble sequences, repeating spreading, etc, which result in spectral correlation.

This means that their statistics can be described by cyclostationary processing. Normally, the analysis of stationary signals is based on the autocorrelation function and the power spectral density. However, the power spectral density is a one-dimensional function of frequency. While cyclostationary behavior, which can be exploited by a related function named *spectral correlation function*, is a complex-valued, two-dimensional function. The main advantage of this spectral correlation function is that it differentiates the noise energy from modulated signal energy, which relies on the fact that the noise is a wide-sense stationary signal with no spectral correlation, while modulated signals exhibit cyclostationarity due to the embedded periodicity. Moreover, different types of modulated signals could have very different spectral correlation features. This cyclostationary detector can thus be applied for the detection of a random signal with a specific modulation type in a background of noise and other modulated signals. Due to its noise rejection property, a cyclostationary feature detector can perform better than the energy detector in discriminating against noise even in very low SNR region. The FCC [1] has suggested the cyclostationary feature detector as a useful alternative to enhance the detection sensitivity in CR networks.

However, it is computationally complex and requires significantly long observation time. Besides, we generally assume that the period of the primary signal is known to the CR terminal. This assumption is reasonable in the early stage of CR application, such as in the TV bands, this information is open to CR users and the characteristics of the primary signals are well known to the public. In the future, CR will be allowed to work in a wide spectrum band, the periods of some modulated primary signals may be unknown to CR users. In this case, an exhaustive search of the cyclic frequencies is needed in cyclostationary detection. This means huge complexity and the loss of the capability to differentiate the primary signal from the interference that is also cyclostationary.

According to the above information, the characteristic for cyclostationary feature detector is therefore concluded as below:

- *Criterion 1*: Since it is not sensitive to noise uncertainty, it can achieve a good detection performance even at a very low SNR but needs long sensing time interval;

- *Criterion 2*: It is robust to noise uncertainty and background interference;

- *Criterion 3*: It well matches the requirement for identity sensing in CR systems. It needs additional implementation structure and complex computation if the period of primary signal is unknown. Therefore, it has a little high implementation complexity but with realistic feasibility;

3.1.5 Conclusion

Different detectors are applicable to different system scenarios and have different properties. Some spectrum sensing algorithms are fast and have a low-complexity. Others provide high sensitivity and reliability, but use more computational resources and may require longer detection intervals. In conclusion, the energy detector is the simplest and quite robust at high SNR. It does not require *a priori* knowledge of the primary signal and works for any signal type. Therefore, it is suitable for the scenario in which the CR user know nothing about the primary signal. In order to implement the identity sensing, it is vital for a detector to be able to differentiate the primary signal from the interference and noise. In practice, such differentiation can be realized if some *a priori* knowledge of the primary signal is known to the CR user. Depending on what types of information the CR user knows about primary signal, different detectors can be applied under different system scenarios. A cyclostationary feature detector is suitable when the period of the primary signal is known. A matched filter is suitable when the pilot signal of the primary system is known. The more the CR user knows about the primary signal, the better the detector works. For example, the characteristics of the digital TV signal in IEEE 802.22 WRAN, are usually well known, and therefore matched filter or cyclostationary detector can be applied for spectrum sensing. Some blind sensing methods without any prior information can refer to [93][94].

In the context of CR, the spectrum sensing functionality consists of: *occupancy sensing* and *identity sensing*. Occupancy sensing is to detect the spectrum occupancy in the local area and identify the idle spectra and occupied spectra, and energy detectors can be applied for this purpose. Identity sensing is to distinguish among the licensed usage by primary users, the opportunistic usage by other CR users, and background noise. Such distinction is crucial in a CR scenario with dense CR users. A cyclostationary detector can be applied to treat noise, interference, and other secondary users differently. In the next section, the cyclostationary detector based on cyclostationary signature for detecting MCM signals is investigated.

3.2 Cyclostationary Signature Detector

Spectral correlation theory for cyclostationary time-series signals has been studied for decades. Explicit formulas of spectral correlation function for various types of analog modulated and digital modulated signals are already derived [20][21].

In this section, we investigate and exploit the cyclostationarity characteristics for two kinds of MCM signals: conventional OFDM and FBMC signals. The spectral correlation characterization of MCM signals can be described by a special Linear Periodic Time-Variant (LPTV) system. Using

this LPTV description, we have derived the explicit theoretical formulas of nonconjugate and conjugate Cyclic Autocorrelation Function (CAF) and Spectral Correlation Function (SCF) for OFDM and FBMC signals. According to theoretical spectral analysis, Cyclostationary Signatures (CSs) are artificially embedded into MCM signal and a low-complexity signature detector is therefore presented for detecting MCM signal. Theoretical analysis and simulation results demonstrate the efficiency and robustness of this CS detector compared to traditional energy detector.

3.2.1 Introduction

The main objective of this section is to obtain the general formulas for calculating the CAF and SCF of MCM signals using a common derivation model. A particularly convenient method for calculating the CAF and SCF for many types of modulated signals is to model the signal as a purely stationary waveform transformed by a LPTV transformation [95][96]. Multicarrier modulated signal can be regarded as a special model with the multi-input transformed by LPTV transformation and one scalar output. By modeling MCM signal into a LPTV system it is convenient to analyze MCM signal using the known LPTV theory. With the help of the mature LPTV theory, herein we derive the explicit formulas for nonconjugate and conjugate cyclic autocorrelation function and spectral correlation function of OFDM and FBMC signals, which are very useful for blind MCM signals detection and classification.

We are interested in various efficient (i.e. low Signal to Noise Ratio (SNR) detection requirement of licensed signal) and low-complex methods for the detection of free bands at the worst situation that we only know few information about the received signal. Cyclostationary based detector is efficient and more robust than energy detector [89], which is highly susceptible to noise uncertainty. In most of practical situations, it is not very likely that the cognitive radio has access to the nature of licensed signal, hence rendering noise estimation impossible. The worse thing is that energy detector can not differentiate between modulated signals, noise and interference. Feature detector such as cyclostationarity is, therefore, proposed for signal detection in CR context. An inherent cyclostationary detection method, by detecting the presence of nonconjugate cyclostationarity in some non-zero cyclic frequency, is proposed in [22]. Although this detector exhibits good detection performance, it can't achieve the low SNR requirement of CR system specified by FCC. In addition, the computation of the proposed cyclostationarity detection algorithm is complex.

Therefore, in order to alleviate the computation complexity and achieve better detection performance for low SNR level, we apply a conjugate cyclostationarity detector by inserting Cyclostationary Signature [97] (CS), which is realized by redundantly transmitting message symbols at some predetermined cyclic frequency based on the theoretical spectral analysis and the fact that most of the MCM

signals and noise don't exhibit conjugate cyclostationarity. Previous works introducing artificially cyclostationarity for OFDM signal at the transmitter can be found in [97][98][99].

In this section, the signal detection between FBMC signal and noise is investigated. We implement the spectral detection of FBMC signal embedded by CS using a low-complexity conjugate cyclostationarity detector considering both Additive White Gaussian Noise (AWGN) and Rayleigh fading environments in the CR domain. Experimental results are provided to show the efficiency and the robustness compared to the traditionary energy detector.

The remainder of this section is organized as follows: *Section 3.2.2* presents the basic definition of spectral correlation. The fundamental concepts of LPTV system are mentioned in *Section 3.2.3*. Through the aforementioned theoretical knowledge, *Section 3.2.4* analyzes and derives the theoretical formulas of nonconjugate and conjugate cyclic autocorrelation and spectral correlation functions of OFDM and FBMC signals. In *Section 3.2.5*, corresponding spectral analysis for FBMC signals with CS is investigated. A low-complexity CS detector is presented in *Section 3.2.6*. Simulation results are given in *Section 3.2.7*. Finally, conclusions are drawn in *Section 3.2.8*.

3.2.2   Definition of Cyclic Spectral Correlation

A complete understanding of the concept of spectral correlation is given in the tutorial paper [96]. This section is a very brief review of the fundamental definitions for spectral correlation.

The probabilistic nonconjugate autocorrelation of a stochastic process $x(t)$ is

$$R_x(t, \tau) = \mathbb{E}\Big[x(t + \tau/2)x^*(t - \tau/2)\Big] \tag{3.1}$$

where the superscript asterisk denotes complex conjugation. $x(t)$ is defined to be second-order cyclostationary (in the wide sense) if $R_x(t, \tau)$ is a periodic function about t with period T_0 and can be represented as a Fourier series

$$R_x(t, \tau) = \sum_{\alpha} R_x^{\alpha}(\tau)e^{j2\pi\alpha t} \tag{3.2}$$

which is called *periodic autocorrelation function*, where the sum is taken over integer multiples of the fundamental frequency $1/T_0$. The Fourier coefficients can be calculated as

$$R_x^{\alpha}(\tau) = \lim_{T \to \infty} \frac{1}{T} \int_{-\frac{T}{2}}^{\frac{T}{2}} R_x(t, \tau)e^{-j2\pi\alpha t}dt \tag{3.3}$$

where $\alpha = integer/T_0$, and $R_x^{\alpha}(\tau)$ is called the *cyclic autocorrelation function*. The idealized *cyclic spectrum function* can be characterized as the Fourier Transform

$$S_x^{\alpha}(f) = \int_{-\infty}^{\infty} R_x^{\alpha}(\tau)e^{-j2\pi f\tau}d\tau \tag{3.4}$$

3. SPECTRUM SENSING

In the nonprobabilistic approach, for a time-series $x(t)$ that contains second-order periodicity, synchronized averaging applied to the lag product time-series $y(t) = x(t + \tau/2)x^*(t - \tau/2)$ yields

$$\widehat{R}_x(t, \tau) = \lim_{N \to \infty} \frac{1}{2N+1} \sum_{n=-N}^{N} x(t + nT_0 + \tfrac{\tau}{2})x^*(t + nT_0 - \tfrac{\tau}{2}) \tag{3.5}$$

which is referred to as the *limit periodic autocorrelation function*. The nonprobabilistic counterpart of (3.3) is given by

$$\widehat{R}_x^{\alpha}(\tau) = \lim_{T \to \infty} \frac{1}{T} \int_{-\frac{T}{2}}^{\frac{T}{2}} x(t + \tau/2)x^*(t - \tau/2)e^{-j2\pi\alpha t} dt \tag{3.6}$$

which is recognized as the *limit cyclic autocorrelation function*. The *limit cyclic spectrum function* can be characterized as the Fourier Transform like (3.4)

$$\widehat{S}_x^{\alpha}(f) = \int_{-\infty}^{\infty} \widehat{R}_x^{\alpha}(\tau)e^{-j2\pi f\tau} d\tau \tag{3.7}$$

The limit cyclic spectrum function is also called *spectral correlation function*. Fourier transform relation in (3.7) is called the *cyclic Wiener relation*.

In summary, the limit cyclic autocorrelation can be interpreted as a Fourier coefficient in the Fourier series expansion of the limit periodic autocorrelation like (3.2). If $\widehat{R}_x^{\alpha}(\tau) \equiv 0$ for all $\alpha \neq 0$ and $\widehat{R}_x^0(\tau) \neq 0$, then $x(t)$ is *purely stationary*; If $\widehat{R}_x^{\alpha}(\tau) \neq 0$ only for $\alpha = integer/T_0$ for some period T_0, then $x(t)$ is *purely cyclostationary* with period T_0; If $\widehat{R}_x^{\alpha}(\tau) \neq 0$ for values of α that are not all integer multiples of some fundamental frequency $1/T_0$, then $x(t)$ is said to *exhibit cyclostationary* [20]. For modulated signals, the periods of cyclostationarity correspond to carrier frequencies, pulse rates, spreading code repetition rates, time-division multiplexing rates, and so on.

In paper [96], a modification of the CAF called *conjugate cyclic autocorrelation function* is given as

$$R_{x^*}^{\alpha}(\tau) = \lim_{T \to \infty} \frac{1}{T} \int_{-\frac{T}{2}}^{\frac{T}{2}} R_x^*(t, \tau)e^{-j2\pi\alpha t} dt \tag{3.8}$$

with $R_x^*(t, \tau) = \mathbb{E}\Big[x(t + \tau/2)x(t - \tau/2) \Big]$, and the corresponding SCF called *conjugate spectral correlation function* is

$$S_{x^*}^{\alpha}(f) = \int_{-\infty}^{\infty} R_{x^*}^{\alpha}(\tau)e^{-j2\pi f\tau} d\tau \tag{3.9}$$

For a non-cyclostationary signal, $R_x^{\alpha}(\tau) = R_{x^*}^{\alpha}(\tau) = S_x^{\alpha}(f) = S_{x^*}^{\alpha}(f) = 0 \ \forall \alpha \neq 0$, and for a cyclostationary signal, any nonzero value of the frequency parameter α, for which the nonconjugate and conjugate CAFs and SCFs differ from zero is called a *cycle frequency*. Both nonconjugate and conjugate CAFs and SCFs are discrete functions of the cycle frequency α and are continuous in the lag parameter τ and frequency parameter f, respectively.

3.2.3 LPTV System

LPTV is a special case of Linear Almost-Periodic Time-Variant (LAPTV), which is introduced in [95]. A linear time-variant system with input $x(t)$, output $y(t)$, impulse response function $h(t, u)$, and input-output relation

$$y(t) = \int_R h(t, u)x(u)du \tag{3.10}$$

is said to be LAPTV if the impulse response function admits the Fourier series expansion

$$h(t, u) = \sum_{\sigma \in G} h_\sigma(t - u)e^{j2\pi\sigma u} \tag{3.11}$$

where G is a countable set.

By substituting (3.11) into (3.10) the output $y(t)$ can be expressed in the two equivalent forms

$$y(t) = \sum_{\sigma \in G} h_\sigma(t) \otimes [x(t)e^{j2\pi\sigma t}] \tag{3.12}$$

$$y(t) = \sum_{\sigma \in G} [g_\sigma(t) \otimes x(t)]e^{j2\pi\sigma t} \tag{3.13}$$

where $\otimes$ denotes convolution operation, and

$$g_\sigma(t) = h_\sigma(t)e^{-j2\pi\sigma t} \tag{3.14}$$

From (3.12) it follows that a LAPTV system performs a linear time-invariant filtering of frequency-shifted version of the input signal. For this reason LAPTV is also referred to as *frequency-shift* filtering. Equivalently, form (3.13) it follows that a LAPTV system performs a frequency shift of linear time-invariant filtered versions of the input.

In the special case for which $G \equiv \{k/T_0\}_{k \in Z}$ for some period T_0, the system becomes the linear periodically time-variant.

LPTV transformation is defined as follows [96]

$$y(t) = \int_{-\infty}^{\infty} \widehat{\mathbf{h}}(t, u)\widehat{\mathbf{x}}(u)du \tag{3.15}$$

where $\widehat{\mathbf{x}}$ is a L-element column vector input (L is any non-zero positive integer) and $y(t)$ is a scalar response. $\widehat{\mathbf{h}}(t, u) = \widehat{\mathbf{h}}(t + T_0, u + T_0)$ is the periodically time-variant (L-element row vector) of impulse response functions that specify the transformation. The function $\widehat{\mathbf{h}}(t + \tau, t)$ is periodic in t with a period T_0 for each τ represented by the Fourier series

$$\widehat{\mathbf{h}}(t + \tau, t) = \sum_{n=-\infty}^{\infty} \widehat{\mathbf{g}}_n(\tau)e^{j2\pi nt/T_0} \tag{3.16}$$

where

$$\widehat{\mathbf{g}}_n(\tau) = \frac{1}{T_0} \int_{-\frac{T_0}{2}}^{\frac{T_0}{2}} \widehat{\mathbf{h}}(t+\tau, t) e^{-j2\pi nt/T_0} dt \tag{3.17}$$

The Fourier transform of function $\widehat{\mathbf{h}}(t+\tau, t)$ is defined as a system function

$$\widehat{\mathbf{G}}(t, f) = \int_{-\infty}^{\infty} \widehat{\mathbf{h}}(t, t-\tau) e^{-j2\pi f\tau} d\tau \tag{3.18}$$

which can be also represented by a Fourier series

$$\widehat{\mathbf{G}}(t, f) = \sum_{n=-\infty}^{\infty} \widehat{\mathbf{G}}_n(f + n/T_0) e^{j2\pi nt/T_0} \tag{3.19}$$

where

$$\widehat{\mathbf{G}}_n(f) = \int_{n=-\infty}^{\infty} \widehat{\mathbf{g}}_n(\tau) e^{-j2\pi f\tau} d\tau \tag{3.20}$$

By substitution of (3.15) and (3.16) into the definition of (3.3) and (3.4), it can be shown that the nonconjugate cyclic autocorrelation and cyclic spectrum of the input $\widehat{\mathbf{x}}(t)$ and output y(t) of the LPTV system are related by the formulas

$$R_y^\alpha(\tau) = \sum_{n,m=-\infty}^{\infty} Tr\left\{ [\widehat{\mathbf{R}}_x^{\alpha - \frac{n-m}{T_0}}(\tau) e^{-\frac{j\pi(n+m)\tau}{T_0}}] \otimes \widehat{\mathbf{r}}_{nm}^\alpha(-\tau) \right\} \tag{3.21}$$

$$S_y^\alpha(f) = \sum_{n,m=-\infty}^{\infty} \widehat{\mathbf{G}}_n(f + \tfrac{\alpha}{2}) \widehat{\mathbf{S}}_x^{\alpha - \frac{n-m}{T_0}}(f - [n+m]/2T_0) \widehat{\mathbf{G}}_m^T(f - \tfrac{\alpha}{2})^* \tag{3.22}$$

where $\otimes$ denotes convolution operation, the superscript symbol T denotes matrix transposition and $*$ denotes conjugation. $\widehat{\mathbf{R}}_x^\beta$ is the matrix of cyclic cross correlation of the elements of the vector $\widehat{\mathbf{x}}(t)$

$$\widehat{\mathbf{R}}_x^\beta(\tau) = \underset{T\to\infty}{Lim} \frac{1}{T} \int_{-\frac{T}{2}}^{\frac{T}{2}} \widehat{\mathbf{x}}^*(t+\tau/2) \widehat{\mathbf{x}}^T(t-\tau/2) e^{-j2\pi\beta t} dt \tag{3.23}$$

and $\widehat{\mathbf{r}}_{nm}^\alpha$ is the matrix of finite cyclic cross correlation

$$\widehat{\mathbf{r}}_{nm}^\alpha(\tau) = \int_{-\infty}^{\infty} \widehat{\mathbf{g}}_n^T(t+\tau/2) \widehat{\mathbf{g}}_m^*(t-\tau/2) e^{-j2\pi\alpha t} dt \tag{3.24}$$

Formulas (3.21) and (3.22) reveal that the cyclic autocorrelation and spectra of a modulated signal are each self-determinant characteristics under an LPTV transformation.

The conjugate cyclic autocorrelation and cyclic spectrum of the input $\widehat{\mathbf{x}}(t)$ and output y(t) of the LPTV system are obtained similarly

$$R_{y^*}^\alpha(\tau) = \sum_{n,m=-\infty}^{\infty} Tr\left\{ [\widehat{\mathbf{R}}_{x^*}^{\alpha - \frac{n+m}{T_0}}(\tau) e^{-\frac{j\pi(n-m)\tau}{T_0}}] \otimes \widehat{\mathbf{r}}_{nm^*}^\alpha(-\tau) \right\} \tag{3.25}$$

$$S_{y^*}^{\alpha}(f) = \sum_{n,m=-\infty}^{\infty} \widehat{\mathbf{G}}_n(f + \tfrac{\alpha}{2})\widehat{\mathbf{S}}_{x^*}^{\alpha - \frac{n+m}{T_0}}\left(f - [n-m]/2T_0\right)\widehat{\mathbf{G}}_m^T(f - \tfrac{\alpha}{2}) \qquad (3.26)$$

$$\widehat{\mathbf{R}}_{x^*}^{\beta}(\tau) = \underset{T \to \infty}{Lim} \tfrac{1}{T} \int_{-\frac{T}{2}}^{\frac{T}{2}} \widehat{\mathbf{x}}(t + \tau/2)\widehat{\mathbf{x}}^T(t - \tau/2)e^{-j2\pi\beta t} dt \qquad (3.27)$$

$$\widehat{\mathbf{r}}_{nm^*}^{\alpha}(\tau) = \int_{-\infty}^{\infty} \widehat{\mathbf{g}}_n^T(t + \tau/2)\widehat{\mathbf{g}}_m(t - \tau/2)e^{-j2\pi\alpha t} dt \qquad (3.28)$$

3.2.4 Spectral Correlation of MCM Signals

Generally, the carrier modulated passband MCM signal $c(t)$ can be expressed as

$$c(t) = Re\{y(t)e^{j2\pi f_c t}\} \qquad (3.29)$$

where Re denotes the real part of $\{.\}$, $y(t)$ is the baseband complex envelope of the actual transmitted MCM signal, and f_c is the carrier frequency.

If the baseband complex envelope signal $y(t)$ is cyclostationary, the spectral correlation function of its corresponding carrier modulated signal $c(t)$ can be expressed as [100]

$$S_c^{\alpha}(f) = \frac{1}{4}\left[S_y^{\alpha}(f - f_c) + S_y^{\alpha}(f + f_c) + S_{y^*}^{\alpha - 2f_c}(f - f_c) + S_{y^*}^{\alpha + 2f_c}(f + f_c) \right] \qquad (3.30)$$

where $S_y^{\alpha}(s)$ and $S_{y^*}^{\alpha}(s)$ are the nonconjugate and conjugate spectral correlation function of the complex envelope $y(t)$, respectively. We can observe that the spectral correlation of the carrier modulated signal $c(t)$ is determined by the nonconjugate and conjugate spectral correlation of the complex envelope signal $y(t)$ and is related to the double carrier frequency, so the problem of spectral correlation analysis of passband carrier modulated signal can be reduced to the spectral correlation analysis of the complex baseband signal.

The spectral correlation analysis of MCM signals is the theoretical basis for further signal processing. In the following, we investigate two typical MCM signals: OFDM and FBMC signals. Other MCM signals share similar spectral correlation properties with these two signals.

3.2.4.1 Spectral Correlation of OFDM Signal using LPTV

Fig. 3.1 shows a filter bank based schematic baseband equivalent of transmultiplexer system, based on the LPTV theory. M parallel complex data streams are passed to M subcarrier transmission filters.
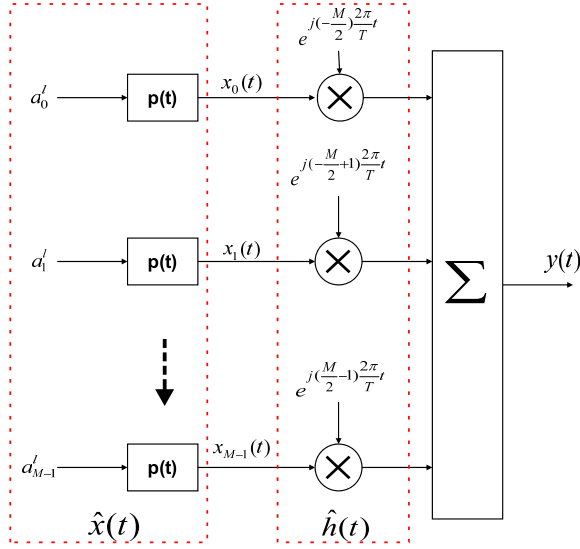
Figure 3.1: Baseband OFDM transmitter

OFDM system is a special filter bank based multicarrier system with the rectangular pulse filters. The baseband OFDM signal can be expressed as a sum of M single carrier signals like (3.15)

$$y(t) = \sum_{k=0}^{M-1} \sum_{l=-\infty}^{\infty} a_k^l p(t - lT_s) e^{jk\frac{2\pi t}{T_0}} e^{-jM\frac{\pi}{T_0}t} = \sum_{k=0}^{M-1} x_k(t) h_k(t) \qquad (3.31)$$

where $x_k(t)$ is the element of the input vector of LPTV system and $h_k(t)$ is the element of impulse response of LPTV

$$x_k(t) = \sum_{l=-\infty}^{\infty} a_k(lT_s) p(t - lT_s), \qquad k = 0, 1, \ldots, M-1 \qquad (3.32)$$

$$h_k(t) = e^{j(k-\frac{M}{2})\frac{2\pi t}{T_0}}, \qquad k = 0, 1, \ldots, M-1 \qquad (3.33)$$

for which a_k is the purely stationary data, $T_s = T_0 + T_g$ is one OFDM symbol duration, where T_0 is the useful symbol duration and T_g is the length of the guard interval where the OFDM signal is extended cyclically. $p(t)$ is the rectangular pulse function, and $h_k(t)$ can be regarded as the periodic function in t with the period T_0 for $k = 0, 1, \ldots, M-1$.

Element of input vector $x_k(t)$ also can be regarded as an inherent LPTV transformation of data a_k with the time-invariant filters $p(t)$

$$x_k(t) = a0(t) \otimes p(t) \qquad (3.34)$$

where

$$a0(t) = \sum_{l=-\infty}^{\infty} a_k(lT_s)\delta(t - lT_s) \tag{3.35}$$

Assuming $\mathbb{E}[a_{l,k}a_{l,k}^*] = \sigma^2$, each entity of matrix $\widehat{\mathbf{R}}_x^\alpha(\tau)$ and $\widehat{\mathbf{S}}_x^\alpha(f)$ in (3.21) and (3.22) reduce to

$$R_{x_k}^\alpha(\tau) = R_{a0}^\alpha(\tau) \otimes r_p^\alpha(\tau) \tag{3.36}$$

$$S_{x_k}^\alpha(f) = S_{a0}^\alpha(f)S_p^\alpha(f) \tag{3.37}$$

where $S_p^\alpha(f)$ is the Fourier Transform of $r_p^\alpha(\tau)$ and

$$
\begin{aligned}
r_p^\alpha(\tau) &= \int_{-\infty}^{\infty} p(t + \tfrac{\tau}{2})p(t - \tfrac{\tau}{2})e^{-j2\pi\alpha t}dt \\
R_{a0}^\alpha(\tau) &= \tfrac{\sigma^2}{T_s}\delta(\tau), \qquad \alpha = \tfrac{integer}{T_s} \\
S_{a0}^\alpha(f) &= \tfrac{\sigma^2}{T_s}, \qquad \alpha = \tfrac{integer}{T_s}
\end{aligned} \tag{3.38}
$$

Other terms corresponding to the LPTV system can be similarly calculated

$$
\begin{aligned}
\widehat{\mathbf{h}}(t,u) &= \left[e^{j(-\frac{M}{2})\frac{2\pi t}{T_0}}\delta(t-u), e^{j(1-\frac{M}{2})\frac{2\pi t}{T_0}}\delta(t-u), \cdots, e^{j(\frac{M}{2}-1)\frac{2\pi t}{T_0}}\delta(t-u)\right] \\
\widehat{\mathbf{G}}(t,f) &= \left[e^{j(-\frac{M}{2})\frac{2\pi t}{T_0}}, e^{j(1-\frac{M}{2})\frac{2\pi t}{T_0}}, \cdots, e^{j(\frac{M}{2}-1)\frac{2\pi t}{T_0}}\right] \\
\widehat{\mathbf{g}}_n(\tau) &= \begin{bmatrix} g_n^0 \\ \vdots \\ g_n^{M-1} \end{bmatrix} = \begin{bmatrix} \delta(\tau) & \cdots & 0 \\ \vdots & \delta(\tau) & \vdots \\ 0 & \cdots & \delta(\tau) \end{bmatrix} \\
\widehat{\mathbf{G}}_n(f) &= \begin{bmatrix} G_n^0 \\ \vdots \\ G_n^{M-1} \end{bmatrix} = \begin{bmatrix} 1 & \cdots & 0 \\ \vdots & 1 & \vdots \\ 0 & \cdots & 1 \end{bmatrix}, n = -\tfrac{M}{2}, \ldots, \tfrac{M}{2} - 1 \quad for \quad M = 8, 16, 32, \ldots;
\end{aligned} \tag{3.39}
$$

Substitution of (3.31)$\sim$ (3.39) into (3.21) and (3.22), the nonconjugate cyclic autocorrelated and cyclic spectra of OFDM signal is transformed into

$$
R_{ofdm}^\alpha(\tau) = \begin{cases} \frac{\sigma^2}{T_s} \cdot \frac{sin[\pi\alpha(T_s-|\tau|)]}{\pi\alpha} \cdot \frac{sin(\pi M\tau/T_0)}{sin(\pi\tau/T_0)}, & \alpha = \frac{integer}{T_s}, |\tau| < T_s; \\ \\ 0, & \alpha \neq \frac{integer}{T_s}; \end{cases} \tag{3.40}
$$

$$
S_{ofdm}^\alpha(f) = \begin{cases} \frac{\sigma^2}{T_s} \sum_{n=-M/2}^{M/2-1} P(f + \frac{\alpha}{2} - \frac{n}{T_0})P^*(f - \frac{\alpha}{2} - \frac{n}{T_0}), & \alpha = \frac{integer}{T_s}; \\ \\ 0, & \alpha \neq \frac{integer}{T_s}; \end{cases} \tag{3.41}
$$

47

where T_s is the time length of one OFDM symbol, $P(f)$ is the Fourier transform of $p(t)$. The magnitudes of nonconjugate CAF and SCF of OFDM signal are drawn in graphical terms as the heights of surfaces above a bi-frequency plane in Fig. 3.2 and Fig. 3.3.

For the conjugate case, according to (3.25) and (3.26), the conjugate cyclic autocorrelation and cyclic spectra of OFDM signal is transformed into

$$R^\alpha_{ofdm^*}(\tau) =$$
$$\begin{cases} \frac{1}{T_s} \sum_{n=-M/2}^{M/2-1} r_p^{\alpha-\frac{2n}{T_0}}(\tau) \mathbb{E}[a_{l,k}a_{l,k}], & \alpha = \frac{integer}{T_s}, |\tau| < T_s; \\ \\ 0, & \alpha \neq \frac{integer}{T_s}; \end{cases} \tag{3.42}$$

$$S^\alpha_{ofdm^*}(f) =$$
$$\begin{cases} \frac{1}{T_s} \sum_{n=-M/2}^{M/2-1} P(f + \frac{\alpha}{2} - \frac{n}{T_0})P^*(f - \frac{\alpha}{2} + \frac{n}{T_0}) \mathbb{E}[a_{l,k}a_{l,k}], & \alpha = \frac{integer}{T_s}; \\ \\ 0, & \alpha \neq \frac{integer}{T_s}; \end{cases} \tag{3.43}$$

Consequently, the explicit spectral correlation function of the carrier modulated OFDM signal can be derived by substituting (3.41) and (3.43) into (3.30)

$$S^\alpha_{c_{ofdm}}(f) =$$
$$\begin{cases} \sum_{n=-M/2}^{M/2-1} \left\{ \frac{\sigma^2}{T_s} P(f - f_c + \frac{\alpha}{2} - \frac{n}{T_0})P^*(f - f_c - \frac{\alpha}{2} - \frac{n}{T_0}) \right. \\ + \frac{\sigma^2}{T_s} P(f + f_c + \frac{\alpha}{2} - \frac{n}{T_0})P^*(f + f_c - \frac{\alpha}{2} - \frac{n}{T_0}) \\ + \frac{A}{T_s} P(f - f_c + \frac{\alpha-2f_c}{2} - \frac{n}{T_0})P^*(f - f_c - \frac{\alpha-2f_c}{2} + \frac{n}{T_0}) \\ \left. + \frac{A}{T_s} P(f + f_c + \frac{\alpha+2f_c}{2} - \frac{n}{T_0})P^*(f + f_c - \frac{\alpha+2f_c}{2} + \frac{n}{T_0}) \right\}, & \alpha = \frac{integer}{T_s}; \\ \\ 0, & \alpha \neq \frac{integer}{T_s}; \end{cases} \tag{3.44}$$

where $A = \mathbb{E}[a_{l,k}a_{l,k}]$. Since $\mathbb{E}[a_{l,k}a_{l,k}] = 0$ for MPSK (M$\neq$2) or QAM modulation types, given that $a_{l,k}$ is centered and i.i.d.. According to (3.43), it can be seen that the OFDM signal does not exhibit conjugate cyclostationarity, that is $R^\alpha_{ofdm^*}(\tau) = S^\alpha_{ofdm^*}(f) = 0, \forall \alpha, \tau, f$. The spectral correlation function of the carrier-modulated signal for MPSK (M$\neq$2) or QAM modulation can be simplified as

$$S^\alpha_{c_{ofdm}}(f) =$$
$$\begin{cases} \frac{\sigma^2}{T_s} \sum_{n=-M/2}^{M/2-1} \left\{ P(f - f_c + \frac{\alpha}{2} - \frac{n}{T_0})P^*(f - f_c - \frac{\alpha}{2} - \frac{n}{T_0}) \right. \\ \left. + P(f + f_c + \frac{\alpha}{2} - \frac{n}{T_0})P^*(f + f_c - \frac{\alpha}{2} - \frac{n}{T_0}) \right\}, & \alpha = \frac{integer}{T_s}; \\ \\ 0, & \alpha \neq \frac{integer}{T_s}; \end{cases} \tag{3.45}$$
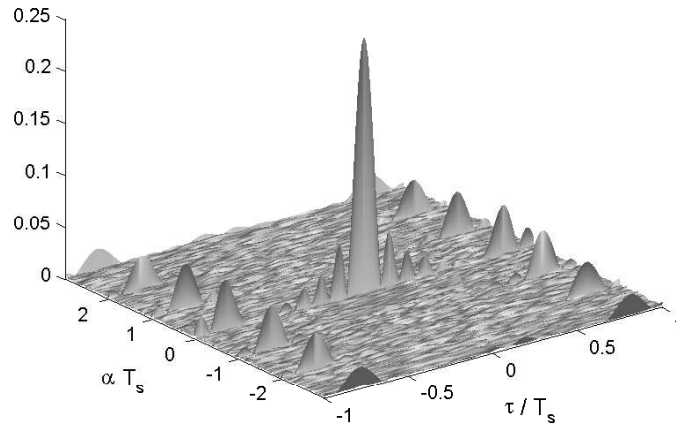
Figure 3.2: 8-channel nonconjugate cyclic autocorrelation of OFDM signal
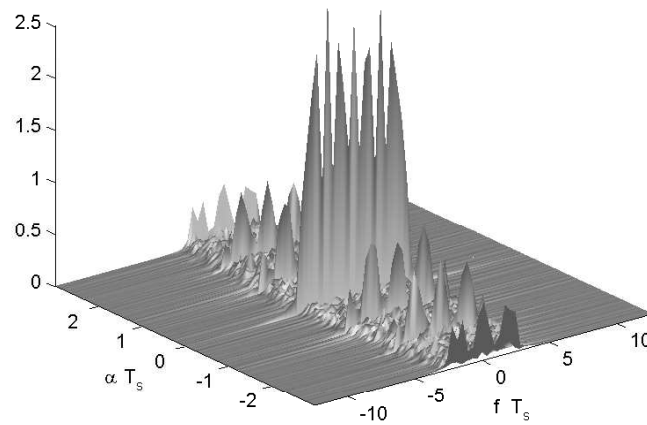
Figure 3.3: 8-channel nonconjugate spectral correlation function of OFDM signal

49

3.2.4.2 Spectral Correlation of FBMC Signal using LPTV
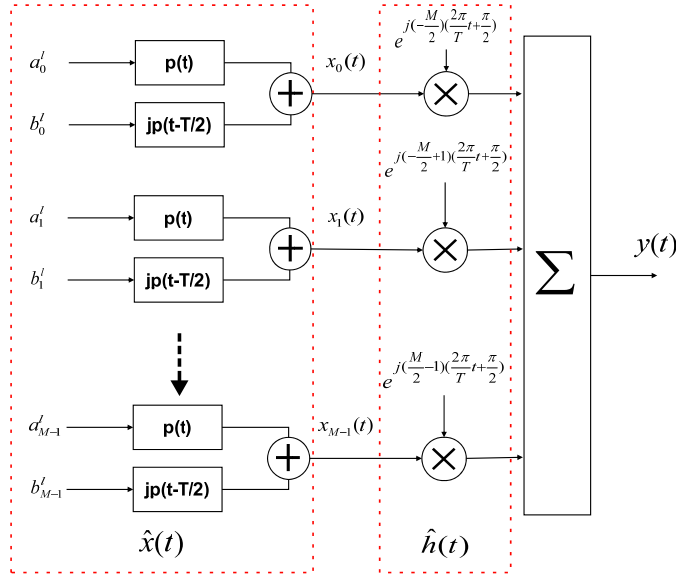
Figure 3.4: Baseband FBMC transmitter

The typical baseband FBMC transmitter system is shown in Fig. 3.4. The transmission is divided into M independent transmissions using M subcarriers. Instead of a rectangular shape filter, a longer prototype filter $p(t)$ is used. Subcarrier bands are spaced by the symbol rate $1/T_0$ (T_0 is one FBMC symbol period). An introduced orthogonality condition between subcarriers guarantees that the transmitted symbols arrive at the receiver free of ISI and ICI, which is achieved through time staggering the in-phase and quadrature components of the subcarrier symbols by half a symbol period $T_0/2$.

Supposing the complex input symbols of FBMC system are

$$x_k^l = a_k^l + jb_k^l \tag{3.46}$$

where a_k^l and b_k^l are respectively the real and imaginary parts of the kth subcarrier of the lth symbol. The complex-values baseband FBMC signal is defined as

$$y(t) = \sum_{k=0}^{M-1} \sum_{l=-\infty}^{\infty} \left[a_k^l p(t - lT_0) + jb_k^l p(t - lT_0 - T_0/2) \right] e^{j(k-\frac{M}{2})(\frac{2\pi t}{T_0} + \frac{\pi}{2})} \tag{3.47}$$

From (3.47) and Fig. 3.4 we can see that FBMC signal is a special model with M-input $\widehat{\mathbf{x}}(t)$ transformed by LPTV transformation $\widehat{\mathbf{h}}(t)$ and one scalar output $y(t)$. The baseband FBMC signal (3.47) can also be expressed as a sum of M single carrier signals like (3.15)

$$y(t) = \sum_{k=0}^{M-1} x_k(t) h_k(t) \tag{3.48}$$

where $x_k(t)$ is the element of the input vector of LPTV system and $h_k(t)$ is the element of impulse response of LPTV

$$x_k(t) = \sum_{l=-\infty}^{\infty} \left\{ a_k(lT_0)p(t - lT_0) + jb_k(lT_0)p(t - lT_0 - \tfrac{T_0}{2}) \right\}, k = 0, 1, \ldots, M - 1 \tag{3.49}$$

$$h_k(t) = e^{j(k-\frac{M}{2})(\frac{2\pi t}{T_0}+\frac{\pi}{2})}, \qquad k = 0, 1, \ldots, M - 1 \tag{3.50}$$

for which a_k and b_k are the purely stationary data, T_0 is one FBMC symbol duration, $p(t)$ is the prototype filter bank pulse function, and $h_k(t)$ can be regarded as the periodic function in t with the period T_0 for $k = 0, 1, \ldots, M - 1$.

$x_k(t)$ also can be regarded as a two-element vector LPTV transformation of input data a_k and b_k with the time-invariant filters $p(t)$ and $p(t - T_0/2)$

$$x_k(t) = a0(t) \otimes p(t) + b0(t) \otimes p(t - T_0/2) \tag{3.51}$$

where

$$a0(t) = \sum_{l=-\infty}^{\infty} a_k(lT_0)\delta(t - lT_0)$$

$$b0(t) = \sum_{l=-\infty}^{\infty} jb_k(lT_0)\delta(t - lT_0) \tag{3.52}$$

Assuming $\mathbb{E}[a_{l,k}a_{l,k}^*] = \mathbb{E}[b_{l,k}b_{l,k}^*] = \sigma^2$, each entity of matrices $\widehat{\mathbf{R}}_x^\alpha(\tau)$ and $\widehat{\mathbf{S}}_x^\alpha(f)$ in (3.21) and (3.22) reduces to

$$R_{x_k}^\alpha(\tau) = \frac{\sigma^2}{T_0}\left[\delta(\tau) \otimes r_{p1}^\alpha(\tau) + \delta(\tau) \otimes r_{p2}^\alpha(\tau)\right] = \frac{\sigma^2}{T_0}r_{p1}^\alpha(\tau)(1 + e^{-j\pi\alpha T_0}), \alpha = \tfrac{integer}{T_0} \tag{3.53}$$

$$S_{x_k}^\alpha(f) = \frac{\sigma^2}{T_0}\left[S_{p1}^\alpha(f) + S_{p2}^\alpha(f)\right] = \frac{\sigma^2}{T_0}S_{p1}^\alpha(f)(1 + e^{-j\pi\alpha T_0}), \alpha = \tfrac{integer}{T_0} \tag{3.54}$$

where $S_{p1}^\alpha(f)$ is the Fourier Transform of $r_{p1}^\alpha(\tau)$ and

$$r_{p1}^\alpha(\tau) = \int_{-\infty}^{\infty} p(t + \tau/2)p(t - \tau/2)e^{-j2\pi\alpha t}dt$$

$$r_{p2}^\alpha(\tau) = \int_{-\infty}^{\infty} p(t + \tfrac{\tau}{2} - \tfrac{T_0}{2})p(t - \tfrac{\tau}{2} - \tfrac{T_0}{2})e^{-j2\pi\alpha t}dt = r_{p1}^\alpha(\tau)e^{-j\pi\alpha T_0} \tag{3.55}$$

Other terms corresponding to the LPTV system can be similarly calculated

$$\widehat{\mathbf{h}}(t,u) = \left[e^{j(-\frac{M}{2})(\frac{2\pi t}{T_0}+\frac{\pi}{2})}\delta(t-u), e^{j(1-\frac{M}{2})(\frac{2\pi t}{T_0}+\frac{\pi}{2})}\delta(t-u), \cdots, e^{j(\frac{M}{2}-1)(\frac{2\pi t}{T_0}+\frac{\pi}{2})}\delta(t-u) \right]$$

$$\widehat{\mathbf{G}}(t,f) = \left[e^{j(-\frac{M}{2})(\frac{2\pi t}{T_0}+\frac{\pi}{2})}, e^{j(1-\frac{M}{2})(\frac{2\pi t}{T_0}+\frac{\pi}{2})}, \cdots, e^{j(\frac{M}{2}-1)(\frac{2\pi t}{T_0}+\frac{\pi}{2})} \right]$$

$$\widehat{\mathbf{g}}_n(\tau) = \begin{bmatrix} g_n^0 \\ \vdots \\ g_n^{M-1} \end{bmatrix} = \begin{bmatrix} \delta(\tau) & \cdots & 0 \\ \vdots & e^{j\frac{\pi}{2}k}\delta(\tau) & \vdots \\ 0 & \cdots & e^{j\frac{\pi}{2}(M-1)}\delta(\tau) \end{bmatrix}$$

$$\widehat{\mathbf{G}}_n(f) = \begin{bmatrix} G_n^0 \\ \vdots \\ G_n^{M-1} \end{bmatrix} = \begin{bmatrix} 1 & \cdots & 0 \\ \vdots & e^{j\frac{\pi}{2}k} & \vdots \\ 0 & \cdots & e^{j\frac{\pi}{2}(M-1)} \end{bmatrix}, n = -\frac{M}{2}, \ldots, \frac{M}{2}-1 \quad for \quad M = 8, 16, 32, \ldots; \tag{3.56}$$

Substitution of (3.48)$\sim$ (3.56) into (3.21) and (3.22), the nonconjugate cyclic autocorrelation and cyclic spectra of FBMC signal is transformed into

$$R_{fbmc}^\alpha(\tau) =$$
$$\begin{cases} \frac{2\sigma^2}{T_0} r_{p1}^\alpha(\tau) \frac{sin(\frac{\pi M \tau}{T_0})}{sin(\frac{\pi \tau}{T_0})}, & \alpha = \frac{2 \cdot integer}{T_0}, |\tau| < KT_0; \\ \\ 0, & \alpha \neq \frac{2 \cdot integer}{T_0}; \end{cases} \tag{3.57}$$

$$S_{fbmc}^\alpha(f) =$$
$$\begin{cases} \frac{2\sigma^2}{T_0} \sum_{n=-M/2}^{M/2-1} P(f+\frac{\alpha}{2}-\frac{n}{T_0})P^*(f-\frac{\alpha}{2}-\frac{n}{T_0}), & \alpha = \frac{2 \cdot integer}{T_0}; \\ \\ 0, & \alpha \neq \frac{2 \cdot integer}{T_0}; \end{cases} \tag{3.58}$$

where KT_0 is the time length of the prototype filter bank, $P(f)$ is the Fourier transform of $p(t)$ and $r_{p1}^\alpha(\tau)$ is described as (3.55). The magnitudes of nonconjugate CAF and SCF of FBMC signal are shown in Fig. 3.5 and Fig. 3.6. We unfortunately found that FBMC signal has very poor inherent cyclostationary property when the cyclic frequency is not equal to zero, which can be interpreted by (3.58), where the value of cross product $P(f+\frac{\alpha}{2})P^*(f-\frac{\alpha}{2})$ tends to zero when $\alpha = \frac{2 \cdot integer}{T_0}$ due to the low side-lobe property of FBMC prototype function.

For the conjugate situation, assuming $\mathbb{E}[a_{l,k}a_{l,k}] = \mathbb{E}[b_{l,k}b_{l,k}] = \sigma^2$, in the same way we can get each entity of matrices $\widehat{\mathbf{R}}_{x^*}^\alpha(\tau)$ and $\widehat{\mathbf{S}}_{x^*}^\alpha(f)$ in (3.25) and (3.26)

$$R_{x_k^*}^\alpha(\tau) = \frac{\sigma^2}{T_0}\left[\delta(\tau) \otimes r_{p1}^\alpha(\tau) - \delta(\tau) \otimes r_{p2}^\alpha(\tau)\right] = \frac{\sigma^2}{T_0}r_{p1}^\alpha(\tau)(1-e^{-j\pi\alpha T_0}), \alpha = \frac{integer}{T_0} \tag{3.59}$$

$$S_{x_k^*}^\alpha(f) = \frac{\sigma^2}{T_0}\left[S_{p1}^\alpha(f) - S_{p2}^\alpha(f)\right] = \frac{\sigma^2}{T_0}S_{p1}^\alpha(f)(1-e^{-j\pi\alpha T_0}), \alpha = \frac{integer}{T_0} \tag{3.60}$$
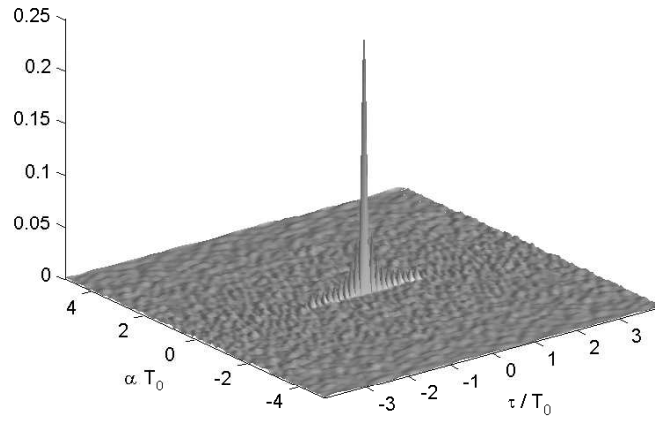
Figure 3.5: 8-channel nonconjugate cyclic autocorrelation of FBMC signal
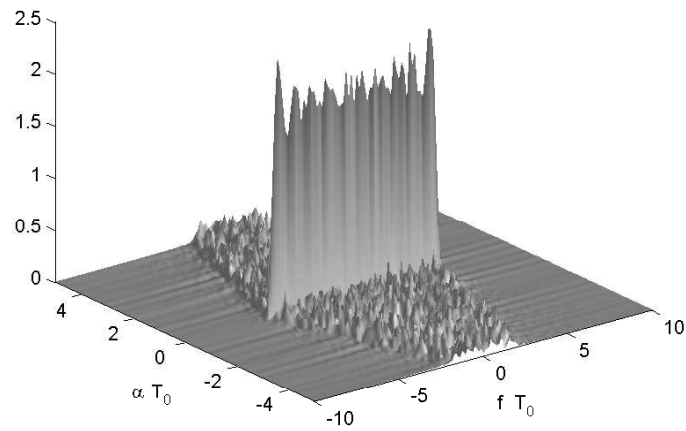
Figure 3.6: 8-channel nonconjugate spectral correlation function of FBMC signal

Substitution of (3.56)(3.59)(3.60) into (3.25) and (3.26), the conjugate cyclic autocorrelation and cyclic spectra of FBMC signal is transformed into

$$
R^{\alpha}_{fbmc^*}(\tau) =
\begin{cases}
\frac{2\sigma^2}{T_0} \sum_{n=-M/2}^{M/2-1} r^{\alpha-\frac{2n}{T_0}}_{p1}(\tau)(-1)^n, & \alpha = \frac{2 \cdot integer - 1}{T_0}, |\tau| < KT_0; \\
\\
0, & \alpha \neq \frac{2 \cdot integer - 1}{T_0};
\end{cases}
\tag{3.61}
$$

$$
S^{\alpha}_{fbmc^*}(f) =
\begin{cases}
\frac{2\sigma^2}{T_0} \sum_{n=-M/2}^{M/2-1} P(f + \frac{\alpha}{2} - \frac{n}{T_0})P^*(f - \frac{\alpha}{2} + \frac{n}{T_0})(-1)^n, & \alpha = \frac{2 \cdot integer - 1}{T_0}; \\
\\
0, & \alpha \neq \frac{2 \cdot integer - 1}{T_0};
\end{cases}
\tag{3.62}
$$

As same as OFDM signal (except BPSK), FBMC signal does not exhibit conjugate cyclostationarity, either. This property can be exactly interpreted by (3.62), where the value of cross product $P(f + \frac{\alpha}{2} - \frac{n}{T_0})P^*(f - \frac{\alpha}{2} + \frac{n}{T_0})(-1)^n$ equals to zero due to neighbored offset effect. The explicit spectral correlation function of the carrier modulated FBMC signal can be obtained by substituting (3.58) into (3.30)

$$
S^{\alpha}_{c_{fbmc}}(f) =
\begin{cases}
\frac{2\sigma^2}{T_0} \sum_{n=-M/2}^{M/2-1} \Big\{ P(f - f_c + \frac{\alpha}{2} - \frac{n}{T_0})P^*(f - f_c - \frac{\alpha}{2} - \frac{n}{T_0}) \\
+ P(f + f_c + \frac{\alpha}{2} - \frac{n}{T_0})P^*(f + f_c - \frac{\alpha}{2} - \frac{n}{T_0}) \Big\}, & \alpha = \frac{2 \cdot integer}{T_0}; \\
\\
0, & \alpha \neq \frac{2 \cdot integer}{T_0};
\end{cases}
\tag{3.63}
$$

3.2.5 Cyclostationary Signature for MCM Signals

The poor inherent cyclostationarity is unsuitable for practically applications in the context of cognitive radio. Even for OFDM signals which contain inherent cyclostationary features due to the underlying periodicities properties (Fig. 3.3), as the power of inherent OFDM features are relative low to the power of signal, reliable detection of these features requires complex architecture and long observation time.

In this part we study the detection problem of MCM signals considering the AWGN and Rayleigh fading environment by using an induced cyclostationary scheme [101], which is realized by intentionally embedding some cyclostationary signatures. Cyclostationarity-inducing method enables the

recognition among primary system and secondary system or among multiple secondary systems competing for the same space spectrum, which is important as it may facilitate the setting of advanced spectrum policy such as multilevel priority or advanced access control [99]. Cyclostationary signature has been shown to be a powerful tool to overcome the challenge of the distributed coordination of operating frequencies and bandwidths between co-existing systems [97]. A cyclostationary signature is a feature, intentionally embedded in the physical properties of a digital communication signal. CSs are effectively applied to overcome the limitations associated with the use of inherent cyclostationary features for signal detection and analysis with minimal additional complexity for existing transmitter architectures. Detection and analysis of CS may also be achieved using low-complexity receiver architectures and short observation durations. CS provides a robust mechanism for signal detection, network identification and signal frequency acquisition.
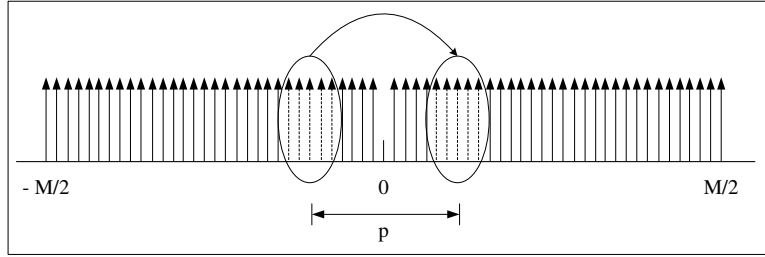
Figure 3.7: Generation of cyclostationary signatures by repeatedly transmitting MCM subcarrier symbols

As illustrated in Fig. 3.7, CSs are easily created by mapping a set of subcarriers onto a second set as

$$\gamma_{n,l} = \gamma_{n+p,l} \qquad n \in N \tag{3.64}$$

where $\gamma_{n,l}$ is the lth independent and identically distributed message at n^{th} subcarrier frequency, N is the set of subcarrier values to be mapped and p is the number of subcarriers between mapped subcarriers. So a correlation pattern is created and a cyclostationary feature is embedded in the signal by redundantly transmitting message symbols.

In order to avoid redundant theoretical analysis, herein we just discuss the cyclostationary signature for FBMC signal. According to (3.21) (3.22) (3.57) (3.58) (3.64), we can rewrite the nonconjugate cyclic autocorrelation and spectral correlation formulas of FBMC signal with cyclostationary

signatures

$$R_{fbmc\cdot cs}^{\alpha}(\tau) =$$

$$
\begin{cases}
\frac{2\sigma^2}{T_0} r_{p1}^{\alpha}(\tau) \frac{sin(\frac{\pi M \tau}{T_0})}{sin(\frac{\pi \tau}{T_0})}, & \alpha = \frac{2\cdot integer}{T_0}, 2 \cdot integer \neq -p, |\tau| < KT_0; \\
\\
\frac{2\sigma^2}{T_0} r_{p1}^{0}(\tau) \sum_{n \in N} e^{-\frac{j\pi(2n+p)\tau}{T_0}}, & \alpha = -\frac{p}{T_0}, |\tau| < KT_0; \\
\\
0, & \alpha \neq \frac{2\cdot integer}{T_0}, \alpha \neq -\frac{p}{T_0};
\end{cases}
\tag{3.65}
$$

$$S_{fbmc\cdot cs}^{\alpha}(f) =$$

$$
\begin{cases}
\frac{2\sigma^2}{T_0} \sum_{n=-M/2}^{M/2-1} P(f + \frac{\alpha}{2} - \frac{n}{T_0})P^*(f - \frac{\alpha}{2} - \frac{n}{T_0}), & \alpha = \frac{2\cdot integer}{T_0}, 2 \cdot integer \neq -p; \\
\\
\frac{2\sigma^2}{T_0} \sum_{n \in N} P(f + \frac{\alpha}{2} - \frac{n}{T_0})P^*(f - \frac{\alpha}{2} - \frac{n+p}{T_0}), & \alpha = -\frac{p}{T_0}; \\
\\
0, & \alpha \neq \frac{2\cdot integer}{T_0}, \alpha \neq -\frac{p}{T_0};
\end{cases}
\tag{3.66}
$$

where N is the set of subcarriers to be mapped and $p \in \mathcal{P}(\mathcal{P} = \pm 2i, i = 1, 2, 3, 4, \cdots)$.

The magnitudes of nonconjugate CAF and SCF of FBMC signal with CS are drawn in Fig. 3.8 and Fig. 3.9, where four cyclostationary signatures are embedded corresponding to two different values of p (choosing $p = 2$ and $p = 4$), and a reference filter bank is designed using the method given in [9]. We can see that for the FBMC signal with CS the strong cyclostationary features appear at the cyclic frequency $\alpha = \pm 2/T_0$ and $\alpha = \pm 4/T_0$.

OFDM and FBMC signals detection utilizing CSs by nonconjugate operation are already investigated in [97] and [102], respectively. They both exhibit good performances, but the experiments using CSs by conjugate operation are still an open topic. In the following, we will insert the CSs by conjugate operation aiming at generating cyclostationary features on some predefined cyclic frequency, which is feasible based on the fact that most of MCM signals and noise[1] do not display cyclostationarity under the conjugate operation for all the cyclic frequencies. Therefore, a simple cyclostationarity detector for the presence of conjugate cyclostationarity over the predefined cyclic frequency can be given to detect MCM signal and noise or detect two different MCM signals[2].

Contrary to the nonconjugate operation, a CS is created by mapping the conjugate formation of a set of subcarriers onto a second set as

$$\gamma_{n,l} = \gamma_{n+p,l}^* \qquad n \in N \tag{3.67}$$

---

[1]Herein the noise is assumed to be circularly symmetric.

[2]Recognition is feasible between the MCM signal embedded by CS and the other MCM signal without CS at a predetermined cyclic frequency.

Figure 3.8: Nonconjugate Cyclic Autocorrelation Function for FBMC signal with cyclostationary features at cyclic frequencies $\alpha = \pm 2/T_0$ and $\alpha = \pm 4/T_0$
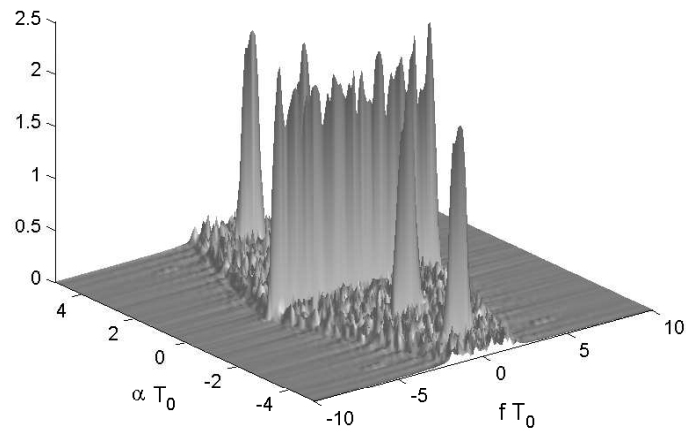
Figure 3.9: Nonconjugate Spectral Correlation Function for FBMC signal with four CSs at cyclic frequencies $\alpha = \pm 2/T_0$ and $\alpha = \pm 4/T_0$
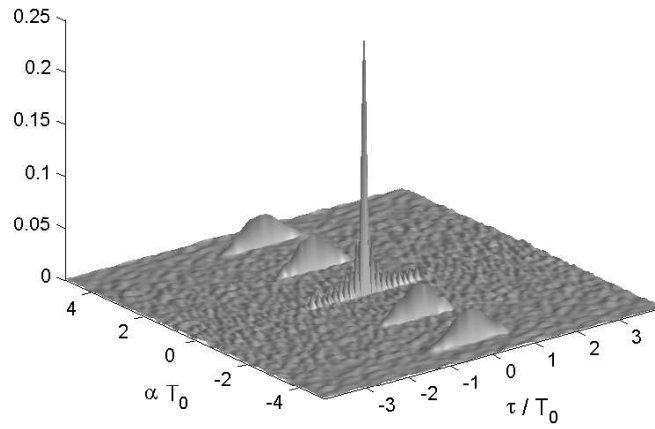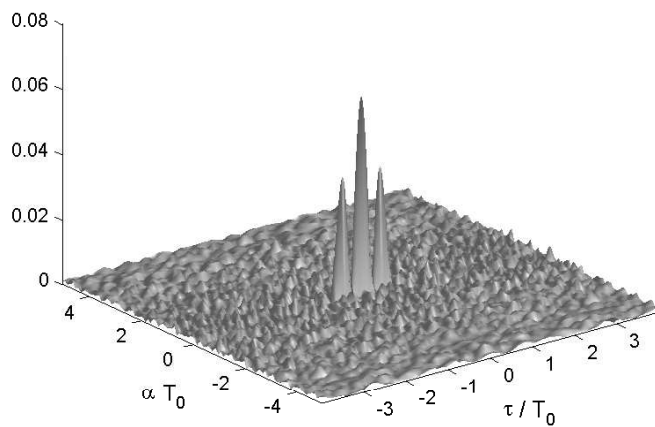
Figure 3.10: Conjugate Cyclic Autocorrelation Function for FBMC signal with cyclostationary features at cyclic frequencies $\alpha = 0$
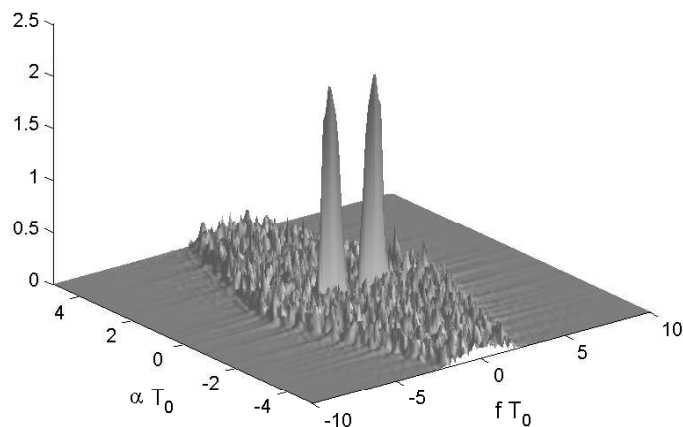
Figure 3.11: Conjugate Spectral Correlation Function for FBMC signal with two CSs at cyclic frequencies $\alpha = 0$

by which a correlation pattern is created and a cyclostationary feature is embedded in the signal.

According to (3.25) (3.26) (3.61) (3.62) (3.67), we can rewrite the conjugate cyclic autocorrelation and spectral correlation formulas of FBMC signal with cyclostationary signatures

$$R^{\alpha}_{fbmc \cdot cs^*}(\tau) =$$
$$\begin{cases} \frac{2\sigma^2}{T_0} \sum_{n=-M/2}^{M/2-1} r^{\alpha - \frac{2n}{T_0}}_{p1}(\tau)(-1)^n, & \alpha = \frac{2 \cdot integer - 1}{T_0}, 2 \cdot integer - 1 \neq 2n + p, |\tau| < KT_0; \\[3mm] \frac{2\sigma^2}{T_0} e^{\frac{j\pi p\tau}{T_0}} r^0_{p1}(\tau), & \alpha = \frac{2n+p}{T_0}, |\tau| < KT_0; \\[3mm] 0, & \alpha \neq \frac{2 \cdot integer - 1}{T_0}, \alpha \neq \frac{2n+p}{T_0}; \end{cases}$$

$$(3.68)$$

$$S^{\alpha}_{fbmc \cdot cs^*}(f) =$$
$$\begin{cases} \frac{2\sigma^2}{T_0} \sum_{n=-M/2}^{M/2-1} P(f + \frac{\alpha}{2} - \frac{n}{T_0})P^*(f - \frac{\alpha}{2} + \frac{n}{T_0})(-1)^n, \\[3mm] \qquad\qquad\qquad\qquad\qquad\qquad \alpha = \frac{2 \cdot integer - 1}{T_0}, 2 \cdot integer - 1 \neq 2n + p; \\[3mm] \frac{2\sigma^2}{T_0} \sum_{n \in N} P(f + \frac{\alpha}{2} - \frac{n}{T_0})P^*(f - \frac{\alpha}{2} + \frac{n+p}{T_0}), & \alpha = \frac{2n+p}{T_0}; \\[3mm] 0, & \alpha \neq \frac{2 \cdot integer - 1}{T_0}, \alpha \neq \frac{2n+p}{T_0}; \end{cases}$$

$$(3.69)$$

where N is the set of subcarriers to be mapped and $p \in \mathcal{P}(\mathcal{P} = \pm 2i, i = 1, 2, 3, 4, \cdots)$. From (3.69) we can embed the CSs at zero cyclic frequency by setting a group of mapping subcarriers according to (3.67) under the condition $2n + p = 0$. The magnitudes of conjugate CAF and SCF of FBMC signal with CS are drawn in Fig. 3.10 and Fig. 3.11, where two subcarriers are repeated transmitted at the value of $p = 2$. We can see that the strong cyclostationary features appear at the cyclic frequency $\alpha = 0$.

3.2.6 Signature Detector

Since complex noise does not exhibit nonconjugate (conjugate) cyclostationarity, the presence of the MCM signal under noise and interference is equivalent to the detection of the presence of non-conjugate (conjugate) cyclostationarity in the received composite signal $x(t) = s(t) + n(t)$ on the predetermined cyclic frequency, where $n(t)$ is the contribution from noise.

The signature detector in [97] can be used for efficient FBMC signal detection. Cyclostationary features generated by subcarriers set mapping can be successfully detected using spectral resolution (subcarrier spacing Δf). So the low-complexity signature detector can be designed by sliding a

window W with the width $N_s \cdot \Delta f$ (N_s is the number of subcarriers in the mapped set) around estimated nonconjugate (conjugate) SCF at the cyclic frequency α_0

$$T_{x^{(*)}} = \max_m \sum_n \widehat{S}_{x^{(*)}}^{\alpha_0}(n) W(m - n) \tag{3.70}$$

where $\widehat{S}_{x^{(*)}}^{\alpha_0}$ is estimated using a time-smoothed cyclic cross periodogram [96].

3.2.7 Numerical Results

In this part, the performance of the conjugate cyclostationary detector between FBMC signal inserted by CS and noise signal is simulated. A 512-subcarrier FBMC signal is chosen and the following assumptions are made:

1. Cognitive radio system with a bandwidth of $5MHz$, and assuming signals are transmitted at carrier frequency $f_c = 2.4GHz$.

2. The AWGN and Rayleigh fading channel are considered, respectively. A typical urban channel [103] is used with a maximum spread delay $\tau \approx 2.2\mu s$ and a Doppler frequency $f_d = 240Hz$, which corresponds to a moving speed $30m/s$.

3. Subcarriers are modulated using FBMC. 6, 12, 18 and 24 subcarriers are respectively used as the mapping subcarrier sets at zero cyclic frequency.

4. Using the detector (3.70), the entry $\widehat{S}_{x^*}^0$ is estimated using time-smoothed cyclic periodogram, where a Hamming window is used. For simplicity, a rectangular sliding window W is chosen.

5. For comparison, the traditional energy detector proposed by Urkowitz [89] is applied under the assumption of noise uncertainty, which is defined in [104]. Assuming the estimation error for noise power $\widehat{\sigma_n^2}$ is bounded by

$$(1 - \epsilon_1)\sigma_n^2 \leq \widehat{\sigma_n^2} \leq (1 + \epsilon_2)\sigma_n^2 \tag{3.71}$$

   where $0 \leq \epsilon_1 < 1$ and $\epsilon_2 \geq 0$. Then the noise uncertainty is defined as

$$U \triangleq 10 log_{10}\left(\frac{1 + \epsilon_2}{1 - \epsilon_1}\right) \tag{3.72}$$

 Receiver Operating Characteristic (ROC) curves are drawn in Fig. 3.12 $\sim$ Fig. 3.15 by averaging 500 Monte Carlo simulations for AWGN channel and Rayleigh fading channel, respectively. Fig. 3.12 gives the experimental results for an AWGN channel at different SNR levels ($0dB$, -$3dB$, -$6dB$, -$9dB$ and -$12dB$) with 6 subcarriers mapping set and an observation time $T = 1ms$ (10 FBMC symbols).

Figure 3.12: Receiver Operating Characteristic performance for AWGN channel with $N = 6$ subcarriers mapping set and an observation time $T = 1ms$
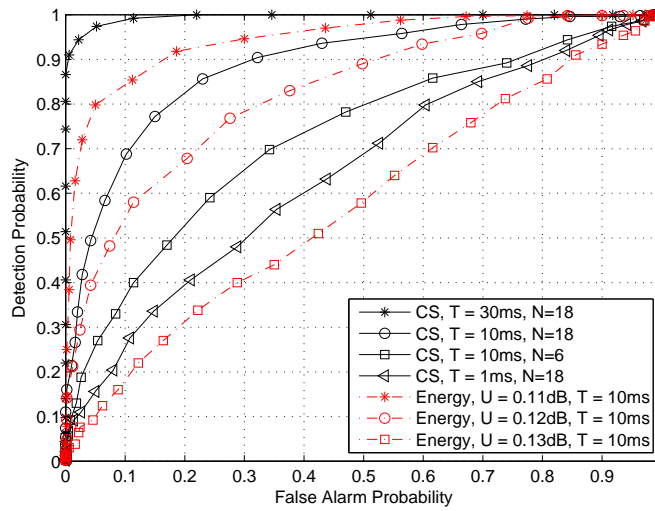
Figure 3.13: Receiver Operating Characteristic performance for AWGN channel with a fixed $SNR = -12dB$
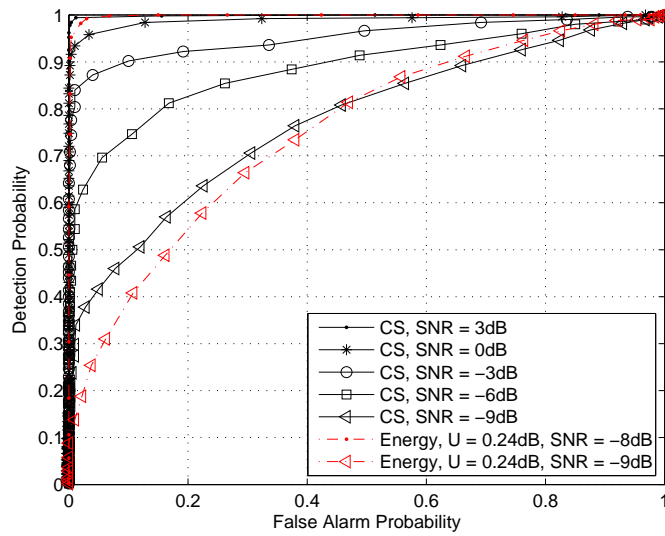
Figure 3.14: Receiver Operating Characteristic performance for Rayleigh fading channel with $N = 12$ subcarriers mapping set and an observation time $T = 3ms$
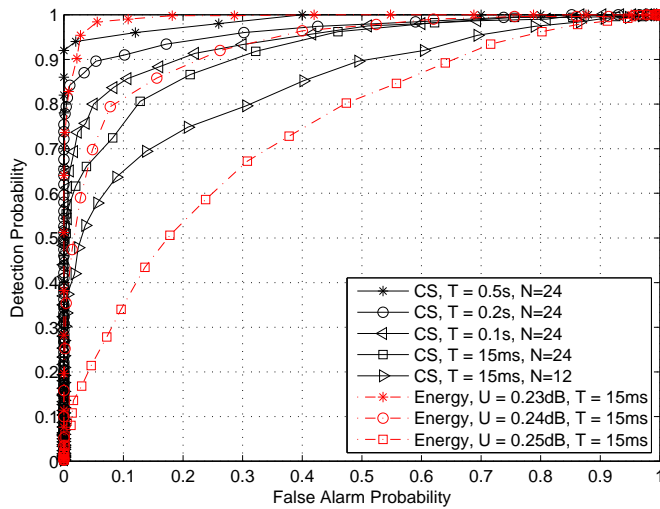
Figure 3.15: Receiver Operating Characteristic performance for Rayleigh fading channel with a fixed $SNR = -9dB$

As a comparison, the energy detector proposed in [89] with a noise uncertainty $U = 0.12dB$ is used. It can be seen that desired detection performance can be achieved for CS detector at the low SNR level, and almost 100% detection rate can be achieved when the SNR level is more than $0dB$. We can also observe that the energy detector significantly outperforms the CS detector when the noise power is well estimated.

Effects of observation time and mapping set are shown in Fig. 3.13 at a fixed $SNR = -12dB$, where the ROC curves show that the performance of the CS detector improves when longer observation time and larger mapping set are applied. In addition, energy detector performance for different noise uncertainty values is depicted in Fig. 3.13, which verifies that energy detector is very susceptible to noise uncertainty at low SNR level. Due to the noise uncertainty, the performance of energy detector does not improve even if the observation time increases. This behavior is predicted by the so called *SNR wall* [1] in [105]. Namely, the energy detector cannot distinguish the weak received signal from slightly higher noise power below some SNR level.

The results deteriorate when more realistic time variant Rayleigh fading channels are considered. As shown in Fig. 3.14, effects of SNR are illustrated at different SNR levels ($3dB$, $0dB$, -$3dB$, -$6dB$ and -$9dB$) with 12 subcarriers mapp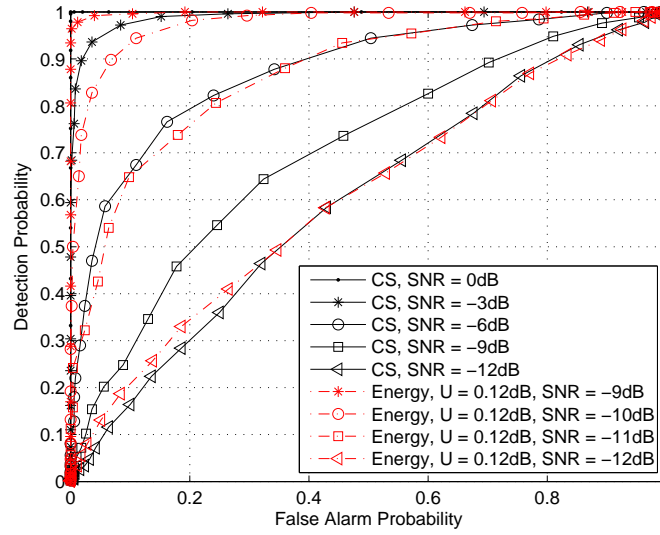ing set and an observation time $T = 3ms$ (30 FBMC symbols). Compared with Fig. 3.12, it can be seen that Rayleigh fading channel affects detection performance significantly. The energy detector with noise uncertainty $U = 0.24dB$ is compared with CS detector in Fig. 3.14, which once again shows the advantage of energy detector when the SNR level is below the SNR wall. In order to achieve higher detection reliability for CS detector, longer observation time or more mapping subcarriers are needed as shown in Fig. 3.15. It can be noted that from Fig. 3.13 and Fig. 3.15 at a low SNR level ($SNR \leq -9dB$) energy detector is not robust under the condition of a noise uncertainty $U \geq 0.13dB$.

Simulations show that the energy detector is very susceptible to noise uncertainties and its performance is dictated by the accuracy of the noise power estimate. Moreover, energy detector can't differentiate different modulated signals, noise and interference. Conversely, good performance can be achieved for CS detector with a short observation time. Detection reliability can be seriously impacted by time-variant Rayleigh fading channel, which can be overcome through the use of longer observation time and more mapping subcarriers. Besides, CS detector is not susceptible to noise uncertainty and can distinguish different modulated signals by inserting CSs at different frequency positions.

---

[1]SNR wall is the SNR below which robust detection is impossible for the given detector.

3.2.8 Conclusion

This section firstly analyzes the cyclic spectral correlation of both OFDM and FBMC signals. By utilizing a LPTV model, we have derived the explicit formulas of nonconjugate and conjugate cyclic autocorrelation and spectral correlation functions for OFDM and FBMC signals, which provide the theoretical basis for further signal detection.

Secondly, a strategy for the detection of MCM signals by embedding cyclostationary signature at the predefined cyclic frequency is investigated. Using the LPTV structure of the FBMC signal, the explicit formulas of nonconjugate and conjugate CAF and SCF with CS for FBMC signal are derived and CS can be accordingly easily inserted into the FBMC signal at some predetermined frequency position. During the simulation, a low-complexity conjugate detector is applied for detecting FBMC signal by embedding the CS at zero cyclic frequency in the AWGN and Rayleigh fading situations, respectively. All the cyclic operations at zero cyclic frequency are actually the conventional correlation and power spectral operations, which in some way reduce the computation complexity. Experimental results show that CS is an effective and robust tool for signal detection in cognitive radio network. We can improve the performance with increased subcarriers mapping size, but this causes a reduction in overall date rate because of the increased overhead. Via flexible CS position design for different MCM signals (different CR networks), identification among different modulated signals can be implemented in the same way.

The proposed cyclostationary detector in this section applies to the whole frequency detection, i.e. single-band detection, simultaneous sensing of multi-band sensing will be examined in the following section.

3.3 Filter Bank based Multi-band Sensing

Spectrum sensing has been identified as an essential enabling functionality for cognitive radio systems to guarantee that CR users could share the spectrum resource with licensed users on a non-interfering basis. Recently, simultaneous sensing of multi-band licensed user activity has been attracting more and more research interest.

In this section, we investigate a multi-band detection architecture based on Polyphase Filter Bank (PFB), which aims to reliably sense multiple active bands by exploiting the low leakage property of PFB. We have theoretically derived the expressions of detection probability and false alarm probability for PFB and FFT based detectors, respectively, and thereby a theoretical detection threshold can be defined. Final experimental results are presented to verify our theoretical analysis and demonstrate that PFB based sensing architecture has a better sensing performance than the conventional FFT.

3.3.1 Introduction

The basic concept of multi-band sensing is to firstly estimate the Power Spectral Density (PSD) and then power detection is applied in the frequency domain based on the observed power spectrum. PFB is proposed as an efficient tool for spectral analysis [16] without additional cost since each secondary user could be equipped with PFB as the receiver front end. This means that the PFB structure for communication will offer a new opportunity for sensing at no extra cost. In [31][32], the performance of the PFB based multi-band sensing is evaluated in comparison with conventional Periodogram Spectrum Estimator (PSE), and the final simulation results demonstrate the significant advantage of the PFB multi-band sensing compared to conventional PSE. Nevertheless, both of these papers employ an optimal Prolate Sequence Window (PSW) [106] as a prototype filter of the PFB. This PSW prototype filter as a spectral analyzer cannot be reused for communication.

In this section, our motivations for multi-band sensing are firstly focused on the PFB based on a prototype filter which has been applied for transmission. The prototype filter advocated in the projet PHYDYAS [19] is considered herein. Secondly, the theoretical expressions of detection and false alarm probabilities for PFB and PSE based detectors are derived, respectively. Thereby, proper threshold levels for different detectors can be achieved to ensure a fair comparison. Specifically, the PFBs using the prototype filter of PHYDYAS and PSW are investigated and compared with the conventional PSE, and experimental results verify the theoretical analysis and reveal that PFB is a better spectrum analyzer instead of PSE.

The rest of this section is organized as follows: In *Section 3.3.2*, we give the system model and the multi-band sensing architecture. In *Section 3.3.3*, theoretical expressions of detection and false alarm probabilities for PHYDYAS based PFB, PSW based PFB and PSE, are derived, respectively. Experimental results are given in *Section 3.3.4*. Finally, *Section 3.3.5* concludes this section.

3.3.2 System Model and Multi-band Sensing Architecture

3.3.2.1 System Model
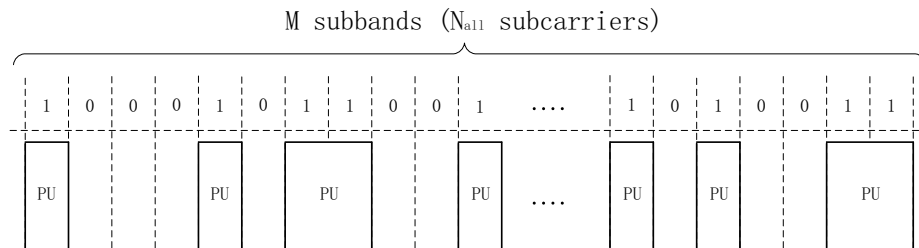
Figure 3.16: Primary channel distribution

In the context of cognitive radio system, an FBMC based primary system operating over a wide-band channel with N_{all} subcarriers is considered. As shown in Fig. 3.16, the whole frequency band licensed to the Primary Users (PUs) is divided into M non-overlapping subbands with N_s subcarriers per subband. In a particular time interval or geographical region, some of the M subbands might not be occupied by the PUs and are available for Secondary Users (SUs). Fig. 3.16 displays the primary channel distribution in some time interval, wherein the subbands occupied by primary users are referred to as "1", whereas the available subbands for SUs are referred to as "0".

According to the above assumed primary model, the crucial task of SU is to sense the M subbands and identify available subbands for opportunistic use. The basic multi-band sensing scheme will be introduced in the next subsection.

3.3.2.2 Multi-band Sensing Architecture
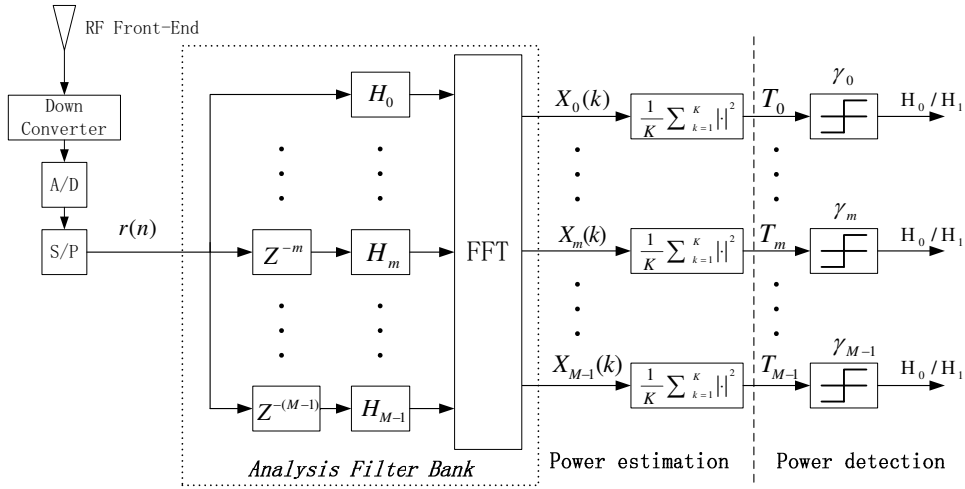
Figure 3.17: Multi-band sensing architecture: joint power estimation and energy detection

In our study, we take into account the detection of PUs for multiple frequency subbands instead of considering one single band at a time. The basic multi-band sensing architecture is given in Fig. 3.17. It is noted that the accomplishment of the multi-band sensing comprises of two basic parts: power estimation and power detection. Every secondary node in the cognitive radio network is equipped with a FFT or a PFB based spectrum analyzer for the power estimation over the band of interest. On the basis of the estimated power density spectrum, the simple energy detector is then applied in different subbands.

For simplicity, the PU signal affected by an AWGN channel is considered herein, and we assume that the noise variance σ_n^2 is perfectly known at the receiver due to the measurements when signal is

absent. The binary test hypotheses at the mth subband are

$$H_0: \quad r_m(n) = w_m(n)$$
$$H_1: \quad r_m(n) = s_m(n) + w_m(n) \tag{3.73}$$

where $s_m(n)$ and $w_m(n)$ are related to the primary transmitted signal and the band limited noise signal at the mth subband, respectively.

The received wideband signal $r(n) = \sum_{m=0}^{M-1} r_m(n)$ including all subbands' information is firstly processed by SU to estimate the frequency spectrum X_m in all the subbands using M point FFT or polyphase AFB

$$X_m(k) = \sum_{n=0}^{M-1} \sum_{l=1}^{L} r\big[(l-1)M+n+kM\big] h\big[(l-1)M+n\big] \cdot e^{-2\pi j \frac{[(l-1)M+n]m}{M}},$$
$$m = 0, 1, \ldots, M-1; \tag{3.74}$$

where $h(n)$ is the $L \times M$ prototype filter (rectangular window is a special filter for PSE where $L = 1$) used by the current spectrum analyzer. Then the test statistic for the mth subband is given

$$T_m = \frac{1}{K} \sum_{k=1}^{K} |X_m(k)|^2 \tag{3.75}$$

where $K = N/M$, and N is the number of samples of received signal. Given the threshold γ_m, the detection rule is: $T_m \geq \gamma_m \rightarrow H_1, T_m < \gamma_m \rightarrow H_0$.

3.3.3 Theoretical Sensing Performance

In this part, the wideband sensing performance are investigated from a theoretical point of view. Three different spectrum analyzers are considered: conventional PSE, PHYDYAS based PFB and PSW based PFB. The prototype filters of PSW and PHYDYAS with $M = 128$ and an overlapping factor $L = 4$ are sketched in Fig. 3.18, where PSW is an optimal window designed by minimizing stopband energy [106], and PHYDYAS is a Square-Root Nyquist filter designed in [13].

When PHYDYAS based PFB or PSE spectrum analyzers are applied, the frequency estimation $X_m(k)$ in Fig. 3.17, are complex independent observations (the proof is provided in *Appendix A.1*). According to the central limit theorem (assuming K is sufficiently large), the distributions of T_m in the absence (H_0) and the presence (H_1) of primary signal are subject to Gaussian approximation (refer to *Appendix A.2*)

$$H_0: \quad T_m \approx \mathcal{N}\big(\sigma_{H_0}^2, \frac{1}{K}\sigma_{H_0}^4\big)$$
$$H_1: \quad T_m \approx \mathcal{N}\big(\sigma_{H_1}^2, \frac{1}{K}\sigma_{H_1}^4\big) \tag{3.76}$$
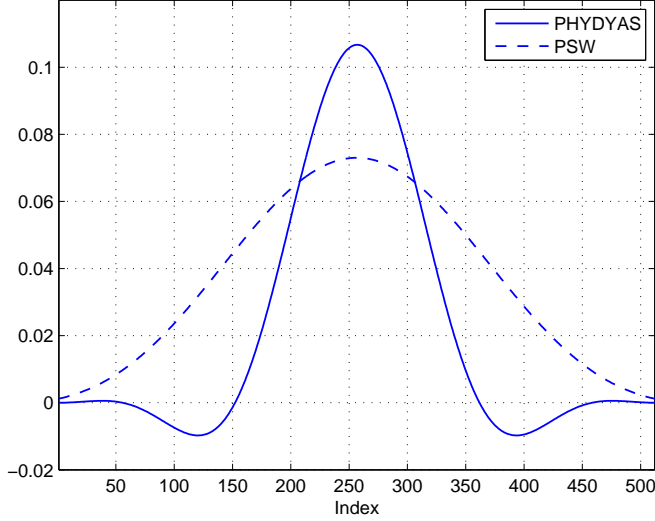
Figure 3.18: The impulse responses of two different prototype filters

here $\sigma^2_{H_0}$ and $\sigma^2_{H_1}$ are the variances of $X_m(k)$ in the absence and the presence of primary signal, respectively.

With respect to PSW based PFB, the central limit theory is no longer valid since $X_m(k)$ are complex correlated observations (refer to appendix $A.1$). In order to facilitate our theoretical analysis, the test statistic T_m using PSW based PFB is approximately treated as Gaussian distribution for a large K, and the distributions in the absence and the presence of primary signal can be written as (the derivation is elaborated in *Appendix A.3*)

$$H_0: \quad T_m \approx \mathcal{N}\big(\sigma^2_{H_0}, \frac{2}{K}\sigma^4_{H_0}\big)$$
$$H_1: \quad T_m \approx \mathcal{N}\big(\sigma^2_{H_1}, \frac{2}{K}\sigma^4_{H_1}\big) \tag{3.77}$$

In the literature [31][32], the variances $\sigma^2_{H_0}$ and $\sigma^2_{H_1}$ in (3.76) and (3.77) are simply regarded as the noise variance σ^2_n and the signal-plus-noise variance $\sigma^2_n + \sigma^2_s$, respectively, and thus the same theoretical threshold was used to implement the subband detection for both windowed FFT and filter bank based spectrum analyzer. For more precise detection and fair detection performance comparison, more stringent requirement of defining a proper detection threshold for various spectrum analyzers should be considered.

Next, we attempt to achieve the corresponding variance values $\sigma^2_{H_{0(1)}}$ of the frequency estimation $X_m(k)$ for conventional PSE, PHYDYAS based PFB and PSW based PFB. In the first instance, our analysis is based on two extreme cases, as illustrated in Fig. 3.19. It is important to note that the
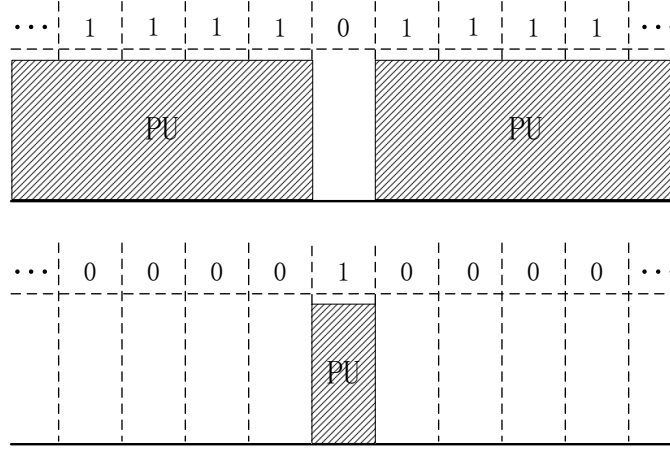
Figure 3.19: Two extreme cases corresponding the absence and the presence of primary signal

spectrum estimation disparity between these two extreme cases will be the smallest. In the absence of primary signals, the extreme (worst) case is in such a way that the detected subband (referred to as "0" in the top graphic of Fig. 3.19) is fully surrounded by primary users, which will contribute to the power estimation result. Conversely, in the presence of primary signal, the worst detection result of the detected subband (referred to as "1" in the bottom graphic of Fig. 3.19) emerges when there is no primary users in the neighborhood.

The detection performance of each detected subband could be well guaranteed provided that the detection requirement of the subbands in the two extreme cases are satisfied. For this reason the theoretical detection threshold can be yielded by analyzing the statistic property of these two extreme cases.

Assuming the received signal $r(n)$ is a Gaussian signal with zero mean, the variance of X_m is calculated by

$$Var(X_m) = \mathbb{E}(|X_m|^2) - \mathbb{E}^2(X_m) = \mathbb{E}(|X_m|^2) = R_{xx}(0)$$
$$= \sum_{i=-(LM-1)}^{LM-1} R(i)\left(h \otimes h[LM+i]\right)e^{-2\pi j \frac{im}{M}} \tag{3.78}$$

According to the property [107] of Fourier Transform, (3.78) can be also expressed as

$$Var(X_m) = S(f) \otimes |H(f)|^2\big|_{f=\frac{m}{M}} \tag{3.79}$$

where $S(f)$ is the true PSD of $r(n)$, and $H(f)$ is the Fourier transform of the prototype filter $h(n)$. Equation (3.79) corresponds to a periodic convolution of $S(f)$ and $|H(f)|^2$.

Fig. 3.20 illustrates the convolution relation between the primary signal PSD ($S_0(f)$ is the PSD of noise and $S_1(f)$ is the PSD of noise plus primary signal) and the frequency spectrum square $|H(f)|^2$

of three different prototype filters for the extreme case at the absence of primary signal. Assuming that $\sum_{n=0}^{LM-1} h^2(n) = 1$, then $\int_0^B |H(f - \frac{m}{M})|^2 df = B$, where $B = \frac{1}{T}$ (T represents the sampling interval). We also assume that $S_0(f) = N_0$, $S_1(f) = N_0 + N_1$, and the SNR is defined as $10log_{10}\frac{N_1}{N_0}$. Then the variance of X_m at the absence of primary signal can be computed as

$$
\begin{aligned}
\sigma_{H_0}^2 &= Var(X_m|H_0) \\
&= \int_{f_1}^{f_2} S_0(f)|H(f - \frac{m}{M})|^2 df + \int^{\mathbb{A}} S_1(f)|H(f - \frac{m}{M})|^2 df \\
&= C_1 N_0 B + C_0(N_0 + N_1)B = \sigma_n^2 + C_0 \sigma_s^2
\end{aligned}
\tag{3.80}
$$

where f_1 and f_2 are indicated in Fig. 3.20. $\mathbb{A}$ denotes the integration region $(0, f_1) \cup (f_2, B)$, $C_0 = \frac{\int^{\mathbb{A}} |H(f-\frac{m}{M})|^2 df}{\int_0^B |H(f-\frac{m}{M})|^2 df}$, $C_1 = \frac{\int_{f_1}^{f_2} |H(f-\frac{m}{M})|^2 df}{\int_0^B |H(f-\frac{m}{M})|^2 df}$, and $\sigma_s^2 = \sigma_n^2 \cdot SNR$.
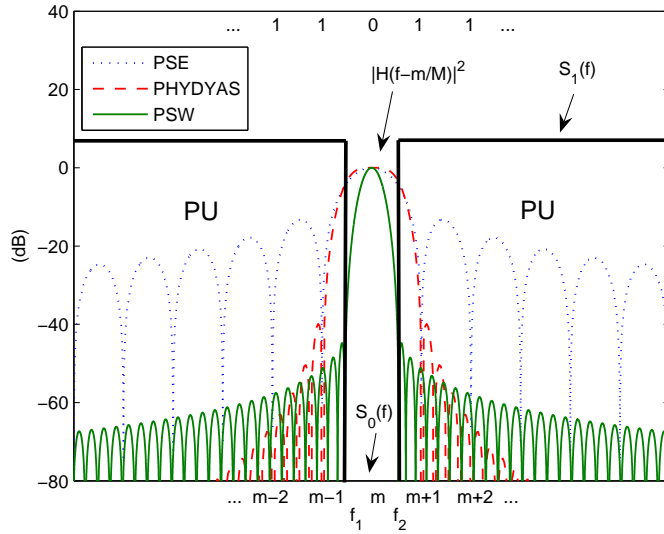
Figure 3.20: The convolution relation between the primary signal spectrum and the spectra of three different prototype filters

The variance of X_m for the extreme case at the presence of primary signals can be derived in the same way

$$
\sigma_{H_1}^2 = Var(X_m|H_1) = \sigma_n^2 + C_1 \sigma_s^2
\tag{3.81}
$$

The coefficient values of C_0 and C_1 corresponding to different prototype filters are presented in Table 3.1.

Table 3.1: Corresponding coefficient values for three prototype filters

Prototype filters	PSE	PHYDYAS	PSW
C_0	0.225	0.126	0
C_1	0.775	0.874	1

As a result, the expressions of false alarm probability and detection probability can be computed by [1]

For PHYDYAS or PSE:

$$P_{FA,m} = Q\left(\frac{\gamma_m - \sigma_{H_0}^2}{\sqrt{\frac{1}{K}\sigma_{H_0}^4}}\right), P_{D,m} = Q\left(\frac{\gamma_m - \sigma_{H_1}^2}{\sqrt{\frac{1}{K}\sigma_{H_1}^4}}\right); \tag{3.82}$$

For PSW:

$$P_{FA,m} = Q\left(\frac{\gamma_m - \sigma_{H_0}^2}{\sqrt{\frac{2}{K}\sigma_{H_0}^4}}\right), P_{D,m} = Q\left(\frac{\gamma_m - \sigma_{H_1}^2}{\sqrt{\frac{2}{K}\sigma_{H_1}^4}}\right); \tag{3.83}$$

3.3.4 Numerical Results

In the following, we numerically evaluate the multi-band sensing scheme in a practical point of view. Assuming a $B = 30MHz$ licensed system containing $N_{all} = 8192$ [2] subcarriers where the wideband channel is equally separated into $M = 128$ subbands with $N_s = 64$ subcarriers per subband. It is also assumed that the channel is AWGN with zero mean and noise power density -174dBm/Hz. The primary system load rate is 50%. The length of the prototype filters of PFB is $\beta = 4M = 512$. The center frequency is $f_c = 3.6GHz$. The received RF signal by RF Front-End is down-converted without frequency offset. $K = 250$ groups of sampled signals with 128 samples per group are used for simulating the multi-band sensing.

At the first stage, we analyze one detected subband which suffers from the extreme situations shown in Fig. 3.19. From a cognitive radio perspective, one of the main challenges is how to deal with an optimal tradeoff between the throughput of Secondary System (SS) and the interference from SS to Primary System (PS). Normally, the PS has the spectrum use priority so the SS should try to avoid introducing severe interference to PS. The amounts of throughput and interference are associated with

---

[1]$Q(\cdot)$ is the tail probability of the standard normal distribution, which can be expressed in terms of the error function $Q(x) = \frac{1}{2}\left(1 - erf(\frac{x}{\sqrt{2}})\right)$.

[2]This parameter set is to ensure that within each subband there are enough subcarriers, thereby the occupancy situation of each subband can be well regarded as "1" or "0".

the false alarm probability and the detection probability, respectively. In other words, low false alarm probability serves to maintain high throughput and high detection probability guarantee the QoS of PS. Therefore, both detection probability performance and false alarm probability performance are simulated. Fig. 3.21 shows the probability density functions for different spectrum analyzers at a fixed $SNR = -6dB$. It can be noted that simulated results match well with theoretical results. Besides, we can envisage that PHYDYAS based spectrum analyzer is able to achieve the highest detection probability than others when the same false alarm probability is prescribed to different spectrum analyzers. As well, the smallest false alarm probability could be achieved when prescribing a fixed detection probability.
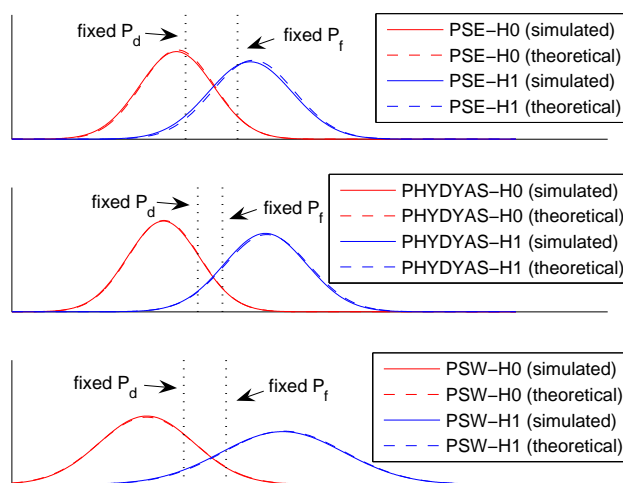
Figure 3.21: Probability density functions for three different spectrum analyzers

Given a fixed false alarm probability $P_f = 5\%$ (denoted with dotted lines in Fig. 3.21), a theoretical threshold can be computed according to (3.82) and (3.83), and then this threshold is used to compute the probability of detection. Similarly, the probability of false alarm can be computed for a given detection probability $P_d = 95\%$. The performance curves of the detection probability and the false alarm probability versus SNR level are plotted in Fig. 3.22 and Fig. 3.23, respectively. Each decision statistic is implemented over 10^3 simulation runs. We can observe that the performance of PFB (PHYDYAS and PSW) exhibits a significant improvement (at maximum 25% performance gain) relative to PSE because of the low spectral leakage property of PFB. It is interesting to find that PHYDYAS performs slightly better than PSW, which can be explained by the fact the variance of PSW based frequency estimation variable is twice as large as that of PHYDYAS (refer to (3.76)(3.77)).
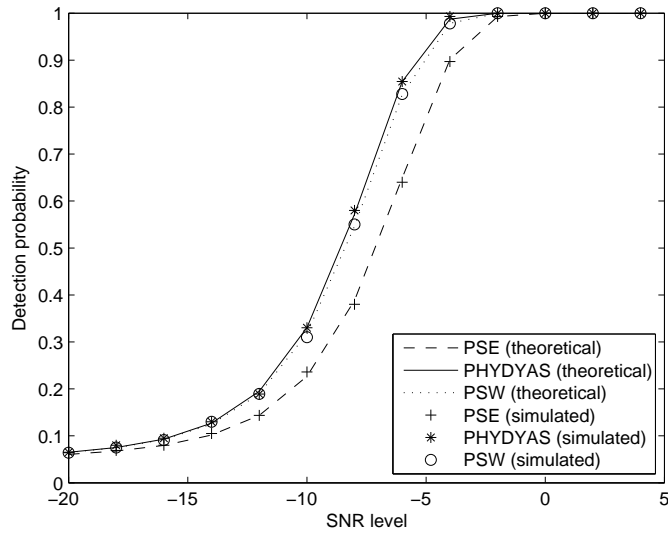
Figure 3.22: Probability of detection vs. SNR level for the extreme cases ($P_f = 5\%$)
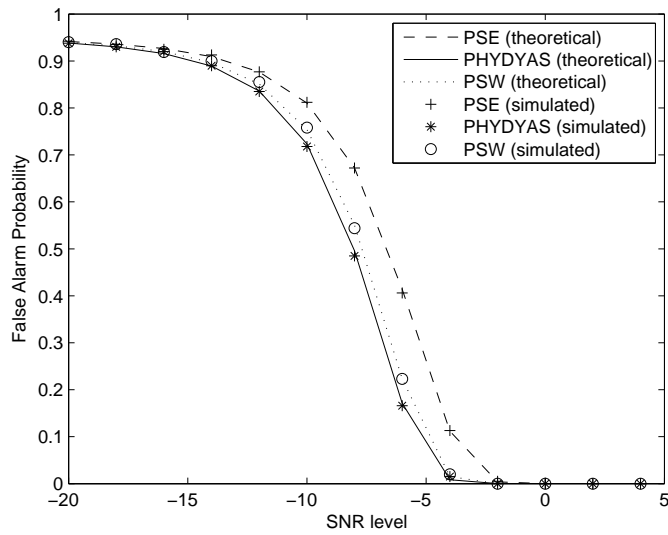
Figure 3.23: Probability of false alarm vs. SNR level for the extreme cases ($P_d = 95\%$)
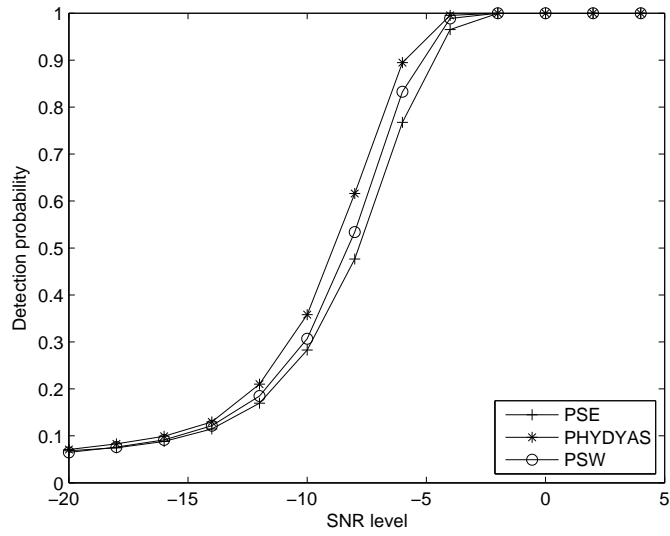
Figure 3.24: Probability of detection vs. SNR level for the general case ($P_f = 5\%$)
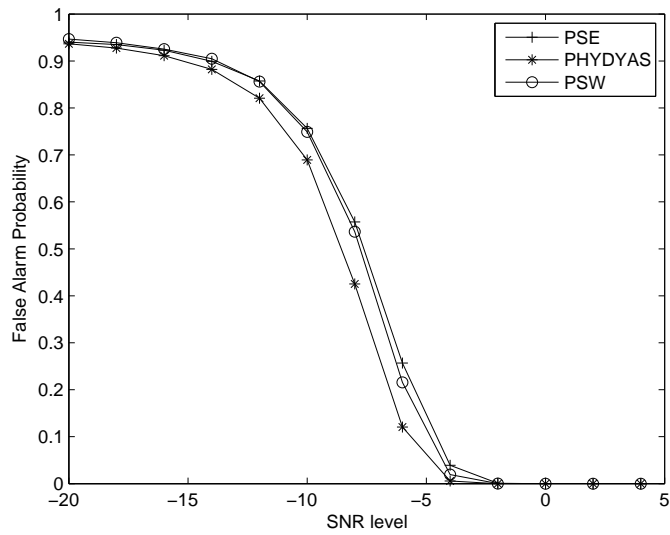
Figure 3.25: Probability of false alarm vs. SNR level for the general case ($P_d = 95\%$)

Next, we compare the experimental results of more general case (as shown in Fig. 3.16) by averaging the detection and the false alarm probabilities over all the detected subbands. In this case, the same detection thresholds determined in the extreme cases are employed to ensure $P_f \leq 5\%$ and $P_d \geq 95\%$. Fig. 3.24 and Fig. 3.25 show the detection probability and the false alarm probability versus SNR level for the general case, respectively. As expected, PHYDYAS and PSE in the general case can achieve better performances than their counterparts in the extreme cases because of the average effect. However, PSW has the same performance in both extreme and general cases due to its well localized frequency spectrum (refer to Fig. 3.20 and Table 3.1). Compared with the extreme cases, the performance gap between PHYDYAS and PSE decreases (at maximum 15% performance gain), but the performance difference between PHYDYAS and PSW increases especially for the probability of false alarm.

In order to examine the detection performance in a more practical case, the frequency offset effect stemming from the oscillator stability is shown in Fig. 3.26 and Fig. 3.27 for the general case with a fixed $SNR = -6dB$. The change of an oscillator in frequency is usually measured in parts per million (ppm). Assuming that the oscillator used for the down-conversion has a stability range between 0 and 30 ppm. We observe that the amount of frequency offset has an influence on the detection performance. A large amount of frequency offset leads to a significant performance degradation. At the same time, it can be seen that PFB always outperforms the PSE at different frequency offset levels. Additionally, PSW has a different performance curve from those of PHYDYAS and PSE. The reason lies in the very localized frequency response of PSW (Fig. 3.20), which leads to perfect sideband rejection. That is why the performance of PSW remains almost unchanged for insignificant frequency offset, while drops faster than PHYDYAS and PSE for significant frequency offset.

Lastly, we analyze the effect of primary system load rate on the detection performance. In Fig. 3.28 and Fig. 3.29, we show the probabilities of detection and false alarm as a function of primary system load rate with a fixed $SNR = -6dB$. It should be noted that PSW is invulnerable to the system load rate because of its ideal sideband rejection. As regards PHYDYAS and PSE, the detection probability performance improves as the rate of system load increases. On the contrary, the false alarm probability performance degrades as the increase of system load rate. In particular, the performance of PHYDYAS dominates PSE over all the different load rates as illustrated in Fig. 3.28 and Fig. 3.29, wherein we observe that the large performance gap of detection probability between PHYDYAS and PSE can be achieved in a low system load rate, whereas the large performance gap of false alarm probability is achieved in a high loaded system.
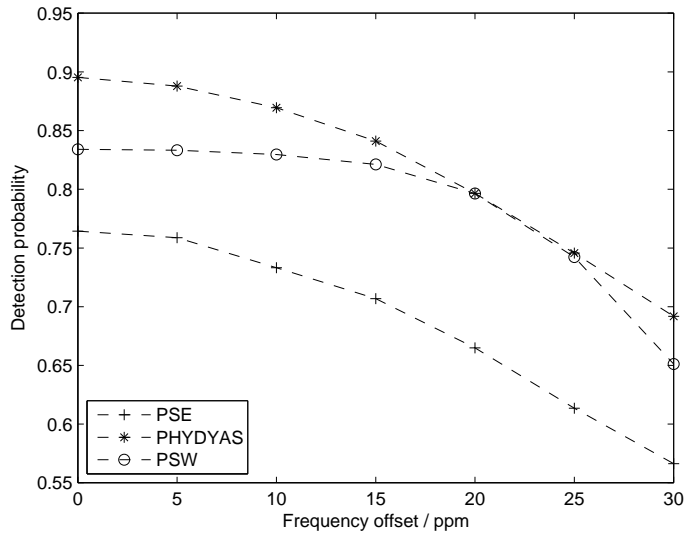
Figure 3.26: Probability of detection vs. frequency offset level with a fixed SNR=-6dB ($P_f = 5\%$)
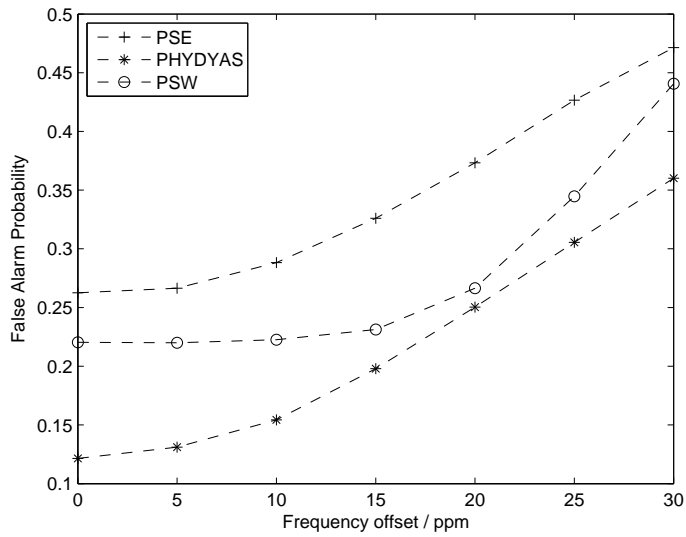
Figure 3.27: Probability of false alarm vs. frequency offset level with a fixed SNR=-6dB ($P_d = 95\%$)
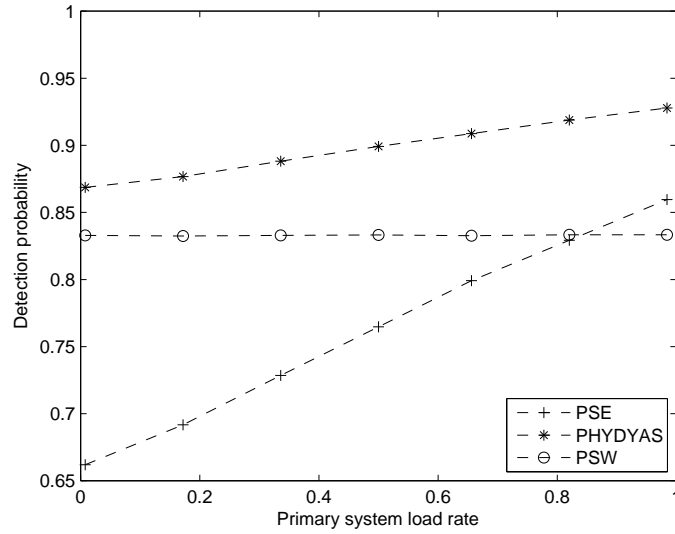
Figure 3.28: Probability of detection vs. primary system load rate with a fixed SNR=-6dB ($P_f = 5\%$)
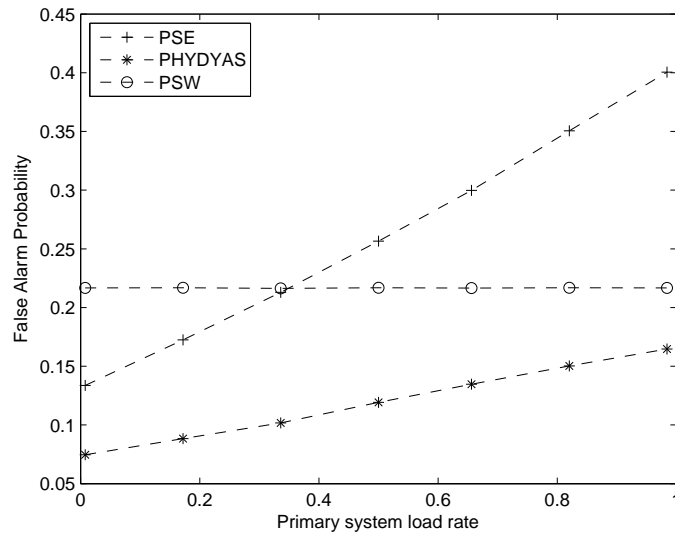
Figure 3.29: Probability of false alarm vs. primary system load rate with a fixed SNR=-6dB ($P_d = 95\%$)

3.3.5   Conclusion

We have investigated the PFB based spectrum analyzer to show its applicability for multi-band sensing in cognitive radio context. Our study includes theoretical and experimental analysis for three kinds of spectrum analyzers: conventional PSE, PHYDYAS based PFB and PSW based PFB. The numerical results reveal that PSE based spectrum analyzer is sensitive to the spectral leakage. Conversely, PFB exhibits more efficient and reliable detection performance by taking advantage of its low spectral leakage property, which further enhances the multi-band sensing application of PFB in cognitive radio networks. From the view of computational complexity, the performance gain obtained by PFB does not come with the penalty of increased complexity due to the inherent parallel structure of PFB.

3.4   Conclusion

In this chapter, we firstly introduce four traditional transmitter detectors, and discuss their advantages and disadvantages in the context of CR. Eventually, cyclostationary feature detector is justified to be a suitable spectrum sensing tool. Thus, cyclostationary characteristics of MCM signals are investigated in the next section, and the explicit theoretical formulas of CAF and SCF for OFDM and FBMC signals are derived. According to these derived formulas, cyclostationary signatures can be easily embedded into the MCM signals, thereby, a CS based cyclostationary detector is proposed for detecting MCM signals and noise. Numerical results exhibit the robustness of the CS detector to noise uncertainty compared to the traditional energy detector. Lastly, filter bank based multi-band sensing architecture is proposed and its sensing performance is compared with the FFT based multi-band sensing architecture. Theoretical analysis and numerical results verify that, compared with the significant spectral leakage of OFDM, higher spectrum resolution and larger dynamic spectrum range can be achieved by applying FBMC due to its low spectral leakage property.

Assuming the available spectrum resource is obtained through certain robust spectrum sensing method, the next task is how to efficiently and fairly share these valuable frequency spectra. In the following chapter, a resource allocation algorithm considering multi-carrier modulation in CR context is proposed, and the channel capacities of OFDM and FBMC based CR systems are evaluated by theoretically analyzing the inter-cell interference resulting from timing offset.

Capacity Comparison of OFDM / FBMC for Uplink CR Systems

To solve the problem of future spectrum scarcity, Cognitive Radio (CR) is proposed to automatically detect and exploit unused spectrum while avoiding harmful interference to the incumbent system. Multicarrier communications have been suggested as a candidate for CR networks due to its flexibility to fill the spectrum holes. In this chapter, we emphasize the spectral efficiency comparison of a CR network using two types of multicarrier communications: conventional Orthogonal Frequency Division Multiplexing (OFDM) with Cyclic Prefix (CP) and Filter Bank based MultiCarrier (FBMC) modulations. Assuming the spectrum sensing is perfectly implemented, then the spectral efficiency on the detected spectrum holes depends on the multicarrier scheme and the resource allocation strategy that the secondary system adopts. In order to reduce the complexity, we propose a resource allocation algorithm in which subcarrier assignment and power allocation are carried out sequentially.

The rest of this chapter is organized as follows: The basic introduction is stated in *Section 4.1*. In *Section 4.2*, we give the system model and formulate our problem, wherein the mean inter-cell interference tables of OFDM and FBMC are introduced. In *Section 4.3* and *Section 4.4*, our proposed resource allocation algorithms for single-user and multi-user are presented, respectively. Simulation results are given in *Section 4.5*. Finally, *Section 4.6* concludes this chapter.

4.1 Introduction

In [33][108], the mutual interference between Primary User (PU) and Secondary User (SU) for FBMC and OFDM based CR systems are investigated, respectively. This kind of mutual interference depends on the out-of-band radiation which is determined by the Power Spectral Density (PSD) models of multicarrier signals. In [45], a power loading scheme to maximize the downlink capacity of the CR system under the interference constraint based on the out-of-band radiation of PSD is proposed, and then according to this proposed scheme, the CR systems based on OFDM and FBMC are evaluated and compared in terms of power allocation and the system throughput in [46], in which an iterative Power Interference constraint algorithm (PI-algorithm) to iteratively allocate the subcarrier power is

proposed. However, the interference induced from PU to SU is assumed to be negligible and channel pathloss is not considered.

In fact, the cross-interference between PU and SU we encounter in an actual CR network does not depend on the out-of-band radiation of PSD, but results from imperfect synchronization, e.g. in a well-synchronized OFDM based CR system, there will be no cross-interference even though the PSD of OFDM signal exhibits significant side-lobe due to its rectangular filter. In [109], inter-cell interferences resulting from timing offset for OFDM and FBMC based systems are firstly investigated and compared. Interference tables of OFDM and FBMC modeling the mean interference are given. These tables give a clear model on the inter-cell interference, and will be used to analyze the resource allocation performance in this chapter instead of out-of-band radiation of PSD. We focus on the comparison of OFDM and FBMC based CR networks in terms of the averaged spectral efficiency of the secondary system, which depends on its resource allocation strategy adopted by the secondary system. If the same resource allocation algorithm is applied for OFDM and FBMC based well-synchronized systems, their capacity performances will be identical under the same system model because no interference issue is involved. So whichever resource allocation algorithm is adopted in CR systems will not change the final comparison conclusion: FBMC is more efficient in spectral use than OFDM, which mainly depends on the inter-cell-interference level. We propose a resource allocation scheme under an uplink scenario considering pathloss and Rayleigh channel, and a maximization of sum-rate is formulated with both power constraint and inter-cell interference constraint based on the interference tables in [109].

The implementation of joint subcarrier assignment and power allocation needs substantial computation and therefore is not considered in practical systems. Without loss of generality, our resource allocation procedure is split into two steps. First of all, SUs are assigned to the detected spectrum holes, which is implemented by using a proposed Averaged Capacity metric (AC-metric) and the Hungarian Algorithm (HA). This AC-metric is proved to offer a better performance than that using traditional SNR-metric. When the SUs are assigned to the spectrum holes, the second part of the procedure: power allocation, is solved by the Gradient Projection Method (GPM) [110] instead of using PI-algorithm and the Lagrangian multiplier method. GPM is an efficient mathematical tool for the convex optimization problems having linear constraints, and optimal power allocation result can be obtained with low computational complexity. The numerical results demonstrate that the spectral efficiency of FBMC based CR secondary network is close to that of the perfectly synchronized case and can achieve higher spectral efficiency than OFDM based CR network.

4.2   System Model and Problem Formulation

In the context of cognitive radio system, a group of secondary users gathering and communicating with a hot spot called Secondary Base Station (SBS), make up a CR system. In the rest of this chapter, we call one CR system with some secondary users and a SBS as *secondary cell*.
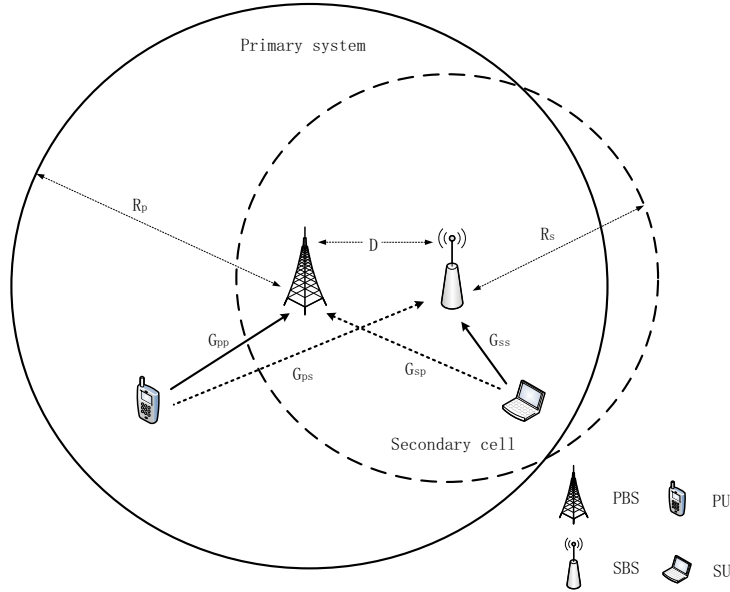
Figure 4.1: Cognitive radio networks with one primary system and one secondary cell
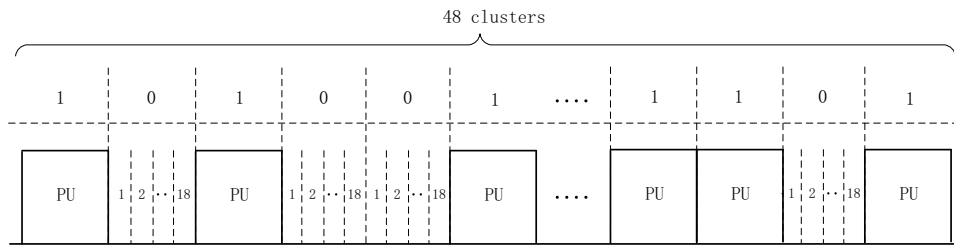
Figure 4.2: Distributions of the primary users and the spectrum holes with $N_{all} = 48$ and $L = 18$

As shown in Fig. 4.1, an uplink scenario of CR networks consisting of one primary system with one PU and one secondary cell with one SU is graphed, where D is the distance between the Primary Base Station (PBS) and SBS, and R_p and R_s are the radius of primary system and secondary cell, respectively. A frequency band of N_{all} clusters with L subcarriers in each cluster is licensed to primary system. Fig. 4.2 shows the distributions of the primary users (referred to as "1") and the

spectrum holes (referred to as "0") with $N_{all} = 48$ and $L = 18$. [1]

Given above basic uplink scenario, we make the following assumptions for our system model:

1. The goal of this chapter is the spectral efficiency comparison, so the simple scenario (Fig. 4.1) with one primary system and one secondary cell is considered.

2. Primary system and secondary cell apply the same multicarrier modulation scheme (OFDM or FBMC).

3. SUs in the secondary cell are synchronized, and SBS can perfectly sense the free bands of the licensed system.

4. SBS has the channel knowledge of G_{ss} (indicated in Fig. 4.1) and full control of its own attached SUs.

5. Primary system and secondary cell are assumed to be unsynchronized, so inter-cell interference exists between primary system and secondary cell.

6. We consider a frequency selective channel with flat Rayleigh fading on each subcarrier, and we assume that the channel changes slowly so that the channel gains will be constant during transmission.

7. Our simulation is conducted without considering nonlinear High Power Amplifier (HPA).

In [109], the authors compare the inter-cell interferences of OFDM and FBMC in an unsynchronized Frequency Division Duplex (FDD) system. All the cells present in the system use the same frequency bands and a perfect frequency and time synchronization between the users of interest and its own base station is assumed, which means that the interference will only come from the other cells. In the analysis process, frequency offset is not considered, nevertheless, different cells are not time-synchronized. To estimate the detrimental effects of interference caused by adjacent cells, a two-cell layout with one user located at the border of the interest cell (the other cell is referred to as *interfering cell*) is assumed. The mean inter-cell interference of the interest user from the interfering cell is computed when the base station in the interfering cell transmits a single complex symbol with power that equals to "1" on the kth frequency slot and the nth time slot. The explicit interference formulas of OFDM and FBMC have been derived in [109]. It is found that the inter-cell interference of OFDM only depends on the timing offset, and inter-cell interference of FBMC depends both the timing offset and the phase offset.

---

[1]Here we have chosen the practical values of WiMAX 802.16 for the number and size of clusters.

The authors in [109] have concluded that the interference level will become lower with the increase of the cyclic prefix duration $\triangle$. Conversely, if we reduce $\triangle$, the interference level will become higher. In our study, we choose the $\triangle$ value of WiMAX 802.16. The mean interference table of CP-OFDM ($\triangle = $ T/8) for an uniformly distributed timing offset $\tau \in [\frac{\triangle}{2}, T + \frac{3\triangle}{2}]$ (T indicates one symbol period) is given in Table 4.1. On the other hand, a filter bank with an overlapping factor "4" designed using the method in the projet PHYDYAS [19] is chosen for our study. Generally, FBMCs with frequency-localized prototype filters have negligible inter-cell-interference because of theirs special filter configurations, therefore, the interference level almost does not change if we use other types of FBMCs. The mean interference table of FBMC in the project PHYDYAS for an uniformly distributed timing offset $\tau \in [T/2, 3T/2]$ and also for an uniformly distributed phase offset $\varphi \in [0, 2\pi]$ is given in Table 4.2. In the mean interference tables, only main interfering slots whose interference powers are larger than "10^{-4}" are considered. We can see that for CP-OFDM systems, inter-cell interference comes from many frequency slots and only two consecutive time slots. On the contrary, the inter-cell interference of FBMC with "15" interfering slots is more localized in frequency than that of OFDM, which has "30" interfering slots. However, the inter-cell interference of FBMC spreads over more time slots which depends on the length of prototype filter.

When we transmit a burst of independent complex symbols, the interference incurred on one subcarrier equals to the sum of the interference for all the time slots. The corresponding frequency inter-cell interference powers which are larger than "10^{-3}" for OFDM, FBMC, and the Perfectly Synchronized (PS) cases are given in Table 4.3. It can be observed that the number of subcarriers that induce harmful interference to primary user of OFDM and FBMC are "8" and "1", respectively.

As shown in Fig. 4.2, the primary users and secondary users share adjacent frequency bands, and one spectrum hole might have one or multiple clusters, that is, one secondary user is permitted to occupy at least L subcarriers. Nevertheless, only "1" subcarrier (FBMC) or "8" subcarriers (OFDM) really induces inter-cell interference to primary user. Inter-cell interferences between primary user and secondary user in OFDM and FBMC based CR networks are graphed in Fig. 4.3. We can see that for primary user, only the eight subcarriers (OFDM) or the one subcarrier (FBMC) adjacent to secondary user suffer from the inter-cell interference, and the same situation for secondary user. For our following theoretical analysis, the simplified interference vectors of OFDM and FBMC are defined as (see Table 4.3)

$$
\begin{aligned}
V^{ofdm} = [&8.94 \times 10^{-2}, \quad 2.23 \times 10^{-2}, \quad 9.95 \times 10^{-3}, \quad 5.60 \times 10^{-3}, \\
&3.59 \times 10^{-3}, \quad 2.50 \times 10^{-3}, \quad 1.84 \times 10^{-3}, \quad 1.12 \times 10^{-3}] \\
V^{fbmc} = [&8.81 \times 10^{-2}, \quad 0, \quad 0, \quad 0, \quad 0, \quad 0, \quad 0, \quad 0] \quad\quad\quad (4.1)
\end{aligned}
$$

Table 4.1: Mean interference power table of OFDM

t / f	n	n+1
k+7	9.19E-04	9.19E-04
k+6	1.25E-03	1.25E-03
k+5	1.80E-03	1.80E-03
k+4	2.81E-03	2.81E-03
k+3	5.00E-03	5.00E-03
k+2	1.13E-02	1.13E-02
k+1	4.50E-02	4.50E-02
k	3.52E-01	3.52E-01
k-1	4.50E-02	4.50E-02
k-2	1.13E-02	1.13E-02
k-3	5.00E-03	5.00E-03
k-4	2.81E-03	2.81E-03
k-5	1.80E-03	1.80E-03
k-6	1.25E-03	1.25E-03
k-7	9.19E-04	9.19E-04

Table 4.2: Mean interference power table of FBMC

t / f	n-2	n-1	n	n+1	n+2
k-1	1.08E-03	1.99E-02	4.60E-02	1.99E-02	1.08E-03
k	1.05E-03	1.26E-01	5.69E-01	1.26E-01	1.05E-03
k+1	1.08E-03	1.99E-02	4.60E-02	1.99E-02	1.08E-03

Table 4.3: Inter-cell interference power tables for three different cases

cases / f	OFDM	FBMC	PS
k+8	1.12E-3	0	0
k+7	1.84E-3	0	0
k+6	2.50E-3	0	0
k+5	3.59E-3	0	0
k+4	5.60E-3	0	0
k+3	9.95E-3	0	0
k+2	2.23E-2	0	0
k+1	8.94E-2	8.81E-2	0
k	7.05E-1	8.23E-1	1
k-1	8.94E-2	8.81E-2	0
k-2	2.23E-2	0	0
k-3	9.95E-3	0	0
k-4	5.60E-3	0	0
k-5	3.59E-3	0	0
k-6	2.50E-3	0	0
k-7	1.84E-3	0	0
k-8	1.12E-3	0	0
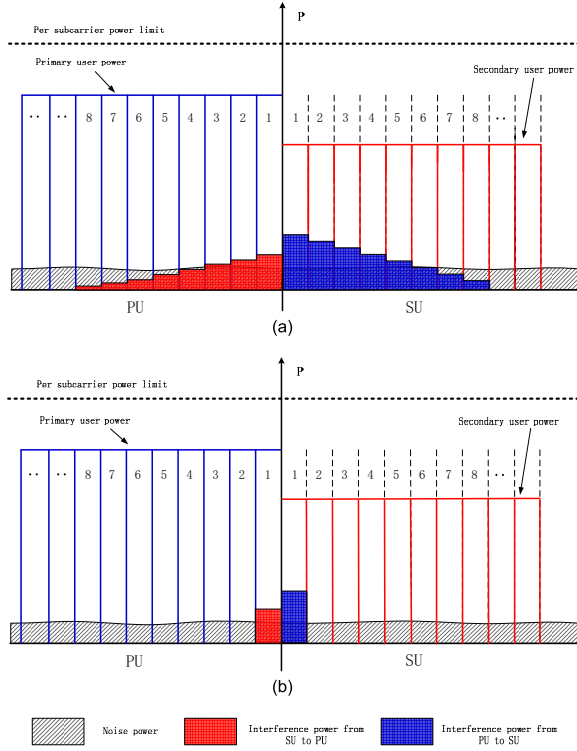
Figure 4.3: (a). Inter-cell interference between PU and SU in OFDM based CR networks (b). Inter-cell interference between PU and SU in FBMC based CR networks

The secondary cell wants to maximize its sum data rate by allocating power into the detected spectrum holes for its own users, this problem can be formulated as

$$\max_{\mathbf{p}} : C(\mathbf{p}) = \sum_{m=1}^{M} \sum_{k=1}^{K} \sum_{f=1}^{F_k} \theta_m^{kf} log_2 \left[1 + \frac{p_m^{kf} G_{ss}^{mkf}}{\sigma_n^2 + I_f^k} \right]$$

s.t.

$$\begin{cases} \sum_{k=1}^{K} \sum_{f=1}^{F_k} \theta_m^{kf} p_m^{kf} \leq P_{th}, & \forall m \\ 0 \leq p_m^{kf} \leq P_{sub} \\ \sum_{m=1}^{M} \sum_{n=1}^{N} \theta_m^{k_{l(r)}n} p_m^{k_{l(r)}n} G_{sp}^{mk_{l(r)}} V_n \leq I_{th}, & \forall k \end{cases} \tag{4.2}$$

where M is the number of secondary users, K is the number of spectrum holes, and F_k is the number of subcarriers in the kth spectrum hole. $\theta_m^{kf} \in \{0, 1\}$ is the subcarrier assignment indicator, i.e. $\theta_m^{kf} = 1$ if the fth subcarrier in the kth spectrum hole is allocated to SU m, p_m^{kf} is the power of SU m on the fth subcarrier in the kth spectrum hole, G_{ss}^{mkf} is the propagation channel magnitude from SU m to SBS on the fth subcarrier in the kth spectrum hole, σ_n^2 is the noise power, and I_f^k is the inter-cell interference from PU to SU on the fth subcarrier in the kth spectrum hole. P_{th} and P_{sub} are the maximum user power limit and per subcarrier power limit, respectively. N is the length of

the interference vector V, $p_m^{k_{l(r)}n}$ is the power of SU m on the left (right) n^{th} subcarrier in the kth spectrum hole, $G_{sp}^{mk_{l(r)}}$ is the propagation channel magnitude from SU m to PBS on the left (right) first primary subcarrier adjacent to the kth spectrum hole, and I_{th} denotes the interference threshold prescribed by the PU on the first primary subcarrier adjacent to SU.

The inter-cell interference from PU to SU I_f^k can be expressed in the mathematical form as follows

$$
I_f^k = \begin{cases}
\sum_{n=f}^N P_p^{k_l} G_{ps}^{k_l f} V_n, & f = 1, 2, \cdots N \\
\sum_{n=F_k-f+1}^N P_p^{k_r} G_{ps}^{k_r f} V_n, & f = F_k - N + 1, \cdots F_k \\
0, & others
\end{cases} \tag{4.3}
$$

where $P_p^{k_{l(r)}}$ is the transmission power of PU located in the left (right) of the kth spectrum hole, and $G_{ps}^{k_{l(r)}f}$ is the channel magnitude from PU located in the left (right) of the kth spectrum hole to SBS on the fth subcarrier of the kth spectrum hole. Practically, the secondary cell is not capable of obtaining the transmission power of PU and the channel information from PU to SU, but I_f^k can be measured during spectrum sensing by SBS without need to know any prior information.

In order to define an interference threshold I_{th} which is predetermined by a practical licensed system [1], we assume that the received primary signal in PBS always has a desired $SNR = \frac{P_p G_{pp}}{\sigma_n^2} \approx 10$. The capacity on the first primary subcarrier adjacent to SU is

$$
C = log_2(1 + \frac{P_p G_{pp}}{\sigma_n^2}) \tag{4.4}
$$

where P_p is the primary transmission power, and G_{pp} is the channel magnitude from PU to PBS. The value of I_{th} can be automatically generated by defining a tolerable capacity loss coefficient λ according to

$$
(1 - \lambda)C = log_2(1 + \frac{P_p G_{pp}}{\sigma_n^2 + I_{th}}) \tag{4.5}
$$

In equation (4.2), the third inequality constraint is related to the interference introduced by the secondary user to the primary base station. This constraint is quite difficult to manage because of the two following reasons: first of all, the threshold I_{th} has to be prescribed by the primary system. It represents the amount of interference that the primary system can accept from secondary system. Standards for multicarriers CR systems are still under study and no common definition for interference threshold is available in literature. Different thresholds corresponding to different penalties in terms of primary system capacity degradation will be used in the following simulation section. Secondly, the SU needs the necessary channel knowledge. Without the information of the channel magnitude G_{sp} between SU and PBS, the third term of the inequality constraint of (4.2) cannot be

---

[1]Considering the absence of a standard interference threshold for CR system, we have derived it using a tolerable capacity loss for the primary system.

computed. This difficulty is common to all CR systems: in order to adjust its emitted power the SU must know the amount of interference brought to the PBS. Under the hypothesis that primary and secondary systems are unsynchronized, it's hard to perfectly estimate the channel magnitude G_{sp}. Nevertheless, a rough estimate of this magnitude can be implemented by the SU during the spectrum sensing phase. The modulus of the channel gain from PBS to SU can be estimated on the subcarriers used by primary system and, by interpolation, the channel magnitude from PBS to SU on free subcarriers can be computed. Alternatively, the information about G_{sp} can be carried out by a band manager that mediates between the primary and secondary users [111]. The channel magnitude of the downlink path (PBS to SU) is not equal to the reverse channel magnitude (SU to PBS) if Frequency Division Duplexing (FDD) is used. However, this downlink channel magnitude can be used as a rough estimate of the uplink channel magnitude. In this case it will be necessary to add some margin on the threshold I_{th} in order to take into account the channel estimation error. Since OFDM based secondary system introduces more interference to primary users than the case of FBMC, the knowledge of G_{sp} is much more important for OFDM, in this case, larger margin value should be added for OFDM based CR systems.

4.3 Single-User Resource Allocation

In this section, the case with only one SU which uses the whole detected spectrum in the secondary cell is studied. The case of multi-user resource allocation will be addressed in the next section.

For the special case of single-user, the problem formulation in (4.2) is simplified

$$\max_{\mathbf{p}} : C(\mathbf{p}) = \sum_{k=1}^{K} \sum_{f=1}^{F_k} log_2 \left[1 + \frac{p^{kf} G_{ss}^{kf}}{\sigma_n^2 + I_f^k} \right]$$

$$s.t.$$

$$\begin{cases} \sum_{k=1}^{K} \sum_{f=1}^{F_k} p^{kf} \leq P_{th} \\ p^{kf} \geq 0 \\ p^{kf} \leq P_{sub} \\ \sum_{n=1}^{N} p^{k_{l(r)}n} G_{sp}^{k_{l(r)}} V_n \leq I_{th}, \quad \forall k \end{cases} \tag{4.6}$$

where the SU is permitted to access all the $F = \sum_{k=1}^{K} F_k$ subcarriers subject to the total power constraint, per subcarrier power constraint, as well as interference constraint.

In mathematical optimization, the method of Lagrangian multipliers can provide a strategy for finding the maximum of (4.6), but the solution of extensive Lagrangian multipliers is computationally complex when F increases. Instead, herein the Gradient Projection Method (GPM) can be applied

to obtain the optimal power allocation for this simple CR uplink scenario in a low computational complexity.

Rosen's gradient projection method [110] is based on projecting the search direction into the subspace tangent to the active constraints. We transform our linear constrained optimization problem into the GPM structure

$$
\begin{aligned}
&\max_{\mathbf{p}} : C(\mathbf{p}) \\
&s.t. \begin{cases}
\mathbf{A}_1\mathbf{p} \leq \mathbf{b}_1 \\
\mathbf{A}_2\mathbf{p} \leq \mathbf{b}_2 \\
\mathbf{A}_3\mathbf{p} \leq \mathbf{b}_3 \\
\mathbf{A}_4\mathbf{p} \leq \mathbf{b}_4
\end{cases}
\end{aligned}
\tag{4.7}
$$

where defining $\mathbf{A} = [\mathbf{A}_1; \mathbf{A}_2; \mathbf{A}_3; \mathbf{A}_4]$ is the coefficient matrix of the inequality linear constraints and $\mathbf{b} = [\mathbf{b}_1; \mathbf{b}_2; \mathbf{b}_3; \mathbf{b}_4]$ is the coefficient vector of the inequality constraints. Making the comparison of (4.7) and (4.6), we can obtain

$$
\begin{cases}
\mathbf{A}_1 = \begin{bmatrix} 1 & 1 & 1 & \cdots & 1 \end{bmatrix}^{1 \times F} \\[4pt]
\mathbf{A}_2 = \begin{bmatrix} -1 & 0 & \cdots & \cdots & 0 \\ 0 & -1 & 0 & \cdots & 0 \\ \vdots & \vdots & \vdots & \ddots & \vdots \\ 0 & \vdots & \vdots & 0 & -1 \end{bmatrix}^{F \times F}, \quad
\mathbf{A}_3 = \begin{bmatrix} 1 & 0 & \cdots & \cdots & 0 \\ 0 & 1 & 0 & \cdots & 0 \\ \vdots & \vdots & \vdots & \ddots & \vdots \\ 0 & \vdots & \vdots & 0 & 1 \end{bmatrix}^{F \times F} \\[4pt]
\mathbf{A}_4 = \begin{bmatrix} G_{sp}^{1_l}V_1 & \cdots & G_{sp}^{1_l}V_N & 0 & \cdots & \cdots & \cdots & \cdots & \cdots & 0 \\ 0 & \cdots & 0 & G_{sp}^{1_r}V_N & \cdots & G_{sp}^{1_r}V_1 & 0 & \cdots & \cdots & 0 \\ \vdots & \vdots & \vdots & \vdots & \vdots & \vdots & \ddots & \vdots & \vdots & \vdots \\ \vdots & \vdots & \vdots & \vdots & \vdots & \vdots & \ddots & \vdots & \vdots & \vdots \\ 0 & \cdots & \cdots & \cdots & \cdots & \cdots & 0 & G_{sp}^{K_r}V_N & \cdots & G_{sp}^{K_r}V_1 \end{bmatrix}^{2K \times F} \\[4pt]
\mathbf{b}_1 = \begin{bmatrix} P_{th} \end{bmatrix}^{1 \times 1}, \quad
\mathbf{b}_2 = \begin{bmatrix} 0 \\ \vdots \\ 0 \end{bmatrix}^{F \times 1}, \quad
\mathbf{b}_3 = \begin{bmatrix} P_{sub} \\ \vdots \\ P_{sub} \end{bmatrix}^{F \times 1}, \quad
\mathbf{b}_4 = \begin{bmatrix} I_{th} \\ \vdots \\ I_{th} \end{bmatrix}^{2K \times 1}
\end{cases}
\tag{4.8}
$$

Let $\mathbf{p}$ be a feasible solution and suppose $\mathbf{A}_1'\mathbf{p} = \mathbf{b}_1', \mathbf{A}_2'\mathbf{p} < \mathbf{b}_2'$, where $\mathbf{A} = (\mathbf{A}_1'; \mathbf{A}_2')$ and $\mathbf{b} = (\mathbf{b}_1'; \mathbf{b}_2')$. Suppose that $\mathbf{M} = \mathbf{A}_1'$, then the gradient projection algorithm is given as follows:

1. Initialization: set t=1, and $\mathbf{p} = \mathbf{0}$.

2. Calculate the projection matrix $\mathbf{Q}$, which is given by

$$\mathbf{Q} = \mathbf{I} - \mathbf{M}(\mathbf{M}^T\mathbf{M})^{-1}\mathbf{M}^T \tag{4.9}$$

   where $\mathbf{I}$ is the unit matrix and T is the transpose operator.

3. Calculate $\mathbf{s}^{(t)} = \mathbf{Q}\nabla_{\mathbf{p}}C(\mathbf{p})$ (∇ is the operator of gradient).

4. If $\|\mathbf{s}^{(t)}\| \leq \varepsilon$, terminate ($\varepsilon$ is a small threshold value).

5. Determine the maximum step size:

$$\alpha_{max} = min\{\alpha_k\}, \qquad k = 1, 2, \ldots, F$$

$$\alpha_k = \begin{cases} \frac{c_k}{d_k} & d_k > 0 \\ \infty & d_k \leq 0 \end{cases} \tag{4.10}$$

$$where \quad \mathbf{c} = \mathbf{b} - \mathbf{Ap}, \quad \mathbf{d} = \mathbf{As}^{(t)}; \tag{4.11}$$

6. Solve the line-search problem to find

$$\alpha = \underset{\alpha}{argmax}\left(C(\mathbf{p}^{(t)} + \alpha\mathbf{s}^{(t)})\right), \quad 0 \leq \alpha \leq \alpha_{max} \tag{4.12}$$

7. Set $\mathbf{p}^{(t+1)} = \mathbf{p}^{(t)} + \alpha\mathbf{s}^{(t)}$, t = t+1, and go to step 2.

GPM is an efficient way with low computational complexity for our single-user optimization problem with linear constraints. Experimental results of one spectrum hole and multiple holes for this single-user case are given in the simulation section.

4.4 Multi-User Resource Allocation

In multicarrier based networks with multi-user , assuming each free subcarrier can be used for transmission to at most one secondary user at any time, then our optimal problem in (4.2) is an integer programming problem, which has a high computational complexity. Generally, instead of searching an optimal solution with an unacceptable computational complexity, the combinatorial suboptimal method of subcarrier assignment and power allocation is proposed: firstly the subcarriers are assigned to the SUs and then the power is allocated to these subcarriers.

For simplicity, we solve our multi-user resource allocation by using this two-step suboptimal algorithm. All the secondary users are firstly allocated to the available spectrum holes according to

some user-selection metrics, and then power allocation is implemented. At the premise of knowing the result of the subcarrier assignment, the power allocation of multi-user system can be virtually regarded as a single-user system and therefore the single-user power allocation algorithm GPM mentioned in last section can be utilized. So our focus is casted on the subcarrier assignment of multicarrier based CR system.

The first task of subcarrier assignment for our uplink multi-user scenario is the bandwidth allocation. In order to guarantee the fairness for different secondary users, the bandwidth allocation method in [112] is applied to assign the number of clusters to each secondary user, which is summarized in Table 4.4. [1]

Table 4.4: Bandwidth allocation with fairness constraint

Given F is the number of free clusters, M is the number of users, and $F > M$.
Assuming N_i denotes the cluster number of ith user, $i = 1, 2, \cdots, M$.

Step 0:　Initialization:
$$N_i = \lfloor F/M \rfloor, i = 1, 2, \cdots, M.$$

Step 1:　Calculate: $C_i = N_i log_2(1 + \frac{\overline{G_i}\frac{P_{th}}{N_i}}{\sigma_n^2}), i = 1, 2, \cdots, M.$
　　　　　Find: $i' = arg\,min_i(C_i)$, then set
$$N_{i'} = N_{i'} + 1;$$

Step 2:　If $\sum_{i=1}^{M} N_i = F$, terminate.
　　　　　If not, go to step 1.

Next, the specific subcarrier assignment is examined. In a traditional multicarrier system, the maximum SNR-metric can be applied to assign each subcarrier to the user with a high value of SNR "$\frac{\overline{P}G_{ss}}{\sigma_n^2}$" (where $\overline{P}$ is the averaged power by dividing the total power limit on the number of the subcarriers). However, the SNR-metric is not always suitable in cognitive radio systems due to the mutual interference between PU and SU, especially with low interference constraint prescribed by PU.

In this section, an Averaged Capacity metric (AC-metric) aiming to maximize the averaged spectral efficiency is proposed. The averaged spectral efficiency not only depends on the channel magnitude G_{ss}, but also on the interference threshold I_{th}, maximum user power limit P_{th}, as well as the channel magnitude G_{sp}. AC-metric makes a balance between all these influence factors.

---

[1]$\lfloor x \rfloor$ is the floor function, which means the largest integer not greater than x. $\overline{G_i}$ is the average channel gain from i^{th} user to the base station.
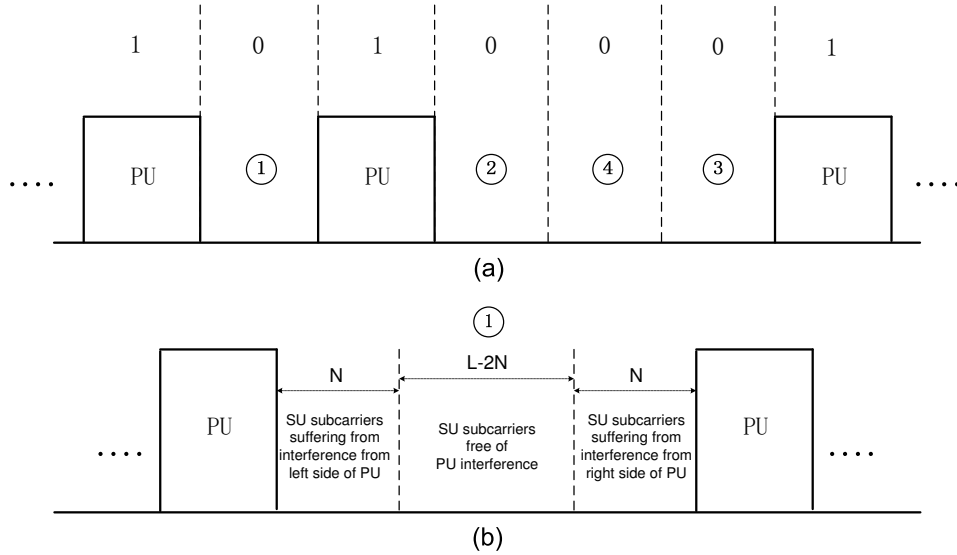
Figure 4.4: (a). Four types of clusters in available spectrum holes (b). The interference situation for the cluster indexed by "1"

It can be envisaged that different clusters in the spectrum holes suffer from different interference strengths introduced by PU. In Fig. 4.4 (a), four possible types of clusters in available spectrum holes are displayed, where the cluster with index "1" suffers from the interferences introduced by both left PU and right PU, the cluster "2" ("3") suffers from the interference introduced by only left (right) PU, and cluster "4" does not suffer from any interference at all. The interference situation of the cluster indexed by "1" is shown in Fig. 4.4 (b).

Considering this practical situation, the AC-metric is defined as

$$
\begin{cases}
\mathbf{C}_1 = \left\{ \sum_{n=1}^{N} log_2(1 + SINR_n^l) + \sum_{n=1}^{N} log_2(1 + SINR_n^r) \right. \\
\qquad\qquad\qquad\qquad\qquad \left. + (L - 2N)log_2\left(1 + \frac{(P_{th} - P_l - P_r)G_{ss}}{(L-2N)\sigma_n^2}\right) \right\}/L \\
\mathbf{C}_2 = \left\{ \sum_{n=1}^{N} log_2(1 + SINR_n^l) + (L - N)log_2\left(1 + \frac{(P_{th} - P_l)G_{ss}}{(L-N)\sigma_n^2}\right) \right\}/L \\
\mathbf{C}_3 = \left\{ \sum_{n=1}^{N} log_2(1 + SINR_n^r) + (L - N)log_2\left(1 + \frac{(P_{th} - P_r)G_{ss}}{(L-N)\sigma_n^2}\right) \right\}/L \\
\mathbf{C}_4 = log_2\left(1 + \frac{\overline{P}G_{ss}}{\sigma_n^2}\right)
\end{cases}
\tag{4.13}
$$

$and:$

$$SINR_n^l = \frac{p_n^l G_{ss}^{ln}}{\sigma_n^2 + I_n^l}, \quad SINR_n^r = \frac{p_n^r G_{ss}^{rn}}{\sigma_n^2 + I_n^r}, \quad P_l = \sum_{n=1}^{N} p_n^l, \quad P_r = \sum_{n=1}^{N} p_n^r$$

$$p_n^l = min\{\overline{P}, \frac{I_{th}}{NV_n G_{sp}^l}\}, \quad p_n^r = min\{\overline{P}, \frac{I_{th}}{NV_n G_{sp}^r}\}$$

where $\mathbf{C}_1 \sim \mathbf{C}_4$ are the averaged channel capacities of the four different clusters in Fig. 4.4, respectively, N is the length of the interference vector V, "$L > 2N$" is the length of one cluster, and $SINR_n^{l(r)}$ is the SINR on the left (right) n^{th} subcarrier of one cluster. $p_n^{l(r)}$ is the power on the left (right) n^{th} subcarrier of one cluster (we assume that each of the N subcarriers adjacent to PU introduces the same quantity of interference to PU), and which is not supposed to overpass the averaged power per subcarrier. $G_{ss}^{l(r)n}$ is the channel magnitude of SU to SBS on the left (right) n^{th} subcarrier of one cluster, $I_n^{l(r)}$ is the interference from PU to SU on the left (right) n^{th} subcarrier of one cluster, $P_{l(r)}$ is the aggregated power on the left (right) N subcarriers of one cluster, and $G_{sp}^{l(r)}$ is the channel magnitude from SU to PBS on the left (right) first primary subcarrier adjacent to one cluster.

Assuming there are K^c free clusters and K^u secondary users, AC-metric can be used for calculating the averaged capacities of each SU on each available cluster. Since we know the number of clusters assigned to each secondary user using the bandwidth allocation method in [112], a $K^c \times K^c$ AC matrix can be obtained. Our task is how to optimally assign these K^c clusters to the K^u secondary users, with the aim of maximizing the averaged spectral efficiency of the secondary cell. This problem equals to the search of the optimum matching of a bipartite graph, so the Hungarian algorithm introduced by H. W. Kuhn [113] is proposed to implement this cluster assignment.

Mathematically, the cluster assignment problem can be described as: Given the $K^c \times K^c$ AC cost matrix $\mathcal{R} = [r_{m,n}]$, find the $K^c \times K^c$ permutation matrix $\Psi = [\psi_{m,n}]$ so that

$$V_\psi = \sum_{m=1}^{K^c} \sum_{n=1}^{K^c} \psi_{m,n} r_{m,n} \tag{4.14}$$

is maximized.

For the low dimension AC matrix, the optimal permutation matrix Ψ can be obtained efficiently by using Hungarian algorithm. The multi-user resource allocation in CR network with multiple spectrum holes will be simulated in next section.

4.5   Numerical Results

In this section, the proposed resource allocation algorithm of OFDM and FBMC based CR networks is evaluated in terms of the averaged spectral efficiency by computer simulations in a comparable

Table 4.5: System simulation parameters

Parameter	Value	Unit
Total bandwidth B	10	MHz
Bandwidth per sub-carrier	9.5	kHz
Center frequency	2.5	GHz
Number of sub-carriers	1024	-
Number of clusters N_{all}	48	-
Number of sub-carriers in one cluster L	18	-
Load rate of primary system	75%	-
Number of free clusters	12	-
Distance between SBS and PBS D	$0.2 \sim 2$	km
Number of secondary cell	1	-
Primary system radius R_p	1	km
Secondary cell radius R_s	1	km
User power limit per subcarrier P_{sub}	5	mWatt
Noise power per subcarrier	-134.10	dBm
Log normal shadowing standard deviation	0	dB
User speed	0	m/s
Pedestrian multipath delays	$10^{-9} \cdot [0, \quad 110, \quad 190, \quad 410]$	s
Pedestrian multipath powers	$[0, \quad -9.7, \quad -19.2, \quad -22.8]$	dB
Channel realization times	200	-

way. We will verify that FBMC based CR network achieves higher spectral efficiency than the case of OFDM.

The CR network as shown in Fig. 4.1 with one primary system and one secondary cell is simulated for different number of users and spectrum holes. Primary and secondary users centering around PBS and SBS, respectively, are uniformly distributed within the cell range (0.1∼1 km). As the increase of transmission distance, the attenuation also increases due to the propagation pathloss. The pathloss of the received signal at a distance d (km) is [114]

$$P(d) = 128.1 + 37.6 \cdot log_{10}(d) \quad dB \tag{4.15}$$

GPM is applied to solve the power allocation problem, where we set the threshold parameter $\varepsilon = 10^{-3}$. Other system simulation parameters are displayed in Table 4.5.

During the following simulation, single-user case as well as multi-user case are considered, and

meanwhile the experimental results of the perfectly synchronized (PS) case are also given for the sake of comparison with the results of OFDM and FBMC based CR networks. First of all, the single-user as well as multi-user cases with perfect Channel State Information (CSI) are experimented. After that, the more practical case, where the CSI is estimated under a prescribed outage probability of primary systems, is simulated.

4.5.1 Single-User Case with Perfect SCI

Firstly, we investigate the single-user case with only one spectrum hole.
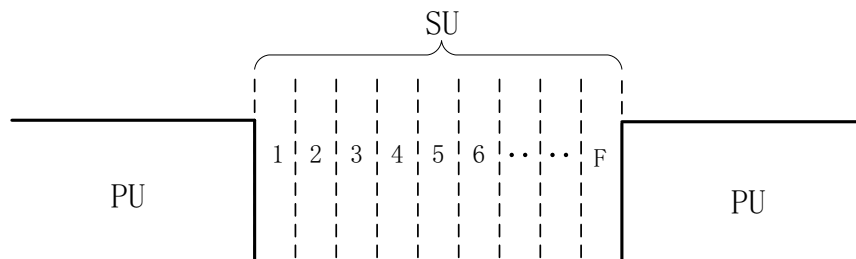
Figure 4.5: Single-user case with F subcarriers in one spectrum hole

As shown in Fig. 4.5, the SU who uses the F available subcarriers is surrounded by the subcarriers allocated to PU. So the SU suffers from the interference introduced by PU from both sides. With respect to the interference from SU to PU, in this paper we consider the interference strength on the first primary subcarrier adjacent to SU, and the interference threshold I_{th} is determined by prescribing a tolerable capacity loss coefficient λ on this primary subcarrier according to (4.5).

Given that the SBS is relatively close to PBS (D=0.2 km), and in the case of one PU and one SU, there are three typical channel situations: (a). The distance from SU to SBS and PBS is larger than that of PU, in other words, PU is closer to the base stations; (b). PU and SU have almost equivalent distance to the base stations; (c). The distance from SU to the base stations is smaller than that of PU.

Table 4.6 gives three examples corresponding to above three typical channel realizations, and their power allocation results of OFDM and FBMC based systems are shown in Fig. 4.6 with the number of subcarriers $F = 18$, the interference threshold determined according to $\lambda = 0.5$, and the maximum user power limit $P_{th} = 36mWatt$. For the first channel situation (Fig. 4.6 (a)), it can be observed that the transmission power of the PU is low because the PU is close to the base stations, whereas the averaged spectral efficiencies of the SU are low because the SU is located relatively far away from the base stations. Furthermore, the gap between the averaged spectral efficiencies of OFDM and FBMC is not obvious mainly due to the low interference induced from SU to PU and slightly

due to the negligible interference from PU to SU. With regard to the second and the third channel realizations (Fig. 4.6 (b) and (c)), the values of the SU's spectral efficiencies increase when the distance between SU and the base stations decreases, and the transmission power of the PU increases when the distance between the PU and the base stations augments. The spectral efficiency gap of OFDM and FBMC augments especially for the third channel realization because the SU is located close to the base stations, which means significant interference will be introduced to the PU. So the power allocation algorithm tries to avoid allocating the power on the subcarriers adjacent to the PU. That's the reason why the power of OFDM in Fig. 4.6 (c) is allocated in such a way that most of the power is localized at the center of a spectrum hole. However, FBMC is insensitive and robust for different channel situations because of its frequency containment property.

Next, the spectral efficiency curves of the single-user case as a function of various system parameters are drawn in Fig. 4.7 by averaging 200 Monte Carlo simulations. Power allocation results for the case of one spectrum hole are presented in Fig. 4.7 (a)(c)(e), and Fig. 4.7 (b)(d)(f) give the simulation results of the single-user case with multiple holes, where the scenario with 12 free clusters and $L = 18$ subcarriers per cluster in Fig. 4.2 is used, and the distributions of the spectrum holes are randomly generated for each channel realization.

The effect of the number of subcarriers is illustrated in Fig. 4.7 (a) and (c). We can see that as the number of subcarriers per cluster decreases, FBMC obtains more spectral efficiency gain over OFDM, which indicates that FBMC is more applicable for the CR system with small size of spectrum holes. For comparison, the averaged spectral efficiencies of the multiple holes at different interference levels ($\lambda = 0.2, 0.3, \cdots, 0.9$) are given in Fig. 4.7 (b) and (d). As expected, OFDM shows a fast decrease of the spectral efficiency when less capacity loss is prescribed by PU, but FBMC is slightly affected by different interference levels. It can be seen that, FBMC is even much better than OFDM when low interference threshold (I_{th} in (4.2)) is prescribed, see Fig. 4.7 (b), where spectral efficiency of OFDM collapses when the interference level decreases compared to FBMC case. We can also find that the spectral efficiencies of one spectrum hole case match well with the case of the multiple holes

Table 4.6: Three typical channel situations

	$D_{SU \to SBS}$ (km)	$D_{PU \to PBS}$ (km)	P_p (mWatt/sub)	C_{ofdm} (bits/Hz/s)	C_{fbmc} (bits/Hz/s)	$C_{fbmc} - C_{ofdm}$ (bits/Hz/s)
(a)	0.84	0.39	0.58	3.15	3.42	0.27
(b)	0.49	0.50	1.30	4.84	5.28	0.44
(c)	0.29	0.89	5.00	6.85	8.28	1.43
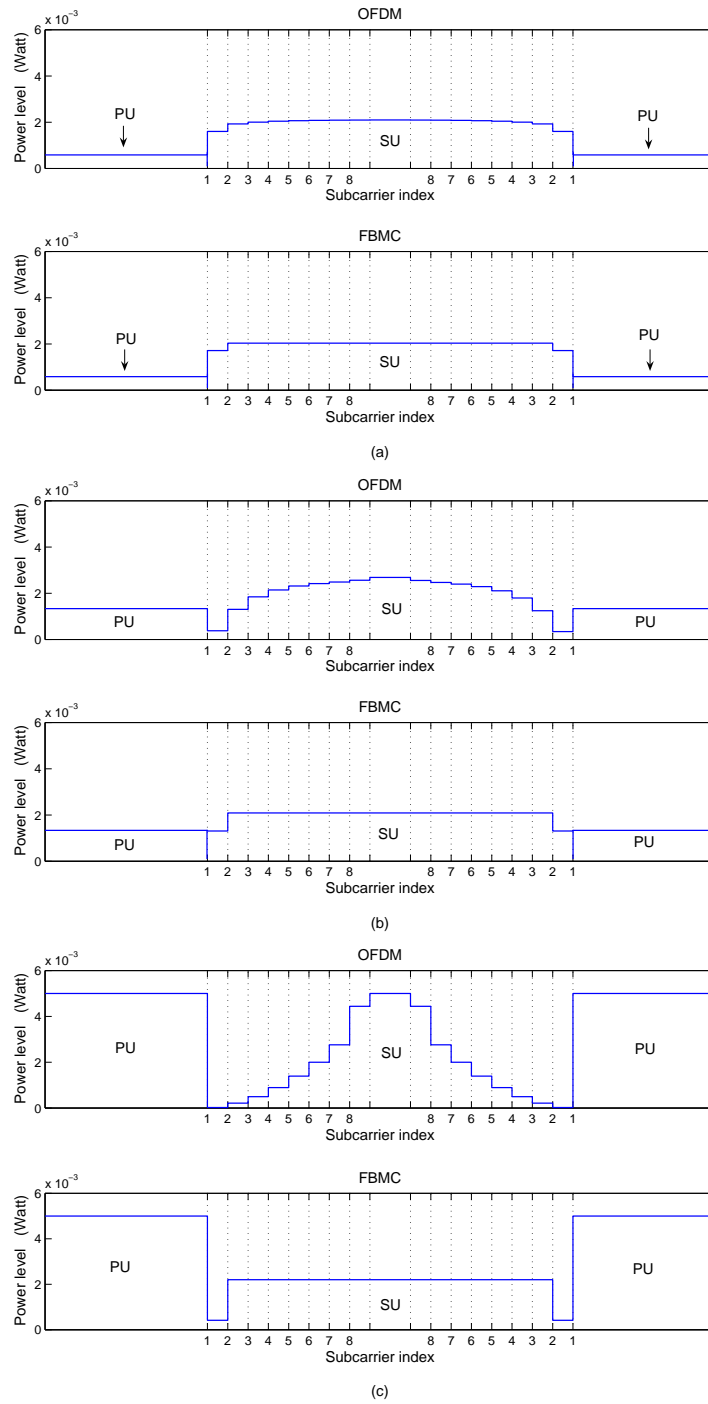
Figure 4.6: Three typical channel realizations of single-user case with F=18, λ=0.5, D=0.2 km, and $P_{th} = 36 mWatt$:   (a). $D_{SU \to SBS} > D_{PU \to PBS}$ (b). $D_{SU \to SBS} \approx D_{PU \to PBS}$ (c). $D_{SU \to SBS} < D_{PU \to PBS}$.

97

Figure 4.7: Experimental results of single-user resource allocation for one and multiple spectrum holes with $D = 0.2\ km$:   (a). Averaged spectral efficiency *vs.* number of subcarriers for one spectrum hole case (b). Averaged spectral efficiency *vs.* interference level for multiple spectrum holes case   (c). (FBMC - OFDM)/OFDM *vs.* number of subcarriers for one spectrum hole case   (d). (FBMC - OFDM)/OFDM *vs.* interference level for multiple spectrum holes case   (e). Averaged spectral efficiency *vs.* total power limit for one spectrum hole case   (f). Averaged spectral efficiency *vs.* total power limit for multiple spectrum holes case.

under the same simulation condition (indicated by the dashed lines in Fig. 4.7 (a) and (b)). Fig. 4.7 (c) and (d) show the ratio of the spectral efficiency gain of FBMC compared to the spectral efficiency of OFDM. When $F = 6$, FBMC can achieve almost 30% spectral efficiency gain over OFDM. The performance of OFDM in the case of the multiple holes is found to behave a little better than the case of one spectrum hole with $F = 18$ subcarriers, which can be explained by the fact each spectrum hole may have two or more than two clusters. Finally, the averaged spectral efficiencies as a function of the total power level P_{th} are given in Fig. 4.7 (e) and (f), and the spectral efficiencies increase with the augmentation of the averaged power per subcarrier $\overline{P}$ ($\overline{P}=P_{th}$/F). Besides, it can be noted that the performance of FBMC approaches the performance of the perfectly synchronized case.

4.5.2   Multi-User Case with Perfect SCI

Without loss of generality for the proposed resource allocation algorithm, the case with multiple PUs and multiple SUs is simulated. In addition, the performance comparison of the SNR-metric and the AC-metric for channel assignment is investigated.

Since 36 clusters (seventy-five percent of the total 48 clusters) are allocated to PUs, we assume that these 36 licensed clusters are occupied by 36 uniformly distributed PUs. The rest 12 clusters are permitted to access by the SUs, each of which can use at least one cluster. The cluster assignment is implemented by the traditional SNR-metric and the proposed AC metric, respectively.

Fig. 4.8 shows the averaged spectral efficiencies of the "6 SUs" and "12 SUs" cases versus different system parameters. The spectral efficiency curves of the multi-user case versus the interference level and the maximum user power plotted in Fig. 4.8 (a) $\sim$ (d) match the case of the single-user, which once again proves the advantage of FBMC. At the same time, we can see that the achieved spectral efficiency of the OFDM based CR system by applying the AC-metric always outperforms the SNR-metric, but there is a slight difference by applying these two metrics for the FBMC based system. This implies that the traditional subcarrier assignment methods in wireless communication system can be used in FBMC based CR network, which reduces the CR system complexity. Nevertheless, some modified methods like AC-metric with computational complexity have to be investigated for OFDM based CR network due to its seriously additional interference. In view of the fact that the distance D between SBS and PBS can be random because of the flexibility of cognitive radio, so the impact of D on spectral efficiency is investigated and shown in Fig. 4.8 (e) and (f). We can observe that as the distance increases, all the performance curves of FBMC and OFDM tend to merge. The reason is that there exists little interference between the primary system and the secondary cell when they are far away from each other.
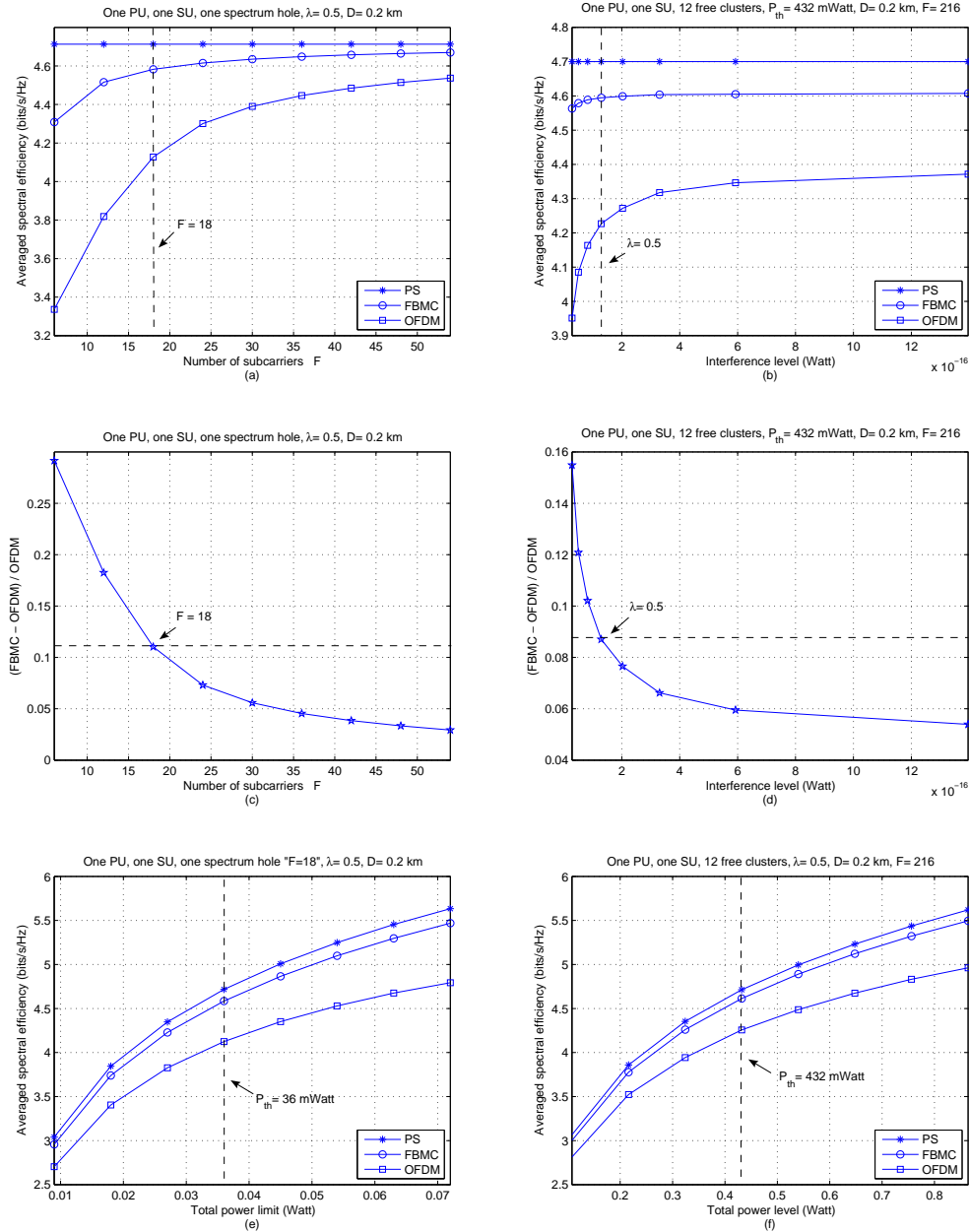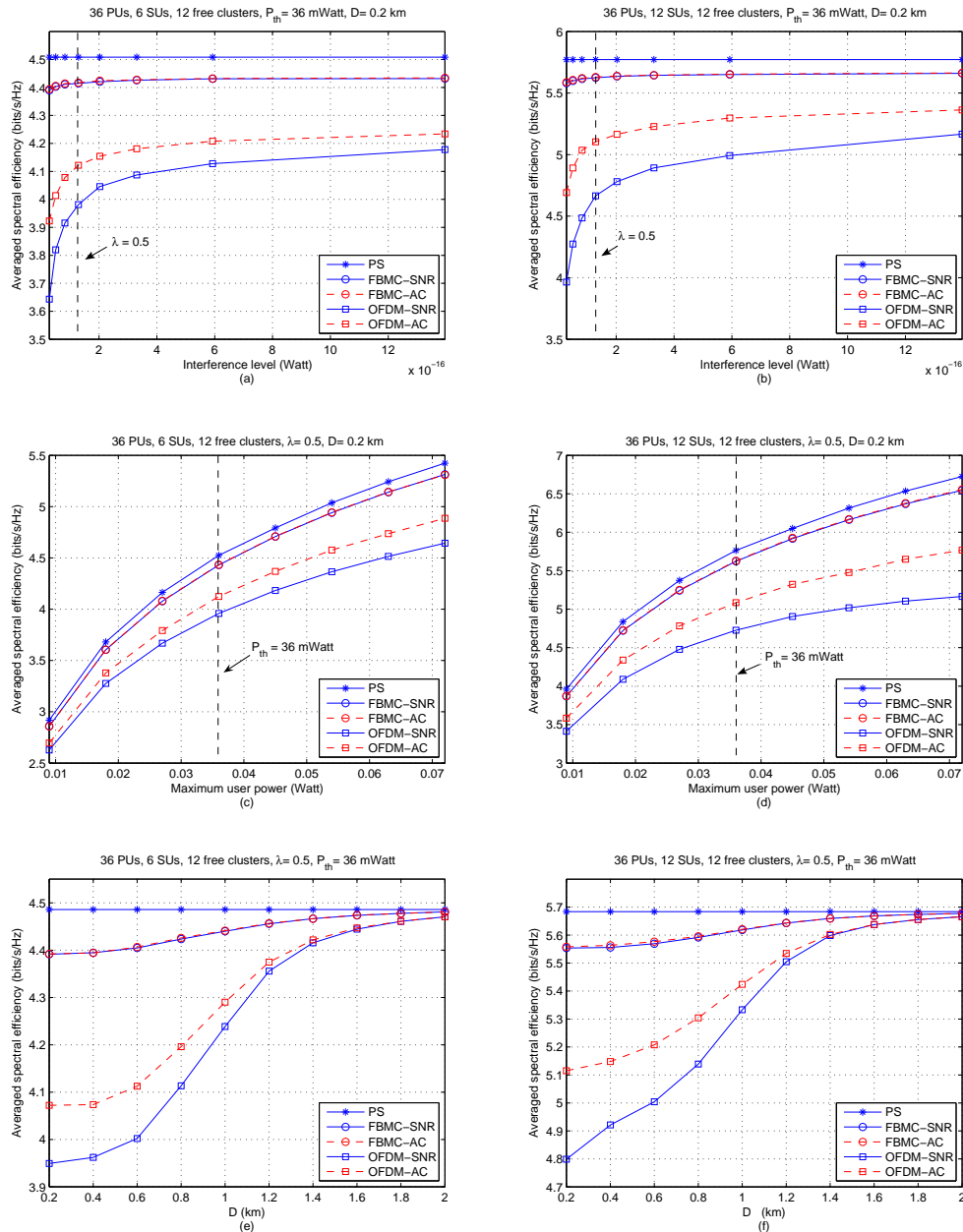
Figure 4.8: Experimental results of multi-user resource allocation for multiple spectrum holes with F=216: (a). Averaged spectral efficiency *vs.* interference level for 6 SUs (b). Averaged spectral efficiency *vs.* interference level for 12 SUs (c). Averaged spectral efficiency *vs.* maximum user power limit for 6 SUs (d). Averaged spectral efficiency *vs.* maximum user power limit for 12 SUs (e). Averaged spectral efficiency *vs.* distance between SBS and PBS for 6 SUs (f). Averaged spectral efficiency *vs.* distance between SBS and PBS for 12 SUs.

100

4.5.3 Multi-User Case with Estimated CSI

Since the channel gain information between SU and PU cannot be precisely estimated, the amount of the interference brought from SU to PU is calculated on the basis of an estimated CSI, which is determined by a prescribed outage probability of primary systems. This part is an extension based on the previous section. The first difference from before is that we consider the capacity loss on all the subcarriers that one PU occupies instead of on the first primary subcarrier adjacent to SU. Secondly, we assume that a rough estimate of the channel gain from SU to PU can be obtained by the SU during the spectrum sensing phase. The estimation error is determined by a prescribed outage probability of primary systems. Based on a rough estimated channel gain, final simulation results show more distinct performance difference between FBMC and OFDM than the case with an ideal channel gain estimation.

The problem can be formulated as

$$\max_{\mathbf{p}} : C(\mathbf{p}) = \sum_{m=1}^{M} \sum_{k=1}^{K} \sum_{f=1}^{F_k} \theta_m^{kf} log_2 \left[1 + \frac{p_m^{kf} G_{ss}^{mkf}}{\sigma_n^2 + I_f^k} \right]$$

$$s.t.$$

$$\begin{cases} \sum_{k=1}^{K} \sum_{f=1}^{F_k} \theta_m^{kf} p_m^{kf} \leq P_{th}, & \forall m \\ 0 \leq p_m^{kf} \leq P_{sub} \\ \sum_{m=1}^{M} \sum_{n=1}^{N} \theta_m^{k_{l(r)}n} p_m^{k_{l(r)}n} G_{sp}^{mk_{l(r)}} \sum_{i=1}^{N-n+1} V_{N-i+1} \leq I_{th}, & \forall k \end{cases} \tag{4.16}$$

In order to guarantee the QoS of primary systems, a channel gain margin G_m is added on the estimated pathloss gain

$$\widehat{G_{sp}} = (1 + G_m)G_{pl} \tag{4.17}$$

where G_m depends on the prescribed outage probability P_{out} tolerated by primary systems. Based on the implicit assumption that downlink and uplink pathloss difference is negligible, the evaluation of $\widehat{G_{sp}}$ only depends on the Rayleigh fading. We define the outage probability as

$$P_{out} = P(G_{sp} > \widehat{G_{sp}}) = P(|H_{sp}|^2 > 1 + G_m) \tag{4.18}$$

where $G_{sp} = |H_{sp}|^2 \cdot G_{pl}$, H_{sp} is the Rayleigh fading frequency response. Since $H_{sp} \sim Rayleigh(\mu)$, then $|H_{sp}|^2$ has a Gamma distribution with shape parameter $\alpha = 1$ and scale parameter $\beta = 2\mu^2$. The Cumulative Distribution Function (CDF) of $|H_{sp}|^2$ is the regularized gamma function, therefore (4.18) can be further expressed as

$$1 - P_{out} = \frac{\gamma\big(\alpha, (1 + G_m)/\beta\big)}{\Gamma(\alpha)} \tag{4.19}$$

where γ is the lower incomplete gamma function. Given an acceptable outage probability P_{out}, the added channel gain margin G_m can be obtained by (4.19) [1]

$$G_m = 2\mu^2 log_e(\frac{1}{P_{out}}) - 1 \tag{4.20}$$

In order to define an interference threshold I_{th} which is predetermined by a practical licensed system, we assume that the received primary signal in PBS always has a desired $SNR = \frac{P_p G_{pp}}{L\sigma_n^2} \approx 10$. The capacity on each cluster occupied by PU is

$$C = log_2(1 + \frac{P_p G_{pp}}{L\sigma_n^2}) \tag{4.21}$$

where P_p is the primary transmission power on one cluster, and G_{pp} is the channel gain from PU to PBS. The value of I_{th} can be automatically generated by defining a tolerable capacity loss coefficient λ according to

$$(1 - \lambda)C = log_2(1 + \frac{P_p G_{pp}}{L\sigma_n^2 + I_{th}}) \tag{4.22}$$

The experimental results of the perfectly synchronized case are given for the sake of comparison with the results of OFDM and FBMC based CR networks. In addition, the performance of the case with perfect channel gain information is also investigated.

The averaged capacities at different interference levels ($\lambda = 0.02 \sim 0.2$) with a given outage probability $P_{out} = 0.06$, a fixed maximum user power $P_{th} = 36mWatt$, and a fixed $D = 0.2km$ are given in Fig. 4.9. As expected, the performance of FBMC always outperforms that of OFDM, which shows a fast decrease of the channel capacity when less capacity loss is prescribed by PU, whereas FBMC is slightly affected by different interference levels. At the same time, we can see a large channel capacity gap between the case with ideal channel gain information and the case with an estimated channel gain for the OFDM based CR system, while there is a slight capacity difference by applying the FBMC based CR system. This could be explained by the fact that the number of subcarriers of OFDM and FBMC that induce harmful interference to PU are "8" and "1", respectively. When a low outage probability is required, more subcarriers adjacent to PU should be deactivated or underutilized for OFDM, which accordingly degrades the amount of channel capacity. On the other hand, FBMC exhibits more distinct advantage than OFDM when a rough estimated channel gain is considered. Besides, it can be noted that the performance of FBMC approaches the performance of the perfectly synchronized case. Fig. 4.10 shows the averaged capacities versus different outage probabilities, where the averaged capacity (with an estimated channel gain) of OFDM based CR system collapses when a low outage probability is prescribed. On the contrary, FBMC based CR

---

[1] In the special case $\alpha = 1$, the lower incomplete gamma function $\gamma(1, x) = 1 - e^{-x}$.

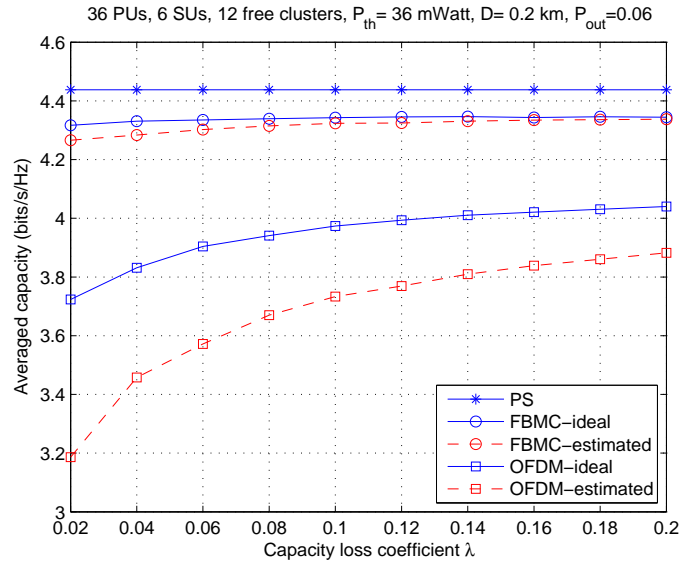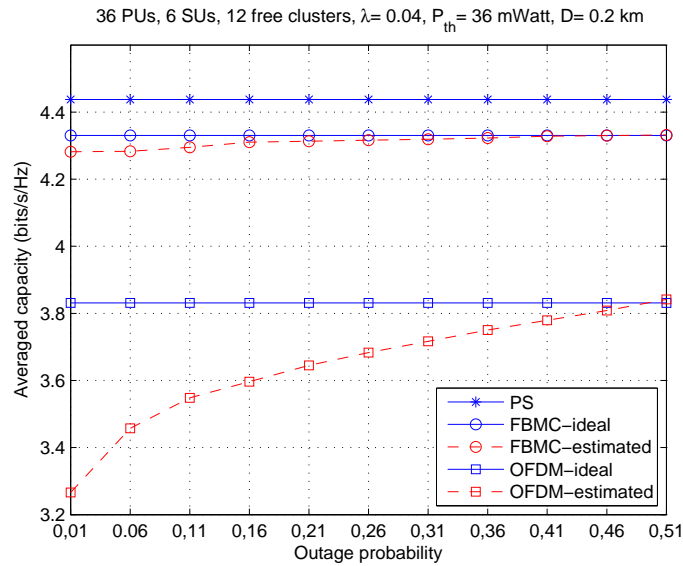**Figure 4.9:** Averaged capacity *vs.* interference level

Figure 4.10: Averaged capacity *vs.* outage probability
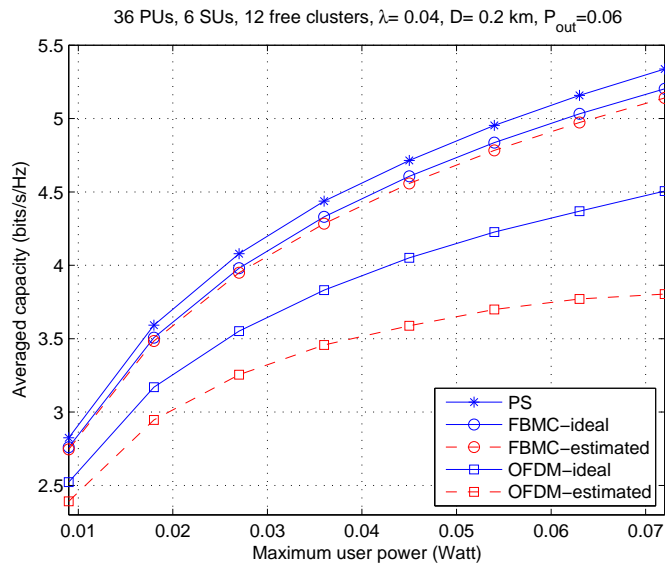
Figure 4.11: Averaged capacity *vs.* maximum user power
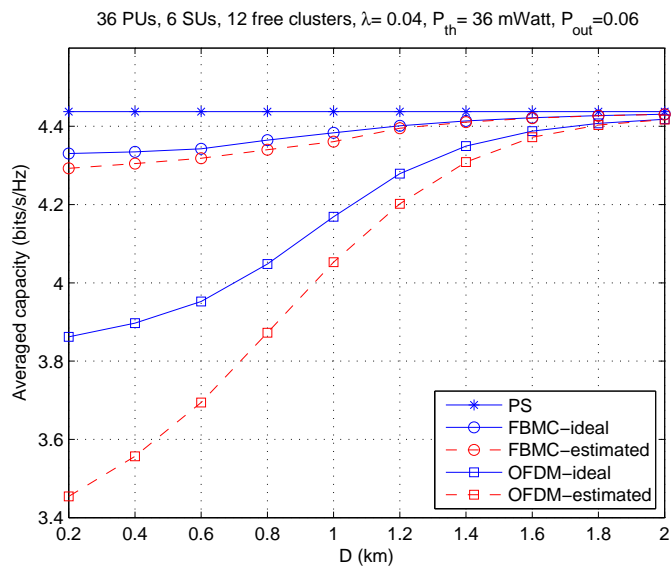
Figure 4.12: Averaged capacity *vs.* distance between SBS and PBS

system is much less vulnerable to different outage probabilities. The effects of the maximum power levels and the distance between SBS and PBS are illustrated in Fig. 4.11 and Fig. 4.12. As before, the channel capacities increase as the averaged power and the distance increase.

In our scenario, all the numerical results have been simulated under the assumption: the primary system and the secondary cell are regarded as mutually unsynchronized, the Rayleigh channel with pathloss is considered, and the practical system parameters and constraints are used for our simulation, all of these hypotheses are close to a realistic CR network. Based on this kind of system model, final simulation results of different cases indicate that FBMC based CR network can achieve higher spectral efficiency than the case of OFDM. Besides, the inserted cyclic prefix [1] in OFDM based CR system lowers the total system spectral efficiency.

4.6 Conclusion

The objective of this chapter is to compare the spectral efficiency performance of OFDM and FBMC based on a realistic uplink CR network. A resource allocation algorithm with the considerations of power constraint and interference constraint is proposed for evaluating the averaged spectral efficiency. Instead of using the interference due to the out-of-band radiation of the power spectral density, inter-cell interferences resulting from timing offset in OFDM and FBMC based networks are considered in our proposed algorithm. Scenario cases with different number of users and spectrum holes are investigated. Like most of the traditional suboptimal resource allocation algorithms, our problem is separated into two steps: subcarrier assignment and power allocation. In the case of multi-user, traditional SNR-metric for subcarrier assignment is not always suitable for CR network because of the existence of mutual interference between PU and SU, thus we propose an enhanced AC-metric for subcarrier assignment, which turns out to be more efficient than SNR-metric. Another contribution of this chapter is that gradient projection method is used for solving the power allocation problem, and optimal solution can be derived with low complexity.

Final simulation results demonstrate that in our scenario FBMC offers higher spectral efficiency and is more applicable for the CR network with small size of spectrum holes than OFDM. Moreover, FBMC can offer higher channel capacity and can achieve much more performance gain if rough estimated channel information is considered. Besides, the performance of FBMC is close to that of the perfectly synchronized case because of its frequency localization and therefore simplified resource allocation schemes could be sufficient for FBMC based CR network. As a result, we conclude that FBMC has practical value and is a potential candidate for physical layer data communication of future CR networks.

---

[1]The spectral efficiency loss due to cyclic prefix is not considered in this chapter.

4. CAPACITY COMPARISON OF OFDM / FBMC FOR UPLINK CR SYSTEMS

The work in next chapter will focus on the study of a scenario with multiple non-cooperative secondary cells, where game theory is used for solving the iterative resource allocation problem.

Non-Cooperative Resource Allocation of FBMC-based CR Systems

In the preceding chapter, the resource allocation issue in the context of single Cognitive Radio (CR) cell was investigated. In order to further study this issue, this chapter considers the resource allocation problem in multiple Filter Bank based Multi-Carrier (FBMC) based CR cells with multiple users per cell, where CR users in different cells reuse the same spectrum resource to enhance the spectral efficiency. Therefore, users assigned with the same spectrum band will interfere with each other, i.e. inter-cell interference exists among different CR cells. From the perspective of applications, a non-cooperative uplink resource allocation algorithm which tries to maximize the total information rate of each CR cell with power constraint on each user in a distributed way is taken into account herein. Game Theory (GT), as a robust mathematical tool to analyze interactive decision process, is used for the distributed resource allocation. Since the game formulation for rate maximization of multiple users in each cell is a non-concave optimization problem, Multiple Access Channel (MAC) technique is proposed. With the aid of MAC, we reformulate the game formulation as a concave optimization problem. When there is only one user in each CR cell, Iterative Water-Filling Algorithm (IWFA) can provide a good solution for the multi-cell distributed game. However, IWFA is no longer suitable for the case when there are multiple users in a cell because subcarrier assignment issue for multi-user of each cell is involved. Hence, the proposed algorithm of this chapter is a generalization of IWFA for distributed resource allocation in multi-cell with multiple users per cell.

This chapter is structured as follows: After a related introduction in *Section 5.1*, we provide the system model and general problem formulation in *Section 5.2*. In *Section 5.3*, we describe the proposed non-cooperative game theoretic algorithm, two mathematical solutions of the concave optimization problem are presented. Numerical results are given in *Section 5.4*. Finally, this chapter is concluded in *Section 5.5*.

5.1   Introduction

Conventional Orthogonal Frequency Division Multiplexing (OFDM) is regarded as a technology which is well-matched for CR physical layer. However, interference avoidance is regarded as an important issue in CR systems. Due to the significant spectral leakage of OFDM, an accurate time synchronization is needed in order to avoid the interference with licensed system and the interference between the CR users belonging to different CR cells. As demonstrated in the previous chapters, FBMC with low spectral leakage property is preferred in CR applications, and therefore is used in this chapter. With FBMC, no time synchronization or only a coarse time synchronization is adequate to suppress the cross-interference between different CR cells. Meanwhile, FBMC strongly relaxes the interference constraint on the licensed system. Thus, the resource allocation strategy without involving interference constraint for a FBMC-based secondary systems can be feasible [1].

Many research studies have been carried out on centralized or cooperative resource allocations [115][116], in which signaling is performed so that resource allocation can be conducted in an optimal way, nevertheless, the signalling overhead is extremely expensive for communication. To avoid excessive signaling and the requirement of coordination among users, one of the possible methods to reduce overhead is to do resource allocation by only using local information. Hence, recent research focus is casted on the distributed resource allocation without any cooperation between CR cells. Distributed resource allocation has been widely recognized as a promising candidate for future cellular systems due to its low-complexity and reasonable overhead. One of the important strategies to analyze this distributed problem is to adopt game theory [117], which is a mathematical model of conflict and cooperation among intelligent and rational players. Each player has to compromise its own demand with the demands of other players, and then makes decisions in a competitive environment using the results of game theory.

This chapter is therefore focused on non-cooperative resource allocation algorithm among multiple independent secondary cells. Relevant research works can be found in the literature [47]∼[53]. However, so far sophisticated distributed resource allocation for non-cooperative multi-cell with multiple users per cell is still an open topic. Herein we investigate this open issue in the framework of game theory. Specifically, we propose an uplink non-cooperative resource allocation algorithm using game theory and multiple access channel technique [118] among multiple FBMC-based CR cells with multiple users per cell. The secondary base station in each CR cell, trying to optimize the requirement of its own users, is a player. The optimization of maximizing total information rate of

---

[1]At the absence of the interference constraint, traditional resource allocation algorithms are suitable for FBMC-based CR systems.

CR users in one cell is considered, subject to power constraint on each CR user. Thanks to the property of MAC technique, the rate maximization problem can be formulated as a concave optimization problem. Since it is complicated to obtain a closed-form solution for multi-user power allocation like water-filling algorithm for single-user, Lagrangian Algorithm (LA) and Gradient Projection Method (GPM) are employed to solve the concave optimization problem, respectively. The proposed distributed algorithm based on GT and MAC technique, which can simultaneously perform iterative subchannel assignment and power allocation for multi-user [1], is regarded as an extension of IWFA which is conventionally applied for iterative single-user power allocation.

Numerical results show that the game theoretic algorithm which allows to share one and more spectrum subchannels for multiple CR users obtains higher information rate and better convergence performance (converge to Nash Equilibrium (NE) with a small number of iterations) than the traditional Frequency Division Multiplexing Access (FDMA) which needs an exhaustive search at each iteration. Since the implementation of MAC requires additional hardware cost in practice [2], a MAC-FDMA transformation algorithm is therefore proposed, i.e. we transform the final resource allocation outcome in the form of MAC into FDMA structure. Compared to traditional FDMA, this transformed FDMA from MAC is shown to have better performance especially when the system dimension is high.

5.2 System Model and Problem Formulation

In this section, we illustrate the system model and clarify its corresponding assumptions. Next, a general problem formulation is given.

5.2.1 System Model

In the context of FBMC-based CR system, multiple Secondary Users (SUs) as well as an access point called Secondary Base Station (SBS) constitute a *CR cell*. As shown in Fig. 5.1, a scenario of CR network consisting of multiple independent CR cells with multiple CR users in each CR cell is illustrated. Unlike well-localized Primary Base Stations (PBSs), the CR cells are assumed to be randomly distributed and can have heterogeneous cell-dimension due to the flexible characteristic of CR systems. We consider a frequency selective channel with flat Rayleigh fading on each subcarrier, and it is assumed that channel changes slowly so that the channel gains will be constant during transmission. Moreover, no interference cancelation techniques are carried out, and the inter-cell interference is treated by each SBS as additive colored noise.

---

[1]The subchannel assignment can be covered by power allocation, e.g. when the allocated power on a subchannel is zero, the subchannel is not used and vice versa.

[2]In general, users belonging to the same cell are not allowed to transmit on the same subchannel.
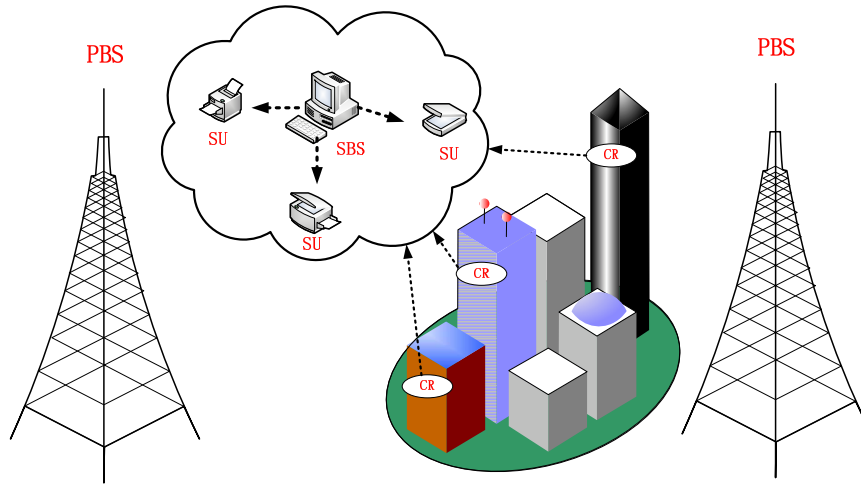
Figure 5.1: A multi-cell CR scenario with multiple CR cells and multiple users per cell

Given the above FBMC-based CR system model, some other assumptions are made:

1. Spectrum sensing has been well implemented, and the available spectrum bands obtained by spectrum sensing are assumed to be fixed and commonly shared by all the CR cells, i.e. the frequency reuse factor is one;

2. Since the random distribution characteristic of available spectrum bands, the channel gains of the available bands are assumed as stationary independent Rayleigh distribution;

3. SUs in each CR cell are synchronized and equalized, and each SBS has full channel state information and control of their own attached SUs, but different CR cells do not share their information, i.e. there is no coordination among CR cells;

4. In the context of FBMC-based CR system, we deactivate one subcarrier adjacent to Primary Users (PUs) in all the spectrum holes [1], thus, the interference from CR cells to primary systems is assumed to be negligible, and vice versa;

5. A coarse time synchronization is implemented, so each SBS can update its system resources by a sensing interval in a sequential way [2] (as shown in Fig. 5.2), and no collision occurs when different SBSs implement their sensing intervals;

---

[1] As highlighted in chapter 4, the number of subcarriers that induce harmful interference to the primary user for FBMC is "1".

[2] We do not consider the addition or removal of secondary cells.
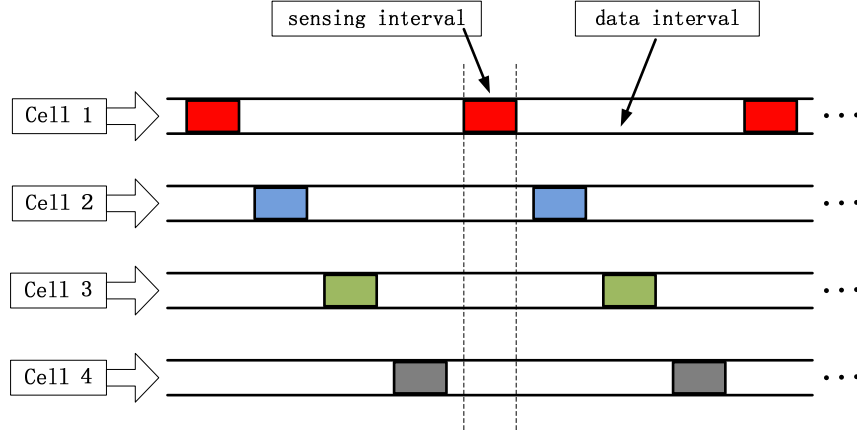
Figure 5.2: Each cell updates its system resource by a sensing interval in a fixed updating order

6. In each cell, every SU has a constant power constraint indicated by P. A number of adjacent subcarriers are grouped into a subchannel. Assuming the number of total available subchannels (free bands) is F;

   The main objective is to find a distributed algorithm that requires no cooperation among the SBSs, and achieve an optimal frequency assignment and power allocation for each CR cell.

5.2.2 Problem Formulation

In the uplink context of CR cells with multiple users per cell, we generally consider the maximization of information rate for the whole system as the objective function, subject to constant power constraint on each user, this optimization problem is formulated as

$$\max_{\mathbf{p}} : \quad \sum_{n=1}^{N}\sum_{m=1}^{M}\sum_{f=1}^{F} \theta_f^{nm} log_2[1 + SINR_f^{nm}]$$

$$SINR_f^{nm} = \frac{G_f^{nmn} p_f^{nm}}{\sigma_n^2 + \sum_{n' \neq n}\sum_{m'=1}^{M} G_f^{n'm'n} p_f^{n'm'}}$$

$$s.t.$$

$$\begin{cases} \sum_{m=1}^{M} \theta_f^{nm} \leq 1, & \forall n, f \\ \sum_{f=1}^{F} p_f^{nm} = P, & \forall n, m \\ p_f^{nm} \geq 0 \end{cases} \tag{5.1}$$

where $\mathbf{p} \in \mathcal{P}$, and $\mathcal{P} \subset \mathbb{R}^{NMF}$ is the possible set of power solution; N is the number of CR cells; M is the number of users per cell; F is the number of free bands; θ_f^{nm} is the subchannel assignment indicator, i.e. $\theta_f^{nm} = 1$ if the fth subchannel in the nth cell is allocated to the mth CR user; $G_f^{n'm'n}$ is

the propagation channel gain from the m'^{th} user of the n'^{th} cell to the SBS of the nth cell in the fth band; $p_f^{n'm'}$ is the power of the m'^{th} user of the n'^{th} cell in the fth band and σ_n^2 is the noise power.

In order to solve (5.1) by centralized constrained optimization algorithms, all the information of channel gains is indispensable, which causes significant computational complexity and large amount of channel estimation overheads especially when the number of CR users is large. Therefore, a distributed resource allocation algorithm should be more appropriate in the realistic CR scenario.

5.3 Non-Cooperative Game Theoretic Algorithm

Notice that the formulation in (5.1) is an integer optimization problem. In order to transform the above optimization problem into a concave optimization problem, we advocate the Multiple Access Channel (MAC) technique, which signifies that multiple CR users in the same cell can occupy one or more spectrum bands.

Simple schemes like Time Division Multiplexing Access (TDMA) and Frequency Division Multiplexing Access (FDMA) are used in many practical situations. When MAC technique is allowed for data transmission in a system, larger capacity region can be obtained than that achieved by TDMA or FDMA by using a common decoder for all the users of this system [118][119]. The bound of MAC capacity region for M users ($M \geq 2$) with powers $(p_1, p_2, \ldots, p_M)$ is given by

$$\sum_{i=1}^{M} R_i \leq log_2[1 + \frac{p_1 G_1 + p_2 G_2 + \cdots + p_M G_M}{N_0}] \tag{5.2}$$

where G_i is the fading channel gain of the ith user, and N_0 is the ambient noise power.

Our interest is casted on a game theoretic resource allocation algorithm without centralized control or coordination among the multiple CR cells. In our distributed game, the secondary base stations are the players, which react and compete with each other for the common resource.

In summary, let $\mathcal{G} = \{\mathcal{N}, \{\mathbf{p}_n\}_{n \in \mathcal{N}}, \{u_n\}_{n \in \mathcal{N}}\}$ denotes the non-cooperative game structure, where $\mathcal{N} = \{1, 2, \cdots, N\}$ is the index set of the players (SBSs), $\mathbf{p}_n = [p_1^{n1}, p_1^{n2}, \ldots, p_1^{nM}, p_2^{n1}, p_2^{n2}, \ldots, p_F^{nM}] \in \mathbb{R}^{MF}$ is the power strategy space of the nth player, and u_n is the utility function of the nth player.

Each CR cell wants to maximize its own information rate by allocating power into different bands for its own users, regardless of other CR cells in a distributed way. For the nth cell, its information

rate maximization problem with power constraint can be formulated as [1]

$$\max_{\mathbf{p}_n}: \quad u_n(\mathbf{p}_n, \mathbf{p}_{-n}) = \sum_{f=1}^{F} log_2[1 + SINR_f^n]$$

$$SINR_f^n = \frac{\sum_{m=1}^{M} G_f^{nmn} p_f^{nm}}{\sigma_n^2 + I_f^{-n}}$$

s.t.

$$\begin{cases} \sum_{f=1}^{F} p_f^{nm} = P, & \forall n, m \\ p_f^{nm} \geq 0 \end{cases} \tag{5.3}$$

where $\mathbf{p}_{-n} = (\mathbf{p}_1, \ldots, \mathbf{p}_{n-1}, \mathbf{p}_{n+1}, \ldots, \mathbf{p}_N)$ is the strategy profiles of all the players except for the nth player and $I_f^{-n} = \sum_{n' \neq n} \sum_{m'=1}^{M} G_f^{n'm'n} p_f^{n'm'}$ is the inter-cell interference from the others cells to the nth cell in the fth band, which is treated as additive noise.

The proposed iterative non-cooperative game is implemented in a sequential way, i.e. each player independently updates its strategy according to a fixed updating order. This sequential algorithm is stated in mathematical terms in Table 5.1 [2].

Table 5.1: The sequential iterative algorithm

Initialization:

　　set t=0 and $\mathbf{p}_n^{(0)} =$ arbitrary feasible power allocation, $\forall n \in \mathcal{N}$;

for　　t=0:T_{it}

　for　　n=1:N

　　　$\mathbf{p}_n^{(t+1)} = arg \, max_{\mathbf{p}_n^{(t+1)}} \left\{ u_n\big(\mathbf{p}_1^{(t+1)}, \mathbf{p}_2^{(t+1)}, \ldots, \mathbf{p}_{n-1}^{(t+1)}, \mathbf{p}_{n+1}^{(t)}, \ldots, \mathbf{p}_N^{(t)}\big) \right\}$;

　end

end

The outcome of the proposed game involving N players based on utility function u_n is expected to achieve a Nash Equilibrium (NE), which is defined as in Definition 1.

Definition 1: *A strategy profile $\mathbf{p}^*$ is a Nash Equilibrium if no unilateral deviation in strategy by any single player is profitable for that player, that is*

$$u_n(\mathbf{p}_n^*, \mathbf{p}_{-n}^*) \geq u_n(\mathbf{p}_n, \mathbf{p}_{-n}), \quad \forall n, \forall \mathbf{p}_n \in \mathcal{P}_n \tag{5.4}$$

where $\mathcal{P}_n$ is the set of admissible strategies defined in the constraint conditions of (5.3).

---

[1]Generally, at the final optimal solution, the constraints are satisfied with equality, that is why we set the first constraint with equality.

[2]Where T_{it} denotes the prescribed iteration times.

5. NON-COOPERATIVE RESOURCE ALLOCATION OF FBMC-BASED CR SYSTEMS

Existence of NE

Theorem 1: *For an utility function $u_n(\mathbf{p}_n, \mathbf{p}_{-n})$ with a support domain $\mathbf{p}_n \in \mathcal{P}_n$, at least a pure strategy NE point exists for any set of channel realizations and power constraint, if $\forall n$, $\mathcal{P}_n$ is a nonempty convex set and u_n is continuous and quasiconvex or quasiconcave.*

Theorem 1 given in [117] can be applied to prove the existence of NE point for the proposed game theoretic algorithm. The proof of u_n being a quasiconcave function is provided in *Appendix B*.

5.3.1 Solutions for Concave Optimization Problem

Next problem is how to achieve the optimal solution $\mathbf{p_n}$ in (5.3) which maximizes the utility function u_n. When $M = 1$, the optimal problem in (5.3) is degraded to the Multi-Cell with single user per cell, in this special case the known closed-form solution of WFA [47] can be used for solving the single-user power optimization problem. Nevertheless, in the general case of $M > 1$, traditional WFA does not work for the power allocation of multi-user case. A closed-form solution for the Multi-Cell with Multi-User per cell (MC-MU) case seems to be difficult to achieve. A variety of mathematic methods, known in the literature can be used to efficiently solve the convex optimization in (5.3), herein Lagrangian Algorithm (LA) and Gradient Projection Method (GPM), are employed to solve the optimization problem of MC-MU.

Lagrangian Algorithm

The optimization problem in (5.3) is a multi-user nonlinear optimization problem with equality and inequality constraints. Herein the method of Lagrange multipliers and Karush-Kuhn-Tucker (KKT) conditions [110] are provided as a strategy for finding the maximum of the utility function u_n subject to constraints. Defining the Lagrangian function of the problem in (5.3) as

$$L(\mathbf{p}_n, \lambda, \mu) = u_n(\mathbf{p}_n, \mathbf{p}_{-n}) + \sum_{i=1}^{M} \lambda_i (P - p_1^{ni} - p_2^{ni} \cdots - p_F^{ni}) + \sum_{i=1}^{M} \sum_{k=1}^{F} \mu_k^i p_k^{ni} \qquad (5.5)$$

The KKT conditions are necessary for a solution in nonlinear programming to be optimal, provided some regularity conditions are satisfied. It is a generalization of the method of Lagrange multipliers to inequality constraints.

Supposing that the objective function to be maximized is f, and the equality and inequality constraint functions are $h_i(i = 1, 2, \ldots, m)$ and $g_j(j = 1, 2, \ldots, n)$, respectively. Further, supposing they are continuously differentiable at a point x^*. If x^* is a local minimum that satisfies some regularity conditions, then there exist constants $\lambda_i(i = 1, 2, \ldots, m)$ and $\mu_j(i = 1, 2, \ldots, n)$, such that

$$
\begin{cases}
\nabla_{x^*} f(x^*) + \sum_{i=1}^{m} \lambda_i \nabla_{x^*} h_i(x^*) + \sum_{j=1}^{n} \mu_j \nabla_{x^*} g_j(x^*) = 0 \\
h_i(x^*) = 0, \quad g_j(x^*) \geq 0 \\
\lambda_i \geq 0, \quad \mu_j \geq 0 \\
\mu_j g_j(x^*) = 0 \qquad\qquad\qquad (\forall i, j)
\end{cases}
\tag{5.6}
$$

where ∇ is the gradient operator. These formulas above are the well-known KKT conditions, which are necessary for a solution to be optimal.

In some cases, the necessary KKT conditions are sufficient for global optimality. This is the case when the utility function and the inequality constraints are continuously differentiable concave functions and the equality constraints are affine functions. Since we already prove the concavity of utility function u_n in (5.3), the KKT condition is sufficient for the uniquely optimal solution of (5.3).

In order to guarantee a maximum point x^* be KKT, it should satisfy some regularity condition, the most used is Linear Independence Constraint Qualification (LICQ). The constraint functions satisfy the LICQ if

$$
[\nabla_{x^*} g_j(x^*); \nabla_{x^*} h_i(x^*)]^T \quad \forall i, j
\tag{5.7}
$$

has full column rank, i.e., the gradients of the active inequality constraints and the gradients of the equality constraints are linearly independent at x^*. For the optimization problem in (5.5), with $g_k^i(\mathbf{p}_n) = p_k^{ni}$ $(\forall i, k)$ and $h_i = (1 - p_1^{ni} - p_2^{ni} \cdots - p_F^{ni})$ $(\forall i)$. Assuming $\mathbf{p}_n^*$ is the optimal solution, according to (5.7), we get

$$
Rank\{[\nabla_{\mathbf{p}_n^*} g_k^i(\mathbf{p}_n^*); \nabla_{\mathbf{p}_n^*} h_i(\mathbf{p}_n^*)]^T\} = M \times F
\tag{5.8}
$$

satisfies the LICQ.

Consequently, the KKT conditions in (5.6) can be used for uniquely solving the global point of (5.3), the Lagrangian functions of the optimal allocation problem can be obtained as

$$
\begin{cases}
\frac{G_k^{nin}}{\sigma_n^2 + I_k^{-n} + (p_k^{n1} G_k^{n1n} + \cdots + p_k^{nM} G_k^{nMn})} \cdot \frac{1}{log_2(2)} - \lambda_i + \mu_k^i = 0, \\
1 - p_1^{ni} - p_2^{ni} \cdots - p_F^{ni} = 0, \\
\mu_k^i p_k^{ni} = 0, \\
\lambda_i \geq 0, \quad \mu_k^i \geq 0, \quad p_k^{ni} \geq 0, \qquad (\forall i, k)
\end{cases}
\tag{5.9}
$$

where $i = 1, 2, \cdots, M$ and $k = 1, 2, \cdots, F$. Under the assumption that aggregated inter-cell interference I_k^{-n} can be measured locally and the SBS knows all the channel information of its own users, the optimal frequency allocation and power control can be iteratively computed between distributed CR cells according to (5.9).

Unfortunately, for a CR cell with M users and F free bands, the number of equations in (5.9) is $M \times (2F + 1)$, which indicates a huge computational complexity in particular when the values of M and F are high.

5. NON-COOPERATIVE RESOURCE ALLOCATION OF FBMC-BASED CR SYSTEMS

Gradient Projection Method

Due to the computation limit of Lagrangian optimization method in (5.9) to high-dimension system, we resort to Gradient Projection Method (GPM) for the linearly constrained problem. Rosen's gradient projection method [110] is based on projecting the search direction into the subspace tangent to the active constraints. We define the constrained optimization problem as

$$
\begin{aligned}
max: \quad & u_n(\mathbf{p}_n) \\
s.t. \quad & \begin{cases} \mathbf{E}\mathbf{p}_n = \mathbf{e} \\ \mathbf{A}\mathbf{p}_n \le \mathbf{b} \end{cases}
\end{aligned}
\tag{5.10}
$$

where $\mathbf{A}$ is a $MF \times MF$ coefficient matrix of the inequality linear constraints and the rows of $\mathbf{E}$ are the coefficient vectors of the equality constraints. Comparing (5.10) with (5.3), we can obtain

$$
\begin{cases}
\mathbf{A} = \begin{bmatrix} -1 & 0 & \cdots & 0 \\ 0 & -1 & \cdots & \vdots \\ \vdots & \vdots & \ddots & 0 \\ 0 & \cdots & 0 & -1 \end{bmatrix}^{MF \times MF} , \mathbf{b} = \begin{bmatrix} 0 \\ \vdots \\ 0 \end{bmatrix}^{MF \times 1} \\[40pt]
\mathbf{E} = \begin{bmatrix} 1 & \cdots & 1 & 0 & \cdots & 0 & \cdots & \cdots & 0 \\ 0 & \cdots & 0 & 1 & \cdots & 1 & 0 & \cdots & 0 \\ \vdots & \vdots & \vdots & \vdots & \vdots & \vdots & \vdots & \vdots & \vdots \\ 0 & \cdots & \cdots & \cdots & \cdots & 0 & 1 & \cdots & 1 \end{bmatrix}^{M \times MF} , \mathbf{e} = \begin{bmatrix} P \\ \vdots \\ P \end{bmatrix}^{M \times 1}
\end{cases}
$$

Let $\mathbf{p}_n$ be a feasible solution and suppose $\mathbf{A}_1\mathbf{p}_n = \mathbf{b}_1, \mathbf{A}_2\mathbf{p}_n < \mathbf{b}_2$, where $\mathbf{A}^T = (\mathbf{A}_1^T, \mathbf{A}_2^T)$ and $\mathbf{b}^T = (\mathbf{b}_1^T, \mathbf{b}_2^T)$. Supposing that $\mathbf{M}^T = (\mathbf{A}_1^T, \mathbf{E}^T)$, then the iterative gradient projection algorithm is given in Table 5.2.

Table 5.2: Iterative steps of gradient projection algorithm

Step 0:	Initialization:
	set t=1, and $\mathbf{p}_n^{(1)}$= any feasible power allocation;
Step 1:	Calculate projection matrix $\mathbf{s}^{(t)} = \mathbf{Q}\nabla u_n$ according to (4.9).
	If $\|\mathbf{s}^{(t)}\| \le \varepsilon$, or $t > T_{max}$, terminate.
	If not, go to step 2.
Step 2:	Determine the maximum step size and solve the line-search
	problem for α according to (4.10)(4.12).
Step 3:	Set $\mathbf{p}_n^{(t+1)} = \mathbf{p}_n^{(t)} + \alpha\mathbf{s}^{(t)}$, t = t+1, and go to step 1.

Given a proper threshold ε, GPM is an efficient way for the optimization problem with linear constraints. To summarize, the above statements show that LA is only applied for low dimension systems due to its computation complexity. Conversely, GPM can be used to solve the optimization problem of high dimension systems.

5.4 Numerical Results

In the context of cognitive radio, we assume that some licensed spectrum band resources are already obtained by CR spectrum sensing. The channels of available spectrum bands are considered as stationary independent Rayleigh distribution because of the random distributed characteristic of spectrum holes. The main objective of this section is to try to demonstrate more optimal sum-rate and stabler convergence using MAC compared to traditional FDMA. Simulations are divided into two parts: low-dimension systems and high-dimension systems.

5.4.1 Simulations for Low-dimension Systems

Since low-dimension systems with small number of CR users per secondary cell are considered, Lagrangian solution in (5.9) can be used for solving the concave optimization in (5.3). More specific, two-cell and five-cell cases are considered (see Fig. 5.1), with two users or three users uniformly distributed within a cell range ($0.01 \sim 1.1\ km$). Assuming the power density of thermal noise is -174 dBm/Hz, in the case of uplink, each user is equipped to transmit signal with fixed $P = 1\ watt$ power. As the increase of transmission distance, the attenuation also increases due to the propagation pathloss. The pathloss of received signal at a distance $d\ km$ is [114]

$$P(d) = 128.1 + 37.6 \cdot log_{10}(d) \quad dB \tag{5.11}$$

by this Macro propagation model the SNR value of the user located at the border of cell (assuming the radius of cell R=1.1 km) fluctuates around 20 dB when the Rayleigh fading channel is considered.

In order to evaluate the proposed MAC game theory (MAC-GT) algorithm, a FDMA based game theory (FDMA-GT) is also implemented in such a way that each secondary base station exhaustively searches for the optimal FDMA strategy which maximizes the whole information rate in a sequential way. Firstly, the numerical results for two-cell case are displayed. In Fig. 5.3, the averaged sum-rate of the whole system with 2 users per cell versus the distance D between base stations is compared for FDMA-GT and MAC-GT, where the optimal centralized algorithm [1] performance for MAC and

---

[1]In this case, all the channel information among different CR cells is assumed to be known by using a centralized controller, thereby the optimal centralized resource allocation can be implemented.
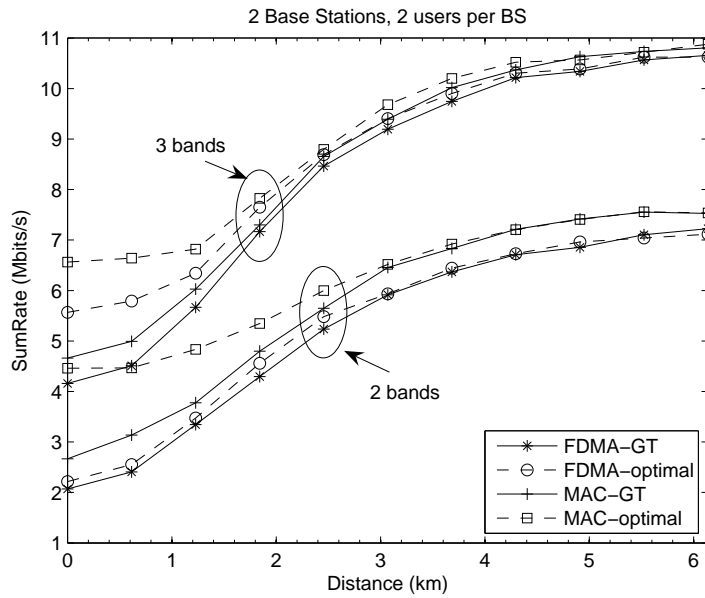
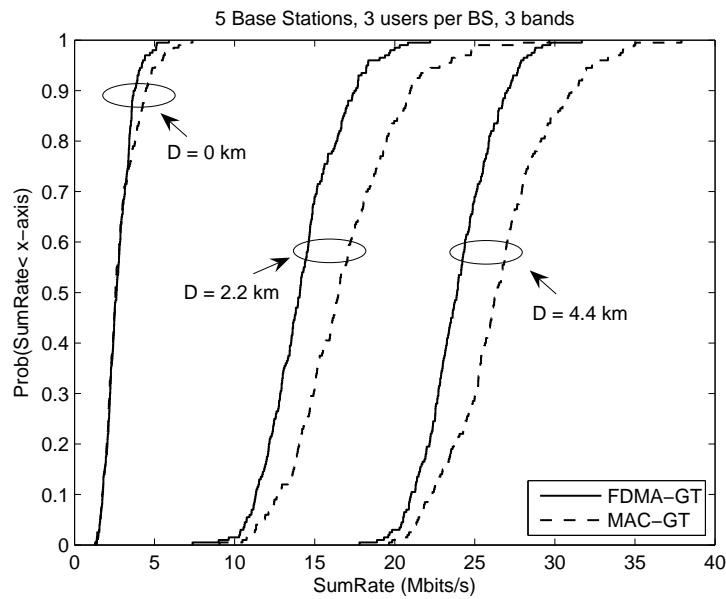**Figure 5.3:** Averaged sum-rate of the whole system vs. Distance D

Figure 5.4: Sum-rate CDFs of FDMA-GT and MAC-GT

FDMA is also given for comparison purpose. 1000 independent network topologies and channel realizations are averaged for two bands and three bands, respectively. It can be seen that a large distance can increase sum-rate performance significantly. The reason is that there exists little interference from other cells when the cells are far away from each other.

In the case of two bands, the optimal centralized sum-rate performance of MAC (MAC-optimal) outperforms that of FDMA-optimal due to the larger capacity region of MAC. These dashed optimal curves in Fig. 5.3 can be used as performance bounds for decentralized game theory algorithm. As expected, MAC-GT always has a better sum-rate performance than FDMA-GT. However, we observe that MAC-GT has low sum-rate compared to its optimal curve when distance D becomes small, which can be explained by the greedy property of each player in game theory, in the presence of small distance (i.e. significant interference), the outcome of the non-cooperative game will finally converge to an inefficient NE point. The same performance results can happen to the case of three free bands, the only difference is that for FDMA, unlike two bands for two users, each user can use one or two bands, e.g. for the user who occupies two bands, power allocation will be implemented on these two bands with a fixed power constraint, which can improve the performance of FDMA. This is the reason why in Fig. 5.3 there is less performance difference between MAC and FDMA compared to the case of two bands.

For the simple case of two cells and two users per cell, both FDMA-GT and MAC-GT can converge with a rapid convergence speed (2 iteration rounds). Next, the case of five cells with three users per cell is considered. As shown in Fig. 5.4, sum-rate Cumulative Distribution Functions (CDFs) of FDMA-GT and MAC-GT algorithms with three available bands and three different distance cases (D = 0, 2.2 and 4.4 km) over 200 independent channel realizations are compared. In the case of distance $D = 0$ km, these two algorithms both suffer from significant interferences, which causes that the final solution converges to some undesired NE points. In the cases of more practical distances $D = 2.2$ km and $D = 4.4$ km, the performance difference between MAC-GT and FDMA-GT are observed to be larger than the case of two cells with two users per cell in Fig. 5.3. This is expected because the capacity region disparity between MAC and FDMA increases as the increase of users' number.

The convergence rates for FDMA-GT and MAC-GT algorithms in the five-cell case are presented in Table 5.3 and Table 5.4, respectively. It can be noticed that, more iterations are needed if the distance D is enough small (which means significant interference between cells). Although FDMA-GT has a little more rapid convergence speed than that of MAC-GT, there exists some Nonconvergent Points (NPs) resulting from some channel situations. Conversely, MAC-GT can always converge to a NE point within a limited iteration times. Hence, we can conclude that MAC-GT can exploit more information rate and better convergence stability than FDMA-GT, especially if the number of users in the network is large. In the subsequent part, practical high-dimension system with large number

of CR users per cell is simulated, it will be demonstrated that higher information rate is achieved for MAC-GT compared to FDMA-GT in the context of high-dimension systems.

Table 5.3: Iteration situation for FDMA-GT algorithm in low-dimension systems

$(d = 0km)$		$(d = 2.4km)$		$(d = 4.8km)$	
Iterations	Percent	Iterations	Percent	Iterations	Percent
3	40.50%	3	79.00%	3	98.50%
4	45.50%	4	19.00%	4	1.50%
5	11.00%	30	0.50%	NP	0.00%
NP	3.00%	NP	1.50%	-	-

Table 5.4: Iteration situation for MAC-GT algorithm in low-dimension systems

$(d = 0km)$		$(d = 2.4km)$		$(d = 4.8km)$	
Iterations	Percent	Iterations	Percent	Iterations	Percent
3	13.00%	3	34.00%	3	92.50%
4	45.50%	4	62.00%	4	7.50%
5	29.00%	5	4.00%	NP	0.00%
6	8.00%	NP	0.00%	-	-
7	3.50%	-	-	-	-
8	0.50%	-	-	-	-
9	0.50%	-	-	-	-
NP	0.00%	-	-	-	-

5.4.2 Simulations for High-dimension Systems

In order to generalize the application of the proposed MAC-GT algorithm, as shown in Fig. 5.5, a seven-cell CR scenario (each cell contains a large number of CR users) with a wrap-around structure is considered, in which the seven base stations who know the propagation channels of their own users are the players (N=7) of the game, and maximize their information rate according to a sequential updating order. In each CR cell, multiple CR users are uniformly distributed within the cell range (0.01~1.1 km). The transmitted power of each user is fixed at a more practical value $P = 20\ mW$. The pathloss model of the received signal in (5.11) is applied.
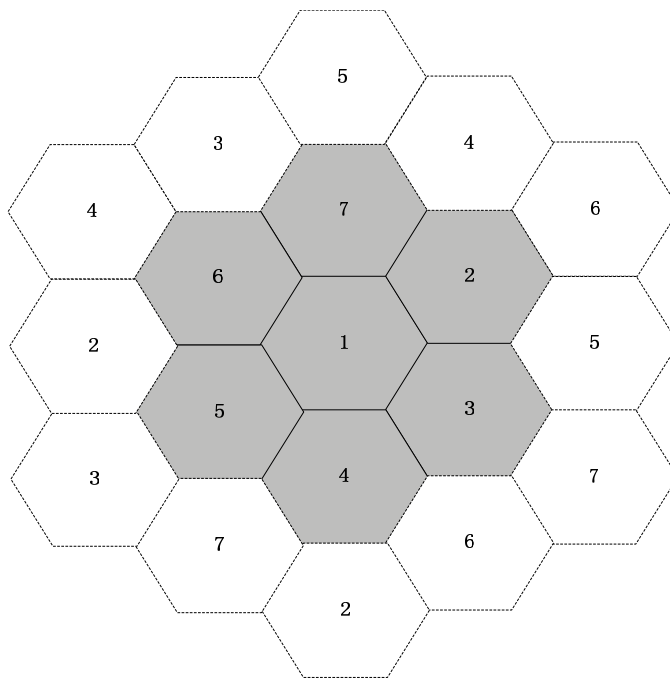
Figure 5.5: A regular seven-cell CR scenario with wrap-around structure

Naturally, the computational complexity increases with the increase of system dimension. Thus, Lagrangian algorithm is no longer efficient for solving the optimization problem in (5.3). Alternatively, we prefer to select GPM in Tab 5.2 to solve the concave optimization problem, where we set the threshold parameter $\varepsilon = 10^{-3}$, and $T_{max} = 500$.

In the first study, we hypothesize that the number of bands is always equal to the number of users per cell [1] ($M = F$). We perform several simulations to corroborate the theoretical results. Firstly, the simulation results with small number of CR users per cell are displayed. In Fig. 5.6, the sum-rate of the whole system with 3 users per cell as well as 5 users per cell, versus the distance D between base stations is compared for FDMA-GT and MAC-GT [2]. 500 independent network topologies and channel realizations are averaged for these two cases, respectively. We can see that MAC-GT always has a better performance than FDMA-GT. Besides, due to the larger capacity region for MAC, MAC-GT benefits more than FDMA-GT with the increase of free bands. As shown in Fig. 5.6, for the case of 5 free bands, there is more performance gap between MAC-GT and FDMA-GT compared to the case of three free bands.

The corresponding convergence rates for FDMA-GT and MAC-GT algorithms are presented in

---

[1] The general case when $M \neq F$ has high simulation complexity but still applies the proposed algorithm.

[2] Here we don't give the numerical results of the optimal centralized algorithm because it requires a global exhaustive search, which has a high computational complexity for high-dimension systems.
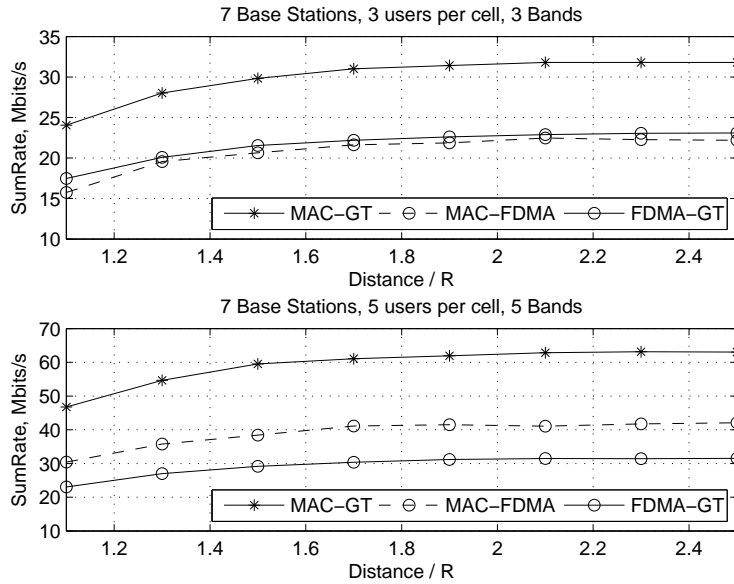
Figure 5.6: Averaged sum-rate of whole system vs. distance

Fig. 5.7 and Fig. 5.8, respectively. The same as the numerical results for low-dimension systems, we observe that more iterations are needed when the distance D becomes small. FDMA-GT converges a little faster than MAC-GT, but there exists some NPs, the rate of which augments as the increase of users' number. Conversely, MAC-GT can guarantee that the non-cooperative game converges to a NE point within a small iteration times.

Secondly, for larger number of CR users per cell, a computation problem appears for FDMA-GT algorithm, because during each iteration process we have to try all the possible FDMA candidates to obtain the optimal FDMA solution. This exhaustive search makes FDMA-GT impractical and some heuristic strategies are expected to solve the high dimension problem of FDMA-GT algorithm. In this chapter, thanks to the MAC-GT algorithm, we propose a MAC-FDMA transformation algorithm. An illustration of this MAC-FDMA algorithm is described in Fig. 5.9. Based on the final MAC-GT result, we firstly search the strongest power value in the MAC table, this value (0.9) corresponds the second band and the first user, therefore we allocate the second band to the first user, and eliminate the second column and the first row from the MAC table. Then we continue to search the strongest power value in the rest of the MAC table, and conduct the previous operation until all the bands are allocated. The experimental results of MAC-FDMA for 3 users and 5 users are shown and compared with FDMA-GT in Fig. 5.6. It is interesting to find that MAC-FDMA algorithm outperforms the exhaustive FDMA-GT algorithm when the number of users in the system increases. In the rest of the simulation, we use MAC-FDMA algorithm to replace the exhaustive FDMA-GT algorithm.
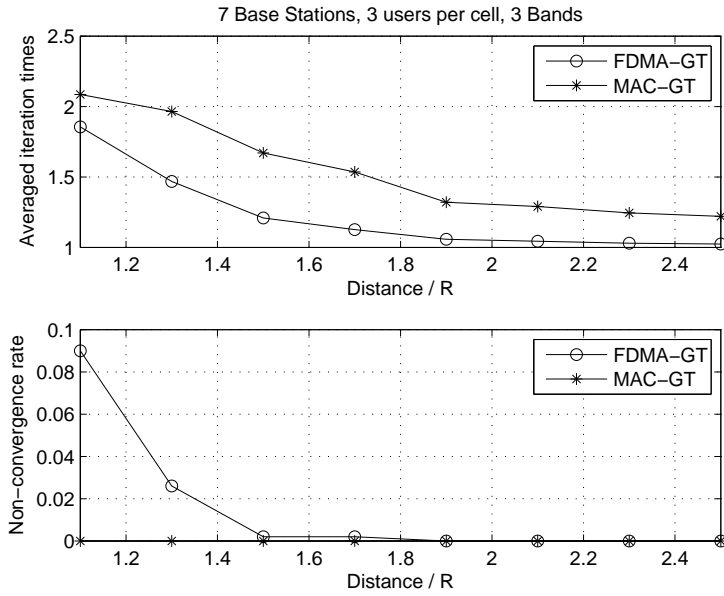
Figure 5.7: Convergence property of the case with 3 bands and 3 users per cell
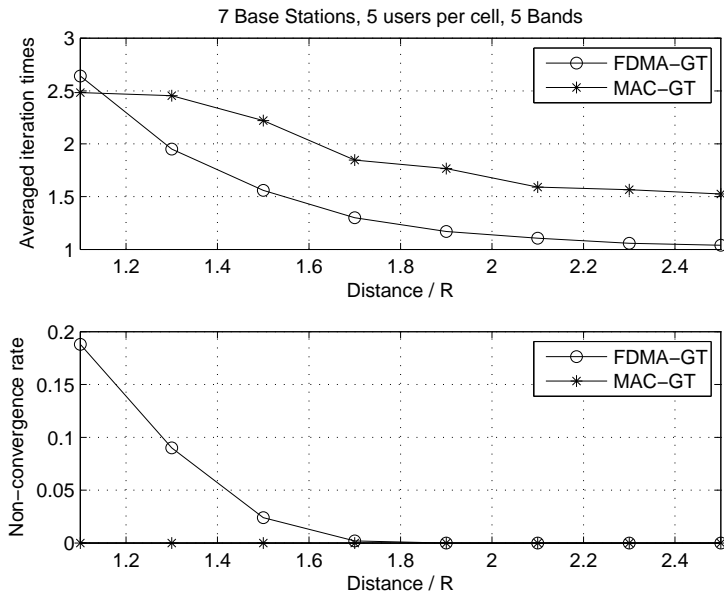
Figure 5.8: Convergence property of the case with 5 bands and 5 users per cell
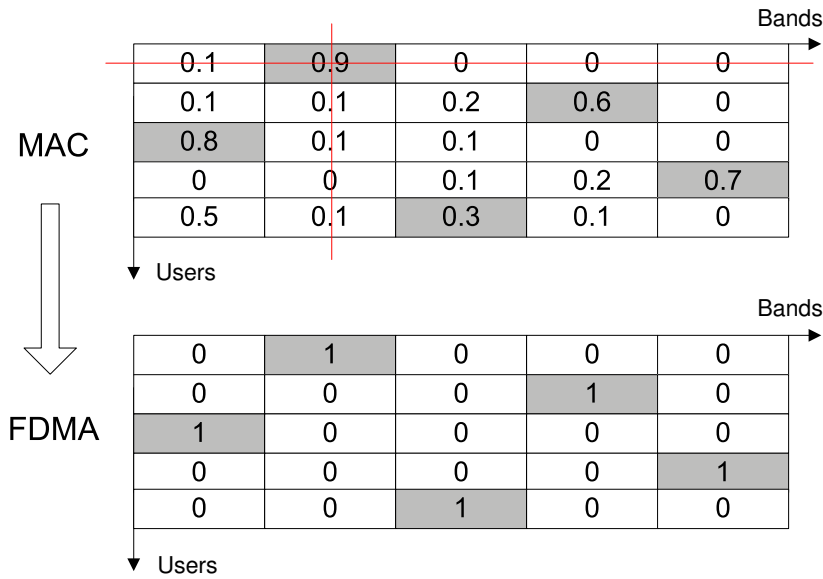
Figure 5.9: A transformation illustration from MAC to FDMA

Next, the situation of a practical distance $(D = 2R)$ with different number of CR users per cell is considered. As shown in Fig. 5.10, the sum-rate CDFs and the averaged user-rate of MAC-FDMA and MAC-GT algorithms with 3, 5, 8 and 10 CR users per cell and a distance $D = 2.2\ km$ over 200 independent channel realizations are displayed, respectively. The performance of MAC-GT algorithm is much better than MAC-FDMA algorithm, and once again, the performance gaps between MAC and FDMA for high user dimension are observed to be larger than the case of small user dimension.

The corresponding convergence properties in Fig. 5.10 are presented in Table 5.5. The higher the user dimension is, the more interference between CR cells. Thus, more iteration times are needed for large user dimension system, which can explain the different convergence rates in Table 5.5.

Table 5.5: Iteration situation for MAC-GT algorithm in high-dimension systems

Users per cell	(3)	(5)	(8)	(10)
Iterations	Percent	Percent	Percent	Percent
1	76.50%	45.00%	16.50%	1.00%
2	22.00%	45.00%	51.00%	30.50%
3	1.00%	9.50%	28.00%	41.50%
4	0.50%	0.50%	3.00%	22.50%
5	-	-	1.50%	4.50%
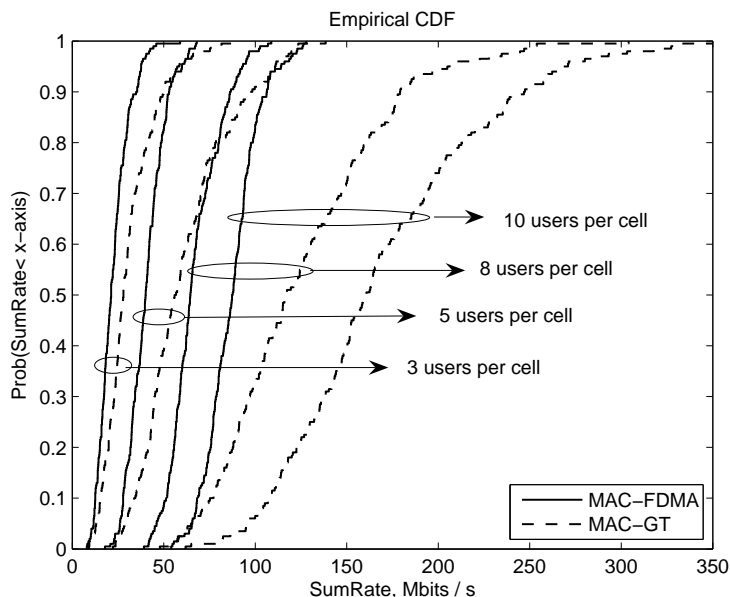
Figure 5.10: Sum-rate CDFs of MAC-FDMA and MAC-GT algorithms

Finally, higher user dimension system with more than 10 users per cell is considered. In this case, the GPM with the hard threshold $\varepsilon = 10^{-3}$ prevents the MAC-GT algorithm from efficiently operating, i.e., large iteration times are needed to achieve the final convergence. To reduce the iteration times and achieve a fast convergence rate, we enlarge the threshold to $\varepsilon = 1$. By using this much more relax threshold, the sum-rate CDFs of MAC-GT algorithms with 8, 10, and 20 CR users per cell and a distance $D = 2.2 \ km$ over 200 independent channel realizations are displayed in Fig. 5.11, and its corresponding convergence properties are presented in Table 5.6. In contrast to Fig. 5.10 and Table 5.5, it is interesting to find that this soft-threshold MAC-GT can achieve almost the same sum-rate performance with faster convergence rate, which indicates that the whole system sum-rate of our MAC-GT algorithm can reach a desired performance after only 2 or 3 iteration times. Herein we have not given out more numerical results for high user dimension system. Higher user dimension system with more than 20 users per cell can be implemented in the same way by changing the threshold ε.

5.5 Conclusion

In this chapter, we propose a non-cooperative MAC-GT algorithm to perform uplink resource allocation with power constraint in the context of multi-cell FBMC based CR network. A convex optimization problem is formulated by taking advantage of MAC technique. We have derived the
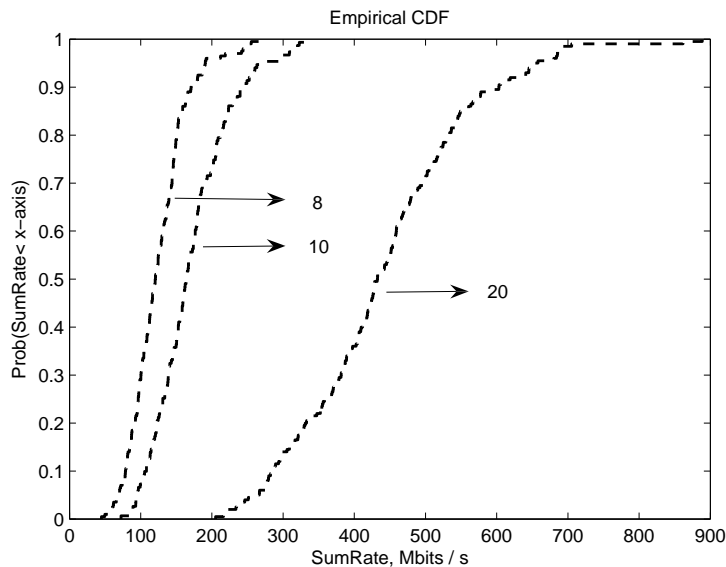
Figure 5.11: Sum-rate CDFs of MAC-GT algorithm with large number of CR users

Table 5.6: Iteration situation for MAC-GT algorithm in high-dimension systems with $\varepsilon = 1$

Users per cell	(8)	(10)	(20)
Iterations	Percent	Percent	Percent
1	87.50%	42.00%	35.00%
2	12.50%	57.00%	62.00%
3	-	1.00%	3.00%

optimization solutions of the proposed algorithm using Lagrangian algorithm and gradient projection method. The MAC-GT algorithm for iterative multi-user power allocation is an extension of IWFA which is applied for iterative single-user power allocation. Besides, since the high implementation cost of MAC scheme, we propose a heuristic MAC-FDMA transformation algorithm to avoid costly implementation of MAC and also to solve the exhaustive search problem of traditional FDMA strategy. Final numerical results exhibit that the distributed MAC-GT and MAC-FDMA algorithms deliver robust convergent behavior and achieve superior sum-rate performance than the traditional FDMA-GT algorithm especially for a high-dimension network with a large number of CR users per cell.

In our CR scenario using FBMC technique, the proposed non-cooperative resource allocation algorithm and the experimental simulation are both based on the assumption that the interference

from CR cells to primary system is neglected by deactivating one subcarrier in the two sides of each spectrum hole. This hypothesis is not far from a realistic CR network without involving interference issue. Nevertheless, there exists significant interference among the CR cells if OFDM technique is applied. As noted in chapter 4, in order to avoid interference with primary system, "8" subcarriers in the spectrum holes should be deactivated, which substantially decreases the capacity of CR system. In summary, FBMC highly relaxes the interference to primary system, and thus can be considered as a potential candidate for future CR physical layer data communication.

CHAPTER 6

Conclusions

It is anticipated that in the future life, the emerging Cognitive Radio (CR) techniques will play a key role in the field of wireless communications due to the increasing wireless services, and a physical layer best suited to CR is needed. In view of this expectation, in this dissertation, we develop a CR framework that advocates Filter Bank based Multi-Carrier (FBMC) for opportunistic spectrum access. The objective of this dissertation is to propose FBMC for the future CR system that is more efficient and flexible than the conventional Orthogonal Frequency Division Multiplexing (OFDM) based CR system. Recently, a great deal of research has focused its attention on OFDM for wireless applications, but few studies in the literature have considered FBMC, especially Offset Quadrature Amplitude Modulation (OQAM), and relatively limited attention from the CR community is received. Thus, another objective of this dissertation is to disseminate the basic knowledge of FBMC and to motivate wireless researchers to strengthen FBMC investigation in the literature.

As a potential candidate of the next generation communication system, FBMC maintains not only the most appealing features of OFDM, e.g. high data rate, robustness to multipath fading, flexible spectral shaping, etc., but also improves the weak points of OFDM thanks to its inherent capabilities. Firstly, FBMC permits to maximize the spectral efficiency of CR system by eliminating the Cyclic Prefix (CP). Secondly, FBMC exploits the low spectral leakage of its prototype filter, which shows a higher robustness to residual frequency offsets and better Inter-Symbol Interference (ISI) and Inter-Carrier Interference (ICI) suppression than OFDM. Moreover, no guard bands are needed for guaranteeing the service quality of licensed system, and a growth of CR system throughput can be hence promoted. Lastly, it has been shown that filter banks can serve as an accurate spectrum analyzer and reception simultaneously at virtually no additional cost, which eases the requirement on the hardware. In this dissertation we show that the analysis filter banks at the receiver can achieve greater dynamic spectrum range than the conventional Fast Fourier Transform (FFT) in OFDM. Besides, compared to OFDM, FBMC can allow a very flexible frequency management on a carrier-by-carrier basis and can provide a more flexible spectral shaping of the transmitted signal that fills the spectrum holes without interfering with the licensed users.

In a word, FBMC techniques offer higher spectrum resolution, higher spectrum efficiency, more flexible spectral shaping, and require only a little increase in computation complexity as opposed to

OFDM. All these important properties of FBMC make it a promising CR physical layer candidate and better suited to the new concept of dynamic access spectrum.

In the following, we review the major contributions of this dissertation and discuss some topics of further research.

6.1 Contributions

After giving the introduction involving motivation, research scope, literature review, thesis outline, and publications in Chapter 1, then an overview of CR and Multi-Carrier Modulation (MCM) schemes are briefly described in Chapter 2, where we describe what is actually meant by cognitive radio, its developments, its applications in different wireless networks, and some research challenges in the deployment of the real-life CR scenario have been outlined. At last, the strengths and weakness of OFDM and FBMC are highlighted. Based on the preliminary and theoretical knowledge provided in the first two chapters, three research issues including: spectrum sensing, spectrum efficiency comparison, and resource allocation in FBMC-based CR context are analyzed and investigated in the subsequent chapters.

In Chapter 3, we first provide a literature review which covers the major categories of traditional transmitter detectors, and discuss their adaptability in the CR system. Next, this chapter proceeds by proposing a cyclostationary signature based single-band detector and a multi-band detection architecture based on polyphase filter bank. Chapter 4 emphasizes the channel capacity comparison between OFDM-based CR systems and FBMC-based CR systems under an uplink scenario. In the last Chapter, we propose a non-cooperative resource allocation algorithm using game theory to efficiently perform uplink frequency allocation and power control for FBMC-based multi-cell CR systems.

In this dissertation, a number of original contributions have been obtained in the area of FBMC-based CR systems, which are summarized as below:

- *Spectrum Sensing*: At first, spectrum sensing as a crucial element of cognition in terms of spectrum awareness is explored. The spectral correlation characteristics of MCM signals are investigated by Linear Periodic Time-Variant (LPTV) model and explicit theoretical formulas of spectral correlation functions are derived. In order to overcome the limitations of energy detector in CR applications, a Cyclostationary Signature (CS) detector based on the theoretical spectral analysis is proposed. This CS detector is demonstrated to be more robust against noise uncertainty, and can discriminate different primary signals, noise and interference. What is worth mentioning is that this CS detector is a good contribution especially for FBMC signal detection since FBMC signal does not exhibit strong cyclostationary feature like OFDM signal.

Additionally, the sensing feature of FBMC is discussed. A multi-band sensing architecture built on Polyphase Filter Bank (PFB) is analyzed and compared to FFT based sensing structure. It is shown that spectral estimation can benefit from PFB due to its high containment of prototype filter, which yields better performance results than FFT.

- *Spectral Efficiency Comparison*: The ideal situation of a CR system the researchers expect is: maximum throughput for the CR system and minimum interference for the licensed system. Since the CR system will inevitably cause some interference to the licensed system, it always needs to make a tradeoff between interference and throughput. In our dissertation, the inter-cell interference resulting from timing offset for OFDM and FBMC are demonstrated, and the mean interference tables for OFDM and FBMC are quantitatively obtained. It has been proven that OFDM causes very significant interference level to the neighboring subcarriers, whereas FBMC causes very small interference. In order to further provide an insight into the spectrum efficiency, the capacities of OFDM and FBMC based CR systems are examined and compared based on their mean interference tables. Numerical results once again verify that FBMC can offer higher channel capacity and can achieve much more performance gain if rough estimated Channel State Information (CSI) is considered.

- *Resource Allocation*: Herein we emphasize on the Non-cooperative Resource Allocation (NRA) based on Game Theory (GT) in FBMC based multi-cell CR system with multi-user per cell. As discussed in the preceding chapter, FBMC is proven to show almost no cross-interference with neighboring subcarriers (i.e. only one secondary subcarrier adjacent to Primary Users (PUs) causes interference to PUs). Therefore, our NRA strategy is proposed under the assumption that the subcarrier adjacent to PUs is deactivated and the multiple secondary cells are coarse-synchronized. Benefiting from these assumptions, the interference constraint is omitted, and a sequential distributed resource allocation algorithm is feasible. In contrast to existing algorithms based on Frequency Division Multiple Access (FDMA), the proposed NRA algorithm formulates a concave optimization by using Multiple Access Channel (MAC) technique, which significantly decreases the non-convergence probability. The proposed MAC based NRA algorithm for distributed multi-user power allocation generalizes Iterative Water-Filling Algorithm (IWFA) which is applied for distributed single-user power allocation. Besides, we propose a pragmatic MAC-FDMA transformation method, which not only avoids costly implementation of MAC but also solves the exhaustive search problem of traditional FDMA strategy. Final numerical results exhibit that MAC and MAC-FDMA based game theoretic algorithms can achieve more stable convergence and higher sum-rate performance than the traditional FDMA algorithm especially for high dimension systems.

According to above descriptions, we demonstrate that when as a CR data communication technique, FBMC offers higher spectral resolution and spectral efficiency than OFDM. As a result, the conclusion can be reached that FBMC is a very appropriate candidate for physical layer data communication in CR systems. Although there is a little additional complexity for FBMC due to the implementation of equalization, it is profitable for achieving better spectral efficiency. Furthermore, the research in this dissertation has significantly advanced the state of the art of FBMC in CR communications.

6.2 Future Research

FBMC has the potential to fulfil the requirements of CR concept, but a major research effort is necessary for full exploitation and optimization of FBMC techniques in all aspects of the CR context. Consequently, advances in FBMC-based CR systems are still required to make it useful for future radio systems. On the basis of the research issues studied in this dissertation, there exists a number of topics that could be continued. Some suggestions of possible extension on existing work are given below:

- *Spectrum Sensing*:

  1. The period of one MCM symbol is assumed to be known to CR receiver for cyclostationary detection in Section 3.2, which is an unrealistic assumption in most of CR scenarios. Thus, it would be interesting to develop sophisticated methods to predict the signal symbol period [120];

  2. In Section 3.2, future work could be undertaken to exploit the use of pilots for generating cyclostationary signatures instead of using transmission data, which will significantly increase the useful data rate;

  3. In Section 3.3, for the sake of simplicity, we compare the multi-sensing performance of PFB and FFT only in white noise environment. However, the shadowing, multipath fading and interference aggregation show large effect on performance. In order to accommodate for practical implementation aspects, future work will concern the effect of High Power Amplifier (HPA), shadowing, fading, and interference related to the utilization of PFB;

  4. With respect to spectrum sensing, there are a number of challenges involving Doppler fading, hidden transmitter, interference from other CR users, etc., which will result in less reliable or even wrong detection. Another solution for future work is to exploit the cooperative spectrum sensing;

- *Spectral Efficiency Comparison*: In this dissertation, the spectral efficiency comparison is implemented from the channel capacity point of view, in the future, the comparison could be extended from the throughput point of view by considering Adaptive Coding and Modulation (ACM). Besides, the influence of nonlinear HPA should also be considered.

- *Resource Allocation*:

    1. Our proposed non-cooperative resource allocation algorithm is at the premise that spectrum sensing is perfectly implemented. However, perfect detection of licensed signals is one of the several research challenges. An interesting research topic may be to analyze resource allocation algorithm in the absence of perfectly spectrum sensing assumption;

    2. Another challenge of resource allocation in CR context is the time-varying property of spectrum holes and channel condition, whereas herein we implicitly assume fixed spectrum resource and constant channel. However, such an assumption may not always be valid in CR networks. Sophisticated resource allocation methods taking these factors into account are required in the future work;

    3. Our future work will also focus on the study of a series of game theory strategies to move from inefficient Nash Equilibrium towards Pareto-efficient solution;

Basic research issues of CR systems are presented in Chapter 2, but there are some general issues which have not been considered herein. This dissertation focuses mainly on the spectrum sensing and spectrum sharing, further research topics (i.e. spectrum management and spectrum mobility) that interact with sensing and sharing are required to investigate for the development of complete CR functionalities:

- *Spectrum Management*: The spectrum management policies and techniques are difficult research problems, yet to be adequately resolved. Completely characterizing the available spectrum holes with various metric parameters is still an open research topic.

- *Spectrum Mobility*: Much future work exists in this area. If a licensed user reappears in a band, the CR user operating in this band must move to another spectrum hole or stop transmitting to avoid interference. Because of the bursty nature of wireless traffic, lightning-fast channel jumping should be required for CR users in order to vacate the current spectrum band for the bursty emergence of licensed user immediately. This problem draws recently more and more attention of system analysis by using Hidden Markov Model (HMM) [121] to predict channel availability. To build up the channel availability state and find out agile solutions of spectrum mobility are the goals we will strive toward.

In the project PHYDYAS, significant emphasis has been put on the energy detection or CP autocorrelation (when PUs use OFDM) based spectrum monitoring [122], i.e. rapid detection of possibly reappearing primary users. By using FBMC waveform for secondary transmission, the simultaneous reception and spectrum monitoring are considered to be feasible. Although some efforts have been devoted to spectrum monitoring in PHYDYAS, a thorough study about this issue is still a future topic;

FBMC and CR are still in their infancy stage, technical issues and regulatory aspects need to be addressed before the FBMC-based system can be realized. Research efforts are particularly important in providing technical support for the spectrum regulatory policies. Given that the research of this dissertation is the preliminary investigation into FBMC-based CR systems, there is plenty of work yet to be explored in both methodological aspects and concrete applications. Looking forward, it is believed that FBMC, as a powerful physical layer technique, will play a significant role in the future CR system, and there is a great chance to emerge a new worldwide CR standard supporting FBMC techniques.

Relative Appendix in Section 3.3.3

A.1 Correlation Property Proof

The equation (3.74) could be equally expressed as

$$X_m(k) = \sum_{n=0}^{LM-1} r\big[n + kM\big] h\big[n\big] e^{-2\pi j \frac{nm}{M}}, \qquad m = 0, 1, \ldots, M - 1; \tag{A.1}$$

thereby the autocorrelation of X_m at lag u is calculated by (A.4), where "$*$" is the conjugate operator, "$\otimes$" denotes convolution operator, and $R_{rr}(i)$ is the autocorrelation function of $r(n)$. Since the spectrum sensing in CR context is operated in a low SNR level, we assume the received samples $r(n)$ are uncorrelated sequences. Therefore, (A.4) is simplified into

$$R_{xx}(u) \approx R_{rr}\big(0\big)\bigg(h \otimes h\big[(L - u)M\big] \bigg) \tag{A.2}$$

PSE

In this case, h is a rectangular filter and $L = 1$, so we have $h \otimes h\big[(1 - u)M\big] = 0$, which demonstrates that $X_m(k)$ based on PSE are independent observations.

PHYDYAS

The prototype filter of PHYDYAS is a Square-Root Nyquist filter. Thus, the function "$h \otimes h$" is a Nyquist filter, which satisfies

$$h \otimes h[kM] = \begin{cases} \sum_{n=0}^{LM-1} h^2(n), & k = L \\ 0, & k \neq L \end{cases} \tag{A.3}$$

due to this property of Nyquist filter, $X_m(k)$ using PHYDYAS based PFB are likewise proved to be independent observations.

PSW

The prototype filter of PSW is a non-Nyquist filter, which is designed especially for sensing task but not suitable for communications. Therefore, $X_m(k)$ using PSW based PFB are correlated observations.

$$
\begin{aligned}
R_{xx}(u) &= \mathbb{E}\left\{X_m(k)X_m^*(k-u)\right\} \\
&= \mathbb{E}\left\{\sum_{n,p=0}^{LM-1} r\big[n+kM\big]r^*\big[p+(k-u)M\big]h(n)h(p)e^{-2\pi j(n-p)\frac{m}{M}}\right\} \\
&\overset{i=n-p}{\Longrightarrow} \sum_{i=-(LM-1)}^{LM-1} \sum_{n=i}^{LM-1} \mathbb{E}\left\{r\big[n+kM\big]r^*\big[n-i+(k-u)M\big]\right\}h(n)h(n-i)e^{-2\pi j\frac{im}{M}} \\
&= \sum_{i=-(LM-1)}^{LM-1} R_{rr}\big[i+uM\big]\sum_{n=i}^{LM-1} h(n)h(n-i)e^{-2\pi j\frac{im}{M}} \\
&= \sum_{i=-(LM-1)}^{LM-1} R_{rr}\big[i+uM\big]\Big(h\otimes h[LM+i]\Big)e^{-2\pi j\frac{im}{M}}, \qquad u=\pm1,\pm2,\pm3,\cdots \quad \text{(A.4)}
\end{aligned}
$$

A.2 Statistic Distribution using PHYDYAS based PFB or PSE

Given the complex frequency estimation $X_m(k)$ with zero mean and variance $\sigma_{H_{0(1)}}^2$, the modulus of $X_m(k)$ satisfies a Rayleigh distribution

$$
|X_m(k)| \approx Rayleigh\left(\sqrt{\sigma_{H_{0(1)}}^2/2}\right) \tag{A.5}
$$

The two-order and four-order raw moments of $|X_m(k)|$ can be therefore calculated as

$$
\mathbb{E}(|X_m(k)|^2) = \sigma_{H_{0(1)}}^2, \quad \mathbb{E}(|X_m(k)|^4) = 2\cdot\sigma_{H_{0(1)}}^4 \tag{A.6}
$$

by which the variance of $|X_m(k)|^2$ is obtained accordingly

$$
Var(|X_m(k)|^2) = \sigma_{H_{0(1)}}^4 \tag{A.7}
$$

Finally, the distribution of the test statistic T_m in (3.75) is derived by applying the cental limit theory

$$
T_m \approx \mathcal{N}\left(\sigma_{H_{0(1)}}^2, \frac{1}{K}\sigma_{H_{0(1)}}^4\right) \tag{A.8}
$$

A.3 Statistic Distribution using PSW based PFB

The derivation of the test statistic distribution using PSW based PFB has the same procedure as the appendix B except the last step. For this special case, the frequency estimation $|X_m(k)|^2$ are a sequence of dependent and identically distributed random observations each having finite values of expectation $\sigma_{H_{0(1)}}^2$ and variance $\sigma_{H_{0(1)}}^4$. With a sufficiently large number of random variables, the test

statistic T_m can be approximately normally distributed, then the mean and the variance of T_m are given by

$$\mathbb{E}(T_m) = \mathbb{E}\left(\frac{1}{K}\sum_{k=1}^{K}|X_m(k)|^2\right) = \sigma^2_{H_{0(1)}}$$

$$Var(T_m) = \frac{1}{K^2}Var\left(\sum_{k=1}^{K}|X_m(k)|^2\right)$$

$$= \frac{1}{K^2}\left[\sum_{k=1}^{K}Var(|X_m(k)|^2) + 2\sum_{i<j}Cov(|X_m(i)|^2, |X_m(j)|^2)\right]$$

$$= \frac{1}{K^2}\left[K\sigma^4_{H_{0(1)}} + 2\sum_{u=1}^{K-1}(K-u)\left(R_{|x|^2|x|^2}(u) - \sigma^4_{H_{0(1)}}\right)\right] \tag{A.9}$$

where Cov denotes covariance operator, and $R_{|x|^2|x|^2}(u)$ is the autocorrelation between $|X_m(k)|^2$ and $|X_m(k-u)|^2$. Assuming $X_m(k) = x_1 + jy_1$ and $X_m(k-u) = x_2 + jy_2$, then $R_{|x|^2|x|^2}(u)$ is computed as

$$R_{|x|^2|x|^2}(u) = \mathbb{E}\left\{(x_1^2 + y_1^2)(x_2^2 + y_2^2)\right\} = \mathbb{E}\left\{x_1^2 x_2^2 + x_1^2 y_2^2 + y_1^2 x_2^2 + y_1^2 y_2^2\right\}$$

$$= \sigma^4_{H_{0(1)}} + 2\left\{\mathbb{E}^2(x_1 x_2) + \mathbb{E}^2(x_1 y_2) + \mathbb{E}^2(x_2 y_1) + \mathbb{E}^2(y_1 y_2)\right\}$$

$$= \sigma^4_{H_{0(1)}} + 4\mathbb{E}^2(x_1 x_2) = (1 + \lambda_u^2)\sigma^4_{H_{0(1)}} \tag{A.10}$$

where $\lambda_u = h \otimes h\left[(L-u)M\right]$. Finally, the variance of T_m in (A.9) can be approximated to

$$Var(T_m) \approx \frac{2}{K}\sigma^4_{H_{0(1)}} \tag{A.11}$$

As a result, the distribution of the test statistic T_m is derived as follows

$$T_m \approx \mathcal{N}\left(\sigma^2_{H_{0(1)}}, \frac{2}{K}\sigma^4_{H_{0(1)}}\right) \tag{A.12}$$

Existence of NE

In (5.3), the support domain $\mathbf{p}_n$ is a nonempty convex set due to the linear constraints. Thus, we only need to prove that the utility function u_n in (5.3) is a quasiconcave function in $\mathbf{p}_n$.

Firstly, we give the inequality of the weighted arithmetic mean and weighted geometric mean that will be helpful for our proof.

Inequality 1: *Let the nonnegative numbers $x_1, x_2, \ldots, x_n$ and the nonnegative weights $\alpha_1, \alpha_2, \ldots, \alpha_n$ be given. Set $\alpha = \alpha_1 + \alpha_2 + \ldots + \alpha_n$. If $\alpha > 0$, then the inequality*

$$\frac{\alpha_1 x_1 + \alpha_2 x_2 + \cdots + \alpha_n x_n}{\alpha} \geq \sqrt[\alpha]{x_1^{\alpha_1} x_2^{\alpha_2} \cdots x_n^{\alpha_n}} \tag{B.1}$$

holds with equality if and only if all the x_k with $\alpha_k > 0$ are equal.

Thanks to the fact that the sum of concave functions is also a concave function, we only need to prove the function

$$f = log_2[1 + \frac{a_1 z_1 + a_2 z_2 + \cdots + a_m z_m}{b}] \tag{B.2}$$

is a concave function, where $a_1, \ldots, a_m, b$ are nonnegative numbers and $\mathbf{z} = (z_1, z_2, \ldots, z_m)$ is in a convex domain C with m elements. Defining $\theta \in [0, 1]$ and $\mathbf{x}, \mathbf{y}$ are two points in the set C. According to the definition of concave function, we have

$$\begin{aligned}
&f(\theta \mathbf{x} + (1 - \theta)\mathbf{y}) \\
&= log_2[1 + \frac{a_1}{b}(\theta x_1 + (1 - \theta)y_1) + \frac{a_2}{b}(\theta x_2 + (1 - \theta)y_2) + \cdots + \frac{a_m}{b}(\theta x_m + (1 - \theta)y_m)] \\
&= log_2[\theta(1 + \frac{a_1}{b}x_1 + \frac{a_2}{b}x_2 + \cdots + \frac{a_m}{b}x_m) + (1 - \theta)(1 + \frac{a_1}{b}y_1 + \frac{a_2}{b}y_2 + \cdots + \frac{a_m}{b}y_m)] \\
&\theta f(\mathbf{x}) + (1 - \theta)f(\mathbf{y}) \\
&= log_2[(1 + \frac{a_1}{b}x_1 + \frac{a_2}{b}x_2 + \cdots + \frac{a_m}{b}x_m)^\theta] + log_2[(1 + \frac{a_1}{b}y_1 + \frac{a_2}{b}y_2 + \cdots + \frac{a_m}{b}y_m)^{1-\theta}]
\end{aligned} \tag{B.3}$$

for simplicity, we set $1 + \frac{a_1}{b}x_1 + \frac{a_2}{b}x_2 + \cdots + \frac{a_m}{b}x_m = x'$ and $1 + \frac{a_1}{b}y_1 + \frac{a_2}{b}y_2 + \cdots + \frac{a_m}{b}y_m = y'$, then

$$\begin{aligned}
f(\theta \mathbf{x} + (1 - \theta)\mathbf{y}) &= log_2(\theta x' + (1 - \theta)y') \\
\theta f(\mathbf{x}) + (1 - \theta)f(\mathbf{y}) &= log_2[(x')^\theta (y')^{1-\theta}]
\end{aligned} \tag{B.4}$$

It is seen that x' and y' are nonnegative numbers, which is a special case of Inequality 1 when $n = 2$ and $\alpha = 1, \alpha_1 = \theta, \alpha_2 = 1 - \theta$ in (B.1). Because of the increasing property of log-function, f in (B.2) satisfies the definition of concave function

$$f(\theta x' + (1 - \theta)y') \geq \theta f(x') + (1 - \theta)f(y') \tag{B.5}$$

Q.E.D.

Bibliography

[1] FCC, "Federal Communications Commission: Spectrum Policy Task Force," *Report of the Spectrum Efficiency Working Group*, Nov. 2002.

[2] FCC, ET Docket No 03-222 Notice of proposed rule making and order, Dec. 2003.

[3] G. Staple and K. Werbach, "The end of spectrum scarcity," *IEEE Spectrum*, vol. 41, no. 3, pp. 48-52, Mar. 2004.

[4] M. A. McHenry, "NSF Spectrum Occupancy Measurements Project Summary," *Shared Spectrum Company Report*, Aug. 2005.

[5] J. Mitola and G. Q. Maguire, "Cognitive radio: Making software radios more personal," *IEEE Personal Communications*, vol. 6, pp. 13-18, Aug. 1999.

[6] T. Weiss and F. Jondral, "Spectrum Pooling: An Innovative Strategy for the Enhancement of Spectrum Efficiency," *IEEE Communications Magazine*, vol. 42, no. 3, pp. 8-14, Mar. 2004.

[7] P. P. Vaidyanathan, "Multirate digital filters, filter banks, polyphase networks, and applications: a tutorial," *Proceedings of the IEEE*, vol. 78, no. 1, pp. 56-93, Jun. 1990.

[8] B. Le Floch, M. Alard, and C. Berrou, "Coded orthogonal frequency division multiplex," *Proceedings of the IEEE*, vol. 83, pp. 982-996, Jun. 1995.

[9] M. Bellanger, "Specification and design of a prototype filter for filter bank based multicarrier transmission," *in Proc. of IEEE ICCASP*, vol. 1, 2001, pp. 2417-2420.

[10] P. Siohan, C. Siclet, and N. Lacaille, "Analysis and design of OFDM / OQAM systems based on filterbank theory," *IEEE Trans. Signal Processing*, vol. 50, pp. 1170-1183, May 2002.

[11] H. Boelcskei, "Orthogonal frequency division multiplexing based on offset QAM," *Advances in Gabor analysis*, Birkhäuser, 2003.

BIBLIOGRAPHY

[12] H. Bölcskei, P. Duhamel, and R. Hleiss, "Orthogonalization of OFDM / OQAM pulse shaping filters using the discrete Zak transform ," *Signal Processing*, vol. 83, iss. 7, pp. 1379-1391, 2003.

[13] M. Bellanger, "Filter banks and OFDM / OQAM for high throughput wireless LAN," *in Proc. of 3rd International Symposium on Communications, Control and Signal Processing. ISCCSP'08*, Malta, Mar. 2008, pp. 758-761.

[14] P. Amini, P. Kempter, RR Chen, and L. Lin, "Filter Bank Multitone: A Physical Layer Candidate For Cognitive Radios," *in Proc. of the SDR Forum technical Conference*, Nov. 2005, pp. 14-18.

[15] B. Farhang-Boroujeny and R. Kempter, "Multicarrier Communication Techniques for Spectrum Sensing and Communication in Cognitive Radios," *IEEE Communications Magazine*, 46(4): 80-85, Apr. 2008.

[16] B. Farhang-Boroujeny, "Filter Bank Spectrum Sensing for Cognitive Radios," *IEEE Transactions Signal Processing*, vol. 56, iss. 5, pp. 1801-1811, May 2008.

[17] TIA-902.BBAB, "Wideband air interface Isotropic Orthogonal Transform Algorithm (IOTA) physical layer specification," *document of the Telecommunications Industry Association*, 2003.

[18] 3GPP TSG-RAN WG1. TR25.892, "Feasibility study of OFDM for UTRAN enhancement," *V1.1.0*, Jun. 2004.

[19] "PHYDYAS-Physical layer for dynamic spectrum access and cognitive radio," *www.ict-phydyas.org: Document5 1 deliverable.*

[20] W. A. Gardner, "Spectral correlation of modulated signal, Part I-Analog modulation," *IEEE Transactions Communications*, vol. COM-35, pp. 584-594, Jun. 1987.

[21] W. A. Gardner, W. A. Brown, and C. K. Chen, "Spectral correlation of modulated signals, Part II-Digital modulation," *IEEE Transactions Communications*, vol. COM-35, pp. 595-601, Jun. 1987.

[22] M. Öner and F. Jondral, "On the Extraction of the Channel Allocation Information in Spectrum Pooling Systems," *IEEE Journal on Selected Areas in Communications*, vol. 25, iss. 3, pp. 558-565, Apr. 2007.

[23] D. Vučić, M. Obradović, and D. Obradović, "Spectral Correlation of OFDM Signals Related to Their PLC Applications," *in Proc. of 6th International Symposium on Power-Line Communications and Its Applications, ISPLC'02*, 2002.

[24] H. Bölcskei, "Blind estimation of symbol timing and carrier frequency offset in wireless OFDM systems," *IEEE Trans. Commun.*, vol. 49, no. 6, pp. 988-999, Jun. 2001.

[25] P. Ciblat and E. Serpedin, "A fine blind frequency offset estimator for OFDM / OQAM systems," *IEEE Trans. on Signal Processing*, vol. 52, no. 1, pp. 291-296, Jan. 2004.

[26] Y. Hur, J. Park, W. Woo, K. Lim, C.-H. Lee, HS. Kim, and J. Laskar, "A wideband analog multi-resolution spectrum sensing (MRSS) technique for cognitive radio (CR) systems," *in Proc. of IEEE Int. Symp. on Circuits and Syst'06*, May 2006, pp. 4090-4093.

[27] B. Chen, T. Liu, F. Shu, and J. Wang, "On Performance Comparison of Wideband Multiple Primary User Detection Methods in Cognitive Radios," *in Proc. of WiCOM'09*, 2009.

[28] Z. Quan, S. Cui, A. H. Sayed, and H. V. Poor, "Optimal Multiband Joint Detection for Spectrum Sensing in Cognitive Radio Networks," *IEEE Transactions on Signal Processing*, vol. 57, pp. 1128-1140, Mar. 2009.

[29] S. Taşcıoğlu and O. Üreten, "Bayesian Wideband Spectrum Segmentation for Cognitive Radios," *in Proc. of 18th International Conference on Computer Communications and Networks*, 2009, pp. 1-6.

[30] R. Mahesh, A. P. Vinod, C. Moy, and J. Palicot, "A Low Complexity Reconfigurable Filter Bank Architecture for Spectrum Sensing in Cognitive Radios," *in Proc. of 3rd International Conference on CrownCom'08*, May 2008, pp. 1-6.

[31] F. Sheikh, S. Masud, and B. Bing, "Harmonic power detection in wideband cognitive radios," *Signal Processing, IET*, vol. 3, pp. 40-50, Jan. 2009.

[32] M. Kim, J. Naganawa, and J. Takada, "Multichannel Spectrum Sensing using Polyphase DFT Filter Bank for Opportunistic Cognitive Radios," *The Institute of Electronics, Information and Communication Engineers (IEICE)*, vol. 109, pp. 121-127, May 2009.

[33] T. Weiss and J. Hillenbrand, "Mutual interference in OFDM-based spectrum pooling systems," *in Proc. of Vehicular Technology Conference*, vol. 4, May 2004, pp. 1873-1877.

[34] W. Rhee, J. C. Chuang, and L. J. J. Cimini, "Performance Comparison of OFDM and Multi-tone with Polyphase Filterbank for Wireless Communications," *in Proc. of Vehicular Technology Conference*, vol. 2, May 1998, pp. 768-772.

[35] D. Lacroix, N. Goudard, and M. Alard, "OFDM with Guard Interval versus OFDM / offset QAM for High Data Rate UMTS Downlink Transmission," *in Proc. of Vehicular Technology Conference*, vol. 4, fall 2001, pp. 2682-2684.

[36] C. S. Lee and K. Y. Yoo, "Polyphase Filter-based OFDM Transmission System," *in Proc. of Vehicular Technology Conference*, vol. 1, Sep. 2004, pp. 525-528.

[37] D. S. Waldhauser, L. G. Baltar, and J. A. Nossek, "Comparison of Filter Bank Based Multicarrier Systems with OFDM," *in Proc. of IEEE Asia Pacific Conference, Circuits and Systems*, Dec. 2006, pp. 976-979.

[38] J. Du and S. Signell, "Comparison of CP-OFDM and OFDM / OQAM in Doubly Dispersive Channels," *Future generation communication and networking*, vol. 2, pp. 207-211, Dec. 2007.

[39] T. Ihalainen, A. Viholainen, and M. Renfors, "On Spectrally Efficient Multiplexing in Cognitive Radio Systems," *in Proc. of International symposium on wireless pervasive computing*, May 2008, pp. 675-679.

[40] T. Ihalainen, T. H. Stitz, A. Viholainen, and M. Renfors, "Performance comparison of LDPC-coded FBMC and CP-OFDM in beyond 3G context," *in Proc. of ISCAS'06*, 2006, pp. 2049-2052.

[41] L. G. Baltar and D. S. Waldhauser, "Out-Of-Band Radiation in Multicarrier Systems: A Comparison," *Lecture Notes in Electrical Engineering*, vol. 1, pp. 107-116, 2007.

[42] T. Qin and C. Leung, "Fair Adaptive Resource Allocation for Multiuser OFDM Cognitive Radio Systems," *in Proc. of ICST ChinaCom*, Shanghai, China, 2007.

[43] P. Wang, M. Zhao, L. Xiao, S. Zhou, and J. Wang, "Power Allocation in OFDM-Based Cognitive Radio Systems," *in Proc. of IEEE GLOBECOM'07*, Nov. 2007, pp. 4061-4065.

[44] G. Bansal, M. J. Hossain, and V. K. Bhargava, "Adaptive Power Loading for OFDM-Based Cognitive Radio Systems," *in Proc. of IEEE ICC'07*, Jun. 2007, pp. 5137-5142.

[45] M. Shaat and F. Bader, "Power Allocation with Interference Constraint in Multicarrier Based Cognitive Radio Systems," *Book Title: Multi-Carrier Systems and Solutions. Chapter 4: Adaptive Transmission .Eds. Plass, S; Dammann, A; Kaiser, S; Fazel, K. Springer*, ISBN: 978-90-481-2529-6 (HB) [4], Netherlands, 2009.

[46] M. Shaat and F. Bader, "Power Allocation and Throughput Comparison in OFDM and FBMC Based Cognitive Radio," *in Proc. of the 22nd Meeting of the Wireless World Research Forum, WWRF'09*, Paris, France, May 2009.

[47] W. Yu, G. Ginis, and J. M. Cioffi, "Distributed multiuser power control for digital subscriber lines," *IEEE Journal on Selected Areas in Commun.*, vol. 20, no. 5, pp. 1105-1114, Jun. 2002.

[48] H. Zhu, J. Zhu, and K. J. Ray Liu, "Non-Cooperative Resource Competition Game by Virtual Referee in Multi-Cell OFDMA Networks," *IEEE Communications Journal*, pp. 1079-1090, Aug. 2007.

[49] L. Wang, Y. Xue, and E. Schulz, "Resource Allocation in Multicell OFDM Systems based on Noncooperative Game," *in Proc. of IEEE PIMRC'06*, 2006, pp. 1-5.

[50] G. Scutari, D. P. Palomar, and S. Barbarossa, "Asynchronous Iterative Waterfilling for Gaussian Frequency-Selective Interference Channels," *IEEE Transactions on Information Theory*, pp. 2868-2878, Jul. 2008.

[51] J. Qiu and Z. Zhou, "Distributed Resource Allocation Based on Game Theory in Multi-cell OFDMA Systems," *International Journal of Wireless Information Networks*, pp. 44-50, Mar. 2009.

[52] H. Kwon and B. G. Lee, "Distributed resource allocation through noncooperative game approach in multi-cell OFDMA systems," *in Proc. of IEEE ICC'06*, Jun. 2006, pp. 4345-4350.

[53] A. M. Kuzminskiy and Y. I. Abramovich, "Decentralized dynamic Spectrum Allocation based on adaptive antenna array interference mitigation diversity: algorithms and Markov chain analysis," *in Proc. of IEEE ICASSP*, 2009, pp. 3645-3648.

[54] "Cognitive Radio, Software-Defined Radio References," *WCSP Group, University of South Florida (USF)*. Available: http://wcsp.eng.usf.edu/cognitive_radio_links.html

[55] P. Pawełczak, "Cognitive radio information centre," *IEEE Standard Association*. Available: http://www.scc41.org/crinfo

[56] Q. Zhao and B. M. Sadler, "A Survey of Dynamic Spectrum Access," *IEEE Signal Processing Magazine*, vol. 24, pp. 79-89, May 2007.

[57] J. Mitola, "The Software Radio," *In Proc. of IEEE National Telesystems Conference*, Digital Object Identifier 10.1109/NTC.1992.267870, 1992.

[58] J. Mitola, "Software radios: Survey, critical evaluation and future directions," *IEEE Aerospace and Electronic Systems Magazine*, vol. 8, pp. 25-36, Apr. 1993.

[59] J. Mitola, "Software Radio Architecture: A Mathematical Perspective," *IEEE Journal on Selected Areas in Communications*, May 1999.

[60] F. K. Jondral, "Software-Defined Radio: Basics and Evolution to Cognitive Radio," *EURASIP Journal on Wireless Communications and Networking*, vol. 2005, iss. 3, pp. 275-283, 2005.

[61] S. Haykin, "Cognitive radio: brain-empowered wireless communications," *IEEE J. Select. Areas Commun.*, vol. 23, pp. 201-220, Feb. 2005.

[62] I. F. Akyildiz, W.-Y. Lee, M. C. Vuran, and S. Mohanty, "Next generation / dynamic spectrum access / cognitive radio wireless networks: a survey," *Computer Networks*, vol. 50, pp. 2127-2159, 2006.

[63] J. Neel, "Analysis and Design of Cognitive Radio Networks and Distributed Radio Resource Management Algorithms," *Ph.D. dissertation, State University*, Blacksburg, VA, Sep. 2006.

[64] "Wireless Innovation Forum," Website: http://www.wirelessinnovation.org

[65] J. Mitola, "Cognitive radio: An integrated agent architecture for software defined radio," *PhD Dissertation Royal Institute of Technology, Stockholm*, Sweden, May 2000.

[66] C. R. Stevenson, G. Chouinard, Z. Lei, W. Hu, S. J. Shellhammer, and W. Caldwell, "IEEE 802.22: The first cognitive radio wireless regional area network standard," *IEEE Communications Magazine*, vol. 47, iss. 1, pp. 130-138, Jan. 2009.

[67] M. Sherman, A. N. Mody, R. Martinez, C. Rodriguez, and R. Reddy, "IEEE Standards Supporting Cognitive Radio and Networks, Dynamic Spectrum Access, and Coexistence," *IEEE Communications Magazine*, vol. 46, iss. 7, pp. 72-79, Jul. 2008.

[68] A. M. Hayar, R. Pacalet, and R. Knopp, "Cognitive radio research and implementation challenges," *in Proc. of Conference on Signals, Systems, and Computers, ACSSC'07*, Nov. 2007, pp. 782-786.

[69] I. Budiarjo, H. Nikookar, and L. Ligthart, "Cognitive radio modulation techniques," *IEEE Signal Processing Magazine*, vol. 25, pp. 24-34, Nov. 2008.

[70] E. Azarnasab, R. Kempter, N. Patwari, and B. Farhang-Boroujeny, "Filterbank Multicarrier and Multicarrier CDMA for Cognitive Radio Systems," *in Proc. of IEEE CrownCom*, Aug. 2007.

[71] H. A. Mahmoud, T. Yucek and H. Arslan, "OFDM for Cognitive Radio: Merits and Challenges," *IEEE Wireless Communications*, vol. 16, iss. 2, pp. 6-14, Apr. 2009.

[72] S. Brandes, I. Cosovic, and M. Schnell, "Reduction of out-of-band radiation in OFDM systems by insertion of cancellation carriers," *IEEE Commun. Lett.*, vol. 10, no. 6, pp. 420-422, Jun. 2006.

[73] H. A. Mahmoud and H. Arslan, "Sidelobe Suppression in OFDM-based Spectrum Sharing Systems Using Adaptive Symbol Transition," *IEEE Commun. Lett.*, vol. 12, no. 2, pp. 133-135, Feb. 2008.

[74] R. W. Chang, "Synthesis of Band-Limited Orthogonal Signals for Multi-carrier Data Transmission," *Bell. Syst. Tech. J.*, vol. 45, pp. 1775-1796, Dec. 1966.

[75] B. R. Saltzberg, "Performance of an efficient parallel data transmission system," *IEEE Trans. On Comm. Tech.*, vol. 15, no. 6, pp. 805-811, Dec. 1967.

[76] B. Hirosaki, "An Orthogonally Multiplexed QAM System Using the Discrete Fourier Transform," *IEEE Trans. On Comm. Tech.*, vol. 29, iss. 7, pp. 982-989, Jul. 1981.

[77] S. D. Sandberg and M. A. Tzannes, "Overlapped Discrete Multitone Modulation for High Speed Copper Wire Communications," *IEEE Journal on selected areas in communications*, vol. 13, no. 9, pp. 1571-1585, Dec. 1995.

[78] B. Farhang-Boroujeny, "Multicarrier modulation with blind detection capability using cosine modulated filter banks," *IEEE Trans. Commun.*, vol. 51, no. 12, pp. 2057-2070, Dec. 2003.

[79] G. Cherubini, E. Eleftheriou, S. Olcer, and J. M. Cioffi, "Filter bank modulation techniques for very high speed digital subscriber lines," *IEEE Communications Mag.*, vol. 38, no. 5, pp. 98-104, May 2000.

[80] A. Skrzypczak, P. Siohan, N. Chotkan, and M. Djoko-Kouam, "OFDM / OQAM: An appropriate modulation scheme for an optimal use of the spectrum," *in Proc. of ISCCSP'08*, Malte, Mar. 2008, pp. 405-410.

[81] P. Amini, R. Kempter, and B. Farhang-Boroujeny, "A comparison of alternative filterbank multicarrier methods for cognitive radio systems". *in Proc. of the SDR Technical Conference and Product Exposition*, 2006.

[82] D. S. Waldhauser, L. G. Baltar, and J. A. Nossek, "Comparison of Filter Bank Based Multicarrier Systems with OFDM". *in Proc. of IEEE Asia Pacific Conference on Circuits and Systems*, Dec. 2006, pp. 976-979.

[83] B. Wild and K. Ramchandran, "Detecting primary receivers for cognitive radio applications," *in Proc. of IEEE DySPAN 2005*, Nov. 2005, pp. 124-130.

[84] G. B. Giannakis and M. K. Tsatsanis, "Signal Detection and Classification Using Matched Filtering and Higher Order Statistics," *IEEE Transactions on Signal Processing*, vol. 38, no. 7, pp. 1284-1296, Jul. 1990.

[85] D. Cabric, S. M. Mishra, and R. W. Brodersen, "Implementation issues in spectrum sensing for cognitive radios," *in Proc. of Asilomar Conf. on Signals, Systems, and Computers*, Nov. 2004, vol. 1, pp. 772-776.

[86] M. Ghozzi, M. Dohler, F. Marx, and J. Palicot, "Cognitive radio: methods for the detection of free band," *Comptes Rendus Physique, Elsevier*, vol. 7, pp. 794-804, Sep. 2006.

[87] H. L. Van Trees, "Detection, Estimation, and Modulation Theory (Part I)," *Wiley, New York*, 1968.

[88] D. Cabric, A. Tkachenko, and R. Brodersen, "Spectrum sensing measurements of pilot, energy, and collaborative detection," *in Proc. of IEEE Military Communications Conf.*, Oct. 2006, pp. 1-7.

[89] H. Urkowitz, "Energy detection of unknown deterministic signals," *Proceeding of the IEEE*, pp. 523-531, Apr. 1967.

[90] I. M. Mendel, "Tutorial on Higher Order Statistics (Spectra) in Signal Processing and Systems Theory: Theoretical Results and Some Applications," *Proc. IEEE*, vol. 79, on. 3, pp. 278-305, Mar. 1991.

[91] W. Akmouche, "Detection of multicarrier modulations using 4th-order cumulants," *in Proc. of IEEE Military Communications Conf.*, Atlantic City, New Jersey, USA, Oct. 1999, pp. 432-436.

[92] C. J. Le Martret and D. M. Boiteau, "Modulation classification by means of different orders statistical moments," *in Proc. of IEEE Military Communications Conf. (MILCOM '97)*, Nov. 1997, pp. 1387-1391.

[93] M. Haddad, A. M. Hayar, M. Debbah, and H. M. Fetoui, "Cognitive radio sensing information-theoretic criteria based," *in Proc. of the 2nd International Conference on Cognitive Radio Oriented Wireless Networks and Communications (CrownCom'07)*, Aug. 2007, pp. 241-244.

[94] B. Zayen, A. M. Hayar, and K. Kansanen, "Blind spectrum sensing for cognitive radio based on signal space dimension estimation," *in Proc. of IEEE International Conference on Communications (ICC'09)*, Jun. 2009, pp. 1-5.

[95] W. A. Gardner, A. Napolitano, and L. Paura, "Cyclostationarity: half a century of research," *Signal Processing*, vol. 86, no. 4, pp. 639-697, Apr. 2006.

[96] W. A. Gardner, "The spectral correlation theory of cyclostationary time-series," *Signal Processing*, vol. 11, pp. 13-36, Jul. 1986.

[97] P. D. Sutton, K. E. Nolan, and L. E. Doyle, "Cyclostationary Signatures in Practical Cognitive Radio Application," *IEEE Journal on selected areas in Communications*, vol. 26, no. 1, pp. 13-24, Jan. 2008.

[98] A. Chevreuil, E. Serpedin, P. Loubaton, and G. Giannakis, "Blind channel identification and equalization using non-redundant periodic modulation precoders: performance analysis," *IEEE Trans. on Signal Processing*, vol. 48, no.6, pp. 1570-1586, Jun. 2000.

[99] K. Maeda, A. Benjebbour, T. Asai, T. Furuno, and T. Ohya, "Cyclostationarity-inducing Transmission Methods for Recognition among OFDM-Based Systems," *EURASIP Journal on Wireless Communications and Networking*, vol. 2008, Jan. 2008.

[100] D. Vučić and M. Obradović, "Matrix-based Stochastic method for the Spectral Correlation Characterization of Digital Modulation," *Facta Universitatis, Series: Electronics and Energetics*, vol. 11, no. 3, pp. 271-284, 1998.

[101] M. K. Tsatsanis and G. B. Giannakis, "Transmitter induced cyclostationarity for blind channel equalization," *IEEE Transactions on Signal Processing*, vol. 45, no. 7, pp. 1785-1794, 1997.

[102] H. Zhang, D. Le Ruyet, and M. Terré, "Signal Detection for OFDM / OQAM System Using Cyclostationary Signatures," *in Proc. of IEEE International Symposium on Personal Indoor and Mobile Radio Communications, PIMRC'08*, Sep. 2008, pp. 1-5.

[103] 3GPP, "ARIB TR-T12-25.943 V4.2.0 Deployment aspects (Release 4)," *3GPP*, Jun. 2002.

[104] A. Sonnenschein and P. M. Fishman, "Radiometric Detection of Spread-Spectrum Signals in Noise of Uncertain Power," *IEEE Transactions on Aerospace and Electronic Systems*, vol. 28, no. 3, pp. 654-660, Jul. 1992.

[105] R. Tandra and A. Sahai, "SNR Walls for Signal Detection," *IEEE J. Sel. Topics Signal Process.*, vol. 2, no. 1, pp. 4-17, Feb. 2008.

[106] P. P. Vaidyanathan, "Multirate Systems and Filter Banks," *Prentice-Hall*, 1993.

[107] M. Bellanger, "Adaptive Digital Filters," *2 edition, Marcel Dekker*, New York, 2001.

[108] H. Zhang, D. Le Ruyet, and M.Terré, "Spectral efficiency comparison between OFDM / OQAM and OFDM based CR networks," *Wireless Communications and Mobile Computing*, Wiley, Vol. 9, pp. 1487-1501, Nov. 2008.

[109] Y. Medjahdi, M. Terré, D. Le Ruyet, D. Roviras, J. A. Nossek, and L. Baltar, "Inter-cell Interference Analysis for OFDM / FBMC Systems," *in Proc. of 10th IEEE Signal Processing Workshop (SPAWC 2009)*, Perugia, Italy, Jun. 2009, pp. 598-602.

[110] M. S. Barzaraa, H. D. Sherali, and C. M. Shetty, "Nonlinear programming: theory and algorithms," *2ed ed, John Wiley & Sons*, 1993.

[111] J. M. Peha, "Approaches to spectrum sharing," *IEEE Commun. Mag.*, vol. 43, no. 2, pp. 10-12, Feb. 2005.

[112] C. Lengoumbi, P. Godlewski, and P. Martins, "An Efficient Subcarrier Assignment Algorithm for Downlink OFDMA," *in Proc. of Vehicular Technology Conference*, Sep. 2006, pp. 1-5.

[113] H. W. Kuhn, "Variants of the Hungarian method for assignment problems," *Naval Research Logistics Quarterly*, 3: 253-258, 1956.

[114] Draft IEEE 802.16m Evaluation Methodology Document C80216m-07-080r2.

[115] M. Haddad, A. M. Hayar, and M. Debbah, "Spectral efficiency of spectrum-pooling systems," *IET Communications*, vol. 2, no. 6, pp. 733-741, Jul. 2008.

[116] B. Zayen, M. Haddad, A. M. Hayar, and G. E. Øien, "Binary power allocation for cognitive radio networks with centralized and distributed user selection strategies," *Physical Communication Journal, Elsevier*, vol. 1, no. 3, pp. 183-193, Sep. 2008.

[117] D. Fudenberg and J. Tirole, "Game theory," *MIT Press, Cambridge, MA*, 1991.

[118] T. M. Cover and J. A. Thomas, "Elements of Information Theory," *New York: Wiley*, 1991.

[119] R. S. Cheng and S. Verdù, "Gaussian Multiaccess Channels with ISI: Capacity Region and Multiuser Water-Filling," *IEEE Transactions on Information Theory*, vol. 39, no. 3, pp. 773-785, May 1993.

[120] J. Wang, T. Chen, and B. Huang, "Cyclo-period estimation for discrete-time cyclo-stationary signals," *IEEE Trans. Signal Process.*, vol. 54, no. 1, pp. 83-94, Jan. 2006.

[121] I. A. Akbar and W. H. Tranter, "Dynamic spectrum allocation in cognitive radio using hidden Markov models: Poisson distributed case," *in Proc. of IEEE SoutheastCon*, Mar. 2007, pp. 196-201.

[122] M. Renfors, "Spectrum monitoring schemes for FBMC cognitive radios," *in Proc. of Future Network and MobileSummit (FNMS 2010)*, Florence, Italy, Jun. 2010.